Parameter identification for a TGV model

Sönke Kraft

Doctoral Thesis

presented by

Sönke Kraft

to obtain the degree

DOCTEUR
DE L'ÉCOLE CENTRALE PARIS

Title:

Parameter identification for a TGV model

Doctoral thesis defended the 30 of March 2012 in front of the jury composed of :

L. Jézéquel	Professor École Centrale Lyon	President
S. Iwnicky	Professor Manchester Metropolitan University	Rapporteur
G. Bonnet	Professor Université Paris-Est Marne la Vallée	Rapporteur
D. Aubry	Professor École Centrale Paris	Supervisor
G. Puel	Maître de Conférences École Centrale Paris	Supervisor
C. Funfschilling	SNCF, Direction de l'innovation et de la recherche	Supervisor

Laboratoire Mécanique des Sols, Structures et Matériaux (MSSMat)
École Centrale Paris
Grande Voie des Vignes
92 295 Châteny-Malabry Cedex

Contents

1 Modelling and parameter identification of a TGV train: technical and theoretical basis 5

1.1 The vehicle track system and its modelling in a multibody approach 6

1.1.1 The mechanical structure of the vehicle track system . 6

1.1.1.1 The wheel-rail contact 6

1.1.1.2 Types and functionality of the suspension elements 11

1.1.1.3 Time scales of vehicle behaviour 12

1.1.2 Modelling of the vehicle track system 12

1.1.2.1 Multi-body description 13

1.1.2.2 Modelling of the suspension elements 13

1.1.2.3 Modelling of the wheel-rail contact 14

1.1.2.4 Impact of nonlinearities on the modelling . . 16

1.1.2.5 Detection of nonlinearities from inline measurements 18

1.2 Identification of the model parameters from inline measurements 20

1.2.1 Choice of an adapted parameter identification method 21

1.2.1.1 Time series analysis 21

1.2.1.2 Frequency analysis: application to nonlinear systems and operational analysis 23

1.2.2 The procedure for the parameter identification using the structural model updating method 28

1.2.2.1 Misfit function criteria 28

1.2.2.2 Regularization 31

1.2.2.3 Detection of identifiable parameters from sensitivity analysis 33

1.2.2.3.1 The screening method 34

1.2.2.3.2 Consideration of nonlinear coupling by the use of global methods 35

1.2.2.4 Minimization of the misfit function 40
1.2.2.4.1 Application of local methods 42
1.2.2.4.2 Application of gradient methods . . 44
1.2.2.4.3 Methods for the calculation of the gradient 46
1.2.2.4.4 Global methods 48
1.2.2.4.5 Combined global-local method: combination between simulated annealing and pattern search 52
1.3 Conclusions 54

2 Selection of an adequate model structure for the representation of the low frequency dynamics of the vehicle track system 55
2.1 Implementation of a bogie model derived from kinematic and dynamic equations 58
2.1.1 Kinematic equations of the wheel-rail contact 58
2.1.2 Derivation of the nonlinear dynamic equations using the Lagrange approach 66
2.1.3 Analysis of the dynamic behaviour of the bogie model . 71
2.2 Vampire bogie model as virtual experimental data 76
2.3 Model of the TGV train implemented in Vampire 79
2.3.1 Modelling of the wheel-rail contact 80
2.3.2 Modelling of the suspension elements 82
2.3.2.1 Air spring model 84
2.3.2.2 Coil springs 89
2.3.2.3 Hydraulic damper 90
2.3.2.4 Rubber spring elements 91
2.3.3 Model properties 94
2.4 Summary of the system and model properties and conclusions 95

3 Application of the parameter identification to the bogie model 97
3.1 Definition of a misfit function as a norm of the distance between model prediction and measurements 99
3.1.1 Analysis of the misfit function solution surface 100
3.1.2 Technical constraints for the suspension parameters . . 107
3.2 Parameter identifiability testing based on sensitivity analysis . 108
3.2.1 Application of the screening method 109
3.2.2 Sensitivity analysis taking into account the parameter interaction 111

3.3 Minimization of the misfit function by applying adequate optimization methods . . . 114
3.3.1 Application of local methods . . . 115
3.3.1.1 Application of the Pattern Search method as a gradient-free local optimization method . . 115
3.3.1.2 Identification with gradient methods . . . 116
3.3.2 Explicit calculation of the gradient . . . 123
3.3.2.1 Gradient calculation from adjoint state approach . . . 124
3.3.2.2 Gradient calculation from automatic differentiation (AD) . . . 129
3.3.2.3 Comparison of the gradient calculations . . . 129
3.3.3 Parameter identification with simulated annealing from Matlab reference simulation . . . 137
3.3.4 Parameter identification with simulated annealing from Vampire reference simulation . . . 141
3.3.5 Parameter optimization for the bogie model: conclusions 142

4 Application of the parameter identification to the TGV model 149
4.1 Introduction . . . 149
4.2 System analysis and calibration of the initial model . . . 151
4.2.1 Analysis of the vehicle-track system with regard to the parameter identification problem . . . 151
4.2.1.1 Analysis of the main excitation of the system : the track . . . 151
4.2.1.2 Analysis of the response of the system to track excitation using transfer functions . . . 155
4.2.1.3 Detection of nonlinearities using transfer functions . . . 158
4.2.1.4 Detection of nonlinearities from phase plots . 162
4.2.2 First Calibration of the initial model estimated from the correlation and misfit function . . . 163
4.2.2.1 Correction of the PK shift . . . 166
4.2.2.2 Computation of the correlation and misfit function per section . . . 167
4.2.3 Sensitivity analysis: coupling between substructures and choice of identifiable parameters . . . 171
4.2.3.1 Calculation of the solution surface by varying one parameter . . . 172
4.2.3.2 Sensitivity taking into account the parameter interaction . . . 175

4.2.3.3 Sensitivity for independent suspension parameters . . . 178
4.3 Parameter identification . . . 184
4.3.1 Misfit function . . . 184
4.3.2 Identification problems . . . 188
4.3.2.1 Bogie A vertical . . . 188
4.3.2.2 Carriage 2 lateral . . . 195
4.3.2.3 Traction unit 1: bogies, car bodies, vertical, lateral . . . 198
4.3.2.4 Traction unit, carriages . . . 198
4.4 Conclusions . . . 200
4.4.1 Discussion of errors in the parameter identification problem . . . 200
4.4.1.1 Modelling errors . . . 200
4.4.1.2 Measurement uncertainties . . . 201
4.4.2 Discussion and Perspectives . . . 204

A Multi-body model of bogie 213

B Vampire model of the TGV train 223

C Optimization methods 231

D Analysis of measurement data and calibration of model 239

E Calibration of the initial model using coherence and misfit functions 253

Symbols and notations

	Signification	**Unit**		**Signification**	**Unit**
D_i	matrix derivative	-	α	regularization factor	-
E	expectance value	-	γ_d	cross level irregularity	rad
E_c	kinetic energy	J	δ_0	angle of conical wheel	rad
F	force vector	N	δ_x	roll angle of wheelset	rad
G	shear modulus	Pa	δ_z	yaw angle of wheelset	rad
H	transfer function	-	μ	slip	-
I	identity matrix	-	π	probability density	-
J	misfit function	-	σ	variance	-
K	stiffness matrix	N/m	∇	gradient	
L	Lagrangian equation	-			
M	mass matrix	kg			
PK	kilometric position	km			
R_R	rail profile radius	m			
R_W	wheel profile radius	m			
S_{xx}	cross-spectrum	-			
S_{xy}	auto-spectrum	-			
T	friction force	N			
V	variance	-			
c	spring rate	N/m			
d	damping rate	Ns/m			
d_j	generalized force	N			
d_k	search direction	-			
d_y	lateral irregularity	m			
d_z	vertical track irregularity	m			
e	error vector	-			
e_0	track gauge	m			
f	force vector	N			
g	vector nonlinear terms	m			
m	mass	kg			
p	parameter vector	-			
Δr	wheel radius difference	m			
u	displacement wheelset	m			
x	response vector	-			
v	translative vitesse	m/s			
w	rotational vitesse	rad/s			

Acklowdegements

This doctoral thesis arised within the framework of a CIFRE contract between the laboratory MSSMat at Ecole Centrale Paris and the research department of SNCF. The subject was initiated by SNCF as a result of experiences with multi-body simulations of the TGV train.

I would like to thank everybody who contributed to this work. In particular my supervisors at SNCF and Ecole Centrale Paris.

At SNCF the thesis was followed by Christine Funfschilling and at Ecole Centrale Paris by Guillaume Puel and Denis Aubry. With their enormous interest in this work and their unresting availability for discussions they brought the thesis forward and created a very constructive environment. I would like to thank them for all their ideas and proposals, all the time spend for discussions and the cordial relations we had.

I also would like to express my gratitude to all my colleagues at the research department of SNCF where I spend most of the time. Right from the beginning, even though my French left a lot to desire, I felt part of the team. The diversity of subjects in the field of railway technology treated their, the discussions and many interesting presentations created a very stimulating environment and allowed me to learn a lot in other fields beyond my own PhD work. Not to forget everything concerning the French culture and language! It was a pleasure to work with you.

And finally, I would like to address my thanks to the personnel and PhD students at MSSMat for support and interesting encounter.

Paris, June 2012

Introduction

The motivation for this work comes from the comparison of the measured dynamic response of a TGV train with the result of a simulation model. The precise measurement of the track irregularities has made it possible to simulate the dynamic behaviour of the TGV train under realistic conditions for the French highspeed lines. It was found that the model represents the dynamic behaviour of the TGV train well but that further improvements would be desirable having in mind new applications of simulation models as the virtual homologation of railway vehicles or model-based condition monitoring. With the excitation signal and the system response exactly known in form of measured track irregularities and accelerations the idea came up to identify the parameters of the vehicle model by solving an inverse problem. This work investigates the properties of the identification problem and proposes an approach for the parameter identification.

The liberalization of the railway market and the need for economic efficiency require the reduction of cost and improved comfort. Less energy consumption, the reduction of wear of rails and wheels and an optimized maintenance are thus of large interest. For all new technical solutions the constructors and operators always have to guarantee the security - the most important criterion and quality feature of the rail traffic.

All these aims are related to the dynamic behaviour of the vehicle-track system. The accelerations on the passenger should not exceed a certain limit guaranteeing a good comfort. The forces in the wheel rail contact should be low reducing wear and material fatigue and in consequence maintenance cost. And the accelerations and forces always have to be within the limits of the norm for the security.

An important tool for the achievement of these aims is the simulation of the dynamic behaviour. Multi-body programs have been used for years by the constructors of railway vehicles during the conception and construction

phase. They allow the comparison and optimization of different technical solutions with respect to the comfort and the security of the vehicle long before the first vehicle runs on the track. The expensive construction of prototypes is no longer necessary. These multi-body programs represent the vehicle by a structure of rigid or elastic bodies with mass connected by suspension elements.

Before a new or modified railway vehicle is allowed to run on a network it has to be certified. The homologation is a costly procedure defined in the norm UIC518 which requires the realization of many inline tests for different track and vehicle conditions and takes several months in some cases years. Due to the strict security requirements the use of simulations is not allowed yet. The validation of the simulation model is not considered as sufficient. This concerns in particular the influence of different running conditions on the validity of the model.

In order to reduce the cost and time needed for the homologation the constructors and operators, among them the SNCF, aim at replacing at least some of the measurements by simulations. This requires an improvement of the simulation programs in order to build precise and reliable measurement substitutes.

One obstacle for more exact simulations has been unavailable or imprecise excitation signals in form of the vertical and lateral irregularities of each rail. With the new measurement train IRIS320 these data are now available in numerical form and high precision. The second difficulty concerns the model of the railway vehicle itself. The exact reproduction of the dynamic behaviour of the real system requires the modelling of the different elements of the primary and secondary suspension. Every suspension element is described by a mechanical model with a certain number of parameters. Often these parameters are not precisely known, on the one hand because the suppliers are not able to specify them and on the other hand due to changes in the parameter values caused by wear and damage during operation. A requirement for the further reaching use of multi-body programs is therefore the validation and parameter identification of the vehicle model from measurement data. An identification of the suspension parameters during operation could be used for improved maintenance procedures based on condition monitoring.

The development of a parameter identification procedure for a TGV train model is the aim of this work. The model represents a TGV train running over a track with measured track irregularities. The response of the model

is compared with the response measured in the train and the suspension parameters are updated by solving an inverse problem.

The identification of the suspension parameters of a railway vehicle model is a so-called white box identification problem. A physical model is constructed beforehand from available information about the real system. Then the parameters of the model are estimated by adjusting the model response to the response of the real system. To perform this identification a large variety of approaches exists each one beeing suitable to particular applications. The parameter identification for a complete train model based on in-line measurements is a fairly new and rarely explored application. It has to take into account the nonlinear characteristics of the wheel-rail contact, the large number of parameters and the limitation to operational measurements obtained from a highly coupled system under non-periodic excitation. This work aims at outlining the particularities of the vehicle-track system and their consequences on the parameter identification. Based on this knowledge a parameter identification procedure is developed and applied.

The work is structured in four chapters. The first chapter gives an introduction to the modelling of the vehicle-track system and the parameter identification. A literature survey presents and discusses relevant methods. For both domains - the modelling of the vehicle-track system and the parameter identification - the focus is laid on the aspects concerning their interaction. Which characteristics of the vehicle-track system have to be considered when applying the parameter identification to this model? And which parameter identification method among the wide range of identification methods can be fitted to the particularities of the vehicle-track system? The first chapter discusses these questions and sets the direction for the following chapters.

In the second chapter the construction and particularities of the vehicle-track model are outlined. Two models are presented in detail: the model of the TGV train for which the parameter identification tends to be applied and the simplified model of a single bogie. It is composed of the wheelsets and the bogie frame and serves as a test model for the parameter identification with relatively simple and completely known properties taking into account the particularity of the wheel-rail contact at the same time.

In the third chapter the parameter identification is applied to the bogie model. Different suitable approaches for the identification of the suspension parameters are compared. Local gradient methods require the sensitivity gradients of the vehicle response relative to the suspension parameters. The

computation of the gradients using the adjoint state method is developed.

Finally, the fourth chapter discusses the application of the parameter identification to the more complex model of the TGV train. The measured track irregularities used as excitation signal of the vehicle model and the in-line measurements of accelerations and forces in the train are analyzed. As a result appropriate identification problems are defined, performed and discussed.

Chapter 1

Modelling and parameter identification of a TGV train: technical and theoretical basis

The system for which the parameter identification should be performed is the TGV Duplex train running on the track. Before working on the different aspects of the identification process, it is indispensable to define the system and its properties. One has to be clear about the physical effects the model is supposed to reproduce. The identification can give reliable results for the parameters only if the model is able to represent these effects. The process of identifying an adequate model, the system identification, is therefore the first step in modelling. The second step aims at identifying the design parameters of the model from the measured system response.

This chapter describes the technical and theoretical basis of these two steps. It is therefore divided into two main sections. The first section 1.1 includes a description of the vehicle track system and its modelling in a multibody approach. The identification of the model parameters from inline measurements is the topic of the second section 1.2.

1.1 The vehicle track system and its modelling in a multibody approach

1.1.1 The mechanical structure of the vehicle track system

A train running on a track is a complicated integrated system composed by several subsystems which are coupled to each other. The vehicle itself and its guidance, the track, can not be regarded separately if the dynamic behaviour is described.

Vehicle and track are coupled by the wheel-rail contact. This enables to support the vehicle, to guide it along the track and to transmit acceleration and braking forces. For the comprehension of the system the geometric and physical properties of the wheel-rail contact is a crucial point. Across a small contact surface all forces are transferred: normal forces compensating the vehicle mass and inertia effects and tangential forces due to friction.

1.1.1.1 The wheel-rail contact

Wheel and track profiles The track is composed of the subgrade, the sleepers and the rails. The rails guide the vehicle. For this purpose the vehicle is equipped with wheelsets - two wheels rigidly connected by an axis - which run on the track as shown in figure 1.1. The geometry of the rail and wheel profile determines this movement. It consists of the running surface and the flange. In the simplest case, the running surface is conical. Due to the conical profile the wheelset returns to the centreline for small lateral displacements. The lateral displacement results in a rolling radius difference between the left and the right wheel. The translational speed of the outer wheel increases turning the wheelset back towards the centreline. The forces acting in the wheel-rail contact can be divided into geometric and friction forces.

At important excitations and narrow curves the conical form of the running surface is not sufficient for the guidance of the vehicle. It is assured by the flange restricting the lateral displacement. Nowadays wheel and rail profiles are standardized. Often used wheel and rail profiles can be seen in figure 1.2. The UIC 60 profile is used for recent lines and is composed of circular profiles of different radii.

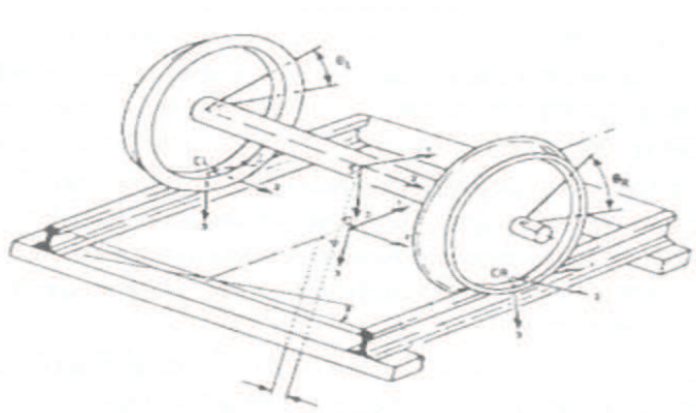

Figure 1.1: Wheelset on track (from [98])

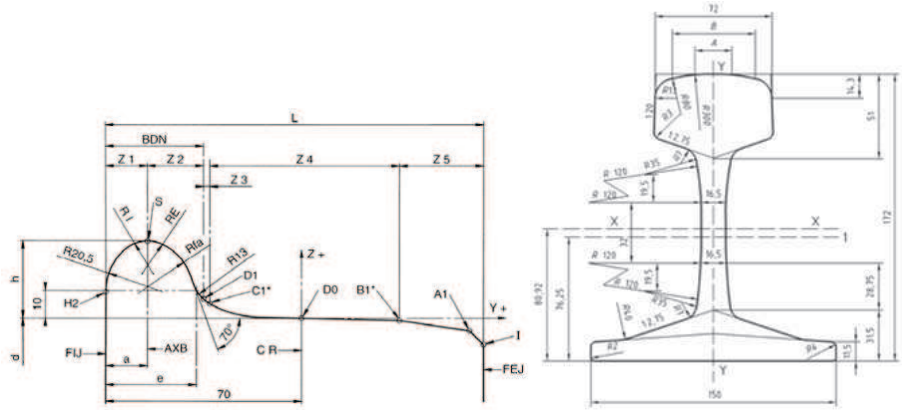

(a) (b)

Figure 1.2: Wheel profile DIN EN 13715 (a) and rail profile 60 E1 DIN EN13674-1 (b)

Contact mechanics Wheel and rail are in contact at one or several points depending on the position of the wheelset relatively to the rail. By displacing the wheelset laterally the contact point moves on the profile. The determination of the contact points is the first step when describing the wheel-rail contact. If the wheel and rail profiles are perfectly circular this relation is continuous and an analytical solution exists. Their derivation can be found in [52]. It shows that among the 6 degrees of freedom for an uncoupled wheelset 4 are independent and 2 are dependent.

The wheel profiles used today are so called wear profiles. As outlined in [8] they have been developed taking into account the wear which changes the profile and therefore the dynamic behaviour during time. In contrast to circular or conical wheel profiles they lead to discontinuities in the contact point. The kinematic equations have no analytical solution. Figure 1.3 (b) shows the difference between left and right wheel contact radii as a function of lateral displacement of the wheelset against the track for a UIC 60/S1002 profile combination (a).

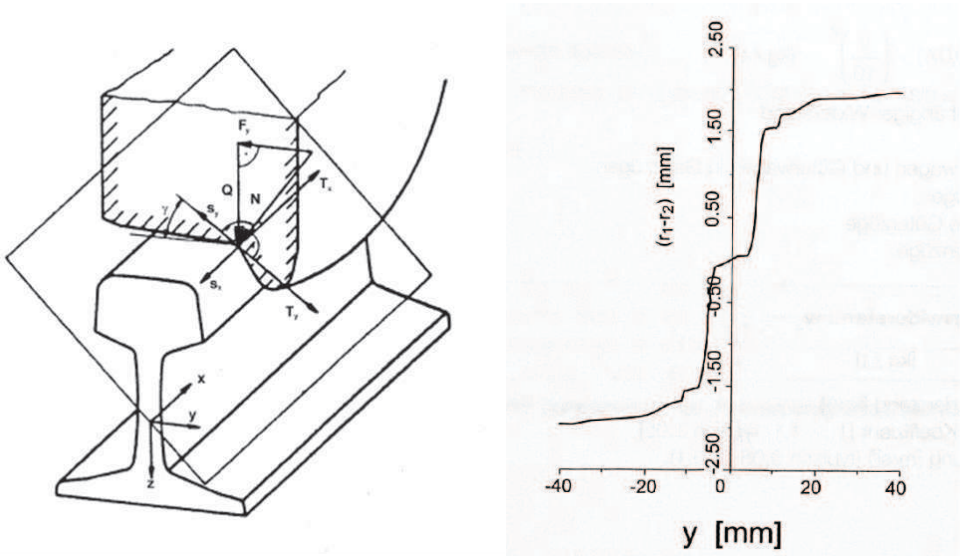

(a) (b)

Figure 1.3: Wheel rail contact (a), Difference between left and right wheel contact radii as a function of lateral displacement y (b) (from [52])

When talking about the contact point one has to bear in mind that - con-

sidering the material elasticity - the contact point is a surface. For circular profiles this surface has the shape of an ellipse. For the geometrically more complicated wear profiles complex non-elliptical forms appear. Figure 1.4 shows the result of measurements of the contact surface for worn profiles obtained by [53]. This complicates the modelling of the wheel-rail contact.

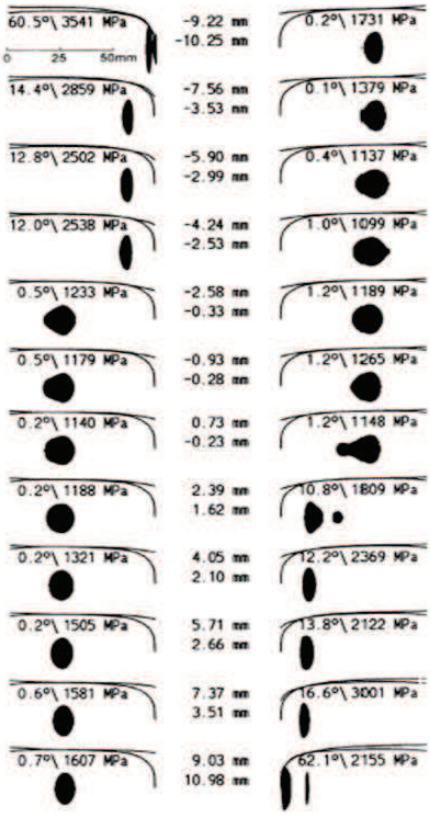

Figure 1.4: Contact surface for worn profiles (S1002, UIC60)[53]

Track irregularities The track does not only fulfil the crucial task to carry and guide the vehicle. It is also the main source for the excitation of unwanted vibrations in the vehicle. The track never has an ideal geometry. Imperfections in the position and geometry of the rails provoke displacements of the wheelset which are transferred into the vehicle as vibrations and noise. Different types of track irregularities can be distinguished: periodic, singular and stochastic irregularities.

Periodic excitations can be caused by a wheel-defect or periodic defects of the rail. Singular excitations are for example track stiffness variations due to switches or bridges appearing at well-defined positions. The most important type of excitation is stochastic track defects.

For a certain position along the track the irregularities are described by four independent parameters. These are the vertical and lateral displacements of the left and the right rail. Often a representation relative to the centreline of the track is used: the horizontal and vertical displacement of the track, its inclination and variations in the gauge. The last parameter only has an importance if nonlinear stability effects are considered. The different track irregularities are depicted in figure 1.5.

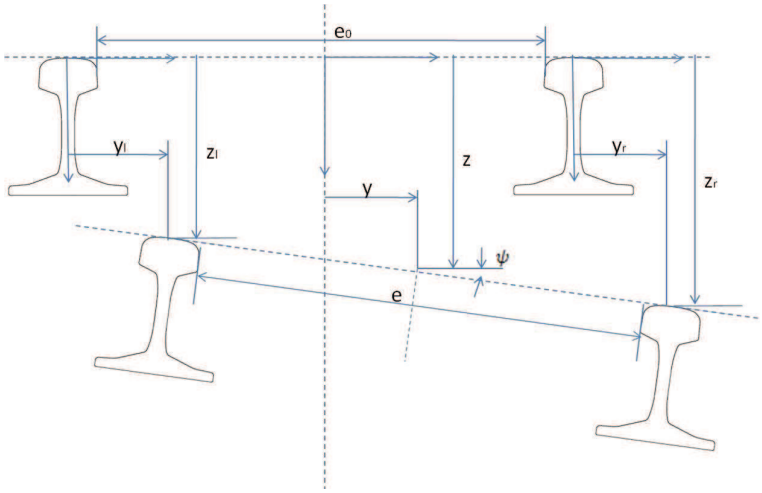

Figure 1.5: Track irregularities described by four degrees of freedom (vertical z, lateral y, cross level ψ, gauge e or vertical left z_l, lateral left y_l, vertical right z_r, lateral right y_r)

At SNCF measurement trains measure continuously the irregularities of the track. The most recent one is a modified TGV train (IRIS320) equipped with camera-and-laser-based light-section measurement systems. Results of the track defects measurements performed for the high speed line TGV Est will be presented in chapter 4.

1.1.1.2 Types and functionality of the suspension elements

The connection between the different bodies of the train (wheelsets, bogies, carbodies) is achieved by suspension elements. Their function is the attenuation of vibrations caused by the track irregularities as well as the guidance of the vehicle along the track.

Primary and secondary suspension levels Most trains are equipped with bogies. Then two suspension levels exist: the primary suspension between the wheelset and the bogie frame and the secondary suspension between the bogie frame and the car body. The same holds for the TGV which has some specific features compared to classical rail vehicles. As shown in figure 1.6 it is an articulated train where each bogie (Jacobs bogie) supports two carbodies leading to a more important dynamic coupling. The carbodies are coupled by elastic pivots and hydraulic dampers.

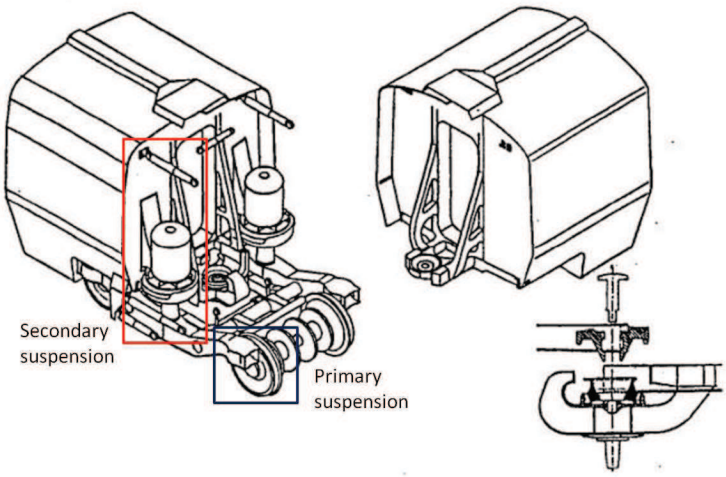

Figure 1.6: Jacobs Bogie in TGV train

The primary suspension ensures the guidance of the wheelset on the track and reduces vibrations transmitted from the wheelsets. The vertical characteristic of the primary suspension is chosen with the objective of vibration attenuation. This is obtained by a relatively weak stiffness. Often coil springs take over this function. The longitudinal and lateral stiffness controls the running stability of the wheelset since it prevents or reduces the hunting

movement. In the TGV train a high transversal stiffness is assured by guidance springs in the power unit or guidance arms for the carrying bogies.

The secondary suspension is crucial for the comfort of the vehicle. It has the function to attenuate the vibration transmission from the bogie frame to the car body. Both low frequency vibrations leading to perturbing accelerations on the passengers as well as structure-borne noise are concerned. During the last decades the air spring has become the standard suspension element. Despite its higher complexity compared to coil springs the good attenuation properties justify its usage. In the TGV Duplex train air springs are used in the secondary suspension of the passenger vehicles.

1.1.1.3 Time scales of vehicle behaviour

In general, two effects can be distinguished when studying the dynamics of railway vehicles. The short time dynamics describes the accelerations and forces in the vehicle due to the track irregularities for a certain vehicle speed. It is the basis for analysis concerning the security and the comfort of the vehicle. Besides, there are processes which arise after many kilometers traveled and which change the dynamic behaviour over a long time. This concerns wear and deterioration processes. An example is the friction forces in the wheel-rail contact which cause material removal on the wheel and rail surface. This changes the profile geometry and eventually the dynamic behaviour of the vehicle.

For this work both aspects are important: the parameter identification for the model is performed using the measured response of the system. By repeating the parameter identification over a longer period one aims to detect deterioration processes in the vehicle.

1.1.2 Modelling of the vehicle track system

After the real system has been determined the modelling may be considered. It has the aim to reproduce the physical effects of the system which are important for the envisaged analysis by a mechanical model. The type of model and its complexity depend on the physical effects one wants to take into account.

1.1.2.1 Multi-body description

In order to analyse the comfort and security of the vehicle the dynamic response in a low frequency range up to 20Hz is sufficient. The eigenmodes of the system in this frequency range are induced by the primary and secondary suspension. The elastic eigenmodes of the vehicle bodies can be neglected. The system is therefore represented by rigid bodies connected by suspension elements. Figure 1.7 shows a railway bogie modeled with a commercial multi-body program.

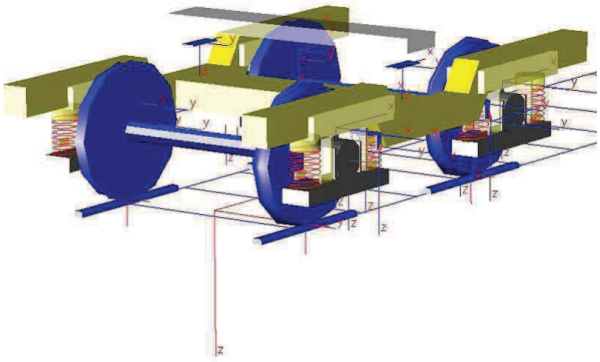

Figure 1.7: Bogie modeled in a multi-body program

In a multi body system (MBS) model with rigid bodies every body is described by 6 degrees of freedom. Coupling elements and constraints reduce the number of degrees of freedom. For the multi body model of the TGV train a total number of around 300 degrees of freedom is obtained.

The bodies which form the multi body model of a train vehicle are basically the wheelset, the bogie and the car body. Depending on the complexity of the model further bodies can be added for example for the detailed description of suspension elements, brake equipment or motor-gear units.

1.1.2.2 Modelling of the suspension elements

The connection between the bodies is ensured by suspension and coupling elements. For the TGV train some are mentioned in the description of the vehicle system above.

The adequate modelling of the suspension elements is a difficult task in the construction of multi-body models. Ideally the inherent dynamic behaviour of a suspension element is known from test rig measurements so that a model can be chosen for the frequency range of interest. If this is not the case theoretical considerations form the basis of the modelling. For coil springs a simple linear description by a constant stiffness is usually sufficient. For more complex elements like the air spring and the rubber spring the construction of an adequate model is by far more difficult.

1.1.2.3 Modelling of the wheel-rail contact

A correct representation of the wheel-rail contact is crucial for the modelling of the vehicle. On a small contact surface all forces between vehicle and track are transmitted. In [90] a comprehensive introduction to the rolling contact is given.

Normal contact model For the modelling of the wheel-rail contact normal and tangential effects are distinguished. The normal contact forces are composed of static forces due to the mass of the vehicle and dynamic forces due to inertia effects. They give rise to a contact surface as a result of the elastic strain of the wheel and the rail.

The form of this contact surface depends on both the normal force and the geometry of the bodies in contact. For its calculation the Hertz theory is applied. The hypothesis of the Hertz theory are the following: the bodies in contact have the same linear-elastic material behaviour, are homogeneous and isotropic and can be considered as half spaces described by second order surfaces. The surfaces are continuous and non-conforming. Under the conditions of the Hertz theory the contact surface has the form of an ellipse with the contact radii a and b (figure 1.8). In the contact surface the stress distribution has the form of a half ellipsoid. Based on the radii of curvature, the material properties and the known normal force, the radii of the ellipse are calculated. The Hertz theory is found in [43] and its application to the wheel-rail contact of circular profiles in [52].

The Hertz theory describes the normal contact problem with a sufficient accuracy for many applications. However, one has to bear in mind that due to curvature discontinuities the UIC60/S1002 profile geometries do not respect the assumptions made in the Hertz theory and lead to other more complicated

forms of the contact surface. An approximation of the non-elliptical contact surface by an elliptical one can lead to errors. Then more complicated models which are able to calculate non-elliptical contact surfaces have to be used.

The properties of the normal contact form the input data to the transversal contact model which aims to calculate the friction forces in the contact surface.

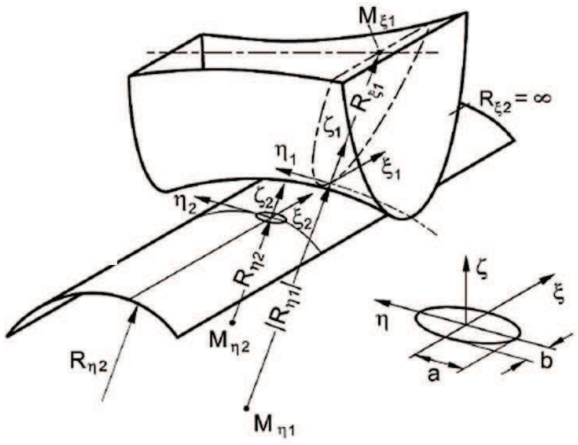

Figure 1.8: Calculation of the contact ellipse with contact radii a and b according to Hertz for a circular rail ($R_{\eta 2}$) and circular wheel profile ($R_{\eta 1}$)(from [52])

Tangential contact model Fundamental works in wheel-rail contact mechanics were developed by Kalker. His theory relates the slip in the contact surface (longitudinal ν_ξ, lateral ν_η, spin ν_ζ) to the friction forces T_ξ, T_η and T_ζ. The slip denotes the normalized relative velocity between the rail and the wheel in the contact point and is computed from the nonlinear geometric relations of the wheelset.

Then the coefficients for the friction model are computed as functions of the slip, the normal forces and the form and dimension of the contact ellipse (a, b). In his linear theory Kalker [44] developed a table including these coefficients (Kalker coefficients C_{ij}) as functions of the named parameters. From the Kalker coefficients, the slip, the ellipse size and the shear modulus G the friction forces are computed according to (1.1).

$$\begin{pmatrix} T_\xi \\ T_\eta \\ M_\zeta \end{pmatrix} = Gab \begin{pmatrix} C_{11} & 0 & 0 \\ 0 & C_{22} & \sqrt{ab}C_{23} \\ 0 & -\sqrt{ab}C_{23} & abC_{33} \end{pmatrix} \begin{pmatrix} \nu_\xi \\ \nu_\eta \\ \nu_\zeta \end{pmatrix} \tag{1.1}$$

This linearised relation between slip and friction forces (1.9) holds only for small slip values. For higher slip values the friction forces reach a saturation level. The reason for this saturation effect is the appearance of two different zones in the contact surface: an adhesion and a slip zone. A point on the wheel entering into the contact surface first adheres. Due to the relative velocity between the wheel and the rail this leads to an increasing tangential tension. When the tangential tension reaches its saturation level defined by the Coulomb friction law the particle begins to slip. It enters the slip zone. With increasing relative velocity the slip zone becomes larger until it represents the whole contact surface. The tangential tensions reach their maximum and saturation appears. It is considered in the theory of Vermeulen and Johnson and in the nonlinear theory of Kalker (FASTSIM) based on a discretisation of the contact surface. For more information it is referred to [44] and [45].

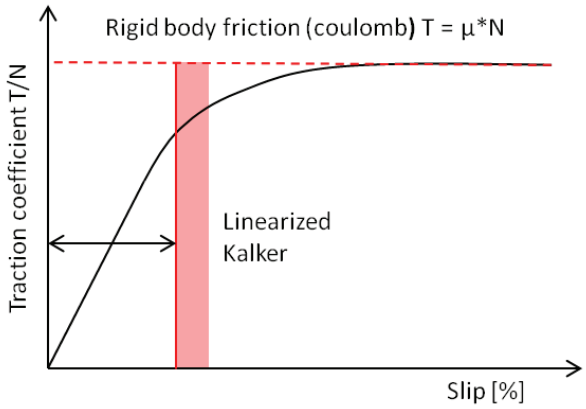

Figure 1.9: Relation between slip and friction forces

1.1.2.4 Impact of nonlinearities on the modelling

The vehicle-track system is characterized by nonlinearities. This raises the question whether the nonlinearities of the system have to be considered for its modelling. In order to answer this question, the effect of the nonlinearities on the dynamic behaviour is analyzed.

In general, nonlinearities appear in all real systems. However, they have often only a weak influence on the system behaviour and can be neglected in the modelling process. This allows to work with linear models and to take advantage of all the properties of linear systems like superposition and modal analysis.

For railway vehicles neglecting nonlinearities is in general not possible. Some nonlinearities determine significantly the dynamic response of the vehicle. In [97] the impact of nonlinearities in railway vehicle dynamics is outlined.

Wheel-rail contact nonlinearities Once again the wheel-rail contact has to be named in the first place. Even if the profiles of the rail and wheel are considered as circular and conical respectively the geometric relations describing the difference in the contact point radius, the contact-angle and the elevation of the centreof gravity of the wheelset as functions of the degrees of freedom are strongly nonlinear. One might use a Taylor development to linearize these terms but for the vertical elevation a nonlinear term of second order remains. The derivation of the nonlinear equations is outlined in chapter 2.

The relation between the friction coefficients and the relative velocities also shows a nonlinear characteristic in form of saturation. Only for small slip values a linear relation can be assumed.

Suspension element nonlinearities The second important source of nonlinearities in railway vehicles is the suspension elements. When analyzed in test rigs, rubber spring elements and the air spring show a significantly nonlinear behaviour. Nonlinearities are also caused by bumpstops which restrict the vehicle movement. In the same way as for a single suspension element in a test rig, inline measurements from the TGV might be used to detect and characterize nonlinearities. However, due to the complexity of the system and numerous sources of error, the analysis is difficult to perform. The detection and identification of nonlinearities in mechanical systems is a current subject in research and a large diversity of articles can be found. A good summary of the current state of research and the different methods is given in [50] and [9].

1.1.2.5 Detection of nonlinearities from inline measurements

When working through the methods and the examples for their application, a difficulty becomes apparent. The presented examples always deal with very simple mechanical systems with only a few degrees of freedom. Due to the individualistic character of the nonlinear problems the application is often limited to a special type of system.

Applications to complex systems like the vehicle-track system considered here are rarely found. Exceptions are the detection and characterisation of nonlinearities for an airplane structure treated in [25] and [27]. However, in these references the measurements are performed in a test rig with well-defined excitation signals. The transferability of the methods on the vehicle track problem is often not possible. The track excitation is neither a periodic excitation with a stationary spectrum nor a white noise signal. Besides, the vehicle is exposed to correlated multiple excitations in form of the contact forces at every wheel.

Eigenmodes from transfer functions The invalidity of the superposition principle is one important indicator for the influence of nonlinearities. The same applies to the dependence of system modes on the excitation. For linear systems the modes described by their eigenfrequencies and eigenforms are system-inherent properties which do not depend on the excitation. For nonlinear systems the modes identified from the transfer functions between excitation and response depend on the excitation level. Due to the characteristics of the real track, the distinction of section with different track defect amplitudes is difficult to perform. However it is found that the level of the wheel forces depends on the speed of the vehicle. Therefore, a comparison of the transfer functions between wheel forces and acceleration responses for different vehicle speeds give important information on nonlinearities. If the effect of nonlinearities is studied for the model of the TGV, analytical track defects with precisely defined properties offer interesting possibilities. The response to sinusoidal excitation is especially suitable for the detection of nonlinearities.

Another characteristic of nonlinear systems is the frequency dependence of the homogeneous solution on the initial conditions and the occurrence of limit cycles. While an undamped linear oscillator vibrates at its eigenfrequencies and an amplitude defined by the initial condition, the homogeneous solution of an nonlinear oscillator shows eigenfrequencies depending on the initial con-

ditions. Using a perturbation method for solving the dynamic equation an amplitude dependent frequency is found.

Correlation analysis The correlation function and the comparison between the H1 and H2 estimates of the transfer function, calculated from the crossspectra S_{ij} and autospectra S_{ii} are an indication for nonlinearities.

$$H_1 = \frac{S_{yx}(f)}{S_{xx}(f)} \qquad H_2 = \frac{S_{yy}(f)}{S^*_{yx}(f)} \tag{1.2}$$

However, it has too be considered that lower values in the correlation function and differences between the transfer function estimation can also be caused by noise in the measurement data.

Higher order spectra An interesting criterion based on the transfer function is the Hilbert transformation applied in [9]. Differences in the Nyquist plot between the transfer function and its Hilbert transform indicate nonlinearities. Hickey [37] proposes the extension of the cross-and autospectra to higher order spectra. Bispectra and trispectra and their correlation functions can be used to identify quadratic and cubic nonlinear modes in a system and their coupling. He presents successful applications to simple systems with a few degrees of freedom. If the approach is applicable to the complex vehicle-track system, the high modal density and disturbing noise effects remains to be figured out.

Restoring force surface method The same applies to the restoring force surface method. In [33] restoring force plots are used to characterize the frequency and amplitude characteristics of nonlinearities from experimental measurements of a tire-vehicle suspension system. Since the restoring force method only uses output acceleration measurements it can be used even when input measurements are not available. Haroon [33] uses the relation between accelerations in the sprung mass and the relative velocity between the sprung mass and the unsprung mass for the charaterisation of nonlinear damping forces.

In the same way the stiffness forces are characterized by using the relative displacements. Displacement and speed are calculated by integrating the measured acceleration in the bogie. For the vehicle-track system the forces

are measured in the specially equipped measurement wheelsets. Accelerations are measured in the axle boxes, the bogies and car bodies.

Glösmann [24] applies the Karhunen-Loève transform (KLT), developed in order to find structures in random process data, on the measurements of a railway wheelset on a test rig. The KLT describes the random process y by a orthonormal basis Ψ as $y = \Psi\alpha$. The basis vectors Ψ_i are referred to as characteristic functions and the realisation α_i as weighting factors. Since the wheelset dynamics is highly nonlinear the measurement of the different degrees of freedom at the time step k is considered as one realization of a multi-dimensional random process. The KLT is used to identify correlations of the different degrees of freedom.

For the application of the KLT it is considered that each track excitation causes a deviation of the wheelset trajectory. Since the track defects are stochastic each initial trajectory position can be seen as the result of a random experiment. Between two excitations at t_k and t_{k+1} the dynamics are assumed to be stationary and can be characterized by the results of the Karhunen-Loève transform. For each stationary time interval $\Delta t = t_{k+1} - t_k$ the weighting factors can be interpreted as the amplitude of the wheelset in the direction of the actual eigenvectors described by the characteristic functions. For the wheelset the characteristic functions describe the principal directions of mouvements. In this way parameter changes of the system due to nonlinearities can be identified as changes in the eigenvalues and eigenvectores.

1.2 Identification of the model parameters from inline measurements

The analysis of the measurement data allows to characterize the dynamic properties of the system. Together with the knowledge of the physical phenomena the analysis of the measurement data provides the basis for the construction of the vehicle model. The detection of nonlinearities from measurement data is an important part of the model identification. Such a model based both on the insight in the physical phenomena and on measurement results is called grey-box model. Contrary to a white-box model which is based on the exact description of the physical effects. Due to the complex nature of many physical processes - the thermodynamic description of the air

spring is a good example - these models become very complex. It is therefore necessary to neglect terms and the attributed physical effects in the model description whose effect on the considered dynamic behaviour is low. This requires the analysis of measurements.

After the model has been built one is confronted with the task of identifying the model parameters so that the model coincides best with the measured response of the real system.

The parameter identification for a multi-body model of a TGV train represents the main objective of this work. The choice of an adequate identification method will therefore be discussed more in detail. From the previous considerations some important aspects can be pointed out:

- The multi-body model of a vehicle-track system is relatively complicated due to the wheel-rail contact and different types of suspension elements.
- Not all nonlinearities can be neglected in the model. Some of the model parameters one aims to identify are therefore related to nonlinear effects.
- The number of parameters the identification methods should deal with is relatively high.

1.2.1 Choice of an adapted parameter identification method

The aim of parameter identification methods is to determine the parameters of a model so that it reproduces best the real system. All methods are therefore based on a criterion which expresses the difference between the real system and the model. The parameter identification methods can be classified depending on how this criterion is defined. An important distinction is made between time domain and frequency domain methods.

1.2.1.1 Time series analysis

ARMAX and NARMAX modelling An application which has been used in control technique for a long time is the time-series analysis. The model of the system is not expressed by a differential equation system but by finite differences equations giving a discrete description of the model. A dynamic model described by a differential equation of the form:

$$\mathbf{M}\ddot{\mathbf{u}} + \mathbf{K}\mathbf{u} = \mathbf{f} \tag{1.3}$$

is transformed into a differences equation using the relations:

$$\dot{\mathbf{u}}(t) = \frac{\mathbf{u}_k - \mathbf{u}_{k-1}}{\Delta t} \quad \ddot{\mathbf{u}}(t) = \frac{\mathbf{u}_k - 2\mathbf{u}_{k-1} + \mathbf{u}_{k-2}}{\Delta t^2} \tag{1.4}$$

giving:

$$\mathbf{u}_k(\frac{1}{\Delta t^2}\mathbf{M} + \mathbf{K}) - \mathbf{u}_{k-1}\frac{2M}{\Delta t^2} + \mathbf{u}_{k-2}\frac{M}{\Delta t^2} = \mathbf{f} \tag{1.5}$$

This Autoregressive Moving average (ARX) is therefore of the form:

$$\mathbf{u}_i = \sum_{j=1}^{n_y} a_j \mathbf{u}_{i-j} + \sum_{j=1}^{n_x} b_j \mathbf{f}_{i-j} \tag{1.6}$$

By fitting the ARX model to the measured time series the coefficients are identified. If noise is present the ARX model is extended to the ARMAX model by the addition of a noise model to the system model.

In [66] and [67] this approach is used for the parameter identification from excitation and response data in presence of noise and unmeasured sources of periodic and random excitation. The parameters of the ARMAX model are estimated by a multistage optimization algorithm and then used to calculate the modal parameters. The method is applied to experimental data from measurements on a beam. The application to a more complex real system can be found in work of Lardies [56].

In order to enable the time series analysis for nonlinear system, the ARMAX model has been extended to nonlinear cases. The identification of nonlinear systems using NARMAX models is treated in [78]. The output is then calculated from delayed input and output variables, the regressors, related by a nonlinear function.

The application of the time series method to the TGV measurements reveals several difficulties. Only if the ARMAX model is built from the continuous differential equation system model the time-series parameters have a physical meaning. They are expressed by the mass, stiffnesses and dampings of the differential equation system. Consequently, if the ARMAX model is applied directly on the measurement data the identified parameters do not have a physical meaning. This represents an important disadvantage for the application to a multibody model. Furthermore, for complex systems like the

vehicle-track system with a high modal density, the order of the ARMAX model that is required for the adequate description can increase significantly.

Temporal structural model updating A time domain approach which is adapted for complex systems is the structural model updating. The system can be described by a complex model with a large number of parameters and nonlinear properties. This is the case for the multi-body model of the vehicle-track system. The criterion is then defined as the distance between the measured and modeled time responses. Typically the distance is expressed by the L1 or L2 norm.

The parameters of the model are identified by applying a parametric optimization method which minimizes the distance between model and measurement response. Kang [47] applies the structural modal updating to measured accelerations from a relatively complicated structure. The identification algorithm minimizes a misfit function defined by the time integral of the least square error between measured and modeled accelerations. He pays attention to the ill-posedness of the inverse problem due to noise and incompleteness of measurements and proposes a new regularization function defined as the time integral of the squared first time derivative of system parameters. It is pointed out that the choice of proper regularization factors is critical for the accuracy of the solution.

The identification of parameters in multi-body dynamic systems by structural model updating is also treated in [88]. A least square misfit function is defined and minimized using the Levenberg-Marquard method. The work deals with the question if an unique solution exists. This is the requirement for the identifiability of the parameters.

1.2.1.2 Frequency analysis: application to nonlinear systems and operational analysis

A drawback of structural model updating methods is the large amount of data used and the sensitivity to measurement errors. Therefore a frequency analysis can be advantageous. The identification is based on spectra or transfer functions. Transfer functions between an input and output signal form the basis of modal analysis methods.

Linear case For linear systems, modal analysis has an outstanding importance in identification problems. If the system is excited with a known input and responses are measured, the transfer functions can be calculated. By different techniques the modal parameters (eigenfrequencies, eigendampings and eigenforms) are extracted. Heylen [35] gives a comprehensive introduction into the theory of modal analysis and its application. In the case of a linear system the transfer functions and modal parameters are inherent properties of the system and describe completely the dynamic behaviour. By superposition of all modes the response of the system can be rebuilt for every excitation. The governing equations of the system are decoupled due to the orthogonality of the modes.

When the dynamic equations are available the eigenvalues can be obtained analytically by solving an eigenvalue problem. To the eigenvalues corresponds a set of eigenvectors describing the shape of the mode. They contain complex modal displacements and can differ in their phases for damped systems. With the modal parameters it is possible to replace the coupled dynamic equations of the systems by decoupled equations. Then the transfer functions can be expressed analytically as the sum of the contributing modes.

It will be shown in chapter 4 that the nonlinearities of the vehicle-track system can not be neglected. The application of the linear modal analysis to this problem is therefore not possible. However, with the concept of nonlinear normal modes presented in the following section some principles of the modal analysis can be assigned to nonlinear systems.

Nonlinear case For nonlinear systems the previously described properties do not hold. Transfer functions and modal parameters now depend on the excitation level and the principle of superposition does not apply. This limits the application of modal analysis to linear systems. However, approaches using the principles of modal analysis for nonlinear systems have been developed.

One is the quasi-linearization of the system by considering a constant excitation level. Then a local modal analysis for this excitation level can be performed using all linear properties. Evidently, the identified modal parameters are only valid for the chosen excitation. For the vehicle-track system this approach would require a constant vehicle speed and track excitation level. It could therefore be used for vehicle tests on a test rig with constant

speed. In this work inline measurements will be used for the identification. Since the speed and the excitation are varying, this approach is unadapted.

Schmidt-Fellner [85] describes an approach for the identification of parameters of nonlinear coupling elements based on transfer functions. It is assumed that the system is composed by linear subsystems connected by nonlinear coupling elements. Each subsystem is described by a linear differential equation system. The nonlinear coupling elements are taken into account as external forces on the subsystems. The coupling parameters are identified by minimizing the misfit function which is defined as the distance between measured and simulated transfer functions.

The same approach is used by the identification through feedback of the output methods (NIFO). Nonlinearities are considered as unmeasured internal forces that act on the underlying linear system together with the measured inputs.

Nonlinear normal modes The principle of normal modes for undamped linear systems has been transferred to nonlinear systems ([72], [51], [73]). The nonlinear normal modes (NNM) have a conceptual relation to linear modal modes even though their properties differ significantly. One difference arises from the frequency-energy dependency of nonlinear systems described before. This prevents a separation between space and time in the governing equations. In [72] the principle of nonlinear normal modes is applied to the modal analysis of nonlinear structures. A main task of his work is the extraction of nonlinear normal modes (NNM) from experimental data.

Nonlinear normal modes can be represented in different ways. In the phase plot the velocity is plotted as a function of the displacement for a degree of freedom. While for a linear system this plot shows a circular form the phase plot of a nonlinear system is deformed. In a similar way the displacements of two degrees of freedom can be plotted. Due to the nonlinear relations between the degrees of freedom curved lines are obtained. They illustrate well that the concept of orthogonality of modes is not valid for nonlinear systems. A representation proposed in [72] is the frequency-energy plot. The eigenfrequencies of the modes are shown as a function of energy brought into the system. Figure 1.10 shows an example of a frequency-energy plot for a 2dof oscillator. It is noticed that the modes behave linearly until a certain energy level is attained. Than the eigenfrequency of both modes increases.

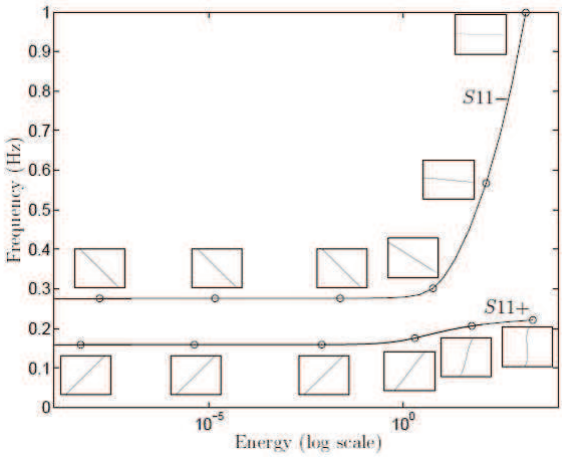

Figure 1.10: Frequency-energy plot of a system with two nonlinear normal modes (from [72])

Beside the frequency-energy dependency mentioned before nonlinear normal modes have other properties which distinguish them from linear modes. One is the modal interaction. Internal resonances in the system lead to an energy transfer from the excited mode to other nonlinear modes. The eigenfrequency of these modes can be very different from the excitation frequency. This coupling explains why even if the system is exited with only one frequency several frequencies can appear in the response spectra. A consequence and further property of nonlinear normal modes is that their number can exceed the number of degrees of freedom of the system. For linear systems this is not possible.

Excitations types The results which can be obtained from modal analysis depend on the excitation signals used. Originally, the modal analysis has been developed for test rig measurements with well-defined excitations. These excitations are applied artificially by a shaker or a similar device and are chosen according to the demand of the analysis.

The most exact results are received if the measurements are repeated a large number of times for a harmonic excitation signal with increasing frequency (stepped or swept sine excitation in [35] and [26]). In this way only the modes which are in resonance at the actual frequency are excited. The modal parameters can be extracted with a good precision. Since nonlinear effects can

not cancel due to averaging the sine stepped is used for the detection of nonlinear behaviour. P. Verboven [104] uses the multi-sine excitations for the detection, qualification and quantification of nonlinear distortions in FRF measurements.

Disadvantageous are the high costs since the measurement has to be repeated for each discretization step of the frequency. By using a white noise excitation all modes are excited uniformly since the amount of energy going into the system is uniformly distributed over frequency. Broad band excitation reduces significantly the cost but can lead to difficulties in the extraction of the model parameters if the modal density is high and the responses of several modes overlaid. Besides, random excitation is exposed to leakage since the signal is not periodic within the observation time window. Broadband excitation results in a linearized estimate of the system since nonlinear effects different in every time section tend to chancel due to averaging.

For the vehicle-track system, measurements in a test rig with a well defined excitation signal can not be performed. Instead, the measurements are performed during operation and the excitation signal is caused by the track irregularities. It is therefore neither a signal with only one frequency nor a fully random white noise signal. From spectral analysis it is found that the frequency content of the track excitations is distributed non-uniformly in the frequency domain of interest. In consideration of these difficulties, modal analysis techniques for operational modal analysis have been developed. They take into account complex excitation signals or even the case that excitation signals are not known at all. Another characteristic of the real track excitation is the presence of multiple excitations which are correlated to each other. This is due to the wheelsets running of the irregularities at a defined distance. In order to calculate the transfer function between one force and response correctly the simultaneous force signals have to be uncorrelated.

Considering these properties of the vehicle-track system, several difficulties become obvious when applying modal analysis: first the measurements are not performed in a test rig under well-defined conditions and the track excitation represents a not fully random non-stationary signal. Secondly nonlinearities exist in the system. For nonlinear systems, transfer functions and modal parameters depend on the excitation making basic concept of classical modal analysis invalid. Finally, the train is exposed to multiple correlated excitation forces perturbing the transfer function computation.

New concepts allowing to apply modal analysis for nonlinear systems and in-operation structures have been developed but are often restricted in their applicability. Gontier [28] uses an energetic criterion for quantifying the contribution of modes in the framework of a stochastic modal analysis. Industrial applications for modal testing of structures under operational conditions are described in [36]. In general, operational modal analysis is often limited to cases where the excitation can be described by stationary white-noise signals thus assuming all modes are excited uniformly.

Conclusion: application of the structural model updating method Based on the properties of the presented identification methods, the choice for the application on the vehicle-track system is made. Taking into account the nonlinearities and the measurement data received from operational measurements, the structural modal updating based on the direct usage of time responses seems to be most suitable.

A comprehensive introduction to the identification of parametric models is given in [99]. It describes the different steps of the parameter identification procedure aiming to answer the following questions: which criterion is used for the misfit function describing the difference between model and measurement? Which parameters are considered in the optimization process? Which parametric optimization method is used for the minimization of the misfit function?

In the following section these questions are discussed and the different steps of the structural model updating outlined.

1.2.2 The procedure for the parameter identification using the structural model updating method

The aim of this section is to propose a survey over the methods used for the different steps of the structural model updating

1.2.2.1 Misfit function criteria

The distance between measurements and model results is described by a misfit function defined in the time domain. Depending on the norm used and the available knowledge on the noise corrupting the measurement data different definitions of the misfit function can be used.

- Least square criterion

Most commonly quadratic misfit functions based on least squares are used. For every time step the error vector $e(p,t)$ between model and measurement is computed $e(p,t) = x_{meas}(t) - x_{model}(t,p)$. Using the square of the L_2 norm and a weighting matrix W the cost function value is calculated and integrated over the time length T

$$J_{ls}(p) = \int_0^T e^T(p,t) W e(p,t) dt \tag{1.7}$$

W is a weighting matrix defining the relative importance of the different measurement channels on the cost function. If W is chosen diagonal the cost function can be written as a sum over the channels k and time steps t_l:

$$J_{ls}(p) = \frac{1}{N} \sum_k \sum_l w_{lk} [x_{meask}(t_l) - x_{modelk}(t_l,p)]^2 \tag{1.8}$$

The weighting can be used to normalize the cost function by choosing $w_{lk} = [x_{meask}(t_l)]^{-2}$ or to reduce the effect of measurement noise by using the result of the Maximum likelihood criterion described below.

- Least modulus criterion

  Another criterion is the least modulus based on the absolute value norm L_1. This criterion lays less importance to large errors between measured and simulated results.

$$J_{ls}(p) = \frac{1}{N} \sum_k \sum_l w_{lk} |x_{meask}(t_l) - x_{modelk}(t_l,p)| \tag{1.9}$$

  In the same way as for the least square criterion weighting factors can be used. $w_{lk} = 1/|x_{meask}(t_l)|$ leads to relative errors. One disadvantage of the least modulus criterion is the non-differentiability preventing the use of series expansions for the cost function.

- Maximum likelihood criterion

  If the measurement data are corrupted by noise more sophisticated cost functions can be defined. They are based on the maximum likelihood method and take into account the measurement noise. In [99] a comprehensive introduction to this method can be found.

The maximum-likelihood estimate maximizes the misfit function:

$$j_{ml}(p) = \pi_x(x^s|p) \tag{1.10}$$

Normally the term $\pi_x(x^s|p)$ describes the probability density of the random vector generated by a model with the parameters p. When used as an optimization criterion, the vector x^s is fixed and describes the measured response while p are the unknown parameters. $\pi_x(x^s|p)$ therefore becomes a function of the parameters p. The maximum likelihood method is based on the maximisation of this likelihood function with respect to the parameters p taking into account measurement noise. Consequently, if prior information on the measurement noise is available it can be considered in the cost function criterion definition.

In the case of a Gaussian noise with known variance the misfit function criterion is obtained from the maximum likelihood method. It is assumed that the measurement data $x(t_i)$ satisfies:

$$x(t_i) = x_m(t_i, p*) + \epsilon_i \tag{1.11}$$

In this formulation the vector $x_m(t_i, p*)$ describes the model result for the true parameter values $p*$. ϵ represents the measurement noise with known variance σ. Based on the assumption that the noise ϵ_i has a Gaussian distribution, its probability density function is described by:

$$\pi_{\epsilon_i}(\epsilon_i) = (2\pi\sigma_i^2)^{-0.5} \exp[-\frac{1}{2}(\frac{\epsilon_i}{\sigma_i})^2] \tag{1.12}$$

Assuming that the difference between the model and the measurements is only given by the Gaussian noise ϵ the likelihood simplifies to the density function of ϵ. Its maximization results in the misfit function:

$$J_{ls}(p) = \frac{1}{2}\sum_{i=1}^{n_t}[\frac{x(t_i) - x_m(t_i, p)}{\sigma_i}]^2 \tag{1.13}$$

This results corresponds to the misfit function obtained from the least square criterion with a weighting factor $w_i = 1/\sigma_i^2$. The weighting factor defined at each time step t_i for a channel is given by the inverse of the noise variance. This has the effect that the influence on the misfit function is reduced when the measurement is corrupted by noise.

- Method based on correlation

  If the measurement signals are corrupted by noise, correlation based misfit function criteria are suitable. In his work Hu [39] has applied this approach to nonlinear systems. It is based on the observation that the noise signals do not correlate after a short time while the vehicle response signals are correlated.

  The least square method minimizes the sum of all modelling errors $e(p,t)$ which is equivalent to the minimization of the trace of the correlation matrix $R_e(\tau)$ for $\tau = 0$.

$$J(p) = E[\mathbf{e}^T(t)\mathbf{e}(t)] = trace[R_e(0)] \tag{1.14}$$

  The result of the minimization is corrupted by the noise contained in the error signal $e(p,t)$. By taking advantage of the fact that the noise is not correlated after a short time the bias error due to noise can be reduced if the correlation matrix for $\tau \neq 0$ is used:

$$J(p) = E[\mathbf{e}^T(t+\tau)\mathbf{e}(t)] = trace[R_e(\tau)] \tag{1.15}$$

  The difficulty is to find a τ for which the noise is uncorrelated while the response signals are still correlated.

  An important requirement for the application of this method is that the excitation of the system is described by a stationary stochastic signal. As outlined in this work this is not the case for real track excitation signals. High frequency noise in the acceleration signals is removed due to the low pass-filtering at maximal 20Hz.

1.2.2.2 Regularization

The identification of the model parameters from the measured response requires the solution of an inverse problem. In general, the correct result can only be obtained if the problem is well-posed. A well-posed problem is a problem for which a solution exists which is unique and depends continuously on the data.

The existence of several solutions requires the choice of one solution using additional information. More problematically is the loss of continuity. If the solution does not depend continuously on the data even a small error in the

measured response can have a large effect on the solution. These characteristics of inverse problems are outlined in [48] and [49]

The regularization of an ill-posed inverse problem allows to obtain a well-posed problem. By adding a regularization term to the misfit function one aims to assure a unique and continuous solution to the problem. In return a bias is introduced. This error is accepted when it allows the convergence to a solution.

Tikhonov regularization A well-known regularization method is the Tikhonov regularization. It is based on the introduction of a penalty term using a priori information of the parameter values p:

$$J_{ls}(p) = \frac{1}{2}\int_0^T \|x_{meas}(t) - x_{model}(t,p)\|^2 dt + \frac{1}{2}\alpha\|p - p*\|^2 \qquad (1.16)$$

where α is the regularization parameter. The idea is that the penalty term will attract the parameter values towards a reasonable region of the parameter space defined by the a priori parameter estimation $p*$. This problem assures a unique solution. Studies and application of the Thikhonov regularization are numerous in literature. In [49] and [42] an introduction to the Tikhonov regularization is given. [17] studies the convergence rates for the Tikhonov regularization. Depending on the noise in the measured data convergence rates for the regularized solution are defined.

The accurate choice of the regularization parameter α is a crucial step when applying the Tikhonov regularization. Evidently, if it is chosen too small the regularization has no influence on the solution and the inverse problem remains ill-posed. Too important values will force the parameter to converge to the initial estimation $p*$. The parameters can not converge to the optimal solution and the optimization then becomes useless. The aim is therefore to find a compromise between a stable convergence and a bias which is as small as possible. An approach for the choice of the regularization parameter is to take the measurement noise into account.

Morozov discrepancy principle In order to choose the regularization parameter α the Morozov's discrepancy principle [2], [49] is used in this work. The discrepancy principle is based on the assumption that the measurement data are corrupted by noise. Even if the model represents perfectly

the real system an error persists due to the measurement noise. It is therefore reasonable to choose a regularization factor which causes a bias of the same dimension as the measurement noise without losing the precision of the solution. With x the ideal response and x^δ the available noisy data the noise level is defined as:

$$\|x - x^\delta\| \leq \delta \tag{1.17}$$

The condition for the choice of the regularization parameter is therefore given by a constraint on the result of the minimization:

$$\|x_{model}(p_{opt}(\alpha)) - x^\delta\| = \delta \tag{1.18}$$

$p_{opt}(\alpha)$ is the parameter vector obtained from the minimization of the misfit function with α as regularization parameter.

The determination of the regularization factor α requires therefore the computation of the root for the nonlinear problem:

$$\|x_{model}(p_{opt}(\alpha)) - x^\delta\| - \delta = 0 \tag{1.19}$$

If the model can be described by a linear equation system of the form $Ax = y$ an analytical solution can be found. For the nonlinear equation system the root is determined numerically.

1.2.2.3 Detection of identifiable parameters from sensitivity analysis

Before choosing the parameters for the identification process an important question has to be considered: Which parameters are identifiable from the available measurement data. In [99] identifiability is defined for the idealized case that the model and the real system have an identical structure and that the measurement is noise free. In this case the model is able to reproduce exactly the measurements if the true parameter values are chosen for the model parameters. *Structural global identifiability* is fulfilled under the condition that the identical input-output behaviour implies the same parameters values for the model and the system:

$$M(p_{model}) = M(p_{true}) \Rightarrow p_{model,i} = p_{true,i} \tag{1.20}$$

If this is valid only around a neighbourhood of p_{true} *structural local identifiability* is fulfilled. In the case that several parameter vectors lead to the same

input-output behaviour of the model, they are not structurally identifiable.

From literature [99] and [100] several methods for testing the identifiability of parameters are available. Some apply only to time-invariant linear models represented by state-space models while others can be used for non-linear models also. However, all methods are based on the analytical equation system of the model. If the model equations are not available or the system is too complex the identifiability of the parameters is studied using a sensitivity analysis. It is based on a simple principle: the evaluation of the system is repeated for different values of one or several parameters and the influence on the system response is compared. Parameters which have an influence on the response are identifiable.

It is distinguished between deterministic local methods and probabilistic global methods.

1.2.2.3.1 The screening method The factor screening method is a deterministic method where only one parameter varies while the others are held constant as illustrated in figure 1.11. The variation is performed between the minimal and the maximal value of the tolerance. This approach allows to calculate the influence of one parameter on the misfit function. Its advantage is the easy graphical representation of the solution surface of the misfit function.

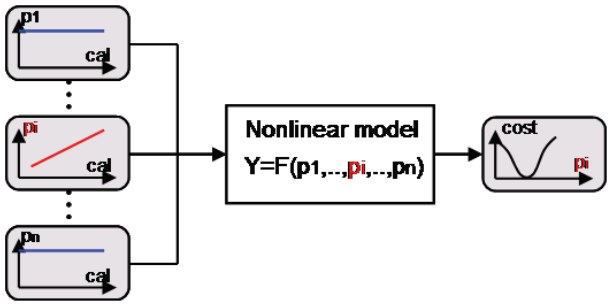

Figure 1.11: Screening method: the parameter p_i is varied while the others are held constant (cal: number of calculations)

However, the sensitivity obtained from the deterministic screening approach has several drawbacks. The influence of a parameter on the misfit function does not only depend on the gradient obtained above but also on the variability of the parameter. In order to consider the variability of the parameter

values the sensitivity analysis has to be based on the variances.

Besides, the screening method can not take into account interactions between more than two parameters on the misfit function. These interactions are important for systems that are nonlinear in their parameters. Then the superposition principle is not fulfilled and the effect of changing several parameter values simultaneously is different from the sum of their individual effects. Evidently, the sensitivity obtained from the screening method is only valid for one parameter set with fixed values.

1.2.2.3.2 Consideration of nonlinear coupling by the use of global methods In order to overcome these limitations, probabilistic global methods have been developed. These methods take into account the parameter variances and the interactions. They allow all input parameters to vary simultaneously by treating the input parameters as random variables with assumed probability density distributions. Then a Monte-Carlo calculation is performed on the multi-body model. As a result the probability density distribution of the misfit function is received. The principle is illustrated in figure 1.12.

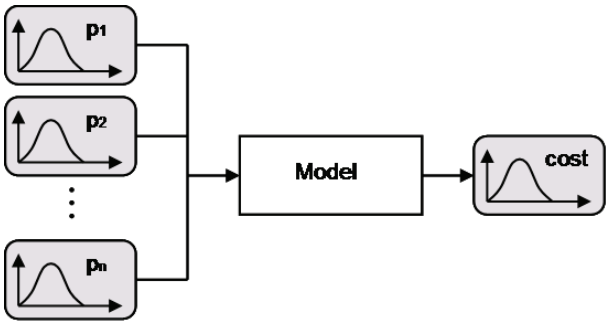

Figure 1.12: Principle of global optimization: the input parameters are given as probability density functions. As a result the probability density function of the misfit function is obtained

As inputs the global methods require the probability density functions of each parameter. For the suspension parameters their determination represents a difficulty. Ideally the parameter has been measured for many suspension elements of the same type allowing to determine the probability density function from a statistical analysis. For the TGV suspension elements these

measurements are not available and the probability density functions have to be estimated. Under the assumption that the variability of the suspension parameters is caused by a large number of independent random effects the central limit theorem holds and Gaussian distributions are chosen. The mean value and the variance of the distribution are based on the nominal values and tolerances specified by the manufacturers.

Another difficulty with global methods is their enormous computational cost due to the probabilistic operators which require a large number of model evaluations. Efforts have been undertaken to develop global methods demanding less computational cost. One result is the Morris method presented in the following section.

Morris method The Morris method is a one-factor-at-a-time method which can take into account nonlinear interactions between the parameters. The method proposes two measures: one which represents the overall effect of the parameter and another estimating the second-and higher order effects of the parameter.

The basic idea of the Morris method is to repeat a local one-factor-at-a-time method several times for randomly chosen data sets. This allows to take into account the interactions between the parameters. As described before, the one-factor-at-a-time method describes the influence of one parameter on the misfit function J when the others are fixed. The gradient of J with respect to p_i is therefore:

$$\nabla_{p_i} J = \frac{J(p_1, ..., p_{i-1}, p_i + \Delta p, p_{i+1}), ..., p_n) - J(\mathbf{p})}{\Delta p} \tag{1.21}$$

This calculation is repeated for randomly chosen samples of the parameter set $\mathbf{p}$ giving a distribution of elementary effects for each parameter. The average of this distribution describes the overall effect of the parameter and the standard deviation the interaction between the parameters. A high value of the standard deviation means that the elementary effect of the parameter depends strongly on the values of the other parameters. If the interaction is low the elementary effect is not influenced by the other parameters and the standard deviation is small.

The cost needed for the computation of the sensitivity is an important criterion. Basically, if r samples are calculated for a set of n parameters the number of misfit function evaluations is $eval = 2nr$. Morris proposes an

approach which reduces the computational cost.

The samples of the parameter vector are constructed outgoing from an initial vector. The following samples are obtained by changing only one component with respect to the previous vector. The component is randomly selected among all parameters apart the ones which have been varied before. Therefore two consecutive samples differ only in one component and each component has been varied at least once. The parameters are varied using a small number of values which are chosen within the range of tolerance. Figure 1.13 illustrates the sampling procedure for the case of two parameters (k=2) and 5 value levels (p=5). The sampling procedure is repeated 4 times (r=4).

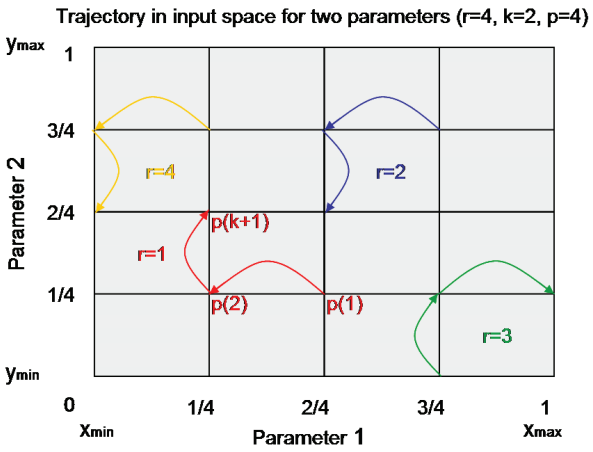

Figure 1.13: Sampling for Morris method with two parameters x and y (k=2, p=5, r=4)

For more details it is referred to [82].

Variance-based methods The Morris method presented in the previous section has the main advantage of low computational cost. The required number of model evaluations is low. In return, its precision is less high. The Morris method provides a sensitivity measure which tends to be qualitative. If the exact quantitative effect of each parameter on the misfit function is of interest variance-based methods have to be used. Their main disadvantage is the enormous computational cost.

Variance-based methods use Monte-Carlo calculations with probability density functions as inputs and outputs. If all parameters are left free to vary

over their range of tolerance the unconditional variance $V(J)$ of the misfit function is obtained. Then, by fixing one parameter to its true value and performing the Monte-Carlo computation the reduction of the misfit function variance due to the fixed parameter is received. This Monte-Carlo calculation is repeated n times where n is the number of parameters. In each calculation one parameter is fixed. Now importance factors can be defined which take into account the nonlinear interactions between the parameters. The approach is illustrated in figure 1.14.

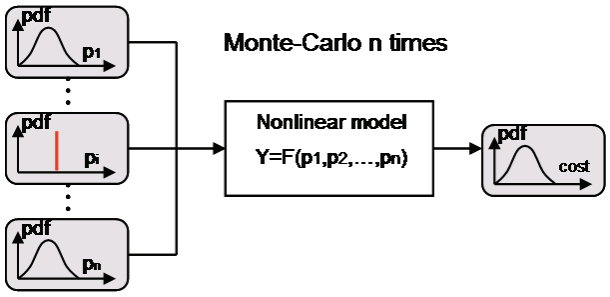

Figure 1.14: Probabilistic sensitivity analysis considering nonlinear interactions

The result received for each calculation is the variance of the misfit function under the condition that p_i is fixed at its true value p_i^*:

$$V(J|p_i = p_i^*) \tag{1.22}$$

If a simulation and not the real measurements are used as reference in the misfit function, the true parameter values are known and the conditioned variance from equation (1.22) can be used directly. If instead real measurements are used the true values p^* are not known. In this case it is required to average the conditioned variance $V(J|p_i = p_i^*)$ over all possible values of p_i giving the mean value of the variance:

$$E(V(J|p_i)) \tag{1.23}$$

Due to the relation:

$$V(J) = E(V(J|p_i)) + V(E(J|p_i)) \tag{1.24}$$

it is possible to use the variance of the mean value of the misfit function V_i as a measure for the importance of the parameter p_i. The importance factor becomes:

$$S_i = \frac{V_i}{V(J)} = \frac{V(E(J|p_i))}{V(J)} \tag{1.25}$$

This importance measure is called first order effect. It represents the effect of one parameter in a decomposition of the misfit function variance:

$$V(J) = \underbrace{\sum V_i}_{\text{First order effect}} + \sum_i \sum_{j>i} V_{ij} + ... + V_{1,2,...,k} \tag{1.26}$$

By dividing the equation with $V(J)$ the sensitivity indices are obtained as:

$$\sum_i S_i + \sum_i \sum_{j>i} S_{ij} + ... + S_{1,2,...,k} = 1 \tag{1.27}$$

Interactions are described by higher order effects on the misfit function variance. The effect of the interaction between two parameters p_i and p_j on the misfit function is given by:

$$V_{ij} = V(E(J|p_i, p_j)) - V(E(J|p_i)) - V(E(J|p_j)) \tag{1.28}$$

The term $V(E(J|p_i, p_j))$ represents the joint effect between the parameters p_i and p_j by fixing both parameters in the Monte-Carlo calculation. By subtracting the first-order effects of each parameter from the joint effect the so called second order effect is obtained. Consequently, third-and higher-order effects are evaluated by fixing three parameters and more.

An important drawback of the variance-based sensitivity analysis is the enormous computational cost. Therefore different estimates of the $V(E(J|p_i))$ calculation have been developed. One of them is the Sobol method which can be found in [82].

For the approaches presented above another simplifying assumption is made. It is assumed that the parameter values are not correlated. For each computation step of the Monte-Carlo simulation the parameter values are chosen by a probabilistic operator according to their probability density distribution. A possible correlation between the parameter values is not taken into account. In [105] the effect of correlated parameters on the sensitivity analysis is studied.

Correlation between parameters If available, correlation between parameter values as shown in figure 1.15 can be obtained from statistical analysis of measurements or from physical and technical considerations. For the

TGV, correlation measurements are not available. From the technical point of view the assumption of independence is justifiable. Variabilities in the suspension parameters will mainly depend on production or weather condition but less on other parameter values. However, interactions between different elements leading to a correlation of the parameter values can not be excluded either. In this works a determination of these interactions is not possible.

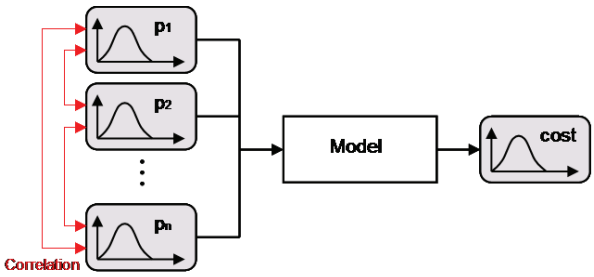

Figure 1.15: Probabilistic sensitivity analysis

1.2.2.4 Minimization of the misfit function

Local versus global methods When the misfit function is defined and the identifiable parameters found one can turn toward the solution of the inverse problem. By minimizing the misfit function one aims to identify the parameter values for which the model reproduces best the measured system response. The misfit function is minimized using an optimization method. In literature the optimization methods are numerous. It can be distinguished between local deterministic methods and global methods based on probabilistic operators. Local methods can be further classified in direct methods which only use the misfit function and gradient methods. Gradient methods seek the minimum of the misfit function by use of the gradient.

The choice of a suitable optimization method depends on the properties of the system and the model. Important properties are the number of parameters and the form of the solution surface of the misfit function which might have one or several minima. If the misfit function has only one minimum or if it can be assumed that the starting point is situated in the attractor region of the global minimum, local optimization methods are the suitable choice. Due to their deterministic operator the convergence to the minimum is guaranteed. Instead, if the misfit function has several minima local methods converge to the closest local minimum. They are not able to leave it in

order to find a better minimum.

Therefore, if several local minima exist global optimization methods have to be used. Thanks to their probabilistic operators they can leave a local minimum. One of their drawbacks is the calculation cost due to the large number of iterations needed. Besides, the convergence to the global minimum is not guaranteed and no well defined convergence criterion exists. Syrjakow [94] therefore proposes the combination of a global and a local optimization method. The same approach is pursued by Ismael [40] who combines a heuristic global method (particle swarm) with the pattern search method for local optimization. This new designed particle swarm pattern search solver has been compared to other global optimization methods and showed good features. Among the large amount of references on optimization methods, the general introductions of Geiger [21] and Nocedal [69] are recommended.

Gradient calculation For some optimization methods the cost increases significantly with the number of parameters. Others are less dependent. If gradient-based optimization methods are used, the calculation of the gradient causes most of the computational cost. The chosen technique for gradient calculation therefore plays an important role. Finite differences offer a simple approach but become very costly if the number of parameters increases.

An analytic calculation of the gradient from adjoint equations reduces the cost. A comprehensive introduction can be found in the inverse engineering handbook [102]. In [23], [14], [21], [76], [71], [1] and [60] the construction and application of adjoint states on optimization problems is outlined. Martins [60] uses adjoint states for an airfoil shape optimization problem characterized by a large amount of parameters and complex system equations. The adjoint approach allows to compute the gradient of the misfit function at the cost of an equivalent flow solution. In [71] the adjoint state approach is used for the computation of the second order sensitivities of the objective function in an viscous flow problem. The second order sensitivities are needed in the Hessian matrix used in the Newton optimization method. By using an adjoint approach the computation of the Hessian matrix requires the solution of N+1 flow system solutions for N design parameters.

The use of the adjoint approach for models solved with Runge-Kutta schemes is treated in [1]. The adjoint solution of a nonlinear model depends on the direct model response. Since the adjoint model is integrated backwards in

time the computation of the direct response has to be performed before. In order to obtain high accurate adjoint solutions an interpolation of the forward model response is needed. Protas [76] deals with the regularization of adjoint analysis.

In the references named above the adjoint state approach is used in the field of flow mechanics. Applications of the adjoint method to multibody problems are less numerous in literature. Ding [16] computes the first- and second-order derivatives of a misfit function for a multibody model. The results are compared and validated with the direct computations of the derivatives. In his work Sandel [84] uses the adjoint method for the sensitivity analysis of a simple multi-body model. He shows the good performance of the adjoint method in the case of a large number of constructive parameters. The non-linearity of the multibody model is taken into account.

The automatic/algorithmic differentiation of differential equation systems is another interesting approach for the gradient calculation. In the book of Griewank [31] its principles and practical implementation are treated comprehensively.

Noise and other sources of error can significantly alter the parameter identification results. Approaches to analyze the uncertainty attached to the results are summarized in [99]. Measurement noise is an important error source. Depending on if the noise variance is known or not different approaches for the calculation of confidence region of the identified parameters are available. Beside, other error sources specific to the studied identification problem have to be considered. The lack of information about the measurement setup or unknown excitations has to be mentioned in this context.

In the following sections some relevant methods are presented.

1.2.2.4.1 Application of local methods Since local methods are based on deterministic algorithms using the misfit function and its derivatives they show generally a faster convergence than global methods. When possible they should be preferred. The requirement is however, that the misfit function is convex or that the starting point is assumed to be situated in the attractor region of the global minimum (figure 1.16) .

A method which only uses the misfit function is called direct method. A widely used method is the pattern search method introduced in the following

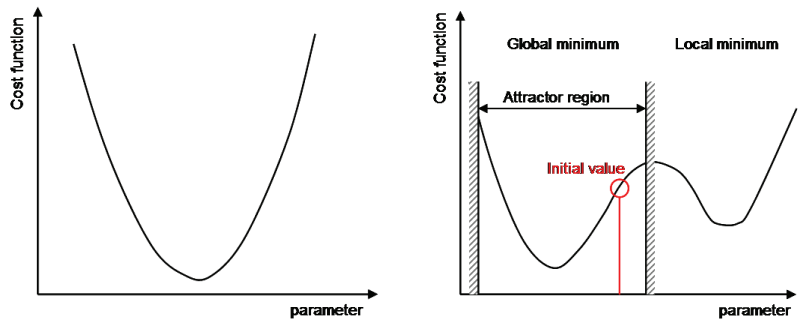

(a) (b)

Figure 1.16: Misfit function: convex solution surface (a), solution surface with local and global minima (b)

section. Gradient methods instead, according to their name, require also the gradient of the misfit function. They get by with a lower number of function evaluations but require the calculation of the gradient.

The pattern search method The pattern search method is based on the principle of slightly varying the parameters at every step until a smaller value of the misfit function has been found. The method stands out due to its good convergence properties, low memory demand and a simple algorithmic structure. The pattern search method is outlined in the work of Lewis [58].

In order to initialize the algorithm, initial parameter values, initial step sizes and a tolerance ϵ are chosen. The optimization is based on two types of steps: first, each parameter is varied with a defined stepsize h_i and the misfit function values are compared. If a reduction of the misfit function is found for a step an extrapolation in the direction v_i of this step is performed. This allows to choose a suitable step length. The combination of these two types of steps leads to a fast convergence.

The step size h_i and the direction vector v_i are adapted to the misfit function during the minimization process. However, the convergence speed depends strongly on the choice of the initial step length which should be adapted to the problem. If the initial step length is chosen too small many iterations are needed in order to increase them. Besides, too small step sizes can cause problems if the misfit function surface is perturbated forming a solution surface with many local minima.

1.2.2.4.2 Application of gradient methods A faster convergence is obtained if information about the derivatives of the misfit function is used. This is the main feature of gradient methods. They use the gradient and optionally the Hessian matrix of the misfit function for the determination of the search direction. A detailed introduction to these methods can be found in the books of Nocedal [69] and Geiger [21].

In general two groups of gradient methods can be distinguished: line search methods and trust region methods. Line search methods require two computational steps. In a first step the search direction in which the misfit function decreases is determined. Then a unidimensional minimization is performed along this direction. Trust region methods are based on the definition of a trust region around the actual parameter value in which the misfit function can be approximated by a quadratic function. Then the minimum in this region is sought. Trust region methods thus require the solution of a quadratic optimization problem with constraints. In return, a method for the choice of the step length is not necessary.

In table 1.1 an overview of the different gradient optimization methods is given.

The steepest descent method is the simplest approach. It is based on a first order expansion of the misfit function gradient. Basically, the search direction is simply chosen as the opposite direction of the maximal slope or gradient respectively. For the choice of the step length different approaches can be considered. The simplest one, a constant step length, is not suitable. A small step length leads to a very slow convergence while for large step lengths the first-order approximation is no longer valid. Instead a unidimensional optimization is performed in the search direction in order to identify the step-length.

The Newton method implemented in the Matlab function *fmincon* minimizes a quadratic approximation of the misfit function $m(d_k)$. The search direction is given by the first and second-order derivatives. The Newton method requires the calculation of the Hessian matrix which can be computationally expensive. This can be avoided if a specific estimation of the Hessian matrix is used such as the one implemented in the Quasi-Newton method.

Gradient methods	
Method	Description
Steepest descent method	For the line search direction the negative gradient value is used: $$d_k = -\nabla J_k / ||J_k|| \quad (1.29)$$ Unidimensional minimization in line direction
Newton	Minimization of quadratic approximation of the misfit function $$m(d_k) = J(p_k) + d_k^T \nabla J(p_k) + \frac{1}{2} d_k^T \nabla^2 J(p_k) d_k \quad (1.30)$$ with line search direction: $$\nabla m(d_k) = \nabla J(p_k) + \nabla^2 J(p_k) d_k = 0 \quad (1.31)$$ $$d_k = -(\nabla^2 J(p_k))^{-1} \nabla J(p_k) \quad (1.32)$$
Quasi Newton	For the calculation of the line search direction an estimation is used for the Hessian matrix: $$d_k = -B_k^{-1} \nabla J(p_k) \quad (1.33)$$ BFGS is a common method for the estimation of B_k.
Nonlinear conjugate gradient methods	For the line search direction the conjugate direction is used: $$d_k = -\nabla J(p_k) + \beta_n d_{k-1} \quad (1.34)$$ Unidimensional minimization in search direction. Different formulas for β_n are available: Fletcher-Reeves: $$\beta_n = \frac{(-\nabla J(p_k))^T (-\nabla J(p_k))}{(-\nabla J(p_{k-1}))^T (-\nabla J(p_{k-1}))} \quad (1.35)$$
Levenberg-Marquardt	The method is based on Newton and uses a Tikhonov regularisation. $$d_k = -[\nabla^2 J(p_0)^T \nabla^2 J(p_0) + \nu I]^{-1} \nabla^2 J(p_0)^T \nabla J(p_0) \quad (1.36)$$
Trust Region	Quadratic approximation m of J in trust region. Acceptance criteria for trust region radius r_k: $$\rho_k = \frac{J(p_k) - J(p_k + d_k)}{m(0) - m(d_k)} \simeq 1 \quad (1.37)$$ and optimization : $$min\ m_k(d_k) = J(p_k) + \nabla J(p_k) d_k + \frac{1}{2} d_k^T B_k d_k \quad ||d_k|| \leq r_k \quad (1.38)$$

Table 1.1: Gadient methods

1.2.2.4.3 Methods for the calculation of the gradient The gradient methods require the computation of the first- and eventually second-order derivatives of the misfit function relative to the design parameters. For a complex system with a large number of parameters as the one considered in this work, the gradient computation can represent the most expensive step in the optimization algorithm. The choice of an adapted method for the computation of the gradient is therefore crucial and will be outlined in this section.

Evidently, a simple but rarely the best way of obtaining approximated numerical values of the misfit function gradient is the finite differences method. For the parameter value p the gradient is estimated by evaluating the misfit function at one or two other points aside. In equation (1.39) the misfit function values at p and $p + h$ are used:

$$D_{+h}J(p) = \frac{J(p+h) - J(p)}{h} \tag{1.39}$$

For a large number of parameters this method is very costly. Besides, the choice of the steplength h is difficult. If h is too large, then truncation errors become significant. Even if h is optimally chosen, the derivative of the misfit function J will be accurate to only about 1/2 or 2/3 of the significant digits of J.

Therefore alternative computation methods have been studied. If the differential equations describing the system are available, analytical approaches can be used. For simple linear-in-parameters systems the derivation of the dynamic equations relative to the parameters is straight forward. However, if the equations are complex and nonlinear in the parameters the analytical calculation of the gradient becomes a difficult task. From the literature survey on sensitivity analysis and parameter identification two analytical methods appear suitable: the adjoint state method which is in particular adapted to systems with a large number of parameters and the algorithmic differentiation method.

Gradient calculation from adjoint state approach The main advantage of the adjoint state method is that its complexity does not depend on the number of parameters. This makes it suitable for problems requiring the identification of a large number of design parameters. Typically these problems appear in flow mechanics where numerous applications were found in literature. The application to complex nonlinear multi-body model is still

at the beginning.

The aim of the adjoint method is to calculate the gradient of the misfit function $J(x(p), p)$ used in the optimization algorithm:

$$\nabla_{p_i} J(\mathbf{x}(\mathbf{p}), \mathbf{p}) = 0 \quad for\ i = 1...n \tag{1.40}$$

n: number of parameters

The misfit function depends directly on the parameters p_i and on the response $x(p)$ of the system. Therefore, the total derivative of the misfit function with respect to the parameters p_i gives:

$$\frac{dJ}{dp_i} = \frac{\partial J}{\partial p_i} + \frac{\partial J}{\partial x}\frac{dx}{dp_i} + \frac{\partial J}{\partial \dot{x}}\frac{d\dot{x}}{dp_i} \tag{1.41}$$

In this equation the derivative of the forward model response x with respect to the parameters are not known. The adjoint approach allows to eliminate these derivatives by using the Lagrangian equation given by the sum of the misfit function and the state equation times the adjoint state solution. If the stationary point of the Lagrangian equation is found one also obtains the minimum of the misfit function.

Gradient calculation from automatic differentiation (AD) From literature another interesting approach for the computation of the gradient is retained: the automatic differentiation. A detailed description of this method can be found in [31].

The code describing the equations of motion of the multibody model is rewritten as a sequence of basic operations. Then the gradient is calculated by applying the chain rule. Finally, AD gives a program code for the calculation of the gradient. It does not apply a symbolic expression for the gradient.

Several AD packages are available. Outgoing from the program code of the model they produce a transformed program that calculates the derivatives. The accuracy of the gradient satisfies the same accuracy as the response calculated from the original program. Generally, AD tools are able to transform even very complex program structures including loops. This is of importance for the multibody models used here which are solved by a numerical integration algorithm like the Runge-Kutta algorithm.

The principle of automatic differentiation is based on transforming the program in a sequence of basic operations resulting in an evaluation trace. First, the input variables are defined. Then the result of each basic operation is represented by an intermediate variable. Each intermediate variable is therefore simply calculated from previously defined variables by applying a basic operation.

Two different principles of automatic differentiation can be distinguished: the forward and the reverse mode.

The forward mode The forward mode calculates the derivatives of every intermediate variable relative to the input variables of interest by applying the chain rule. The derivatives are calculated together and in the same order as the values themselves. It should be pointed out that the symbolic expression of the gradient is never calculated. The numerical value of the derivative for each intermediate variable is calculated from the previously calculated numerical values.

The reverse mode The reverse mode starts with an output variable and calculates the derivative of that output variable with respect to all intermediate variables. The derivatives are therefore calculated backwards.

The transform of the underlying program into the transformed program providing the derivatives is automated in the automatic differentiation tools. In some cases it can however be necessary or advantageous to rewrite the underlying code before the application of an automatic differentiation tool.

1.2.2.4.4 Global methods For complex multibody systems the solution surface of the misfit function has several minima. The aim is therefore to identify the global minimum. The exclusive use of local methods is therefore unsuitable since the convergence to the global minimum is not guaranteed. Depending on the initial parameter values they converge to the closest local minimum.

In order to identify the global minimum of the misfit function global optimization methods have to be applied. They are able to leave the attractor region of a local minimum in order to converge to the global minimum of

the solution space. This capacity is achieved by a probabilistic operator. In the simulated annealing method ([94]) the probability for the acceptance of an increase of the misfit function values depends on a parameter called temperature. The method simulates the cooling process of a material and is presented in the following. Another widely-used approach are the genetic algorithms discussed in [63].

The capability to identify the global minimum comes along with several drawbacks which still constrain the use of global optimization methods. Due to the probabilistic operators a very large number of misfit function evaluations is necessary even for relatively small problems. This leads to the slow convergence of global algorithms especially when the algorithm has already approached the global optimum.

Besides, the global optimization algorithms do not guarantee the convergence to the global minimum. Only if the whole solution surface is exploited the identification of the global minimum is guaranteed. However, this is normally impossible to perform and heuristic methods are used. Consequently, it is not possible to define clear convergence and termination criteria for global algorithms. Depending on the choice of the control parameters suboptimal solutions can be obtained.

Simulated annealing The simulated annealing method reproduces the physical cooling process. The material is heated until it reaches the melting point. In this high-energy state the atoms are arbitrary distributed. Then the material is slowly cooled down with the aim to reach the state with the lowest energy corresponding to an ideal atomic structure. An important criterion is the gradient of the temperature reduction. If the material is cooled down too fast higher energetic states are obtained.

The basic principle of this cooling process has been transformed to the optimization problem. The different solutions of the misfit function correspond to the energy states of the material. The optimization problem is represented by the solution space of the parameter values and the misfit function. Important elements of the simulated annealing algorithm are the probabilistic generator which creates a new parameter set from the previous one, the loop for the temperature reduction and the maximal number of tries and successes within one temperature.

The calculation of a new parameter set from the previous one is performed by

a probabilistic generator. At each iteration only one parameter is changed. A value is obtained which lies in the tolerance defined initially. Then the misfit function value is compared to the previous one. If a reduction is obtained, the new parameter set is accepted. If the misfit function increases the new parameter set is accepted with a probability which depends on the temperature. This allows the algorithm to leave local minima.

At the beginning of the optimization high temperature values correspond to an important probability that increases in the misfit function are accepted. If instead the temperature is approaching zero the probability decreases exponentially and the algorithm behaves like a local method.

Consequently, the choice of the control parameters of the simulated annealing algorithm has an important effect on the results. If the temperature decreases too fast the algorithm can converge to a local minimum because the local search charateristics are emphasized. The choice of the temperature algorithm and the number of function evaluations for every temperature is difficult since standard adjustments of the control parameters are not known yet. In this work several adjustments have been tested and compared. In the work of Azizi [5] two approaches for the control of the temperature are presented. They are based on the number of consecutive improving moves and the adding of a tabu list.

Another difficulty which all global methods have in common is the choice of a termination condition. The temperature or the number of iterations without any improvement of the misfit function can be used.

Genetic Algorithms Genetic optimization methods are based on the principles of evolution. They belong to the probabilistic optimization methods and are suitable for complex optimization problems with many local minima. Like the simulated annealing algorithm they combine deterministic and probabilistic elements. A crucial difference to the simulated annealing method is that they provide not only one solution but a set of possible solutions. Referring to natural genetics this set of possible solutions is called population and every potential solution individual. In this application the individual is therefore represented by a suspension parameter set. The misfit function value for a parameter set is referred to as the fitness of the individual. It serves as the selection criterion in the evolution process.

The initial population is created outgoing from the initial parameter set. The initial parameters are varied in accordance with the defined value constraints and distributions using a probabilistic operator in order to obtain the individuals of the initial population. The number of individuals per population is a control parameter chosen by the user which has an important influence on the performance of the algorithm.

The creation of a new population from the previous one is based on the principles of evolution selection and recombination. Individuals with a better fitness show a higher probability to be selected. These individuals might then be modified due to crossover and mutation. Crossover combines the properties of two parent individuals hence in this application the creation of a new parameter set from two previous parameter sets. Mutation describes the probabilistic modification of one parameter set. The probability for a mutation is defined by the mutation rate another important control parameter. This process is repeated according to the defined number of generations.

The consideration of a large number of possible solutions in parallel combined with probabilistic operators taking into account the performance of each solution is the main advantage of genetic algorithms. They can be used for complex optimization problems with many local minima and are therefore of large interest for the application to the parameters identification discussed here. However, despite these advantages the genetic algorithm is exposed to the same conflict of objectives as the simulated annealing method described in the previous section: the exploiting of the best solution with low computational cost on the one hand and exploring the search space on the other hand. The size of the population and the evolutionary pressure allow the user to control the importance of these conflicting objectives. The right choice giving the best balance between exploration and exploitation of the search space depends on the optimization problems and is the main difficulty for the application of genetic algorithms.

An unsuitable choice of the control parameters can provoke the convergence to a local minimum. This is the case when the selective pressure is chosen too high. Instead, a large population diversity emphasizes the exploitation of the search space but might make the algorithm ineffective and costly.

A detailed description of the genetic algorithm, application examples and strategies to prevent premature convergence can be found in the book of Michalewicz [63].

1.2.2.4.5 Combined global-local method: combination between simulated annealing and pattern search The literature survey on the application of the simulated annealing method has revealed several drawbacks. One is the large number of function evaluations needed. Especially close to the minimum the convergence speed is very slow. Besides, the definition of termination criteria is difficult leading to large variations in the performance. Global optimization methods are therefore subject of research aiming to reduce calculation misfit and improving the convergence stability.

An approach used in [94], [96] and [64] is the combination of a global heuristic optimization algorithm with local deterministic ones. By combining a local with a global search mechanism the advantages of both methods are used: the exact localization of minima with a fast convergence using local methods and the capacity of global methods to leave local attractor regions.

Syrjakow [94] divides the optimization into two phases: the pre-optimization and the fine-optimization. The pre-optimization phase uses the simulated annealing method and aims at identifying a parameter set which lies in the attractor region of the global minimum. Then in the second phase a local direct or gradient method is used in order to converge fast to the global minimum.

The main difficulty is evidently to switch from the first phase to the second since no precise convergence criteria for the global algorithm exist. In general, the control parameters of the global algorithm should be chosen in a way so that the whole parameter space of interest is exploited and a too early convergence avoided.

The global optimization is finished when a termination criterion is reached. The choice of the termination criterion has to follow two opposed aims: on the one hand the misfit of the evaluation should be low, and on the other hand the convergence of the global algorithm in the attractor region of the global minimum should be avoided. This requires that the whole solution space is covered in order to identify the global attractor region. The solution of the global optimization has to be located in the global attractor region with a high probability. The exact localization of the minimum is then achieved by the local optimization.

Well-defined criteria for the switching from the global to the local optimization do not exist. Heuristic criteria are used which guarantee to locate the global attractor region with a high probability. They are based on the num-

ber of iterations performed during the global optimization, the distribution of the generated parameter values in the solution space and the corresponding misfit function values. For genetic algorithms the accumulation of parameter values in a region of the solution space indicates the convergence in a attractor region. Evidently, the difficulty is that each local minimum has an attractor region in which solutions can accumulate. The use of the variance is therefore not suitable.

Instead, several accumulation regions have to be defined and the one corresponding to the global minimum chosen. This can be done by taking into account the number of points included in the accumulation region, its dimension and variance. Accumulation regions are defined by measuring after each iteration the distance of the parameter value to the previously calculated values. Beginning at a define number of iterations the distance between all parameter values is computed and used as a criteria for their classification in accumulation regions. The global optimization is terminated if one of the accumulation regions passes a defined size. However, the application to the models has shown that the choice of this criterion is difficult and can lead to errors.

The evolution of the misfit function values should be taken into account also. If the misfit function value stabilizes on a low level this indicates that the global attractor region is reached.

Miettinge [64] does not call the local solver after the global one. He shows different ways how to integrate the local solver directly into the simulated annealing algorithm.

It is difficult to choose the optimization methods the most suitable for the parameter identification problem discussed here. It depends principally on the characteristics of the multi-dimensional solution surface. Even though exact knowledge about the solution surface is not available the sensitivity analysis will give important indications. Generally both approaches, the global and the local methods will be considered. With regard to the complexity of the model a complex solution surface of the misfit function is probable, requiring the application of global methods. However, in order to overcome the disadvantage of slow convergence the combination of global methods with local methods is a promising approach.

1.3 Conclusions

In the first chapter the identification problem has been characterized. Based on the properties of the vehicle-track system an adequate approach for the parameter identification has been chosen.

Due to the wheel-rail contact and nonlinear suspension elements the system shows a nonlinear behaviour which can not be neglected. Therefore an identification in the frequency domain using modal analysis has been rejected. The modal parameters would depend on the excitation and running conditions. The requirement of identifying physical parameters of the multi-body model makes the identification of a nonlinear filter from time series analysis inappropriate also. As a result the structural model updating in the time domain will be used in the following. It compares directly the time signals of the measurement and the simulation and minimizes a misfit function describing the distance between these signals. For the definition of the misfit function and its minimization different approches will be studied.

In the following chapter the selection of an adequate model is outlined before applying the parameter identification in the chapters 3 and 4.

Chapter 2

Selection of an adequate model structure for the representation of the low frequency dynamics of the vehicle track system

The first step in modelling is the selection of an adequate model. It starts from the question which physical effects of the real system the model is supposed to take into account. It is therefore preceded by an analysis of the dynamic behaviour of the system under consideration. Then the properties of the system which the model should reproduce are selected and a model is built. Based on this model the parameter identification is performed. If the results of the parameter identification are not satisfying, the model has to be improved.

Criteria for selection As outlined in chapter 1, the aim of this work is the identification of suspension parameters for a TGV train. The system under consideration is a complete TGV train running on a track. All dynamic properties of the system which have an influence on the security and comfort of the vehicle and which lie in the frequency range of interest have to be taken into account. One decisive criterion for the model selection is therefore the reproducibility of these properties.

But it is not the only criterion. Since the parameters of the model are not exactly known from the beginning, the system identification is followed by the second step of the modelling process, the parameter identification. The

response of the model is compared with the measured response of the system. By minimizing a misfit function describing the difference between the model and the system response one aims at improving the estimate of the model parameters. The parameter identification leads therefore to an inverse problem.

Model parameters with physical meaning This implies two important criteria for the choice of the model: first, the aim is the identification of the suspension parameters. It is therefore necessary that the model parameters can be related to the suspension elements of the system. In other words, a model whose parameters do not have any physical meaning even if it fits well the measured response is not suitable. This is the reason why in chapter 1 the use of the ARMAX analysis has been rejected. For the nonlinear vehicle-track system it would be very complicated to relate the ARMAX model to a physical model. Instead, a multi-body model which is composed of rigid masses and suspension elements connecting them allows to rebuild the structure of the system and to relate the model parameters to system parameters with a physical meaning.

Identification method requirements The second criterion concerns the optimization algorithms used for the misfit function minimization. Some algorithms require more information about the model than others. From chapter 1 it is known that the adjoint method requires the nonlinear dynamic equations of the vehicle model for the calculation of the adjoint equations. Commercial multi-body programs do not provide this information because they are developed as black box systems. They require input parameters and give the dynamic response of the system but do not provide access to the equations of motion.

Use of commercial multi-body programs Commercial multi-body programs have many advantages. They offer predefined elements for the different types of suspension elements and notably for the wheel-rail contact. Due to these elements and a predefined structure, they simplify considerably the construction of large multi-body models of trains. By placing rigid bodies and connecting them with suspension elements, the user builds the model without having to set up the equations of motion himself. For this reason the multi-body program Vampire is used in this work for the modelling of the TGV train. It allows to set up a complex model which takes into account

a nonlinear description of the wheel-rail contact and all the different types of suspension elements in the primary and secondary suspension and between the vehicles. A detailed description of the Vampire TGV model is given in section 2.3. Notably the modelling of the complex elements like the rubber spring in the primary suspension, the air spring in the carrying bogies and the wheel-rail contact are discussed in detail.

The important drawback of the Vampire model is the lack of information about its mathematical description. As mentioned before, commercial multi-body programs are designed as black box systems. The user has no access to the nonlinear dynamic equations of the model. If the model parameters are assumed to be known and the model is used for simulating the dynamic response, this represents no difficulty. Such use as a forward model is the normal case in vehicle dynamics.

However, in this work the model is integrated in an optimization algorithm requiring the solution of an inverse problem. Then the lack of information concerning the nonlinear dynamic equations of the model becomes important. It makes the use of the optimization algorithms which require these equations impossible. As outlined in chapter 1 an important group of local optimization methods are based on the calculation of the gradient of the misfit function. The adjoint state method and the automatic differentiation method, giving a better accuracy and a lower calculation cost than the finite difference approach, need the knowledge of the dynamic equations. At present, they can not be applied to the commercial multi-body model.

Use of a simplified model For this reason a second multi-body model is used. It is derived from the equations of motion of the multi-body system and implemented in Matlab. Thanks to the known analytical description, the model can be used with all parameter identification methods, notably with the gradient calculation from adjoint states and analytical differentiation. However, the aim is not to have a complete model of the TGV train with the same precision as the Vampire model. This would require an enormous modelling effort comparable to the implementation of a complete multi-body code and could not be the objective of this work. Such a complex problem is much better handled with a well-established multi-body code like Vampire. The parameter identification for the TGV train based on actual measurement data is therefore exclusively performed on the Vampire model.

The motivation for a multi-body model in Matlab is to identify a relatively simple model structure which represents nevertheless important characteristics of the vehicle-track system. Nonlinearities due to the wheel-rail contact and suspension elements as well as the excitation by rail irregularities should be taken into account by this model. For this reason the model of a bogie including two wheelsets running on the track, the primary suspension and the bogie frame is chosen.

In the section 2.1 the multi-body model of the bogie will be described before presenting the Vampire model of the TGV in section 2.3.

2.1 Implementation of a bogie model derived from kinematic and dynamic equations

The bogie model is composed of three bodies: the bogie frame and two wheelsets. It runs on the track with a constant speed v. The model is excited by the irregularities spatially defined along the track. With the vertical and horizontal displacement of the right and the left rail relative to the theoretical position four degrees of freedom are necessary for their description. Otherwise the track is supposed to be rigid. In figure 2.1 the structure of the model is shown.

2.1.1 Kinematic equations of the wheel-rail contact

In order to formulate the equations of motion for the model, the position and velocity have to be described for each body. This is done relatively to an inertial frame moving on the track centreline with the constant vehicle speed v. The position of each body is described by three translational and three rotational degrees of freedom. Kinematic constraints lead to a reduction of this number of degrees of freedom. The remaining degrees of freedom form the vector of generalized coordinates which describes completely the dynamic behaviour of the system.

Degrees of freedom For the bogie the identification of the degrees of freedom is evident since no kinematic constraint exists.

The determination of the degrees of freedom for the wheelset and its position relatively to the track requires the solution of the kinematic relations.

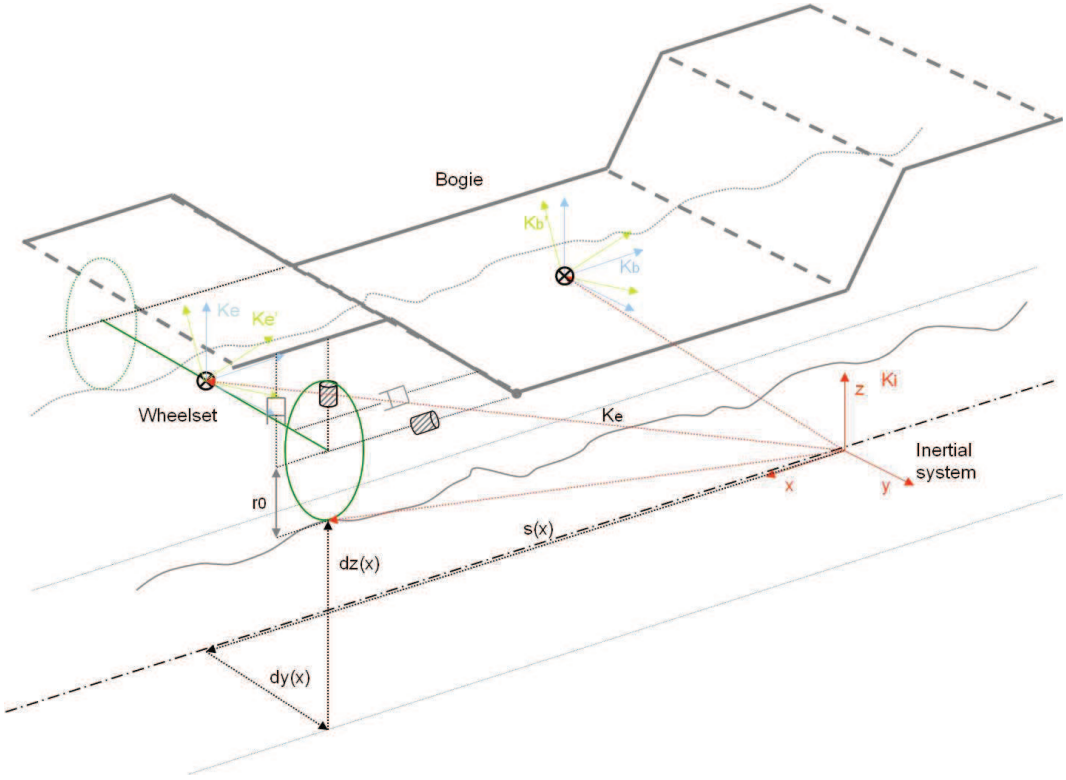

Figure 2.1: Model of the bogie including two wheelsets

Supposing that the wheel and the rail are always in contact and that there are no strains in the rail, two kinematic constraints exist. This reduces the number of degrees of freedom for the wheelset to 4: the lateral displacement u_y, the rotation around the z axis δ_z, the longitudinal displacement u_x relatively to the constant vehicle speed and variations of the constant rotational velocity of the wheelset $\dot{\delta}_y$. Vertical displacements and rotation around the longitudinal x-axis are prevented by the track.

If acceleration and braking effects are not considered, the relative longitudinal displacement u_x and the relative rotational velocity δ_y can be neglected. It is assumed that the vehicle and also the centres of gravity of the wheelsets move with constant speed. This implies that no longitudinal friction forces appear when the wheelset is not skewed. As outlined later this assumption is justified since mainly lateral effects determine the dynamic of the wheelset. This approximation reduces the number of degrees of freedom per wheelset to two.

Finally, 10 degrees of freedom are identified for the model: two for each wheelset and six for the bogie frame. The vector of generalized coordinates relative to the inertial system is composed of the following degrees of freedom:

$$\underline{x} = (r_{bx}, r_{by}, r_{bz}, \delta_{bx}, \delta_{by}, \delta_{bz}, u_{e1y}, u_{e2y}, \delta_{e1z}, \delta_{e2z})^T \tag{2.1}$$

with:
r_{bx}, r_{by}, r_{bz}: *bogie position*, δ_{bx}, δ_{by}, δ_{bz}: *bogie rotation*, u_{e1y}, u_{e2y}: *lateral displacements of wheelsets*, δ_{e1z}, δ_{e2z}: *yaw rotations of wheelsets*.

The aim of the kinematic equations is to describe the position of the wheelset and the contact points as functions of the degrees of freedom. The vertical position of the centreof gravity u_z as well as the rotation around the longitudinal axis δ_x depend on the generalized coordinates and track irregularities.

Kinematic constraints for ideal track As described in chapter 1 these kinematic relations become very complicated for real profile combinations. In this case analytical relations are not available any longer. In order to obtain an analytic mathematic description, a simplified contact geometry is applied. When both rail and wheel are described by circular profiles, an analytical solution exists. For this bogie model a circular rail profile and a conical wheel profile are used as shown in figure 2.2. In the following the derivation of the dynamic equations for this profile combination is outlined for an ideal track

without irregularities. It is based on the detailed descriptions given in [52] and [62].

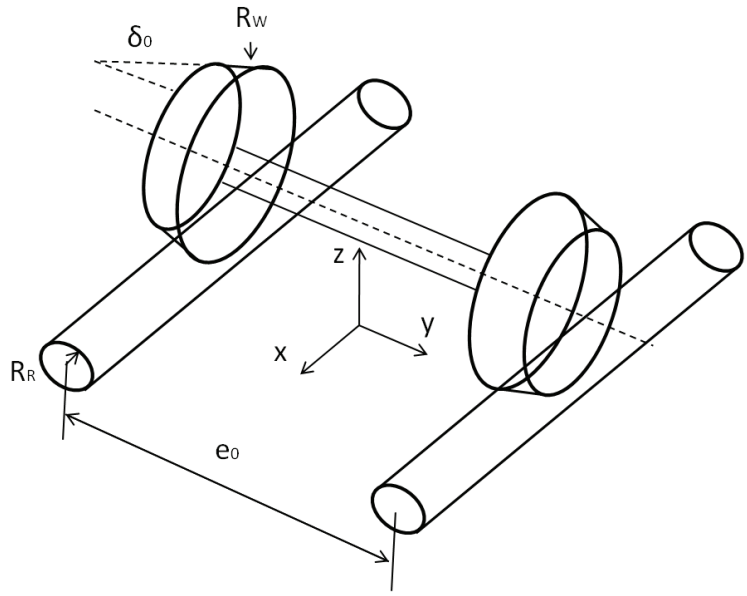

Figure 2.2: Model of the wheelset with conical profile on a circular track

In the first step the independent coordinates of the wheelset have been identified. The next and difficult step is to relate the two dependent coordinates u_z and δ_x to the degrees of freedom. Beside the position of the centre of gravity, two values are important for dynamic calculations of the vehicle: the difference between the left and right contact radii Δr and the contact angle $\delta_{r(l)}$ in the contact point for the right and left rail respectively. $\delta_{r(l)}$ describes the angle of the contact surface between wheel and rail and is shown in figure 2.4. For real profiles the contact angle and the conicity respectively depend on the track gauge e_0 describing the distance between the two rails. The calculation of these kinematic relations is rather complicated and not outlined here. It results in the following nonlinear equations which can be found in [52]:

$$[u_y + h_W \sin\delta_x]^2 = (R_W - R_R)^2 \frac{g_W^2 \sin^2\delta_x}{g_W^2 - 2g_W g_R \cos\delta_x + g_R^2} \tag{2.2}$$

$$[u_z + h_W \cos\delta_x + h_R]^2 = (R_W - R_R)^2 \frac{g_W^2 \sin^2\delta_x}{g_W^2 - 2g_W g_R \cos\delta_x + g_R^2} \tag{2.3}$$

with the terms :

$g_W = e_0 + R_W \sin \delta_0$
$h_W = e_0 + R_W \cos \delta_0$
$g_R = e_0 + R_R \sin \delta_0$
$h_R = e_0 + R_R \cos \delta_0$

with:
R_W: wheel radius, R_R: rail radius, e_0: track gauge, δ_0: angle of conical wheel.

By applying a Taylor development these relations are linearized except for the vertical displacement where quadratic terms persist. Details of these calculations are given in the appendix A.

$$\Delta r \cong \lambda u_y \tag{2.4}$$

$$\tan \delta_{l(r)} \cong \tan \delta_0 \pm \epsilon \frac{2}{e_0} u_y \tag{2.5}$$

$$\delta_x \cong \sigma \frac{2}{e_0} u_y \tag{2.6}$$

$$u_z = \frac{1}{2} \zeta u_y^2 - \frac{1}{2} \xi \delta_z^2 \tag{2.7}$$

λ, ϵ, σ, ζ and ξ are geometry parameters defined in [52] which depend on the radius of the wheel and of the rail. As outlined in the appendix A, they are given for the general case that wheel and rail profiles are circular. The case of circular profiles is illustrated in figure 2.3. They are described by the curvatures in lateral direction. Since the wheel profile used in this study is conical the equations are simplified by letting the radius of the wheel going to infinity.

The kinematic relations describe the radius difference, the contact angle for the left and right wheel, the rotation around the x-axis and the vertical displacement as a function of the two degrees of freedom and the geometric parameters of the wheel-rail contact. In order to better understand the results it is interesting to relate them to the geometric relations obtained from a graphical representation.

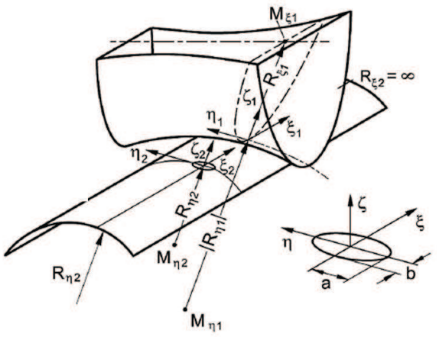

Figure 2.3: Wheel-rail contact for circular profiles represented by the lateral curvatures R_W for the wheel and R_R for the rail(from [52])

Graphical representation For this graphical consideration the rail radius is assumed to be infinitesimal small. The rail is therefore degenerated to a line. The geometry parameters are reduced to:

$$\lambda = \delta_0 \tag{2.8}$$

$$\epsilon = \delta_0 \tag{2.9}$$

$$\sigma = \delta_0 \tag{2.10}$$

$$\zeta = 4\delta_0/e_0 \tag{2.11}$$

$$\xi = \frac{1}{2}\delta_0 e_0 \tag{2.12}$$

The contact angle in the contact surface is the sum of the cone angle δ_0 and the wheelset angle around the x-axis δ_x:

$$\delta_l' = \delta_0 - \delta_x \tag{2.13}$$

From the trigonometric relations in figure 2.4 the contact angle is expressed by the lateral displacement u_y and the length l:

$$\cos\delta_l' = \frac{u_y}{l} \qquad \Rightarrow l = u_y \frac{1}{\cos\delta_l'} \tag{2.14}$$

From the same trigonometric relations the radius difference for the left wheel Δr_l is obtained:

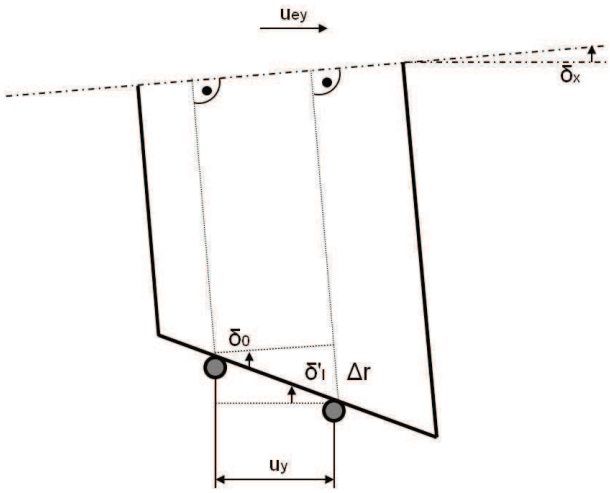

Figure 2.4: Geometric relations between contact point radius, contact point angle and lateral displacement for the left rail

$$\Delta r_l = l \sin \delta_0 = u_y \frac{\sin \delta_0}{\cos \delta_l'} = u_y \frac{\sin \delta_0}{\cos(\delta_0 - \delta_x)} \tag{2.15}$$

If the rotation of the wheelset around the x-axis δ_x is neglected an estimate for the radius difference Δr_l is obtained which corresponds to the estimate (2.4) obtained from the nonlinear kinematic relations:

$$\Delta r_l \cong u_y \tan \delta_o \tag{2.16}$$

The rotation angle of the wheelset δ_x is calculated from the track gauge e_0 and the radius difference between right and left rail $2\Delta r$ with $\Delta r_l = \Delta r_r = \Delta r$:

$$\sin \delta_x = 2\frac{\Delta r}{e_0} = 2\frac{u_y \frac{\sin \delta_0}{\cos(\delta_0 - \delta_x)}}{e_0} \tag{2.17}$$

For small rotation angles the same estimate as for the kinematic relation (2.6) is found again:

$$\delta_x \cong 2\frac{\tan \delta_0}{e_0} u_y \cong 2\frac{\delta_0}{e_0} u_y \tag{2.18}$$

If this result is inserted into equation (2.13) for the contact angle a result is obtained which corresponds to the estimation (2.5) received from the nonlinear kinematic relations.

The last coordinate which one wants to estimate from graphical considerations is the vertical displacement of the wheelset. From trigonometric considerations it can be easily seen that it depends on the lateral displacement u_y and the rotation around the z-axis δ_z.

$$u_z(u_y, \delta_z) = u_y \tan \delta_x - \frac{1}{4}\delta_0 e_0 \delta_z^2 \tag{2.19}$$

Using the result received for the rotation angle δ_x in 2.18 and the dependence on the rotation around the z-axis the vertical displacement becomes:

$$u_z(u_y, \delta_z) = 2u_y^2 \frac{\delta_0}{e_0} - \frac{1}{4}\delta_0 e_0 \delta_z^2 \tag{2.20}$$

This is the same term obtained from nonlinear equations.

Kinematic constraints for real track So far the position vector of the wheelset has been described relatively to the two degrees of freedom of the wheelset. Evidently, the position of the wheelset relatively to the inertial system depends also on the track irregularities, expressed by the vertical displacement d_z, a horizontal displacement d_y and a cross level irregularity of the track γ_d relative to its ideal position. Variations in the track gauge are neglected. Taking into account the track irregularities in the kinematic relations obtained before, the vertical displacement u_z, the angle δ_x, the contact radius difference Δr and the contact angle $\tan \delta_{l(r)}$ are given by:

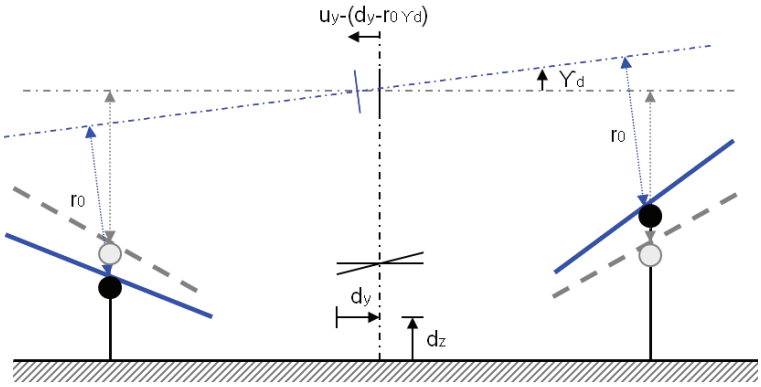

Figure 2.5: Geometric relation between the position of the wheelset and the geometric track irregularities

$$u_z = d_z - \frac{1}{2} r_0 (\gamma_d)^2 + \frac{1}{2} \zeta (u_y - d_y + r_0 \gamma_d)^2 - \frac{1}{2} \xi \delta_z^2 \tag{2.21}$$

$$\delta_x = \gamma_d + \sigma \frac{2}{e_0} (u_y - d_y + r_0 \gamma_d) \tag{2.22}$$

$$r_{l(r)} = r_0 \pm \lambda (u_y - d_y + r_0 \gamma_d) \tag{2.23}$$

$$\tan \delta_{l(r)} = \tan \delta_0 \pm \epsilon \frac{2}{e_0} (u_y - d_y + r_0 \gamma_d) \tag{2.24}$$

The nominal contact radius r_0 represents the wheel radius at the contact point when the wheelset is centreed on the track. No lateral displacement exists and the contact radii on the left and right wheel are identical.

From the two-dimensional representation in figure 2.5 some of the additional terms in the kinematic equations can be illustrated. The lateral displacement of the wheelset relative to the ideal centreline of the track is now described by the difference between the wheelset displacement u_y and the track displacement due to the lateral and cross track irregularity $d_y - r_0 \gamma_d$. Besides, additional terms appear in the vertical displacement of the wheelset.

2.1.2 Derivation of the nonlinear dynamic equations using the Lagrange approach

Outgoing from these kinematic relations the position vectors of the bogie frame and of the two wheelsets can be described with respect to the degrees of freedom and the track irregularities. It forms the basis for the setup of the equations of motion. Two different approaches can be applied: the Euler/Newton and the Lagrange approach. If Euler/Newton is used the equilibrium of forces and moments has to be derived for every body. Here the Lagrange approach is used. The equations of motion are derived from the kinetic energy of the system.

Lagrange's equations For each degree of freedom x_i of the vector of generalized coordinates (2.1) the Lagrangian equations have the form:

$$\frac{d}{dt} \left(\frac{\partial E_c}{\partial \dot{x}_j} \right) - \frac{\partial E_c}{\partial x_j} = d_j, \qquad j = 1, ..., 10 \tag{2.25}$$

E_c is the kinetic energy of the system calculated with the translational v_i and rotation velocities ω_i at the centre of gravity for every body i described by its mass m_i and inertia J_i:

$$E_c = \frac{1}{2}\sum_{i=1}^{3}(v_i^T m_i v_i + \omega_i^T J_i \omega_i) \tag{2.26}$$

The generalized forces d of the Lagrangian equations are calculated with the forces f_{Ei} and moments m_{EiP} acting on the centre of gravity of every body. J_{Ti} and J_{ri} are the Jacobian matrices of translation and rotation:

$$d = \sum_{i=1}^{3}(J_{Ti}^T f_{Ei} + J_{ri}^T m_{EiP}) \tag{2.27}$$

In order to calculate the kinetic energy E_c the translational and rotational velocities have to be calculated for every body relativ to the inertial system. The vector d of the generalized forces is composed of the spring and damping forces of the primary suspension and the friction forces of the wheel-rail contact. The spring and damping forces are calculated using the displacements and velocities at the coupling points of the suspension expressed in inertial coordinates. The derivations of the translational and rotational velocities as well as the force terms can be found in the appendix A.

The friction forces are related to the slip in the contact surface between wheel and rail through the coefficient of friction. The slip ν is defined as the relative velocity in the contact point normalized by a reference velocity. Here the constant vehicle speed v is used as reference velocity giving for the slip ν:

$$\nu = \frac{v_{rel}}{v} \tag{2.28}$$

Three different slips are distinguished: the lateral slip ν_ξ, the vertical slip ν_η and the rotational slip ν_ζ. They are described relatively to the inertial system. The objective is thus to determine the friction forces T and moments M as functions of these slips. It is distinguished between the longitudinal friction force T_ξ, the lateral friction force M_ζ and the spin M_ζ. The spin describes the moment due to the rotation in the contact surface.

$T_\xi = T_\xi(\nu_\xi, \nu_\eta, \nu_\zeta)$
$T_\eta = T_\eta(\nu_\xi, \nu_\eta, \nu_\zeta)$
$M_\zeta = M_\zeta(\nu_\xi, \nu_\eta, \nu_\zeta)$

The relative velocities are illustrated in figure 2.6. Figure (a) shows a top view of the left wheel and figure (b) the front view of the wheelset. The relative velocities are described in a local coordinate system in the contact point whose ζ axis is normal to the contact surface.

The longitudinal relative velocity $v_\xi^{r(l)}$ is caused by a rotation δ_z of the wheelset around the z-axis. It is the difference between the vehicle speed v, the component due to the constant rotational velocity Ω of the wheel and the rotational speed $\dot{\delta}_z$ around the z-axis. If the yaw angle of the wheelset is zero ($\delta_z = 0$) and ideal rolling without friction is assumed, the longitudinal relative velocity becomes zero.

$$v_\xi^{r(l)} = r_{r(l)}\Omega\cos\delta_z \pm \dot{\delta}_z e_0/2 - v \tag{2.29}$$

The lateral relative velocity is illustrated in figures 2.6 (a) and (b). It is composed by three components: the speed of the contact point due to the rotational velocity Ω of the wheelset when the yaw angle δ_z is non-zero (1), the lateral velocity due to changes in the lateral displacement (2) and the lateral velocity due to a rotational speed of the wheelset around the x-axis (3).

$$\begin{aligned} v_\eta^{r(l)} = \underbrace{r_{r(l)}\Omega\sin\delta_z\cos\delta_{r(l)}}_{(1)} - \underbrace{\frac{d}{dt}[(u_y - d_y + r_0\gamma_d)\cos\delta_{r(l)}]}_{(2)} \\ - \underbrace{\frac{d}{dt}[\delta_x(\frac{e_0}{2}\sin\delta_0 + r_{r(l)}cos\delta_0)]}_{(3)} \end{aligned} \tag{2.30}$$

Perpendicular to the contact surface a rotational relative velocity appears. It depends on the contact angle and is composed by two components: the normal part of the rotational speed of the wheelset (4) and the velocity due to the rotation around the z-axis (5).

$$v_\zeta^{r(l)} = \underbrace{\pm\Omega\sin\delta_{r(l)}}_{(4)} - \underbrace{\frac{d}{dt}[\delta_z cos\delta_{r(l)}]}_{(5)} \tag{2.31}$$

For the calculation of the friction forces and moments, the linearized Kalker theory is applied. As outlined in chapter 1 it assumes that the slip rates are small so that a linear ratio between slips and friction forces can be applied. More information on the linear and other theories developed by Kalker can

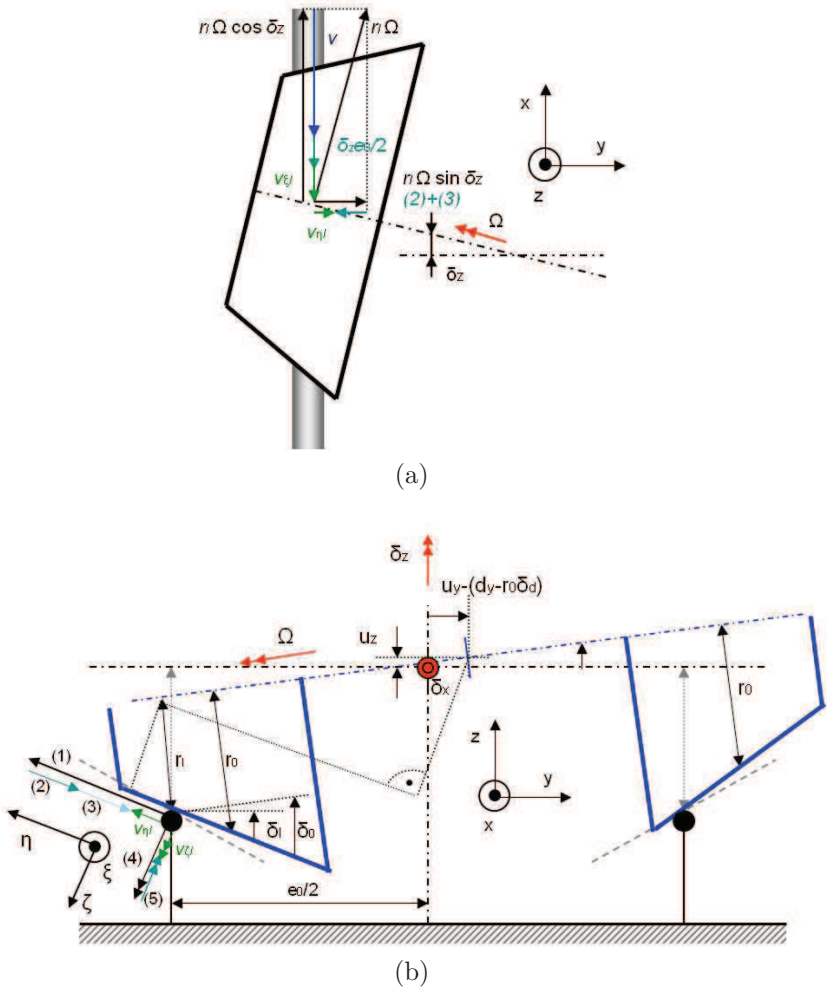

Figure 2.6: Relative velocities between the wheel and the rail: top view of a wheel turned with angle δ_z to the track (a) and front view of a wheelset displaced laterally by $(u_y - d_y + r_0\gamma_d)$(b)

be found in [107]. The values for the Kalker coefficients C_{ij} depend on the form of the contact ellipse and can be found for example in [52].

$$\begin{pmatrix} T_\xi \\ T_\eta \\ M_\zeta \end{pmatrix} = Gab \begin{pmatrix} C_{11} & 0 & 0 \\ 0 & C_{22} & \sqrt{ab}C_{23} \\ 0 & -\sqrt{ab}C_{23} & abC_{33} \end{pmatrix} \begin{pmatrix} \nu_\xi \\ \nu_\eta \\ \nu_\zeta \end{pmatrix} \tag{2.32}$$

with: G: shear modulus

The form of the contact surface is elliptic and described by the contact radii a and b. They are obtained from the Hertz theory of the normal contact problem. The Hertz theory has been introduced in chapter 1.

The Hertz theory allows to compute for a known normal force the contact radii, the elastic strain and the stress in the contact surface. Input parameters are the radii of curvature for the rail and the wheel and the modulus of elasticity. The normal force is composed by static forces due to the mass and a dynamic part. The calculation itself can be found in the appendix A.

Finally, the nonlinear equations of motion for the bogie model are obtained from the Lagranges's equations in the form:

$$\mathbf{M}(\mathbf{x}, t)\ddot{\mathbf{x}}(t) + \mathbf{g}(\mathbf{x}, \dot{\mathbf{x}}, t) = \mathbf{d}(\mathbf{x}, \dot{\mathbf{x}}, t) \tag{2.33}$$

$\mathbf{M}$ is the mass matrix and depends generally on the parameter vector $\mathbf{x}$ and time. The vector $\mathbf{g}$ regroups all nonlinear terms depending on the parameter vector $\mathbf{x}$ and its first derivative $\dot{\mathbf{x}}$. The vector $\mathbf{d}$ is the nonlinear vector of generalized forces.

For the computation of the friction forces at every time step the vertical wheelforces have to be known. Basically, the vertical wheelforces are composed by a static component given by the mass of the bogie and car-body and a dynamic component due to the inertia of the bogie and car-body. For the computation of the dynamic forces the accelerations of the masses at each time step are required. They are obtained from the two previous time step by differentiating the velocity.

$$a_k = \frac{v_{k-2} - v_{k-1}}{\Delta t} \tag{2.34}$$

2.1.3 Analysis of the dynamic behaviour of the bogie model

The bogie model is described by a nonlinear differential equation system with initial conditions and an excitation. Equation (2.35) gives the state space equation of the system received above with $\mathbf{w} = [\mathbf{x}, \dot{\mathbf{x}}]$. It is not possible to solve this equation system analytically. Numerical integration algorithms have to be used instead.

$$\dot{\mathbf{w}} = \begin{pmatrix} 0 & \mathbf{I} \\ 0 & 0 \end{pmatrix} \mathbf{w} + \begin{pmatrix} 0 \\ \mathbf{M}^{-1}(\mathbf{d}(\mathbf{x}, \dot{\mathbf{x}}, t) - \mathbf{g}(\mathbf{x}, \dot{\mathbf{x}}, t)) \end{pmatrix} \tag{2.35}$$

All numerical integration algorithms are based on a discretization of the analysis time interval $[0, T]$. For every time step an estimation of the solution is calculated. The distance between two time steps, the step length, has an important effect on the accuracy of the results. Generally, two types of integration algorithms can be distinguished: one-step algorithms and multi-step algorithms. For computing the estimation at a time step the one-step solver only uses the solution of the previous step. Multi-step solvers use the estimations of several steps before.

In Matlab both one- and multi-step solvers are available. For this problem the one-step solver ODE45 based on the explicit Runge-Kutta formulas and the multi-step solver ODE113 are used.

For the choice of the solver and the integration step length h, the required accuracy is important. This necessitates the calculation of the local error for an integration step. Normally, solvers for practical applications offer an automatic control of the integration step length. The step length h is chosen so that a given tolerance, the absolute tolerance, is kept. The method is based on the calculation of two approximations, one of order p and one of order $p + 1$. Based on the two approximations Y_{k+1}^{p} and Y_{k+1}^{p+1} the local discretization error is estimated. If it is smaller than the absolute tolerance the steplength is accepted otherwise the integration step is repeated with a smaller steplength h.

The local discretisation error τ is given by:

$$\tau = \frac{Y_{k+1}^{p+1} - Y_{k+1}^{p}}{h_{old}} \approx C h_{old}^{p} \tag{2.36}$$

If the local error is smaller than the defined tolerance TOL ($\tau < TOL$) the integration steplength h is accepted. If not the new steplength h_{new} is

calculated as follows:

$$h_{new} = h_{old}(\frac{TOL}{\tau})^{1/p} \tag{2.37}$$

The forward response of the bogie model has been calculated for the solvers ODE45, ODE113 and ODE15s for different tolerances and initial time steps. The accuracy of the result and the calculation time are compared since they will play an important role in the parameter identification methods outlined in the next chapter. As excitation signal a lateral track irregularity shown in figure 2.7 is used.

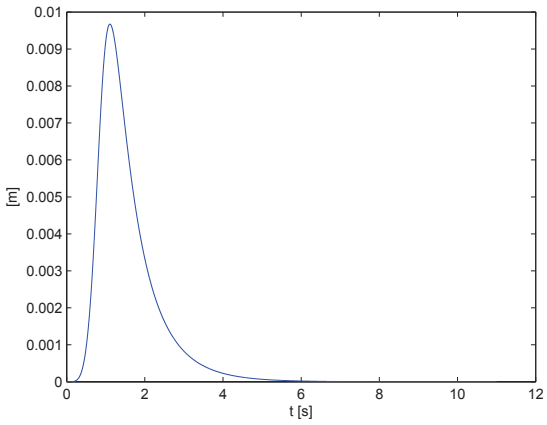

Figure 2.7: Lateral track defect as excitation signal

Besides, the forward model allows to analyze the dynamic behaviour of the bogie model. Although it is relatively simple, important properties of vehicle track systems are reproduced. If the lateral displacement and the rotation of the wheelsets are plotted the typical hunting movement is found: a wheelset which has been displaced laterally is exposed to lateral geometric and longitudinal friction forces leading to a rotational movement toward the centre of the track. Due to the moment of the lateral friction forces it crosses the centreline and continues to turn until the moment of the longitudinal friction forces which is now opposed becomes larger. The cycle is illustrate in figure 2.8.

Below the so-called critical speed the wheelset behaves in a stable way and the oscillation decays. If the vehicle speed is increased and the critical speed is attained the behaviour changes abruptly. An initial displacement leads

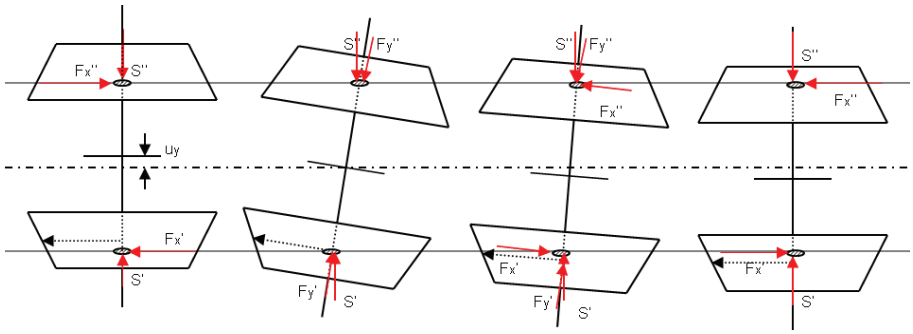

Figure 2.8: Hunting movement of wheelset due to friction and geometric wheel forces (F: friction forces, S: geometric forces)

to an oscillatory movement with increasing amplitude. The system becomes unstable. When analyzing the poles of the linearized wheelset model in the complex plane this corresponds to poles in the positive half plane. For the nonlinear system the amplitude increases until a limit cycle is obtained as shown in figure 2.9.

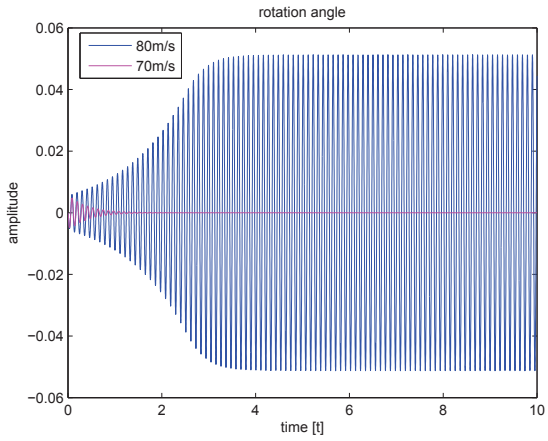

Figure 2.9: Yaw angle of the wheelset for a vehicle speed below and above the critical speed

The critical speed of the wheelset depends on the suspension properties. By changing the suspension parameters the critical speed is increased or reduced. Notably the longitudinal stiffness of the primary suspension has an important effect on the critical speed as shown in figure 2.10.

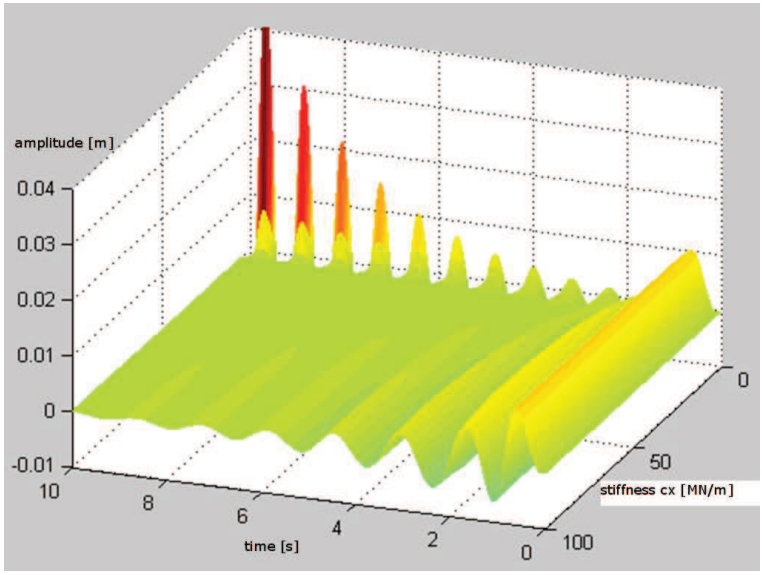

Figure 2.10: Dynamic response of the bogie model as a function of the longitudinal stiffness

The parameters of the bogie model which may be considered in the identification are summarized in table 2.1. It is distinguished between inertia parameters, suspension parameters and parameters of the wheel-rail contact. Even though the conicity of the wheel-rail contact and the coefficients of the Kalker friction model are listed here there identification is unlikely due to their unstationarity and nonlinear effects.

Bogie model parameters			
Name	Unit	Valeur	Description
Geometry			
ls	$[m]$	2.5	wheelset distance
Inertia			
m	$[t]$	1.8	mass wheelset
I_x	$[Kgm^2]$	960	Inertia x wheelset
I_y	$[Kgm^2]$	450	Inertia y wheelset
I_z	$[Kgm^2]$	960	Inertia z wheelset
m	$[t]$	2.38	mass bogie frame
I_x	$[Kgm^2]$	1924	Inertia x bogie frame
I_y	$[Kgm^2]$	1080	Inertia y bogie frame
I_z	$[Kgm^2]$	2970	Inertia z bogie frame
Suspension			
cx	$[MN/m]$	52	stiffness x
cy	$[MN/m]$	3.5	stiffness y
cz	$[MN/m]$	1.0	stiffness z
dx	$[MN/m]$	0.0003	damping x
dy	$[MN/m]$	0.0003	damping y
dz	$[MN/m]$	0.012	damping z
Wheel-rail contact			
δ_0	$[rad]$	0.2	conicity
e	$[m]$	1.435	track gauge
sfV	$[-]$	1	factor Kalker coefficients

Table 2.1: Parameters of bogie model

2.2 Vampire bogie model as virtual experimental data

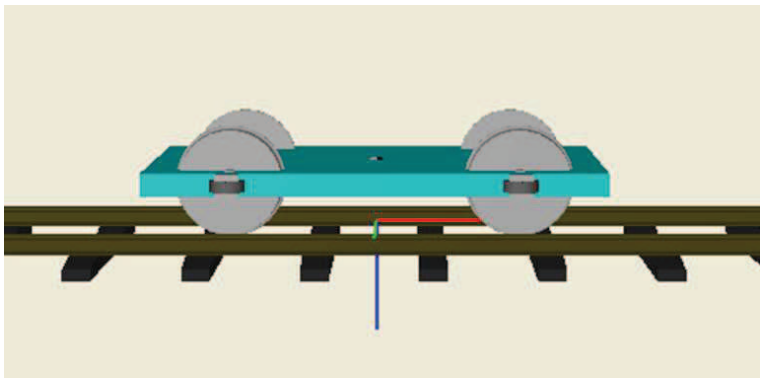

Figure 2.11: Bogie model implemented in Vampire

The model of the bogie described in section 2.1 has been implemented in Vampire. The model is used to validate the Matlab model and will serve as measurement substitution for the parameter identification of the bogie model in the following chapter.

The model is composed of two wheel-sets and a bogie frame connected by the primary suspension. The parameter values for the inertia and suspension elements are the same as outlined in table 2.1. The exact description of the wheel rail contact is not known.

As outlined before Vampire proposes different models of the wheel-rail contact. For the bogie model the linear creep law and the nonlinear creep model have been compared. The linear creep law assumes a linear relationship between the slip and the friction forces. Therefore it is only applicable for low slip values when no saturation appears. Besides, it is assumed that the wheels are perfectly coned. For the non-linear creep law the real profiles of the wheel and the rail are used.

The comparison between the bogie models implemented in Matlab and Vampire is shown in the figures 2.13 to 2.15. Even though the same masses and model parameters have been used differences in the dynamic response of the two models appear. They might be due to differences in the model structure notably the kinematic description of the wheel rail contact which is not exactly known for the Vampire model.

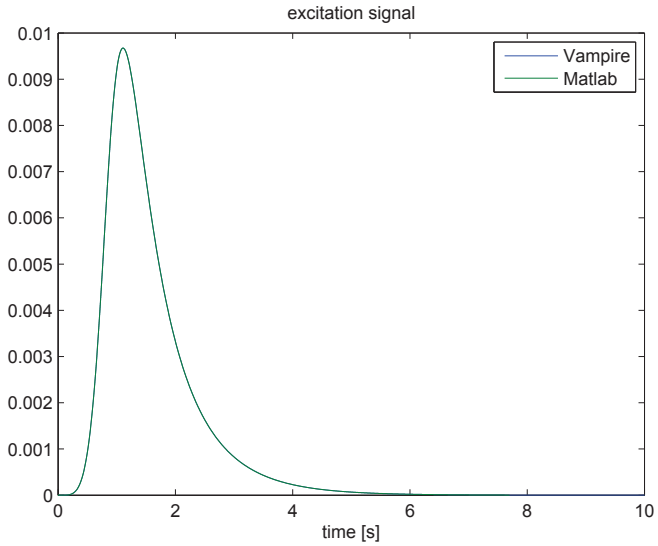

Figure 2.12: Lateral track irregularity signal to Vampire and Matlab model

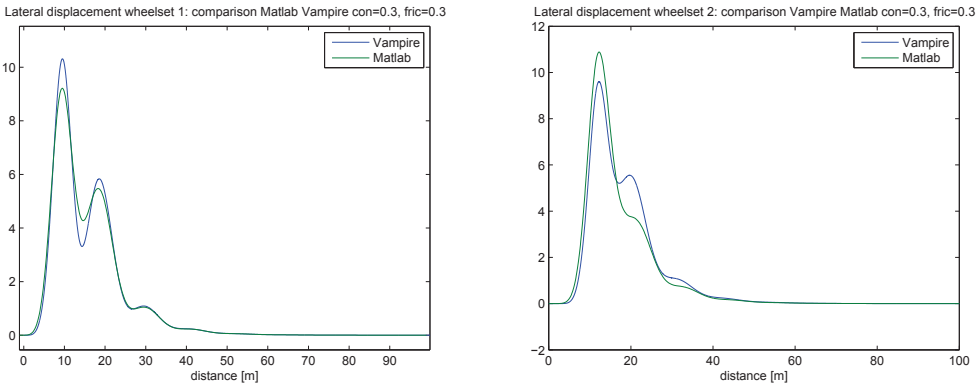

(a) (b)

Figure 2.13: Lateral displacement for wheelset 1 (a), and wheelset 2 (conicity=0.3, friction=0.3)(b)

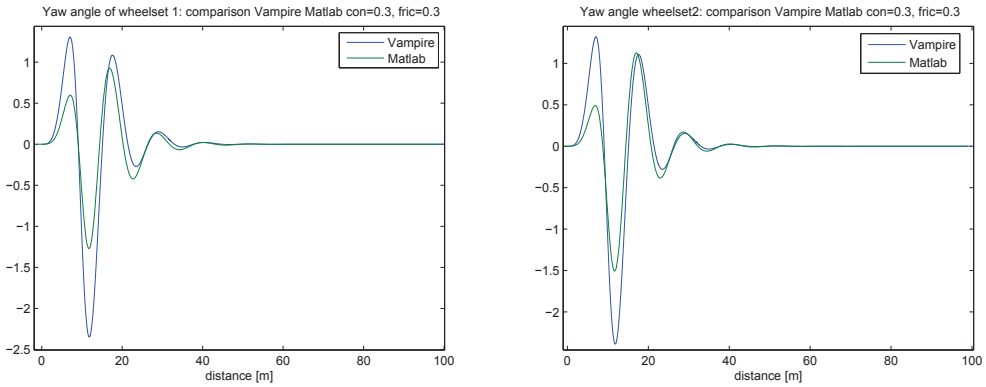

(a) (b)

Figure 2.14: Yaw angle for wheelsets 1 (a), and 2 (conicity=0.3, friction=0.3)(b)

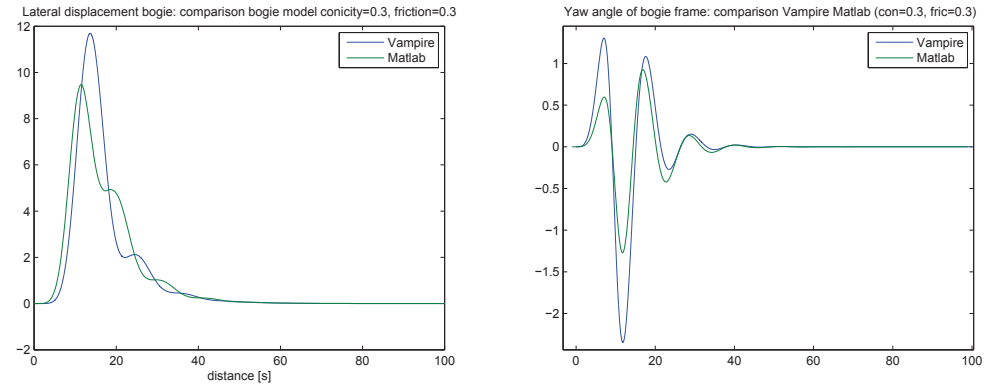

(a) (b)

Figure 2.15: Lateral displacement of bogie frame (a), and yaw angle (conicity=0.3, friction=0.3)(b)

2.3 Model of the TGV train implemented in Vampire

The model of the TGV Duplex train is implemented with the commercial multi-body program Vampire. The system is assembled from rigid bodies and connected by suspension elements. This is done by defining the masses, inertias and positions of the bodies as well as the types and parameters of the suspension elements. Predefined elements and a graphical interface reduce the effort for building a model.

After the model setup, different kinds of computations can be performed: transient analysis for the nonlinear model with the track excitation and modal analysis for the linearized model. The dynamic equations are automatically created and solved. The functionality of the Vampire program will not be outlined here. For more details it is referred to the Vampire manual [103].

In the following the focus is laid on the selection of an adequate model for the TGV train. Once again the important questions of model selection are treated: which properties of the real system the model is supposed to reproduce? Which model structure and complexity are needed in order to model these properties?

One limitation is made from the beginning. The model is entirely composed of rigid bodies and can not represent effects due to elastic modes of the real system. The frequency domain covered by the model ranges to 30Hz approximately. For the analysis of the passengers comfort and criteria concerning the security of the vehicle, this is sufficient.

From the description of the vehicle-track system in chapter 1, the crucial points for the model selection are known. One is the wheel-rail contact. Several models of different complexities and precisions have been developed in railway vehicle dynamics. In the first part of this chapter which is about the model implementation for a bogie, the kinematic relations for a circular rail and conical wheel profile and the linear Kalker theory have been implemented. This approach enables an analytical description of the wheel-rail contact mechanics but implies important simplifications.

In Vampire more accurate models are available leading to a better representation of the real system. They will be discussed in the following paragraphs. The second important point in the model selection concerns the suspension

elements. Situated in the primary and secondary suspension as well as between the carriages they assure the coupling between wheelsets, bogies and carbodies. Some of them, mainly the airsprings in the secondary suspension and the rubber elements have complicated dynamic properties. Their modelling is a difficult task and will be discussed in section 2.3.2. The used suspension element models, their properties and modelling are summarized in the appendix B.

2.3.1 Modelling of the wheel-rail contact

The wheel-rail contact, implemented in Vampire, involves the calculation of the relative velocities in the wheel-rail contact and the creep law relating the friction forces to the relative velocities. Three relations are provided for the friction law: the linear, the square root and the non-linear creep law.

The longitudinal creepages, calculated as the relative velocity in the contact normalized with the vehicle speed, for the left and the right wheel are [103]:

$$\nu_\xi^l = 1 + \frac{e_0\dot{\delta_z}}{2v} + \frac{r_l\Omega}{v} + \frac{e_0}{2R_{curve}} + \frac{\dot{u_x}}{v} \tag{2.38a}$$

$$\nu_\xi^r = 1 - \frac{e_0\dot{\delta_z}}{2v} + \frac{r_r\Omega}{v} - \frac{e_0}{2R_{curve}} + \frac{\dot{u_x}}{v} \tag{2.38b}$$

with: δ_z: yaw angle, Ω: roll rotation, e_0: track gauge, $\dot{u_x}$: variation from vehicle speed, R_{curve}: curve radius.

If these expressions are compared to the creepages calculated for the bogie model two additional terms are found. The third term describes the longitudinal creepage due to track curvatures with the radius R_{curve}. It does not appear in the bogie model since a straight track is considered. The last term describes variations from the constant vehicle speed which are not taken into account in the bogie model in order to reduce the number of degrees of freedom from 4 to 2.

In the lateral direction the creepage is calculated:

$$\nu_\eta^l = (\frac{\dot{u_y}}{v} + \frac{r_l\Omega\delta_z}{v})\frac{1}{\cos\delta_l} \tag{2.39a}$$

$$\nu_\eta^r = (\frac{\dot{u_y}}{v} + \frac{r_r\Omega\delta_z}{v})\frac{1}{\cos\delta_r} \tag{2.39b}$$

with: u_y: lateral displacement, $\delta_{l(r)}$: contact angle for left and right wheel

For the lateral creepage an additional term is considered in the bogie model. It describes the creepage due to the rolling rotation of the wheelset around the x-axis. Since the rolling movement of the wheelset is small the term is neglected in Vampire.

Finally, the spin creepage is described by the expressions:

$$\nu_\zeta^l = -(\frac{\Omega}{v}) \sin \delta_l + \dot{\delta_z} \tag{2.40a}$$

$$\nu_\zeta^r = (\frac{\Omega}{v}) \sin \delta_r + \dot{\delta_z} \tag{2.40b}$$

This corresponds to the description used for the bogie model.

The creepage relations presented above are used in the non-linear creep law model. For the linear and the square root model simplifications are introduced. As recommended by Vampire, the nonlinear transient analysis program has been chosen for analyzing the TGV model.

In order to allow an analytical calculation of the kinematic relations in the wheel rail contact, a circular rail profile and a conical wheel are used in the bogie model. However, as outlined in chapter 1 real wheel and rail profiles have more complicated geometries. For these profiles a closed analytical solution is no longer available. The nonlinear creep law implemented in Vampire uses wheel-rail contact data files in forms of two tables. One table contains the contact data with respect to the lateral displacement and the other, optional table, the contact data with respect to the yaw angle of the wheelset relative to the track. For a straight track or very large curve radii the contact data for zero yaw angle should be used.

The table describing the contact data as a function of the lateral displacement gives precisely the position of the contact point. It involves the left and right wheel contact radii, the contact angles, the longitudinal, lateral and vertical positions of the contact surface as well as the area of the contact ellipse and its semi-axes ratio a/b. According to the Hertz theory, the contact area and the ratio of the ellipse semi-axes depend also on the axleload. The calculation of the table is performed for static axleloads and dynamic wheelloads are taken into account by supplying a factor on the static load.

For each time step during the numerical integration process the lateral displacement of the wheelset is calculated. It is then used for a linear interpolation of the contact data table in order to obtain the contact point parameters needed for the calculation of the creepages. Finally, the friction forces are obtained from the relation between creepage and friction forces.

If the full non-linear contact theory of Kalker is used the creep forces are calculated by interpolating the tabulated creepage-force relation. Consequently, for each time step the procedure can be divided into three steps: the location of the contact point, the calculation of the creepages and the calculation of the friction forces. A good introduction to the theories developed by Kalker for the wheel-rail contact is given in [107]. For more information it is referred to the papers of Kalker [46],[44] and [45].

2.3.2 Modelling of the suspension elements

The suspension elements have an outstanding influence on the dynamic behaviour of the vehicle. A proper modelling is therefore an important requirement for accurate model results.

In the TGV train different types of suspension elements are used. From the design drawing in figure 2.16 the suspension elements are identified: the primary suspension of the power car is composed by vertical coil springs, guidance springs and a vertical damper. In the secondary suspension, vertical coil springs as well as vertical, lateral, and anti-yaw dampers are used. In the carrying bogies, the function of the guidance spring is fulfilled by a motion link. In the secondary suspension, air springs are used instead of coil springs in order to obtain a better comfort.

The suspension has to meet several criteria. One is the attenuation of the vibrations of the wheelset caused by track irregularities. The other concerns the running stability of the vehicle. As shown before for the bogie model, the stiffness of the suspension in longitudinal direction determines the critical speed at which the hunting movement occurs. Therefore, in order to ensure running stability up to very high speeds the value of the longitudinal stiffness in the primary suspension of the TGV is important.

The modelling of the suspension elements is complicated. From test rig measurements of suspension elements, it is known that some show a considerable nonlinear behaviour. In these tests the suspension element is mounted in a test rig and excited by a known displacement with varying amplitudes and

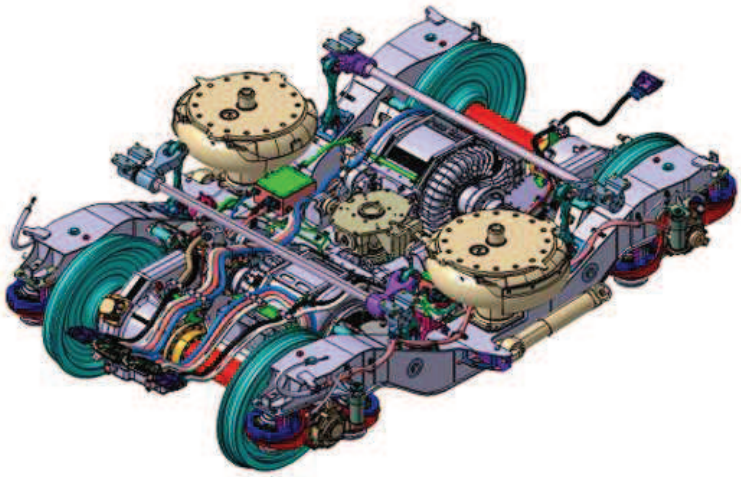

Figure 2.16: Motor bogie of a high speed train (source: Alstom)

frequencies. From the measured spring forces, the spring characteristic is identified as a function of amplitude and frequency. The results stand as a basis for the modelling of the suspension element.

In literature, test rig measurements for different suspension elements and dampers can be found. Generally, the setup for the experimental testing of the dynamic properties is similar. The test component is mounted in a servo-hydraulic test machine between two masses. While one is fixed, the other is excited by a piston imposing a defined displacement on the suspension element. The motion and the force of the suspension element are measured by displacement sensors and load cells respectively. From these data the displacement-force curves and stiffnesses can be analyzed as functions of the amplitude and frequency of the piston displacement.

For example, in [95] rubber spring elements are analyzed. The dependence between displacement and force and the dynamic stiffness are measured in a test rig and compared to results received from a material model. Dynamic tests with different amplitudes have been performed over a frequency range from 1 to 100Hz. Some results are shown in figure 2.17.

In the following sections the different suspension elements of the TGV train are described and approaches for their modelling presented. The focus lies in the modelling and implementation of these elements in Vampire. The physical principles, results of test rig measurements if available and derivation

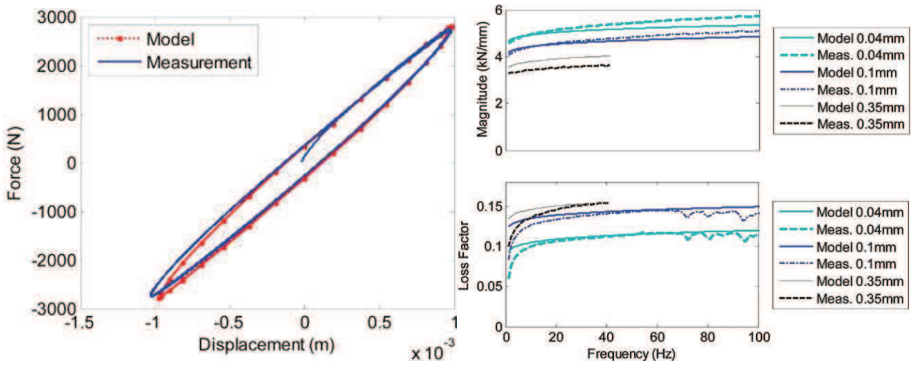

(a) (b)

Figure 2.17: Rubber bushing: measured and modeled hystereis loop (a), magnitude and dynamic loss factor for dynamic stiffness (b)

of model equations can be found in the appendix B.

2.3.2.1 Air spring model

The air spring is a complicated thermodynamic system composed of variable volumes and interconnecting pipes. It takes advantage of the compressibility of the air. The reasons for the widespread use of airsprings in railway vehicles lie in the possibility to control the height by changing the pressure level and the progressive stiffness characteristic. Besides, self-damping can be achieved by an orifice between the air bellow and the reservoir. Due to the air flow in the orifice the airspring system has non-linear characteristics. The dynamic response depends on the amplitude as well as the frequency.

The general structure of an air spring system is shown in figure 2.18. The coupling between the bogie and the car body is provided by the air spring bellows (6). The stiffness of the air spring in the vertical direction is inversely proportional to the volume. By adding air reservoirs (2) and (5) to the bellow volume, the spring stiffness is reduced. Depending on the orifice in the pipe (4) between the bellow and the reservoir self damping is achieved. The compressor (1) and the level controller (3) provide the required air pressure in the system.

The modelling of the air spring is based on the thermodynamic equations describing the air exchange between the bellow and the reservoir. Important work has been performed by Krettek [55] and Grajnert [29]. Their thermo-

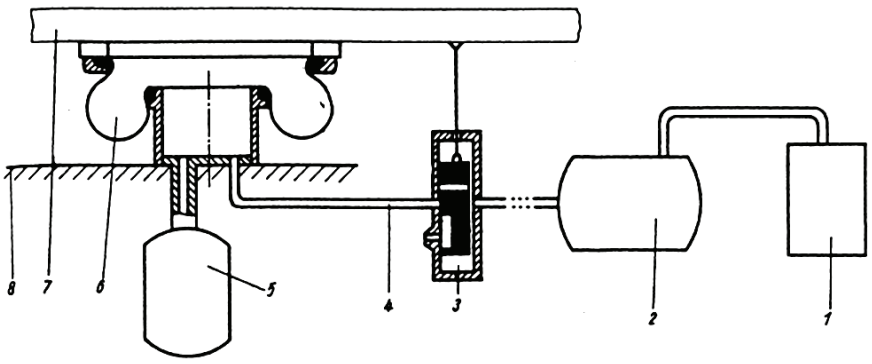

Figure 2.18: Airspring (1: compressor, 2: main air reservoir, 3: level controller, 4: pipe, 5: auxiliary air reservoir, 6: air spring, 7: car body, 8: bogie (from [32])

dynamic model describes most accurately the dynamic behaviour of the air spring and forms the basis to the air spring models in ADAMS rail ([30] and [61]) and Simpack. A short introduction to this model can be found in the appendix B.

Vampire provides a special air spring element. It belongs to the group of the shear elements tending to model suspension elements where large vertical loads are carried with lateral flexibility. The airspring model is divided into a vertical and a lateral model which are to a large extent independent from each other. The vertical air spring model is shown in figure 2.19.

It is based on the model developed by Nishimura and Oda [70] extended by a mass. The model is simpler than the complete thermodynamic model proposed by Krettek. It does not describe the heat and mass flow relations between the bellow and the reservoir. The calculation of the spring stiffness is based on the ideal gas law. The spring rate c_z is given by:

$$c_z = \frac{dF_z}{dz} \tag{2.41}$$

The vertical force F_z is calculated from the pressure difference p_Δ between the system pressure p and the atmospheric pressure p_a and the effective spring surface A_e giving:

$$c_z = \frac{dF_z}{dz} = \frac{d}{dz}(p_\Delta A_e) = p_\Delta \frac{dA_e}{dz} + \frac{dp_\Delta}{dz} A_e = p_\Delta \frac{dA_e}{dz} + \frac{dp}{dz} A_e \tag{2.42}$$

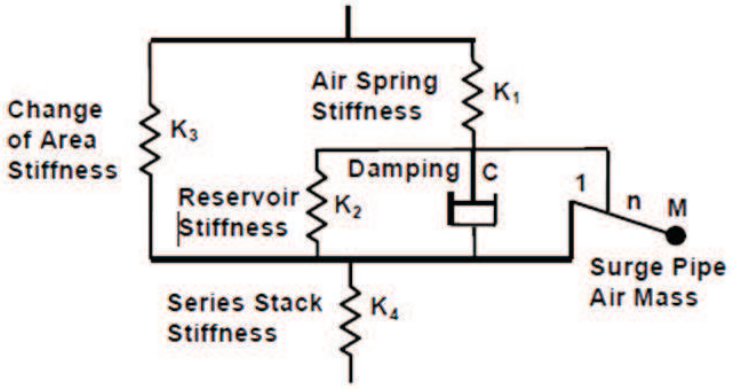

Figure 2.19: Vertical airspring model implemented in Vampire

with $p = p_a + p_\Delta$.

The pressure differential $\frac{dp}{dz}$ is calculated from the ideal gas law:

$$p_1 V_1^n = p_2 V_2^n = constant \tag{2.43}$$

In this equation n is the polytropic rate. Its value depends on the process. If the heat generated during compression is immediately dissipated the process is isothermal and the value of n is 1. In the air spring, due to the fast compression, only a small part of the heat is dissipated. Therefore the air spring is much better described by an adiabatic process so that the polytropic rate becomes the isentropic factor κ given by the ratio of the heat capacity at constant pressure (C_p) to the heat capacity at constant volume (C_V). For air κ is 1.4.

Differentiating the ideal gas law with respect to z and solving the equation for $\frac{dp}{dz}$ with $A_e = -\frac{dV}{dz}$ gives:

$$\frac{d}{dz}(pV^\kappa) = p\kappa V^{\kappa-1}\frac{dV}{dz} + \frac{dp}{dz}V^\kappa = 0 \tag{2.44}$$

$$\frac{dp}{dz} = \frac{-p\kappa V^{\kappa-1}\frac{dV}{dz}}{V^\kappa} = \frac{p\kappa A_e}{V} \tag{2.45}$$

Inserting the result for $\frac{dp}{dz}$ in equation (2.42) gives the spring rate :

$$c_z = \kappa p\frac{A_e^2}{V} + p_\Delta\frac{dA_e}{dz} \tag{2.46}$$

Taking into account that the total volume is composed of the bellow and the reservoir volume two stiffness terms are obtained which are in series in the model. Besides, a damping term is added taking into account the flow resistance caused by the surge pipe. It depends on the flow resistance coefficient R_f, the gravitational acceleration g and the diameter of the surge pipe and is given by:

$$C = R_f A_e^2 pg \tag{2.47}$$

The vertical air spring model in Vampire is extended by a fourth stiffness in series with the Nishimura model representing the stiffness of a series rubber element. Besides, the inertia of the air mass in the pipe is taken into account by the Vampire model represented by the parameter nM. Even though the mass is small the large flow velocities in the pipe can lead to important inertia effects. The final model parameters are: K_1: stiffness of the air bellow, K_2: stiffness of the reservoir, K_3: stiffness change due to variable effective spring area and C: orifice damping. A level controller is not considered in this model.

$$K_1 = \kappa p \frac{A_e^2}{V_{bellow}} \tag{2.48}$$

$$K_1 = \kappa p \frac{A_e^2}{V_{reservoir}} \tag{2.49}$$

$$K_3 = p_\Delta \frac{dA_e}{dz} \tag{2.50}$$

The Vampire air spring element also includes a model for the horizontal behaviour of the air spring shown in figure 2.20. The lateral spring characteristic is determined by the stiffness of the air bellow material. It shows the characteristic of rubber spring elements with nonlinear stiffness and hysteresis. The parameters of the model are the nonlinear lateral stiffness K_y, the hysteresis force F_h, the hysteresis exponential distance constant α, the lateral damping rate C_y and the lateral damping series stiffness K_c.

The model parameters are estimated from technical information about the air spring system and test rig measurements performed by the supplier. However, due to incomplete information, difficulties appear. The geometric parameters like the bellow and reservoir volumes and the length of the pipe are available. For the parameters of the lateral model, notably the nonlinear stiffness, the hysteresis force and the damping, the estimation is more difficult. From the supplier results from test rig measurements are available but

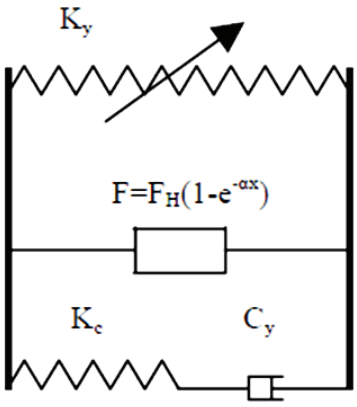

Figure 2.20: Lateral airspring model implemented in Vampire

not extensive. Often these measurements are performed for static charges and do not represent the dynamic behaviour of the air spring.

Figure 2.21a shows the lateral nonlinear stiffness of the air bellow. In 2.21b the dependence of the effective air spring area A_e from the air pressure is shown.

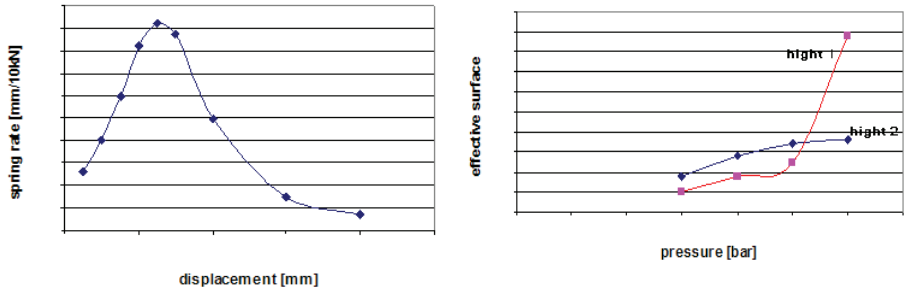

(a) (b)

Figure 2.21: Test rig measurements of air spring: lateral stiffness (a), effective spring area as a function of pressure for different heights (b)

The initial estimation of the parameter values is the main difficulty for all presented models. If the values are not or incompletely given by the supplier the experimental determination of these values in a test rig is the most accurate approach for their identification. If test rig measurements can not be

performed the parameter estimates are exclusively obtained from the physical and technical properties of the system. This is the aim pursued in [75].

2.3.2.2 Coil springs

Coil springs are used in the primary and secondary suspension. They are made by a wire with a circular cross section shown in figure 2.22 (a).

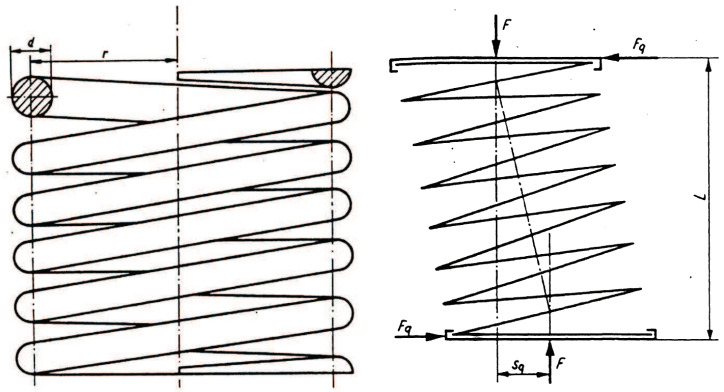

(a) (b)

Figure 2.22: Cylindrical coil spring (a), Transversal stiffness due to Flexicoil effect (b) [32]

Their spring characteristic is approximately linear and is calculated from the material shear modulus G, the number of windings i, the wire diameter d and the diameter of the spring r:

$$c = \frac{d^4 G}{64 i r^3} \tag{2.51}$$

The spring rate in transversal direction is described by the Flexicoil effect represented in figure 2.22b. It is caused by lateral displacements of the air spring. Notably in the secondary suspension of the power unit this effect is important since the coil springs have to compensate the longitudinal displacements due to the yaw movement of the bogie in curves. In the primary suspension this effect is less important since the wheelset is guided in longitudinal direction by the stiff guidance springs. Beside the spring parameters named above, the transversal stiffness depends on the vertical force and is described by the relations:

$$c_x = c_y = \frac{1}{\frac{1}{F_z}(\frac{2}{x}tan\frac{1}{2}xL - L) + \frac{L}{S}} \tag{2.52}$$

with the coefficients:

$$x = \sqrt{\frac{F_z}{B(1 - \frac{F_z}{S})}} \tag{2.53}$$

$$S = 3360\frac{Ld^4}{ir^3} \tag{2.54}$$

$$B = 1460\frac{Ld^4}{ir} \tag{2.55}$$

In the Vampire model the coil spring of the primary and secondary suspension is modelled by a shear element with constant stiffness in the vertical and transversal directions. Shear elements are suitable for the representation of suspension components which carry a static load and provide flexibility in directions perpendicular to this load. This is the case for the flexicoil spring described above.

The dynamic behaviour of the shear spring element is described by six stiffness values: the longitudinal, lateral and vertical stiffnesses as well as the roll bending, pitch bending and torsional stiffness. From figure 2.23 the definition of the lateral stiffness is apparent: it is given by the ratio between the lateral force F and the lateral displacement y and can be calculated from equation (2.52) presented above.

$$c_x = c_y = \frac{F}{y} \tag{2.56}$$

The bending stiffness illustrated in figure 2.23b is defined as:

$$c_\theta = \frac{M_1}{\theta_1} = \frac{M_2}{\theta_2} \tag{2.57}$$

Considering the structure of the TGV bogie it can be assumed that the supporting areas of the coil spring are always in parallel. The bending stiffness is therefore neglected in the model.

2.3.2.3 Hydraulic damper

Coil and air springs do not have sufficiently internal damping. It is necessary to connect hydraulic dampers in parallel. The damping is created by the flow

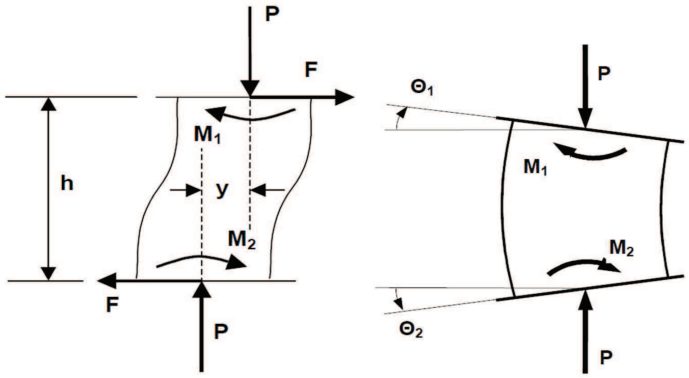

Figure 2.23: Computation of the lateral stiffness (a) and bending stiffness (b) in Vampire (from: [103])

resistance of the oil when pressed through an orifice. In [32] the functional principle of the hydraulic damper is described. The design of a hydraulic damper used in the TGV is shown in figure 2.24. It shows the oil flow between the volumes in the damper for the compression and expansion process.

The velocity force relation of a hydraulic damper is nonlinear. As an example, figure 2.25 shows the measured nonlinear velocity-force characteristics of the transversal damper of the secondary suspension. More measured damper characteristics for the TGV are included in the appendix B.

In Vampire the hydraulic damper is modelled by a viscous damping element (pinlink) shown in figure 2.26. The damping characteristic is given as a nonlinear relation between compression velocity and damping force. For the dampers of the TGV model measured nonlinear damper characteristics are available. In addition a constant stiffness c is defined in parallel.

The position of the damper element is described by the x and y position and the height above the rail for each end. The axis in which the force acts depends on the relative position of the bodies the damper is attached to. Moments can not be transmitted.

2.3.2.4 Rubber spring elements

Rubber spring elements are used at several positions in the TGV train. In the primary suspension of the power unit the guidance springs are made

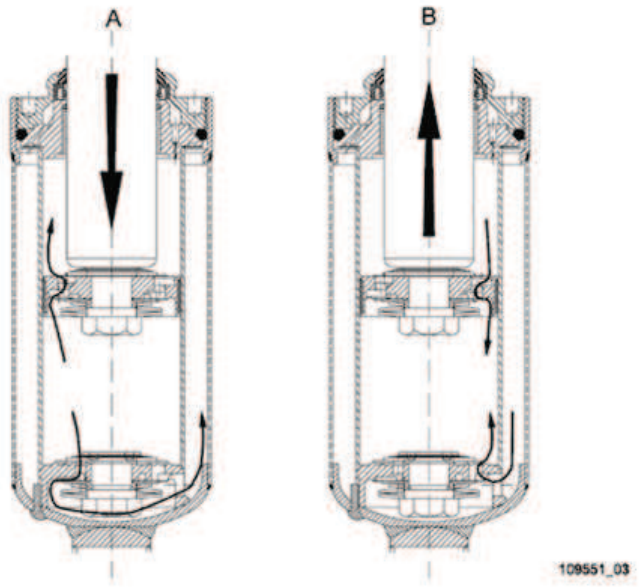

Figure 2.24: Oil flow in a hydraulic damper: compression (a) and expansion (b)

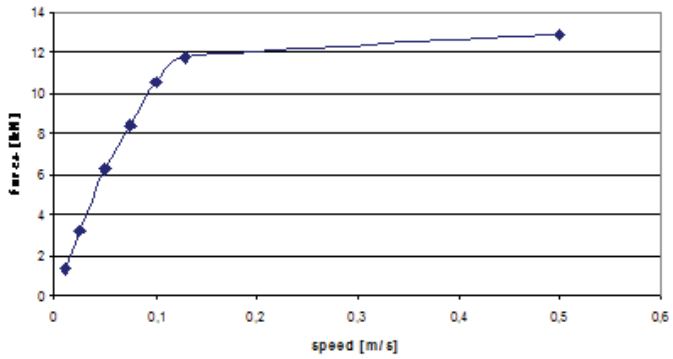

Figure 2.25: Nonlinear damping velocity-force characteristics for the transversal damper of the secondary suspension

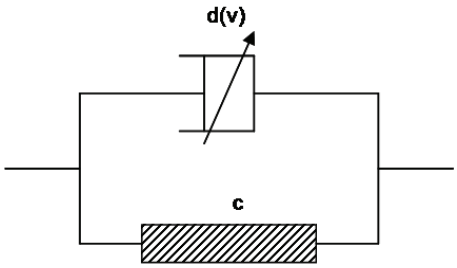

Figure 2.26: Vampire model of hydraulic damper with nonlinear damping d(v) and linear series stiffness c

from rubber. They are composed of steel and rubber segments. As shown in figure 2.27, the displacement-force characteristic of rubber elements is nonlinear and shows a hysteresis. It depends on the deformation rate and the deformation amplitude. The model has to reproduce the dynamic behaviour for the frequency range of interest.

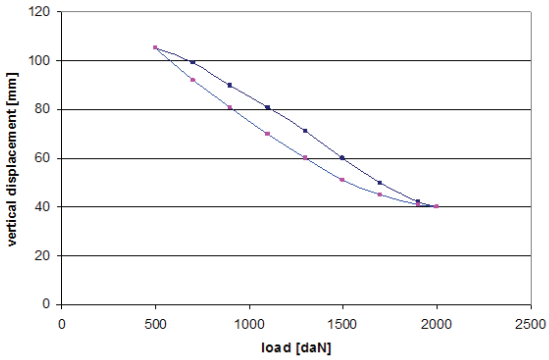

(a)

(b)

Figure 2.27: Load-displacement measurement of power car guidance spring (a), guidance spring in primary suspension (b)

The simplest model for rubber spring elements is the Kelvin-Voigt model composed of a spring and viscous damping in parallel. The spring rate amplitude dependence is not taken into account.

The modelling can be improved by using the generalized Maxwell element presented in figure 2.28. By adding more spring-damper elements in parallel

the accuracy of the model is improved. In return the number of parameters for the identification process increases.

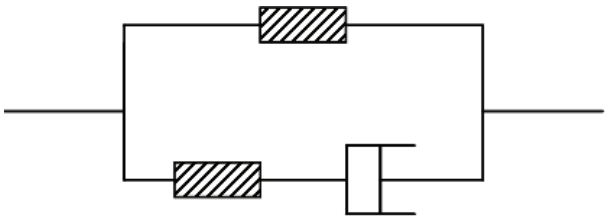

Figure 2.28: Generalized maxwell element

In literature more complex models for rubber elements can be found. Berg [7] presents a nonlinear model which takes into account the dependence of the spring rate on the deformation velocity and amplitude. The model is described by three forces which are superposed: an elastic force, a visco-elastic force and a friction force.

In Vampire the bush element is proposed for the modelling of rubber spring elements. It is a Maxwell model with 18 parameters: the stiffness, damping and series stiffness for all six degrees of freedom.

2.3.3 Model properties

The structure of the TGV Duplex model is represented in figure 2.29. It is composed of two traction units (M1 and M2) and 8 carriages (R1 to R8). Each traction unit rests on two bogies (A,B,C,D) while for the carriages Jacobs bogies are used. The car bodies and bogies frames are described by 6 degrees of freedom respectively. Due to the constraint of the wheel-rail contact each wheelset has only two degrees of freedom. In total the number of degrees of freedom of the TGV train is 300.

The model parameters which may be considered in the identification are summarized in appendix B. They can be distinguished in mass and inertia parameters and parameters of the suspension. The suspension parameters are classified in primary and secondary suspension for the traction units and carriages. In total 117 parameters are considered assuming that all elements of the same type have the same parameter value. If all elements are considered independently the number of model parameters increases significantly.

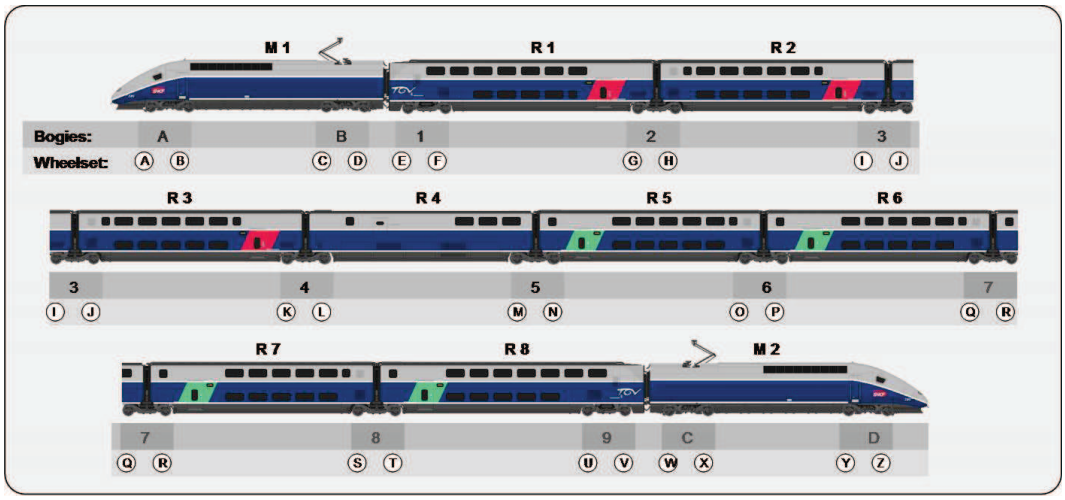

Figure 2.29: Structure of the TGV Duplex model

2.4 Summary of the system and model properties and conclusions

Two models have been selected which will be used for the following parameter identification: a model of a single bogie implemented in Matlab and the model of a complete TGV train. According to their intended use the models have different properties. For the bogie model the complete mathematical description is known allowing the application of the adjoint state gradient calculation. The suspension is modeled by a stiffness and damping element per direction, leading to a low number of parameters. Since measurements for a single bogie have not been performed an identification on real measurement data is not possible. Instead the simulation results of a Vampire bogie model will be used as virtual experimental data.

The TGV model is designed to reproduce the dynamic behaviour of the real train. The parameter identification will be performed on real measurement data. This requires the detailed modelling of the suspension elements leading to more than 100 different parameters in total. The parameters of the wheel-rail contact are not considered.

The properties of the two models are summarized in table 2.2.

Model properties		
Property	TGV model	Bogie model
Model type	▷ Multi-body ▷ Representing physical structure ▷ Degrees of freedom > 300 ▷ Black box	▷ Multi-body ▷ Representing physical structure ▷ Degrees of freedom $= 10$ ▷ Model equations known
Parameters	▷ Physical meaning ▷ Suspension ▷ Masses, Inertia ▷ Number > 100	▷ Physical meaning ▷ Suspension ▷ Masses, Inertia ▷ wheel-rail contact ▷ Number $= 16$
Track irregularity	▷ Real track irregularities ▷ Analytical track irregularities	▷ Analytical track irregularities
Nonlinearities	▷ not linear in inputs ▷ not linear in outputs	▷ not linear in inputs ▷ not linear in outputs

Table 2.2: Comparison of model properties for the TGV and the bogie model

Chapter 3

Application of the parameter identification to the bogie model

After the two multi-body models have been selected one can turn toward the second step of modelling: the parameter identification. It represents the focus of this work. The aim is to identify the parameters of the model so that the simulation results coincide best with the measured results. Outgoing from an initial estimation of the model parameters the identification algorithms seek to minimize the difference between model and simulation results expressed by a misfit function. This requires the coupling between an optimization algorithm and the model. At each step the optimization algorithm updates the parameter vector. Then the model is evaluated for the updated parameters and the misfit function calculated. The principle of the parameter identification is shown in figure 3.1.

The principal aim of this work is to propose an approach for the identification of the TGV suspension parameters. However, from the previous chapter it is known that the TGV model implemented in Vampire is exposed to important restrictions. Due to the black box characteristic of the software the dynamic equations of the model are not accessible. Besides, the complexity of the model might complicate the application and analysis of the identification. Therefore a second much simpler model of a bogie has been realized as a first step. It takes into account the wheel-rail contact and explains the nonlinear dynamics of the railway vehicle.

Following this approach the parameter identification will be first applied to the suspension parameters of the bogie model (c_x,c_y,c_z,d_x,d_y,d_z) outlined in

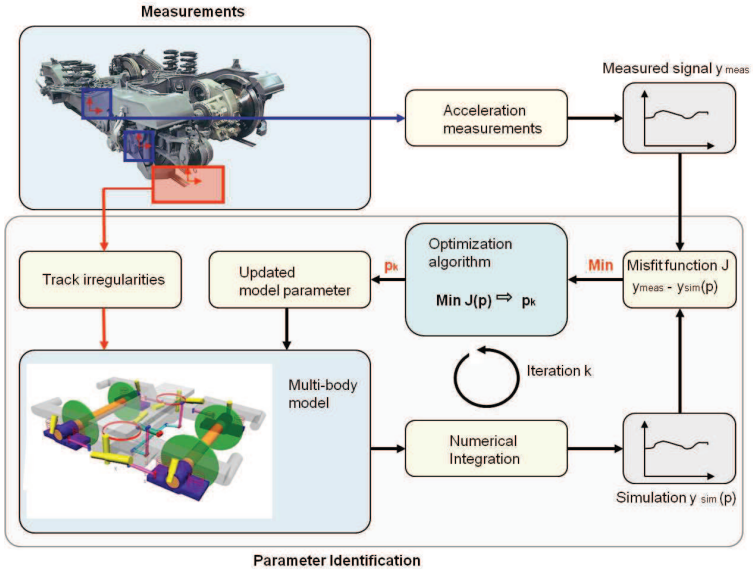

Figure 3.1: Principle of parameter identification

table 2.1. It is the aim of this chapter. The known mathematical description allows the application of all identification methods of interest. The results and their relevance for the TGV model are discussed. The application of the parameter identification on the TGV model will then be treated in chapter 4.

The structure of this chapter therefore follows one aim: outgoing from the defined problem, the bogie model, the different steps of the parameter identification procedure are applied. Even though this work focuses on some aspects of the identification procedure which will be discussed more in detail it is indispensable for the understanding to present the complete identification procedure.

The first step outlined in section 3.1 is the definition of the misfit function. As virtual experimental data, reference simulations of the Matlab model as well as the Vampire bogie model for nominal parameters values will be used. Misfit functions considering a different number of vehicle response degrees of freedom are compared.

In a second step all suspension parameters which have an influence on the misfit function have to be identified. This is done by a sensitivity analysis applied to the bogie model in section 3.2. Suspension parameters with a negligible influence on the vehicle response are not taken into account in the

following identification.

When the misfit function criterion is chosen and the relevant parameters are defined from the sensitivity analysis, one can turn to the optimization. It consists in identifying the parameter values which minimize the misfit function. The relevant methods are applied to the bogie model in section 3.3.

3.1 Definition of a misfit function as a norm of the distance between model prediction and measurements

The identification of the parameters is performed by minimizing a scalar misfit function with respect to the model parameters. The choice of the misfit function is an important step since the precision of the identified parameter values depends on the misfit function.

From section 2.1 it is known that the bogie model is described by 10 degrees of freedom: the lateral displacement and yaw rotation for the wheelsets and all 6 degrees of freedom for the bogie frame.

$$x_{model} = (r_{bx}, r_{by}, r_{bz}, \delta_{bx}, \delta_{by}, \delta_{bz}, u_{e1y}, u_{e2y}, \delta_{e1z}, \delta_{e2z})^T \tag{3.1}$$

The degrees of freedom used in the misfit function have been varied. In general, since virtual experimental data obtained from a simulation is used, all degrees of freedom are available. Of course, in the case of real measurements only some degrees of freedom are measured.

Two types of virtual measurement data are used in the identification: the simulation result of the Matlab model obtained for nominal parameter values and the simulation result of the Vampire bogie model outlined in section 2.3. Since the Vampire model does not have the same structure a identification on these data is adequate for validating the method.

The quality of the measured data which might motivate the exclusion of a perturbated channel will be considered for the TGV model where the identification is based on real measurement data. For the bogie model where a reference simulation replaces the measurements this aspect has no importance. The same holds for the choice of the frequency range. Since the measured and the modeled response are both the result of a simulation they

are valid in the same frequency domain.

As outlined in chapter 1 different misfit function criteria are available: the least squares criterion, the least modulus criterion and the maximum likelihood criterion. The last one should be generally the first choice if the measurements are corrupted by noise and if the characteristic of the noise is known. For the bogie model the virtual measurement data has not been corrupted by noise. In this case the adequate choice for the misfit function criteria is therefore the least squares methods. By adding white noise to the simulated vehicle response the influence of measurement noise on the simulation result can be studied. In this case misfit function criteria which take into account the noise should be used.

If less importance should be laid to large errors between measured and simulated results the least modulus criterion has to be used. Figure 3.2 shows the least square and least modulus criterion for the vertical displacement of wheelset 1 u_{e1y} of the bogie model.

One can see that for the least modulus method the amplitude differences between the peaks are smaller while for the least square method the large errors are amplified.

The misfit function used here is normalized with the integral of the square of the measured signal x_{meas}:

$$J_{ls}(t,p) = \frac{\int_0^T \|x_{meas}(t) - x_{model}(t,p)\|^2 dt}{\int_0^T \|x_{meas}(t)\|^2 dt} \tag{3.2}$$

This allows to evaluate the quality of the model and the improvement obtained by the parameter identification.

3.1.1 Analysis of the misfit function solution surface

For the application of optimization methods the characteristics of the misfit function plays an important role. It is described by a solution surface with a number of dimensions equal to the number of parameters. In order to visualize the solution surface the misfit function is in the following calculated as a function of the two suspension parameters c_x and c_y for the bogie model. Of course, the computation and plotting of the misfit function surface is not realizable in practice. The number of parameters and the high computational cost render this impossible therefore requiring the use of optimization

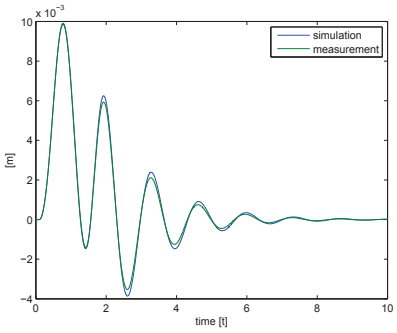

(a) measured (green) and simulated (blue) direct response for dof 7

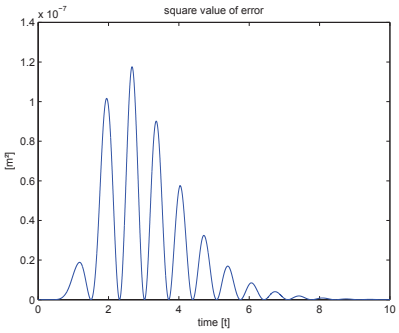

(b) least square criterion between measured and simulated response of dof 7

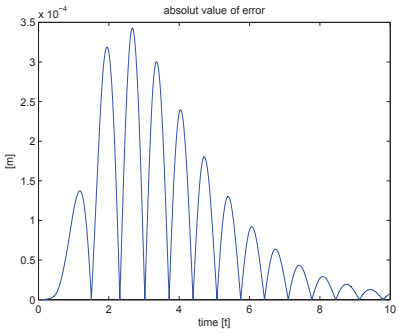

(c) least modulus criterion between measured and simulated response of dof 7

Figure 3.2: Definition of the misfit function from the least square and least modulus criterion

methods.

Figure 3.3a shows the misfit function as a function of the stiffnesses c_x and c_y. The solution surface is characterized by a curved valley with several local minima. This can disturb the convergence of the optimization algorithm. Due to the small gradient and local disturbances in the valley the solution is not unique and depends on the chosen initial values.

In order to improve the convergence of the optimization algorithm a Tikhonov regularization is applied. The properties of an ill-posed inverse problem and the Tikhonov regularization have been outlined in chapter 1. It consists in adding a regularization term to the misfit function:

$$\begin{aligned} J_{ls}([c_x, c_y]) = & \underbrace{\frac{1}{2}\int_0^T \|x_{meas}(t) - x_{model}(t, [c_x, c_y])\|^2 dt}_{\text{solution surface without regularization}} \\ + & \underbrace{\frac{1}{2}\alpha \|[c_x, c_y] - [c_{xinitial}, c_{yinitial}]\|^2}_{\text{solution surface of regularization term introduces bias}} \end{aligned} \tag{3.3}$$

By doing so a convex surface is added to the solution surface of the non-regularized misfit function from figure 3.3a with the aim to obtain a distinct minimum. In return a bias error is introduced in the solution. The choice of the regularization factor α is not trivial. If α is chosen too small the regularization has no influence on the solution surface and the problem remains ill-posed. Instead, a too large α has the effect that the convex surface dominates the regularized misfit function forcing the parameters to converge to the initial values $p*$.

How to choose a suitable value of the regularization parameter? Since the solution surface of the misfit function is known a simple and obvious approach is the trial and error approach. The solution surface of the regularized misfit function is calculated for different values of α and compared with the non-regularized misfit function. Figures 3.3b to 3.3e shows the regularized misfit function for $\alpha = 1$ (3.3b), $\alpha = 0.1$ (3.3c), $\alpha = 0.01$ (3.3d) and $\alpha = 0.001$ (3.3e) for the parameter values:

Parameter values [m/s]			
True values		Initial values	
c_x	c_y	c_x	c_y
5.2e7	3.5e6	4.7e7	3.2e6

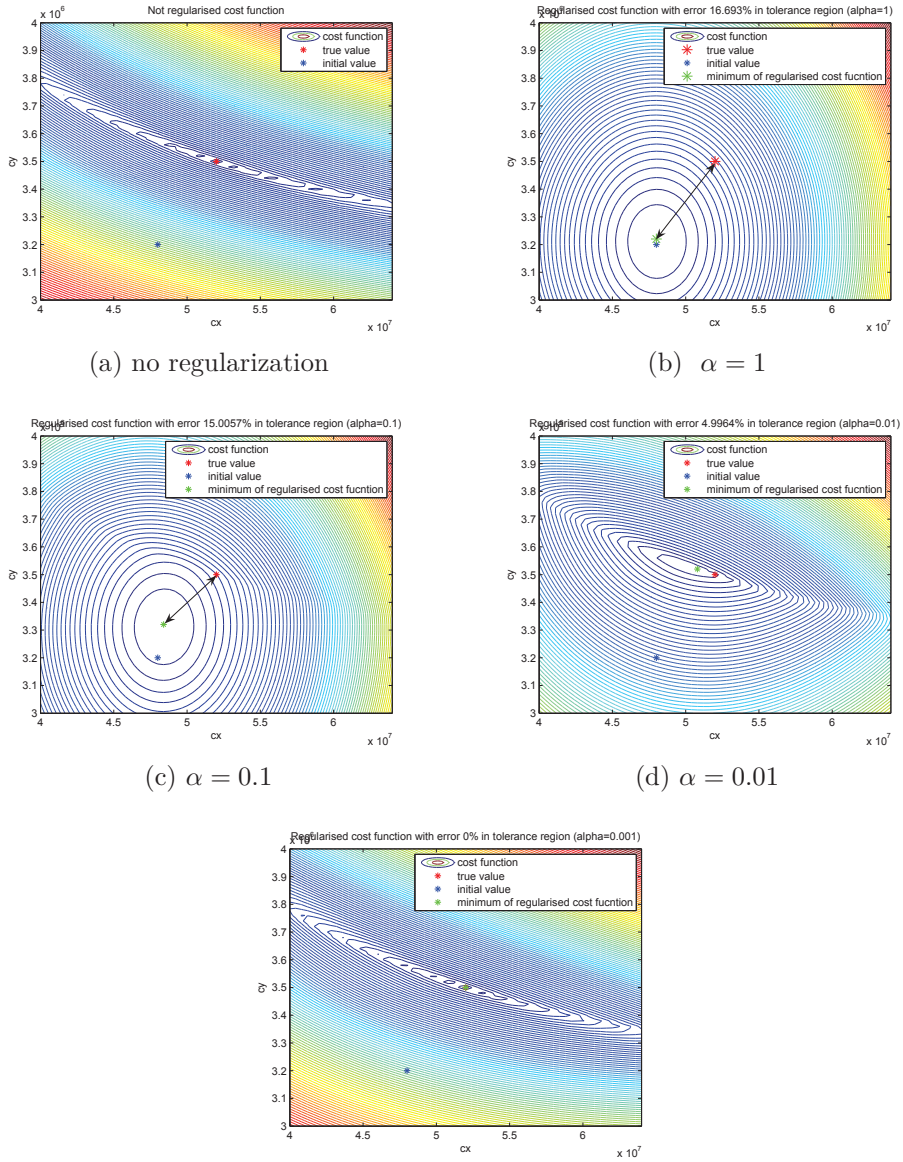

(a) no regularization

(b) $\alpha = 1$

(c) $\alpha = 0.1$

(d) $\alpha = 0.01$

(e) $\alpha = 0.001$

Figure 3.3: Regularization of the misfit function relative to c_x and c_y for different values of the regularization parameter α

For the choice of the suitable α several criteria are considered. One concerns the form of the solution surface. For $\alpha = 1$, $\alpha = 0.1$, $\alpha = 0.01$ the valley with its local minima is avoided and a convex misfit function with one minimum obtained. However, more important is to estimate the error introduced by the regularization. The parameter values and the misfit function values of the regularized misfit function are therefore compared with the non-regularized function. For $\alpha = 1$ and $\alpha = 0.1$ the distance between the true parameter values and the parameter values at the minimum of the regularized misfit function is with 16% important. The same holds for the value of the cost function. The choice $\alpha = 0.01$ represents a good compromise. The regularized misfit function is convex and the errors in the parameter values and the misfit function value are with 5% small.

However, when choosing the value of the regularization factor it has to be considered that the result depends strongly on the initial parameter values. Figures 3.4a and 3.4b show the regularized misfit function for two different initial parameters.

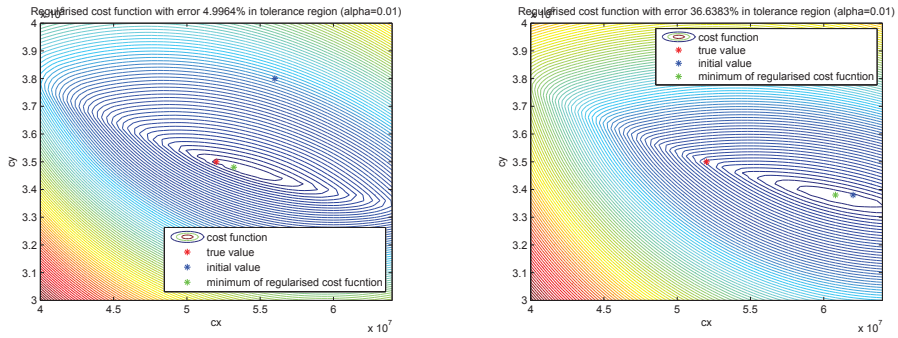

(a) $\alpha = 0.01$, $c_x = 5.7e7$, $c_y = 3.8e6$ (b) $\alpha = 0.01$, $c_x = 6.2e7$, $c_y = 3.38e6$

Figure 3.4: Regularized misfit function for different initial parameter values

It can be seen that an initial value situated in the valley leads to a larger error relative to the true value than an initial value outside the valley.

The comparison of the non-regularized and regularized misfit functions for different values of α is not convenient. It requires the misfit function to be known a priori and is time consuming. Therefore, in chapter 1 an approach was presented which allows to determine the regularization parameter as a function of the noise level in the measurement data. The Morozov's discrepancy principle [2] is based on the idea that the error between model and

measurements can not be smaller than the noise corrupting the measurement data. It is therefore reasonable to choose a regularization factor which causes a bias of the same dimension as the measurement noise.

The discrepancy principle is applied to the misfit function J relative to c_x and c_y even though the used virtual measurement data is not corrupted by noise. For a supposed noise level δ one seeks the value for α which fulfils the condition:

$$J_{non-regularized}(p_{opt}(\alpha)) - \delta = 0 \tag{3.4}$$

where $p_{opt}(\alpha) = arg \;\; min J_{regulaized}(p, \alpha)$.

The determination of the root of equation 3.4 is performed numerically with the function *fzero*. Each iteration requires the minimization of the regularized misfit function in order to obtain the optimized parameter vector p_{opt}. The principle is illustrated in figure 3.5.

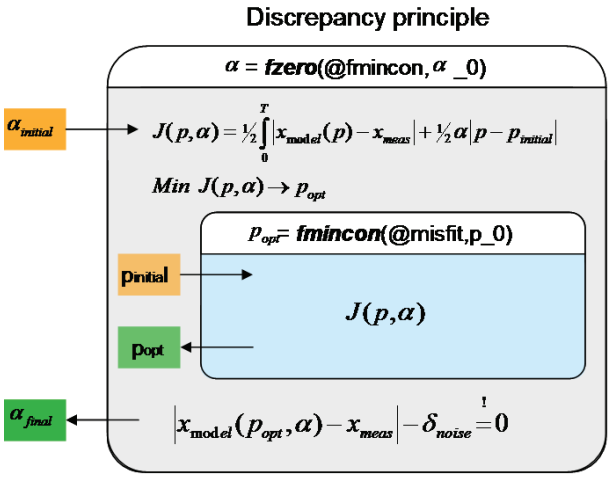

Figure 3.5: Determination of the regularization factor from the discrepancy principle

Figure 3.7 shows the value of α for different values of the noise level.

However, if the solution surface of the misfit function is not known a priori and/or if it is depending on more than two parameters a numerical mini-

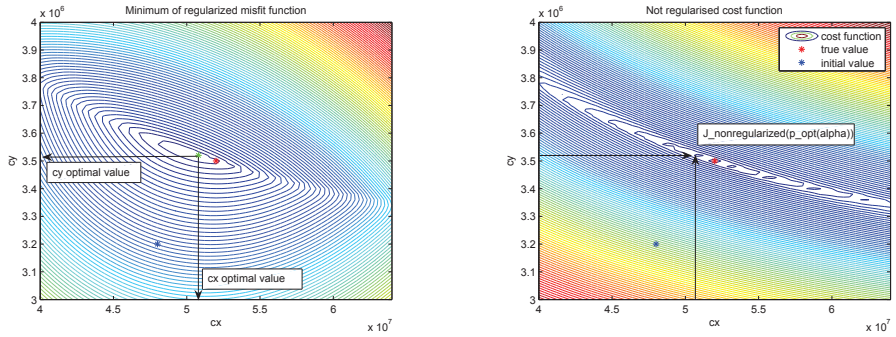

(a) Optimized parameter values for cx and cy from minimum of regularized misfit function

(b) Value of nonregularized misfit function for optimize parameter values of cx and cy

Figure 3.6: Application of the discrepancy principle for the determination of the regularization factor α

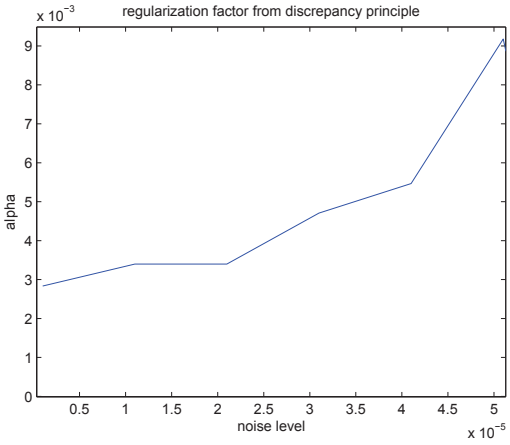

Figure 3.7: Regularization factor α as a function of the noise level δ calculated from the discrepancy principle

mization is required.

The analysis of the misfit function solution surface for the simple two parameter case illustrates a difficulty for the parameter identification. Several local minima appear which will perturb the convergence of optimization methods. If more than two parameters are considered in the misfit function hypersurfaces with order k are obtained. A way to avoid or reduce the effect of local minima is the regularization.

3.1.2 Technical constraints for the suspension parameters

The parameters of the bogie model represent physical properties of the primary suspension. Their values are therefore restricted to a range given by the tolerance of the suspension element.

As outlined in chapter 1 the tolerances lead to inequality constraints. They indicate that the parameters can only take values in a certain range. In figures 3.8a and 3.8b the effect of constraints on the solution space of the misfit function is demonstrated. In figure 3.8a the global minimum is situated in the tolerances while in figure 3.8b it is outside indicating an insufficient model description.

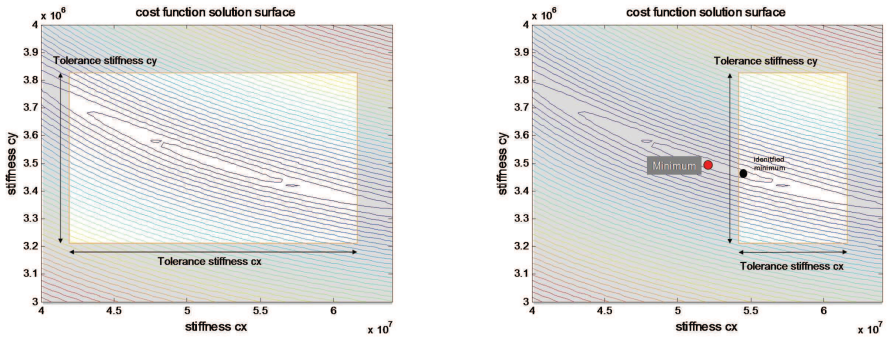

(a) Unequality constraints for stiffnesses c_x and c_y

(b) Global minimum outside of tolerances

Figure 3.8: Parameter constraints on the solution surface of the misfit function

In the optimization the parameters tolerances are taken into account by ap-

plying a constrained optimization algorithm. In addition to the function to be minimized the constraints on the parameter values have to be defined.

3.2 Parameter identifiability testing based on sensitivity analysis

When the misfit function of the bogie model is calculated relatively to all suspension parameters c_x, c_y, c_z, d_x, d_y and d_z (figures 3.10a to 3.11b) two observations can be made: first, the effect of the parameters on the misfit function is very unequal. Some parameters have almost no influence on the misfit function. And secondly, the influence of one parameter on the misfit function can depend strongly on the values of the other parameters indicating a coupling between them. Both effects have to be considered in the identification.

Parameters which have an effect on the misfit function are called identifiable. For the bogie model the identifiability is evaluated by performing a sensitivity analysis as described in chapter 1. As a result of the sensitivity analysis a reduced model is obtained which includes only the identifiable parameters. All other parameters are fixed at their nominal values. The procedure is illustrated in figure 3.9.

The sensitivity analysis is based on a simple principle: the simulation is repeated for different values of one or several parameters and the influence on the misfit function is compared. In chapter 1 local and global sensitivity methods were distinguished. Since the bogie model is nonlinear and the effect of the parameters coupled, both types of methods are applied.

In section 3.2.1 the results of the local screening method are presented. They complete the result for the misfit function relatively to the parameters c_x and c_y already used in section 3.1.1.

The coupling between the parameters due to the nonlinear structure of the model is taken into account by performing a global sensitivity analysis. In section 3.2.2 the results of the Morris method are outlined.

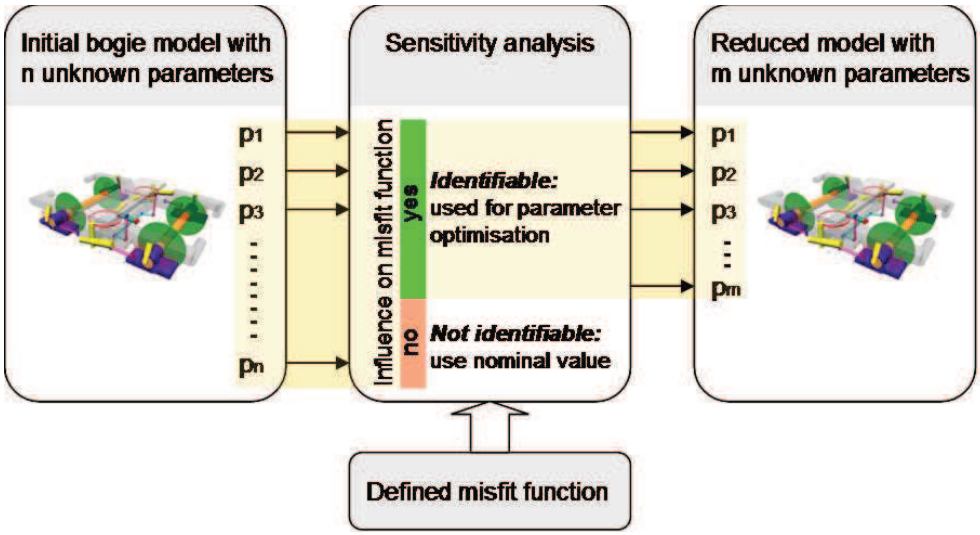

Figure 3.9: Model reduction: Selection of identifiable parameters using a sensitivity analysis

3.2.1 Application of the screening method

The screening of the misfit function is performed relatively to two parameters consecutively providing a three-dimensional solution surface. It has already been used for the analysis of the misfit function solution surface relative to the stiffnesses c_x and c_y in section 3.1.1. In this section the result for all suspension parameters of the bogie model is presented. Their nominal value, minimal and maximal values are given in table 3.1:

Stiffness parameters [N/m]				**Damping parameters [Ns/m]**			
parameter	Values			parameter	Values		
	nominal	min	max		nominal	min	max
c_x	5.2e7	4e7	6.4e7	d_x	300	200	400
c_y	3.5e6	3e6	4e6	d_y	300	200	400
c_z	0.5e6	1e6	1.5e6	d_z	1.2e4	0.7e4	1.7e4

Table 3.1: Parameter values of the bogie model used for the screening method

The misfit function is defined using all 10 degrees of freedom of the bogie model.

For the stiffnesses c_x-c_y, c_x-c_z and c_y-c_z the results shown in figure 3.10 are obtained.

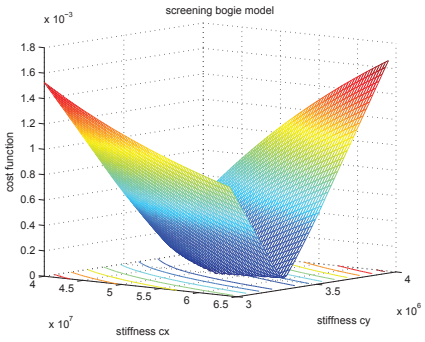

(a) Misfit function surface for c_x and c_y, c_z fixed at nominal value

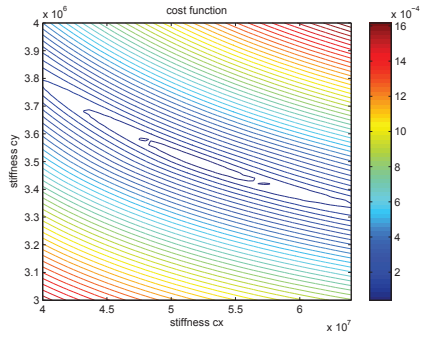

(b) Misfit function contour for c_x and c_y, c_z fixed at nominal value

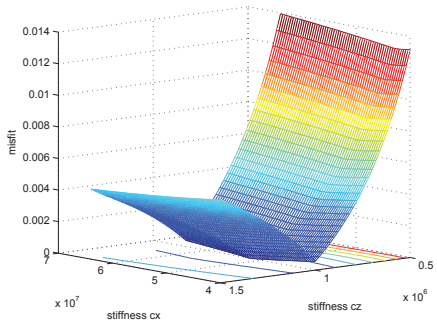

(c) Misfit function surface for c_x and c_z, c_y fixed at nominal value

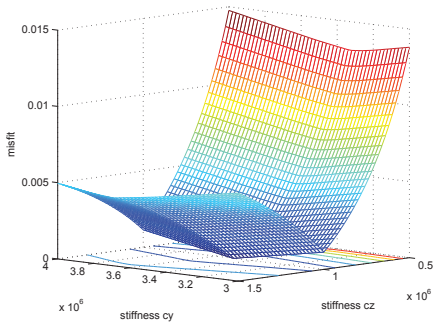

(d) Misfit function surface for c_y and c_z, c_x fixed at nominal value

Figure 3.10: Two-parameter screening for the stiffnesses c_x-c_y, c_x-c_z and c_y-c_z

As already known the misfit function relative to the stiffnesses c_x and c_y is described by a curved valley indicating a nonlinear coupling between these parameters (figures 3.10a and 3.10b). The result of the screening relative to the stiffnesses c_x-c_z and c_y-c_z reveals that the effect of the parameters on the misfit function is unequal. The vertical stiffness is much more important.

The results of the screening relative to the damping parameters d_x-d_y and d_x-d_z are given in figures 3.11a and 3.11b.

It is found that the influence of the damping parameters on the misfit function is also very unequal. The damping d_z and d_y have much higher influence

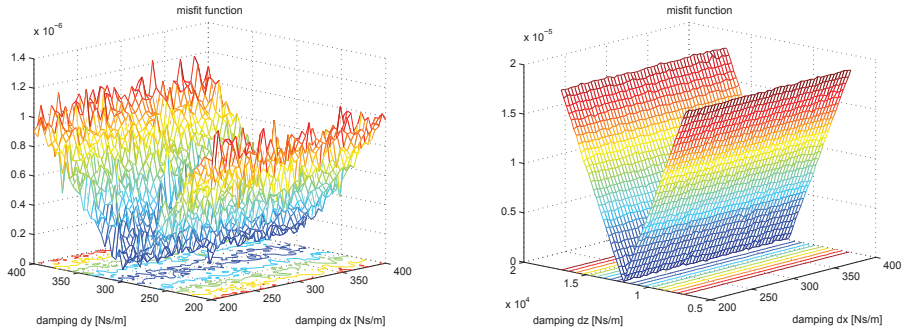

(a) Misfit function surface for d_x and d_y, d_z fixed at nominal value

(b) Misfit function surface for d_x and d_z, d_y fixed at nominal value

Figure 3.11: Two-parameter screening for the stiffnesses d_x-d_y and d_x-d_z

than the damping d_x. However, more important is the fact that the influence of the damping on the misfit function is in general negligible compared to the stiffnesses. It is 2 to 3 orders of magnitude smaller. Besides, the solution surface of the misfit function relative to d_x-d_y is very perturbed.

3.2.2 Sensitivity analysis taking into account the parameter interaction

The coupling between more than two parameters can not be taken into account by the local screening method. In order to do so global methods have to be used. Therefore the Morris method which has been presented in chapter 1 is applied to the bogie model also. It proposes two measures: one which represents the overall effect of the parameter and another estimating the second and higher order effects of the parameter.

The Morris method is applied to the stiffness and damping parameters of the secondary suspension defined in table 3.2. The misfit function is defined using all 10 degrees of freedom of the bogie model.

The result of the Morris method is given by a point for each parameter in a two dimensional graph. On the abscissa the average and on the ordinate the standard deviation of the elementary effect $\nabla^n_{p_i} J = \frac{J(p_{n+1})-J(p_n)}{\Delta p}$ are shown. They represent the overall effect of each parameter and the coupling between them respectively.

Stiffness parameters [N/m]				**Damping parameters [Ns/m]**			
Parameter	Values			Parameter	Values		
	nominal	min	max		nominal	min	max
c_x	5.2e7	4e7	6.4e7	d_x	300	200	400
c_y	3.5e6	3e6	4e6	d_y	300	200	400
c_z	0.5e6	1e6	1.5e6	d_z	1.2e4	0.7e4	1.7e4

Table 3.2: Parameter values of the bogie model used for the Morris method

$$\mu_{p_i} = \sum_{n=1}^{r} \nabla_{p_i}^n J/r \qquad \sigma_{p_i} = \sqrt{\sum_{n=1}^{r} (\nabla_{p_i}^n J - \mu_{p_i})^2/r} \tag{3.5}$$

The sampling procedure which consists in varying randomly step by step each parameter of the initial parameter vector according to the procedure described in chapter 1 is repeated r times. The choice of r determines with which precision the overall effect and the coupling of each parameter are identified. In order to estimate the scattering of the Morris method for a given r the calculation is repeated several times with the same r.

First the Morris method has been repeated 20 times with $r = 10$ for the parameters c_x and c_y. The result is shown in figure 3.12 a. It shows a large dispersion reducing the reliability of the results. Therefore the number of sampling has been successively increased. Figure 3.12 b shows the result of 20 calculations for $r = 50$.

Figure 3.13 shows the result of the Morris method for 50 samplings. The calculation has been repeated 20 times in order to estimate the dispersion of the result. For all suspension parameters the dispersion lies between 20 and 30%. The result of the Morris method is coherent with the result obtained by the screening. The lateral stiffness c_y has the highest influence on the vehicle response. The variance indicates a important coupling with the other parameter values. If the coefficient between the variance and the mean is calculated for the parameters c_x, c_y and c_z approximately the same value is found. The influence of the damping parameters is negligible.

From the sensitivity analysis two conclusions for the following parameter identification are made:

- Due to the negligible influence on the misfit function and the perturbed solution surface an identification of the damping parameters of the

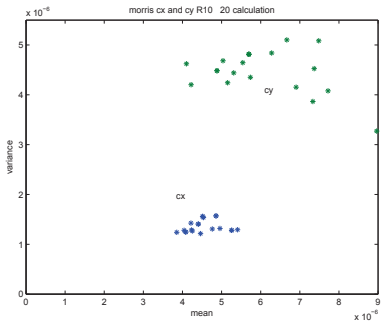

(a) Morris method for c_x and c_y: 20 calculations for r=10

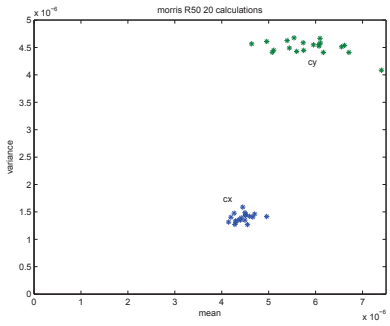

(b) Morris method for c_x and c_y: 20 calculations for r=50

Figure 3.12: Morris method for the parameters c_x and c_y for two different values of r

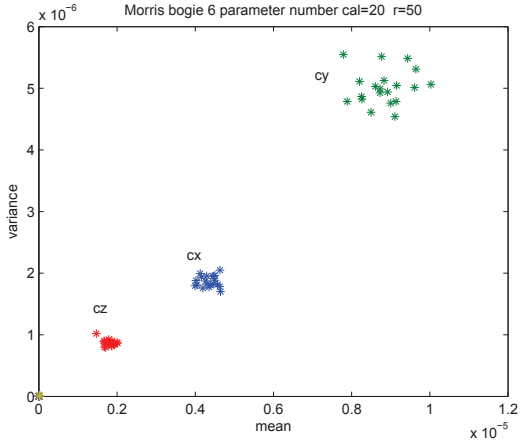

Figure 3.13: Result of the Morris method for the suspension parameters c_x, c_y, c_z, d_x, d_y and d_z

bogie model is not possible. They are therefore excluded from the identification process.

- The coupling between the parameter values is not negligible requiring all parameters to be considered simultaneously in the optimization.

3.3 Minimization of the misfit function by applying adequate optimization methods

After the definition of a misfit function and the extraction of the identifiable model parameters the optimization can be applied. It is the crucial step of the parameter identification and aims at minimizing the misfit function in order to identify the parameter values of the model.

The sensitivity analysis showed that among the suspension parameters of the bogie model only the three stiffnesses c_x, c_y and c_z are identifiable. In contrast to the Vampire model with a large number of parameters the computational cost is therefore less important.

In the following sections suitable optimization methods are applied to the bogie model. Their performances are tested and compared. This may provide important information for the later application on the TGV model.

From the sections 3.1.1 and 3.2 important informations about the properties of the misfit function have been obtained. They have to be taken into account when applying the optimization methods and are shortly summarized here. If possible the consequences for the choice of the optimization method are outlined likewise:

- **Unequal effect of the suspension parameters on the misfit function**:
  From the sensitivity analysis in section 3.2 it is found that the influences of the stiffnesses c_x, c_y and c_z on the misfit function are different. This leads to small gradients in one direction compared to another and might perturb the convergence of the optimization algorithm. By regularizing the misfit function the convergence can be improved.

- **Different dimensions of the suspension parameters**:
  The dimensions of the stiffnesses c_x, c_y and c_z differ considerably. A normalization of the parameter vector with the vector of the initial parameters can improve the convergence .

- **Constraints on the parameter values**:
  The constraints on the parameter values due to the tolerances have to be taken into account by the optimization algorithm. If unconstrained optimization methods lead to parameter values outside the tolerances constrained optimization methods have to be used.

- **Existence of local minima**:
  The solution surface of the misfit function relative to the stiffnesses c_x and c_y in figure 3.10a revealed the existence of local minima. Depending on the initial parameter values local optimization methods described in chapter 1 can therefore converge to the local instead of the global minimum. As outlined in section 3.1.1 this can be avoided by regularizing the misfit function or by the use of global optimization methods.

An introduction to the different optimization methods which are considered in this work can be found in chapter 1.

3.3.1 Application of local methods

The screening analysis in section 3.2.1 showed that the regularized misfit function of the bogie model relative to the stiffnesses has a smooth solution surface with only one minimum. The local minima which occur in the valley of the misfit function relative to c_x and c_y can be avoided by regularizing the misfit function.

It is therefore possible to solve the parameter identification problem for the suspension parameters c_x and c_y by the use of local optimization methods. As outlined in chapter 1 local methods use the misfit function value and its derivatives at the considered point allowing generally a faster convergence than global methods. For the bogie they should be preferred.

3.3.1.1 Application of the Pattern Search method as a gradient-free local optimization method

The suspension parameters of the bogie model c_x and c_y are identified using the Pattern Search method. It has been chosen due to its good convergence properties and a simple algorithmic structure. A description of this gradient-free direct method can be found in chapter 1.

Initial step length The two control parameters of the algorithm, the step size h_i and the direction vector v_i are adapted to the misfit function during the minimization process. However, the convergence speed depends strongly on the choice of the initial step length which should be adapted to the problem. If the initial step length is chosen too small many iterations are needed in order to increase them. Besides, too small step sizes can cause convergence problems if the misfit function surface is perturbated forming a solution surface with many local minima. Therefore, different initial step lengths have been tested for the bogie model.

In order to visualize the optimization in the misfit function solution surface the pattern search method is applied to the parameters c_x and c_y for different initial step lengths (table 3.3). The parameters c_z, d_x, d_y and d_z are held constant at their nominal values.

Stiffness parameters [N/m]						
Parameter	Values				Initial step length	
	true	initial	min	max	step1	step2
c_x	5.2e7	4.5e7	4e7	6.4e7	5e4	5e3
c_y	3.5e6	3.2e6	3e6	4e6	5e3	5e2

Table 3.3: Parameter values used for the Pattern search method

The misfit function is defined using all 10 degrees of freedom of the bogie model.

The parameter values for each iteration are plotted in the misfit function solution surface shown in figure 3.14.

The result shows the effect of two different initial step lengths. If the solution surface of the misfit function is irregular containing local minima, as it is the case here, a small stepsize can lead to convergence problems. By choosing a sufficiently large stepsize this can be avoided since perturbances and local minima on the solution surface are not visible. An alternative is to use the regularized misfit function from figure 3.3d.

3.3.1.2 Identification with gradient methods

The Pattern Search method is a direct method and does not take advantage of the derivatives of the misfit function for the determination of the search

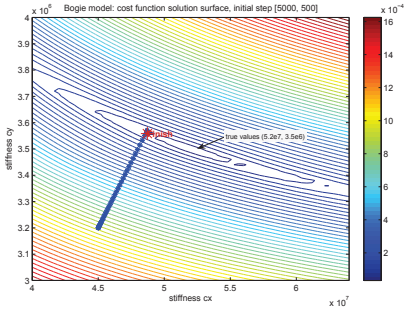

(a) Short stepsize

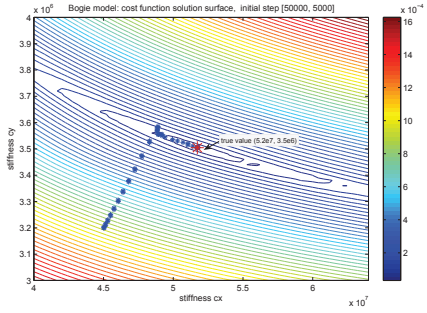

(b) Large stepsize

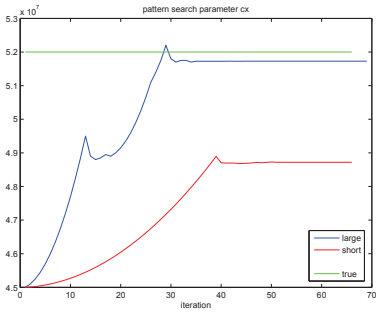

(c) Parameter value c_x as a function of iteration steps

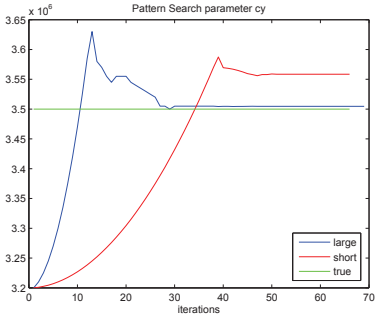

(d) Parameter value c_y as a function of iteration steps

Figure 3.14: Application of the Pattern search method for the parameters c_x and c_y using two different initial step lengths

direction. It is therefore interesting to apply also gradient methods to the bogie model. Since they use also information about the derivatives a faster convergence should be obtained.

From chapter 1 it is known that many different gradient methods can be distinguished. For the optimization of the bogie model Newton and Trust region methods are applied. They are implemented in the Matlab function *fmincon* which is adapted to the solution of nonlinear constrained optimization problems. By using an analytically calculated misfit function gradient - the available methods are outlined in the following sections - the trust region method can be applied to the bogie model. It belongs to the large scale option and is adapted to optimization problems with a large number of parameters.

Important numerical control parameters of the optimization algorithms are the relative and absolute error tolerances defined in Matlab by the variables *TolX* and *TolFun*. By reducing *TolX* and *TolFun* the precision but also the computational cost are increased. This might be necessary if the misfit function is very flat and the small gradient values lead to an early termination of the minimization. Besides, the choice of the initial values has an important influence on the convergence of the algorithm. If several local minima exist as it is the case for the non-regularized misfit function relatively to c_x and c_y the algorithm will, depending on the initial values, converge to the closest local minimum.

The function *fmincon* is applied to the identification of the spring stiffnesses c_x and c_y. The parameters c_z, d_x, d_y and d_z are held constant at their nominal values. The cost function is defined using all 10 available degrees of freedom of the bogie model.

The stiffnesses and the corresponding tolerances have the values given in table 3.4.

The optimization is performed for the Newton and Trust-region method with and without regularization as summarized in table 3.5 (with: TolFun: Termination tolerance on the function value; TolCon: Termination tolerance on the constraint violation; TolX: Termination tolerance on parameter values). For the Newton method the Hessian matrix is calculated using the BFGS method.

In the following the result for each configuration is illustrated by the param-

Stiffness parameters [N/m]				
Parameter	Values			
	true	initial	min	max
cx	5.2e7	4.5e7	4e7	6.4e7
cy	3.5e6	3.2e6	3e6	4e6

Table 3.4: Parameters used for the application of the gradient methods to the bogie model

Optimization parameter					
Cal.	α	Method	TolFun	TolCon	TolX
1	no	Newton method	1e-100	1e-100	1e-100
2	no	Trust-region-reflective	1e-100	1e-100	1e-100
3	0.01	Newton method	1e-100	1e-100	1e-100

Table 3.5: Control parameters of the gradient methods

eter values on the solution surface of the misfit function and the decrease of the misfit function as a function of the iteration steps.

- *Calculation 1: Direct minimization with Newton method*

  The misfit function is not regularized and has several local minima. The convergence of the Newton-method is analysed for two different initial parameter sets with the values $[c_x = 4.5e7N/m, c_y = 3.2e6N/m]$ and $[c_x = 5.8e7N/m, c_y = 3.2e6N/m]$ as shown in figure 3.15. Both optimizations converge to the closest local minimum but not to the global minimum indicated by the red circle on the misfit function solution surface.

- *Calculation 2: Trust-region method*

  The trust-region method is applied to the initial parameter set $[c_x = 4.5e7N/m, c_y = 3.2e6N/m]$ in figure 3.16. It converges to the global minimum by requiring a low number of iteration steps.

- *Calculation 3: Tikhonov regularization*

  In order to improve the convergence of the algorithm the Tikhonov regularization is applied to the problem. The regularization parameter is determined with the discrepancy principle as outlined in section 3.1.1. For the given initial point figure 3.17 shows the relation between the

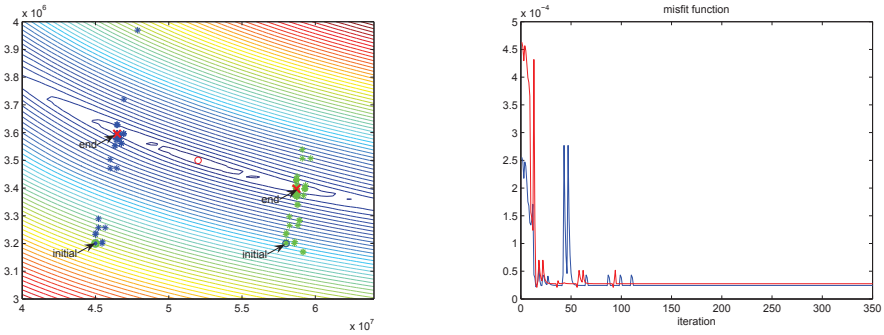

(a) parameter values on misfit function solution surface

(b) misfit function

Figure 3.15: Calculation 1: Newton method for two initial parameter sets, no regularization

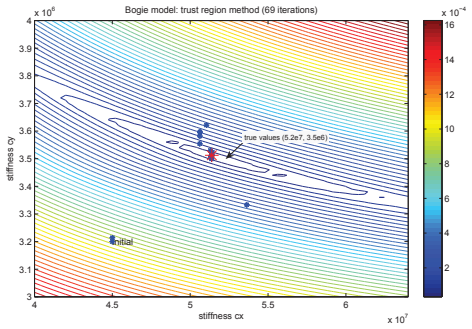

Figure 3.16: Calculation 2: Trust-region reflective method, no regularization

noise level on the measurement data and the regularization factor alpha.

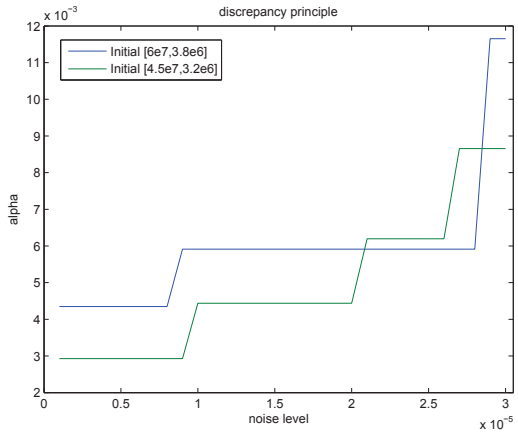

Figure 3.17: Regularization factor as a function of the noise level for the used initial parameter value

For a real system the noise level can be estimated from a statistical analysis of the measurement data. Since for the bogie model measurement data is not available and a reference simulation is used instead the noise level is zero. A choice of the regularization parameter leading to a bias of the same order as the noise level is therefore not possible. The regularization factor is chosen from knowledge of the misfit function solution surface so that local minima are avoided.

If the misfit function is regularized with $\alpha = 0.01$ a smooth solution surface with one minimum is obtained. The local Newton method (interior point) therefore converges to the global minimum of the regularized problem shown in figure 3.18b. Nevertheless, the misfit function (figure 3.18a) does not decrease to zero and the identified parameter values (figure 3.18c and 3.18d) differ slightly from the true values. This bias is due to the error introduced by the regularization.

The three optimizations show the performances and limits of local optimization methods. The convergence is fast. The trust-region method converges after less than 70 iteration steps. For the non-regularized Newton method the convergence is obtained after 120 iterations. The regularization of the misfit function reduces the required iterations to around 40. The limitation of the

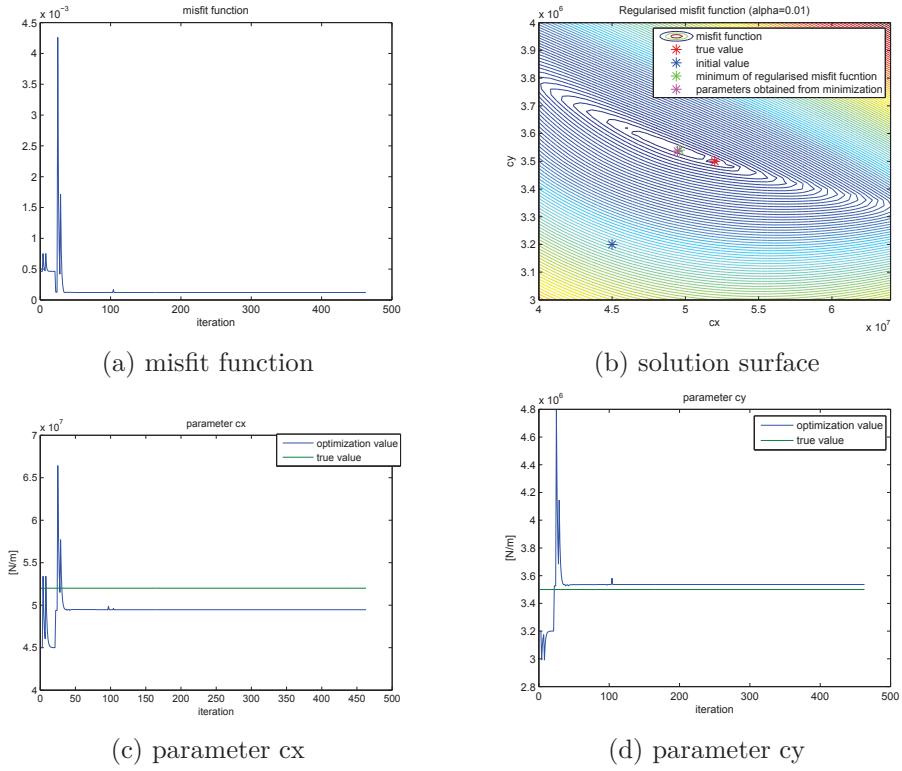

(a) misfit function

(b) solution surface

(c) parameter cx

(d) parameter cy

Figure 3.18: Calculation 3: Newton method with finite differences gradient and regularization $\alpha = 0.01$

local methods is the already evoked fact that they are not suitable for optimization problems with many local minima. In the first example the Newton method converges to different local minima as a function of the initial conditions. Here, the trust region method converges to the global minimum but in general it has the same limitation in common with the other local methods.

Even though the number of iteration steps is low for the gradient methods the calculation times can increase significantly for large models. This is due to the numeric calculation of the gradient necessary at every iteration.

3.3.2 Explicit calculation of the gradient

The gradient methods necessitate the calculation of the gradient. From chapter 1 it is known that for complex systems with a large number of parameters the gradient calculation can represent the most expensive step in the optimization algorithm. In this case the choice of an adapted method for the calculation of the gradient is crucial.

For the bogie model described by a small number of parameters the cost required for the computation of the gradient is less relevant. The application of different methods for the calculation of the gradient is nevertheless a focus of this work and of this chapter in particular. The potential of the gradient calculation methods is studied on the bogie model with regards to the model of the complete train. As outlined in the next chapter the complete TGV train is described by several hundred parameters if the parameter values are considered to be independent. The cost required for the calculation of the gradient with respect to each parameter becomes important.

Of course a simple but rarely the best way for obtaining approximated numerical values of the misfit function gradient is the finite differences method. For the parameter value p the gradient is estimated by evaluating the misfit function at one or two other points aside. In equation (3.6) the misfit function values at p and $p + h$ are used:

$$D_{+h}J(p) = \frac{J(p+h) - J(p)}{h} \tag{3.6}$$

For a large number of parameters this method is very costly. Besides, the choice of the steplength h is difficult. If h is too large, then truncation errors become significant. Even if h is optimally chosen, the derivative of the misfit function J will be accurate to only about 1/2 or 2/3 of the significant digits

of J.

Therefore alternative calculation methods should always be taken into account. If the equations of motion describing the system are available analytical approaches can be used. In chapter 1 two approaches for complex nonlinear systems have been proposed: the adjoint state method which is in particular adapted to systems with a large number of parameters and the automatic differentiation method.

3.3.2.1 Gradient calculation from adjoint state approach

The gradient methods applied to the bogie model in section 3.3.1.2 require the calculation of the misfit function gradient relative to the unknown parameters. The aim of the adjoint method outlined in this section is to calculate the gradient of the misfit function $J(p)$ in an analytical way requiring less computational cost than the numerical calculation.

The minimization of the misfit function requires the zero value of the gradient $\nabla_{p_i} J(\mathbf{p})$:

$$\nabla_{p_i} J(\mathbf{p}) = \nabla_{p_i} \frac{1}{2} \int_0^T \|\mathbf{x}_{meas}(t) - \mathbf{x}_{model}(t,p)\|^2 dt \quad for\ i = 1...n \tag{3.7}$$

n: number of parameters

The misfit function depends on the parameters p_i through the response $\mathbf{x}(\mathbf{p})$ of the bogie model. The total derivative of the misfit function with respect to the parameters p_i is therefore:

$$\frac{dJ}{dp_i} = \frac{\partial J}{\partial p_i} + \nabla_{\mathbf{x}} J(\mathbf{p}) \frac{d\mathbf{x}}{dp_i} \tag{3.8}$$

with the gradient relative to x: $\nabla_{\mathbf{x}} = [\frac{\partial}{\partial x_1}, ..., \frac{\partial}{\partial x_n}]$: gradient

The derivatives $\frac{d\mathbf{x}}{dp_i}$ of the result of the forward model $\mathbf{x}$ with respect to the parameters p_i are not known. Due to the complexity of the nonlinear model a straightforward calculation is not feasible.

In order to overcome this problem the following approach is used: instead of minimizing the misfit function J the stationarity of the Lagrangian equation L given by the sum of the misfit function and the state equation along with a Lagrange multiplier is sought. This is possible since the stationarity of

the Lagrangian equation implies the minimization of the misfit function. It is supposed that the variables $\mathbf{p}$, $\mathbf{x}$ and $\mathbf{z}$ in the Lagrange equation are independent giving the derivative:

$$dL(\mathbf{p},\mathbf{x},\mathbf{z}) = \nabla_p L(\mathbf{p},\mathbf{x},\mathbf{z})d\mathbf{p} + \nabla_x L(\mathbf{p},\mathbf{x},\mathbf{z})d\mathbf{x} + \nabla_z L(\mathbf{p},\mathbf{x},\mathbf{z})d\mathbf{z} \tag{3.9}$$

In the following this approach is illustrated for the bogie model. In chapter 2 the nonlinear equation of motion was found to be:

$$\mathbf{M}(\mathbf{x},\mathbf{p})\ddot{\mathbf{x}}(t) + \mathbf{F}(\mathbf{x},\dot{\mathbf{x}},\mathbf{p},t) = 0 \tag{3.10}$$

From the Lagrangian equation L the gradient and the adjoint state equations are calculated. The Lagrangian equation has the form:

$$L = J(\mathbf{p},\mathbf{x}) - \int_0^T (\mathbf{z}^T, (\mathbf{M}(\mathbf{x},\mathbf{p})\ddot{\mathbf{x}}(t) + \mathbf{F}(\mathbf{x},\dot{\mathbf{x}},\mathbf{p},t)))dt = \mathbf{0} \tag{3.11}$$

For the misfit function $J(\mathbf{p},\mathbf{x})$ displacement, velocities or acceleration signals can be used. The derivative of the Lagrange equation relatively to the parameters $\mathbf{p}$ gives the gradient equation $\nabla_p L$. It does not depend on the signal type used in the misfit function. If the Tikhonov regularization is used as outlined in chapter 1 a regularization term is added to the misfit function. It depends on $\mathbf{p}$ giving a gradient equation:

$$\nabla_p L = \alpha(\mathbf{p} - \mathbf{p}_{initial}) - \int_0^T ((D_p \mathbf{M}\ddot{\mathbf{x}})^T \mathbf{z} + D_p \mathbf{F}^T \mathbf{z})dt \tag{3.12}$$

In order to minimize the misfit function the Lagrange equation gradient $\nabla_p L(\mathbf{p},\mathbf{x},\mathbf{z})$ must vanish and provides the optimal parameters:

$$\nabla_p L(\mathbf{p},\mathbf{x},\mathbf{z}) = \mathbf{0} \tag{3.13}$$

The derivative of the Lagrangian equation with respect to $\mathbf{x}$ gives the adjoint state equation:

$$\int_0^T \mathbf{z}^T (D_{\mathbf{x}} \mathbf{M}\ddot{\mathbf{x}}\delta\mathbf{x})dt + \int_0^T \mathbf{z}^T (\mathbf{M}\delta\ddot{\mathbf{x}})dt + \int_0^T \mathbf{z}^T (D_{\mathbf{x}} \mathbf{F}\delta\mathbf{x})dt + \int_0^T \mathbf{z}^T (D_{\dot{\mathbf{x}}} \mathbf{F}\delta\dot{\mathbf{x}}) = \int_0^T (\mathbf{x} - \mathbf{x}_{exp})^T \delta\mathbf{x} dt \tag{3.14}$$

The right-hand term in (3.14) describes the derivative of the misfit function $J(\mathbf{p},\mathbf{x})$ relatively to $\mathbf{x}$. It depends on the type of signal used in the misfit function. Here the displacement of the model and measurement are used.

Alternatively the misfit function can be defined using the velocities or accelerations. For this description the three cases are outlined in parallel and are denoted by (a), (b) and (c). The adjoint equations for the three cases are given by:

(a) displacement

$$\int_0^T \mathbf{z}^T(D_{\mathbf{x}}\mathbf{M}\ddot{\mathbf{x}}\delta\mathbf{x})dt + \int_0^T \mathbf{z}^T(\mathbf{M}\delta\ddot{\mathbf{x}})dt + \int_0^T \mathbf{z}^T(D_{\mathbf{x}}\mathbf{F}\delta\mathbf{x})dt + \int_0^T \mathbf{z}^T(D_{\dot{\mathbf{x}}}\mathbf{F}\delta\dot{\mathbf{x}}) = \int_0^T (\mathbf{x}-\mathbf{x}_{exp})^T\delta\mathbf{x}dt \tag{3.15}$$

(b) velocity

$$\int_0^T \mathbf{z}^T(D_{\mathbf{x}}\mathbf{M}\ddot{\mathbf{x}}\delta\mathbf{x})dt + \int_0^T \mathbf{z}^T(\mathbf{M}\delta\ddot{\mathbf{x}})dt + \int_0^T \mathbf{z}^T(D_{\mathbf{x}}\mathbf{F}\delta\mathbf{x})dt + \int_0^T \mathbf{z}^T(D_{\dot{\mathbf{x}}}\mathbf{F}\delta\dot{\mathbf{x}}) = \int_0^T (\dot{\mathbf{x}}-\dot{\mathbf{x}}_{exp})^T\delta\dot{\mathbf{x}}dt \tag{3.16}$$

(c) acceleration

$$\int_0^T \mathbf{z}^T(D_{\mathbf{x}}\mathbf{M}\ddot{\mathbf{x}}\delta\mathbf{x})dt + \int_0^T \mathbf{z}^T(\mathbf{M}\delta\ddot{\mathbf{x}})dt + \int_0^T \mathbf{z}^T(D_{\mathbf{x}}\mathbf{F}\delta\mathbf{x})dt + \int_0^T \mathbf{z}^T(D_{\dot{\mathbf{x}}}\mathbf{F}\delta\dot{\mathbf{x}}) = \int_0^T (\ddot{\mathbf{x}}-\ddot{\mathbf{x}}_{exp})^T\delta\ddot{\mathbf{x}}dt \tag{3.17}$$

In the next step the derivatives of $\mathbf{x}$ are separated and the terms from the equations (3.15) integrated by parts in order to eliminate all derivatives of $\delta\mathbf{x}$ from the adjoint state equation. For the left-hand side terms the integration by parts is identical for the displacements, velocity and acceleration case. Using the relation $(\mathbf{A}\mathbf{x})^T\mathbf{z} = (\mathbf{A}^T\mathbf{z})^T\mathbf{x}$ one obtains the following results for the four left-hand side terms:

$$1: \quad \int_0^T (D_x\mathbf{M}\ddot{\mathbf{x}}\delta\mathbf{x})^T\mathbf{z}\ dt = \int_0^T ((D_x\mathbf{M}\ddot{\mathbf{x}})^T\mathbf{z})^T\delta\mathbf{x}\ dt \tag{3.18a}$$

$$2: \quad \int_0^T (\mathbf{M}\delta\ddot{\mathbf{x}})^T\mathbf{z}\ dt = \int_0^T (\mathbf{M}^T\mathbf{z})^T\delta\ddot{\mathbf{x}}\ dt$$

$$= [(\mathbf{M}^T\mathbf{z})^T\delta\dot{\mathbf{x}}]_0^T - [\overbrace{(\mathbf{M}^T\mathbf{z})^T}^{\dot{}}\delta\mathbf{x}]_0^T + \int_0^T (\overbrace{(\mathbf{M}^T\mathbf{z})^T}^{\ddot{}}\delta\mathbf{x})\ dt \tag{3.18b}$$

$$3: \quad \int_0^T (D_x\mathbf{F}\delta\mathbf{x})^T\mathbf{z}dt = \int_0^T (D_x\mathbf{F}^T\mathbf{z})^T\delta\mathbf{x}\ dt \tag{3.18c}$$

$$4: \quad \int_0^T (D_{\dot{\mathbf{x}}}\mathbf{F}\delta\dot{\mathbf{x}})^T\mathbf{z})\ dt = \int_0^T (D_{\dot{\mathbf{x}}}\mathbf{F}^T\mathbf{z})^T\delta\dot{\mathbf{x}}\ dt$$

$$= [(D_{\dot{\mathbf{x}}}\mathbf{F}^T\mathbf{z})^T\delta\mathbf{x}]_0^T - \int_0^T (\overbrace{(D_{\dot{\mathbf{x}}}\mathbf{F}^T\mathbf{z})^T}^{\dot{}}\delta\mathbf{x}\ dt \tag{3.18d}$$

For the right-hand side term three different cases have to be considered. If displacements are used in the misfit function no further operation is necessary. Instead, for the misfit function defined with the velocity or acceleration integrations by part are needed in order to eliminate the derivatives of $\delta\mathbf{x}$:

$$\text{(b)}\ \int_0^T (\dot{\mathbf{x}} - \dot{\mathbf{x}}_{exp})^T \delta\dot{\mathbf{x}}\, dt = [(\dot{\mathbf{x}} - \dot{\mathbf{x}}_{exp})^T \delta\mathbf{x}]_0^T - \int_0^T (\ddot{\mathbf{x}} - \ddot{\mathbf{x}}_{exp})^T \delta\mathbf{x}\, dt \quad (3.19a)$$

$$\begin{aligned}\text{(c)}\ \int_0^T (\ddot{\mathbf{x}} - \ddot{\mathbf{x}}_{exp})^T \delta\ddot{\mathbf{x}}\, dt &= [(\ddot{\mathbf{x}} - \ddot{\mathbf{x}}_{exp})^T \delta\dot{\mathbf{x}}]_0^T - \int_0^T (\dddot{\mathbf{x}} - \dddot{\mathbf{x}}_{exp})^T \delta\dot{\mathbf{x}}\, dt \\ &= [(\ddot{\mathbf{x}} - \ddot{\mathbf{x}}_{exp})^T \delta\dot{\mathbf{x}}]_0^T - [(\dddot{\mathbf{x}} - \dddot{\mathbf{x}}_{exp})^T \delta\mathbf{x}]_0^T + \int_0^T (\mathbf{x}^{IV} - \mathbf{x}_{exp}^{IV})^T \delta\mathbf{x}\, dt\end{aligned} \quad (3.19b)$$

From the integration by parts terms remain which are calculated at $t = 0$ and $t = T$. They depend on $\delta\mathbf{x}$ and $\delta\dot{\mathbf{x}}$. Due to the initial condition $\mathbf{x}(t = 0) = \mathbf{0}$ they become zero at $t = 0$. For $t = T$ the final conditions are obtained by separating the left and right-hand side terms depending on $\partial\mathbf{x}$ and $\partial\dot{\mathbf{x}}$:

(a) Displacements:

$$\mathbf{z}(T) = 0 \quad \dot{\mathbf{z}}(T) = 0 \quad (3.20)$$

(b) Velocity:

$$\mathbf{M}^T\mathbf{z}(T) = \mathbf{0} \quad (3.21a)$$

$$-\dot{\mathbf{M}}^T\mathbf{z}(T) - \mathbf{M}^T\dot{\mathbf{z}}(T) + D_{\dot{\mathbf{x}}}\mathbf{F}^T\mathbf{z}(T) = (\dot{\mathbf{x}}(T) - \dot{\mathbf{x}}_{exp}(T)) \quad (3.21b)$$

(c) Acceleration:

$$\mathbf{M}^T\mathbf{z}(T) = (\ddot{\mathbf{x}}(T) - \ddot{\mathbf{x}}_{exp}(T)) \quad (3.22a)$$

$$\dot{\mathbf{M}}^T\mathbf{z}(T) + \mathbf{M}^T\dot{\mathbf{z}}(T) - D_{\dot{\mathbf{x}}}\mathbf{F}^T\mathbf{z}(T) = (\dddot{\mathbf{x}}(T) - \dddot{\mathbf{x}}_{exp}(T)) \quad (3.22b)$$

Now all the integral terms in the adjoint equation depend only on $\delta\mathbf{x}$ which can be eliminated. For the three cases the adjoint equations are therefore given by:

$$\text{(a)}\ \overbrace{(\overbrace{\mathbf{M}^T\mathbf{z}}^{\ddot{}})}^{\ddot{}} + (D_x\mathbf{M}\ddot{\mathbf{x}})^T\mathbf{z} + D_x\mathbf{F}^T\mathbf{z} - \overbrace{(D_{\dot{\mathbf{x}}}\mathbf{F}^T\mathbf{z})}^{\dot{}} = \mathbf{x} - \mathbf{x}_{exp} \quad (3.23a)$$

$$\text{(b)}\ \overbrace{(\overbrace{\mathbf{M}^T\mathbf{z}}^{\ddot{}})}^{\ddot{}} + (D_x\mathbf{M}\ddot{\mathbf{x}})^T\mathbf{z} + D_x\mathbf{F}^T\mathbf{z} - \overbrace{(D_{\dot{\mathbf{x}}}\mathbf{F}^T\mathbf{z})}^{\dot{}} = -(\ddot{\mathbf{x}} - \ddot{\mathbf{x}}_{exp}) \quad (3.23b)$$

$$\text{(c)}\ \overbrace{(\overbrace{\mathbf{M}^T\mathbf{z}}^{\ddot{}})}^{\ddot{}} + (D_x\mathbf{M}\ddot{\mathbf{x}})^T\mathbf{z} + D_x\mathbf{F}^T\mathbf{z} - \overbrace{(D_{\dot{\mathbf{x}}}\mathbf{F}^T\mathbf{z})}^{\dot{}} = \dddot{\mathbf{x}} - \dddot{\mathbf{x}}_{exp} \quad (3.23c)$$

The signal in the adjoint state equations depend therefore on the type of signal used in the misfit function. The three cases are summarized in tabel 3.6.

Adjoint state calculation		
	Signal in misfit function	Signal in adjoint state
a	displacements $\mathbf{x}$	displacements $\mathbf{x}$
b	velocities $\dot{\mathbf{x}}$	accelerations $\ddot{\mathbf{x}}$
c	accelerations $\ddot{\mathbf{x}}$	fourth derivative $\dddot{\mathbf{x}}$

Table 3.6: Ajoint state calculation for displacements, velocities and accelerations used in the misfit function

Which of these approaches provides the best result depends on the available data and the error introduced by integrating or differentiating the time signals. As outlined in [49] the differentiation leads often to spurious oscillations and to numerical errors. A small perturbation in the data can lead to large variation in the derivative. Therefore the derivation should be avoided.

Therefore, for the bogie model the use of displacements in the misfit function is advantageous. It leads to displacements in the adjoint equation. Since the results of the numerical integration calculated for state space equations are available as displacements and velocities no differentiation is needed in this case. We will see in the next chapter that for the identification of the TGV parameters the case b should be used. The vehicle response is measured in form of accelerations which could be used directly in the adjoint state equation. In order to obtain the velocities for the misfit function an integration would be required.

In the adjoint state equation several derivatives of the matrix $\mathbf{M}$ appear:

$$\ddot{\mathbf{M}}^T\mathbf{z}+\mathbf{M}^T\ddot{\mathbf{z}}+2\dot{\mathbf{M}}^T\dot{\mathbf{z}}+(D_x\mathbf{M}\ddot{\mathbf{x}})^T\mathbf{z}+(D_x\mathbf{F}^T)\mathbf{z}-\dot{\overbrace{(D_{\dot{\mathbf{x}}}\mathbf{F}^T)}}\,\mathbf{z}-D_{\dot{\mathbf{x}}}\mathbf{F}^T\dot{\mathbf{z}}=\mathbf{x}-\mathbf{x}_{exp} \tag{3.24}$$

The term $D_x\mathbf{M}$ describes the derivative of the matrix $\mathbf{M}$ with respect to a vector $\mathbf{x}$ giving a tensor of order 3. According to the tensor algebra which can be found in the appendix C a second order tensor is obtained when the derivative of $\mathbf{M}$ is contracted with the vector $\ddot{\mathbf{x}}$. Using the index notation

the contraction is given by:

$$(\frac{\partial m_{ij}}{\partial x_s} e_i \otimes e_j \otimes e_s)\ddot{x} = \frac{\partial m_{ij}}{\partial x_s}(e_s, \ddot{x}) e_i \otimes e_j = \frac{\partial m_{ij}}{\partial x_s}(\ddot{x}_s) e_i \otimes e_j \tag{3.25}$$

Accordingly, an index appearing twice in a multiplicative term represents a summation. The equation above can therefore be written as:

$$\sum_s \ddot{x}_s \frac{\partial m_{ij}}{\partial x_s} e_i \otimes e_j \tag{3.26}$$

For the validation of the adjoint state method the scalar product test proposed in [48] is used. It is based on the definition of the adjoint state. At first the differentiated equation of the system is solved for an arbitrary excitation.

$$(D_x \mathbf{M}\ddot{\mathbf{x}})\delta\mathbf{x} + \mathbf{M}\delta\ddot{\mathbf{x}} + D_x \mathbf{F}\delta\mathbf{x} + D_{\dot{\mathbf{x}}} F\delta\dot{\mathbf{x}} = \mathbf{b}(t) \tag{3.27}$$

The result for $\delta\mathbf{x}$ is injected in the right side of the adjoint state equation (3.24) and the following scalar products $(\mathbf{b}, \mathbf{z})$ and $(\delta\mathbf{x}, \delta\mathbf{x})$ are calculated. If the two scalar products give the same result for different choices of $\mathbf{b}$ the result of the adjoint equation is validated.

3.3.2.2 Gradient calculation from automatic differentiation (AD)

In chapter 1 another interesting approach for the calculation of the gradient was outlined: the automatic differentiation.

The code describing the equations of motion for the forward bogie model is rewritten as a sequence of basic operations. Then the gradient is calculated by applying the chain rule. Finally, AD gives a program code for the calculation of the gradient. It does not apply a symbolic expression for the gradient.

For this work the TOMLAB/MAD toolbox [19] in Matlab has been used. The numerical integration needed for the solution of the differential equation system is treated by this automatic differentiation package. For the gradient calculation the forward mode is used.

3.3.2.3 Comparison of the gradient calculations

The misfit function gradients obtained from the finite differences, adjoint state and automatic differentiation approach are compared. The criteria for the comparison are the accuracy of the gradients and the computational cost.

The latter becomes important with regard to the TGV model where the gradient is calculated relatively to a large number of parameters.

In addition to the method used the result and cost needed for the calculation of the gradient depends of course on the numerical control parameters. Both the calculation of the forward model response and the gradient require control parameters which are summarized in table 3.7. All gradient methods require the solution of the forward model. As outlined before it is described by a system of nonlinear differential equations and solved by numerical integration. If the gradients are calculated from finite differences only the forward model response is needed. It is calculated at several parameter values shifted by a certain steplength. The adjoint state approach requires the solution of the adjoint state equation. As the forward model equation it is described by a nonlinear differential equation system which is solved by numerical integration. The automatic differentiation requires no more than the choice of the mode.

Numerical control parameters			
Forward model	Solver	type of solver	ODE113
	MaxStep	max step size	0.01
	RelTol	relative tolerance	1e-4
	AbsTol	absolute tolerance	1e-6
Finite Differences	Steplength		0.01
Adjoint state	Solver	type of solver	ODE113
	MaxStep	max step size	0.001
	RelTol	relative tolerance	1e-4
	AbsTol	absolute tolerance	1e-6
	Type	signal in misfit function	displacement
Automatic differentiation	Mode		forward

Table 3.7: Control parameters for the gradient calculation methods

The control parameters of table 3.7 concern for the most part the numerical integration algorithm used for solving the differential equation systems.

- Solver:
  The solvers ODE are used for solving initial value problems for ordi-

nary differential equations. Among the seven different solvers available in Matlab the ODE45 and the ODE113 solvers have been used. The ODE45 solver is an explicit Runge-Kutta(4,5) one-step solver which uses only the result of the previous time step. It is recommended to use this solver at first for most problems. If the numerical integration is slow due to an expensive evaluation the ODE113 solver should be used. It is a multi-step solver using the solution at several preceding time steps. The order given by the number of preceding steps is variable.

- MaxStep:
  The upper bound of the solver step size is defined by the parameter MaxStep.

- RelTol:
  The parameter RelTol defines the relative error tolerance that applies to all components of the solution vector $\mathbf{x}$. The relative error is a measure of the error relative to the size of each solution component.

- AbsTol:
  The parameter AbsTol describes the absolute error tolerance that applies to the individual components of the solution vector. If the value of the i_{th} solution component is below this threshold it is neglected and convergence to zero is assumed.

From section 3.3.2.1 it is known that the misfit function can be defined using the displacements, velocities and acceleration signals of the simulation and measurement response. This choice concerns the forward model. The integration by parts needed for the calculation of the adjoint state equations leads to higher order derivatives. The relation between the signals used in the misfit function and in the adjoint state equation has been summarized in table 3.6.

The choice of the signal type depends on the available data and the error introduced by a possible differentiation. In the following the displacement, acceleration and 4th derivative of the direct model response are compared. From the numerical integration the result is obtained as displacement and velocity. In order to obtain the acceleration and the 4th derivative numerical differentiation are applied. As outlined before the differentiation can lead to an important amplification of errors in the original signal.

The gradients of the misfit function have been calculated relative to all degrees of freedom. All three types can be used in the optimization algorithm. As an example the forward model response for the dof 7 of the bogie model is shown in figure 3.19.

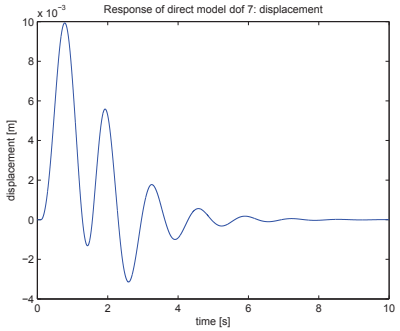

(a) Forward model dof 7: displacement

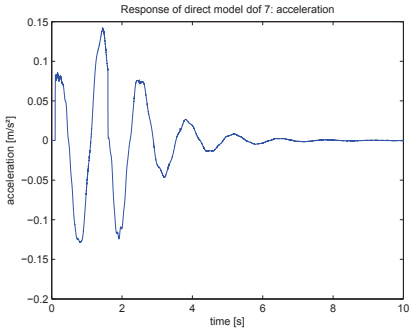

(b) Forward model dof 7: acceleration

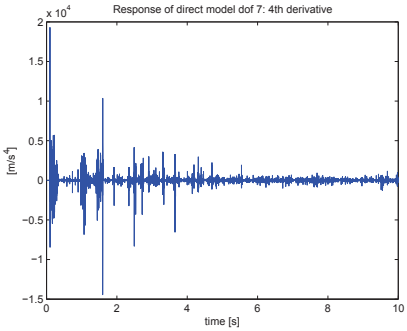

(c) Forward model dof 7: 4th derivative

Figure 3.19: Displacement, acceleration and 4th derivative of dof 7 of the vehicle response

It is found that the acceleration signal and in particular the 4th derivative are disturbed. While the acceleration signal can be calculated directly by evaluating the system equation for $\ddot{x}$ the calculation of the 4th derivative requires a numerical differentiation. Due to the large errors introduced by the differentiation the accelerations can not be used in the misfit function.

Computation of the adjoint state:
The forward model and the adjoint equation are solved by numerical integration using the Matlab functions ODE45 or ODE 113. At every iteration step of the optimization algorithm the following operations are required for

the calculation of the adjoint state:

- Solution of the forward model:
  The forward model described by equation (3.10) is solved for the time interval $t = 0$ to $T = 10s$ using the defined maximal step size and tolerances. In figure 3.20 the inversed dof 7 of the forward model response $x_{forwardmodel}$ is shown for the model and the measurement.

- Solution of the adjoint equation:
  In the next step the adjoint equation (3.24) is solved for the time interval $t = T$ to $t = 0$ using the defined maximal step size and tolerance. The adjoint equation is solved inverse in time requiring the forward model to be solved for the whole time range chosen. The result is shown in figure 3.20.

- Calculation of the gradient:
  After the forward model and the adjoint equation have been solved the gradient can be calculated from equation (3.24) by implementing the adjoint variable for $t = 0$ to $t = T$.

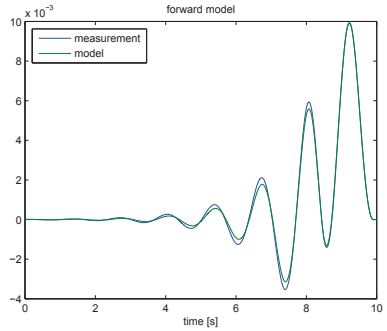

(a) Forward model dof 7

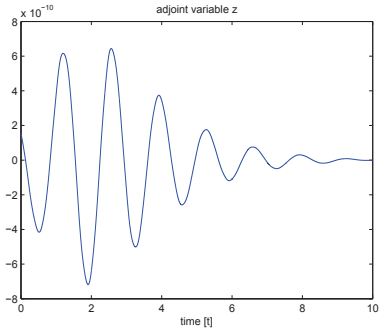

(b) Adjoint state dof 7

Figure 3.20: Forward model response and adjoint state for bogie model (dof 7)

Automatic differentiation:
For the calculation of the gradient by automatic differentiation the toolbox tomlab/Mad is used. The automatic differentiation requires only the forward model. The code for the gradient calculation is created automatically. Then the forward model and its derivative are solved using an numerical integration algorithm.

Comparison of gradients:
The misfit function gradients relative to the stiffnesses c_x, c_y and c_z have been calculated with the finite differences, adjoint state and automatic differentiation method. In the following the results for the gradients are compared. The criteria are the accuracy of the gradient calculation on the one hand and the needed calculation time on the other hand.

The gradients of the misfit function have been calculated for different configurations. For configuration 1 (table 3.8) a low friction value is used. For configuration 2 (table 3.9) the friction value is increased. Finally, in configuration 3 (table 3.10) the velocity signal is used in the misfit function instead of the displacement signals.

Gradient calculation

Model	Misfit	Conicity	Friction	Time	Track	Para
Single Wheelset	displ.	0.2	0.1	2	con	cy
Complete bogie	displ.	0.2	0.1	10	con	cy

Table 3.8: Parameters for gradient calculation, configuration 1

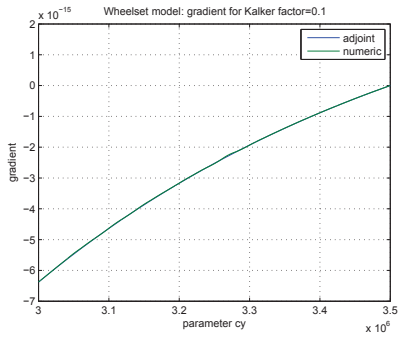

Figure 3.21: Gradient from adjoint state and finite differences for single wheelset model, configuration 1

In a first step a special case is considered. The bogie frame is fixed moving with constant speed so that the two wheelsets are not coupled any longer. In this case the same gradients are obtained for all three cases. However, an influence of the friction coefficient is recognizable. If the friction coefficient and therefore the level of the friction forces is reduced the difference between

Gradient calculation

Model	Misfit	Conicity	Friction	Time	Track	Para
Single Wheelset	displ.	0.2	0.3	2	con	cy
Complete bogie	displ.	0.2	0.3	10	con	cy

Table 3.9: Parameters for gradient calculation, configuration 2

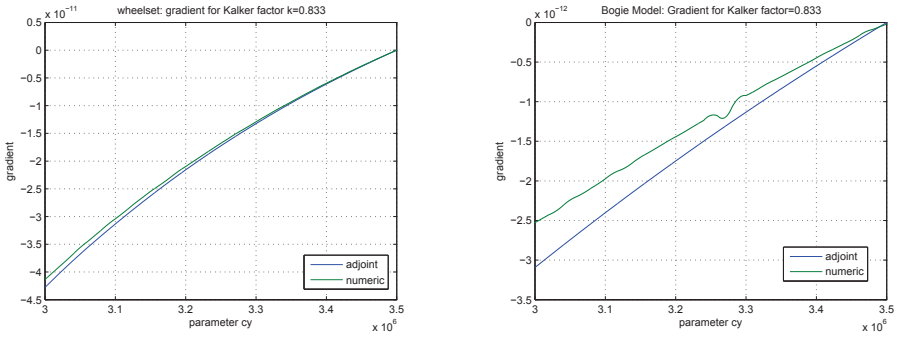

(a) uncoupled wheelset (b) complete bogie

Figure 3.22: Gradient calculated from adjoint state and finite differences, configuration 2

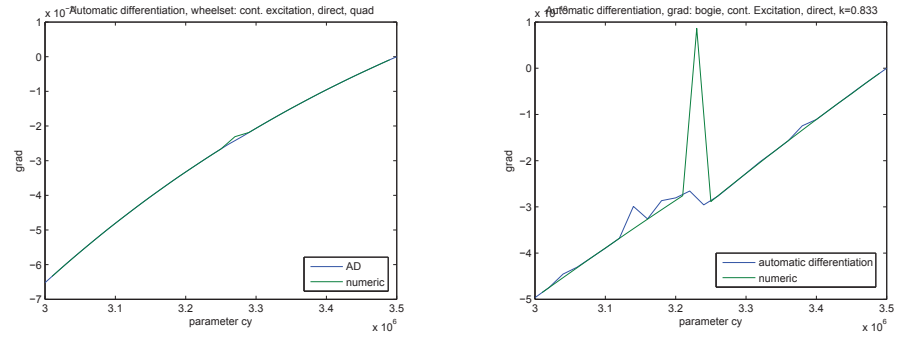

(a) uncoupled wheelset (b) complete bogie

Figure 3.23: Gradient calculated from automatic differentiation and finite differences, configuration 2

Gradient calculation

Model	Misfit	Conicity	Friction	Time	Track	Para
Single Wheelset	speed	0.2	0.1	2	con	cy
Complete bogie	speed	0.2	0.1	10	con	cy

Table 3.10: Parameters for gradient calculation, configuration 3

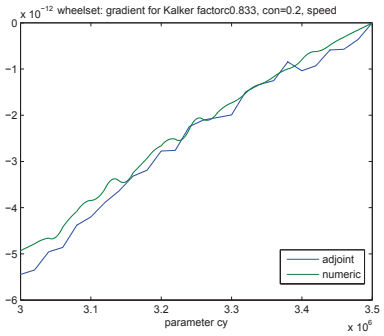

Figure 3.24: Gradient calculated from adjoint state and finite differences for single wheelset model, configuration 3

state gradient and numerical gradient is reduced either.

If the full dynamics of the bogie model is considered the interpretation of the results becomes more complicated. Between the numerical and adjoint state gradient an important error occurs. No clear explanation of the differences could be found. For the linearized model of the wheelset the adjoint method could be validated with the scalar product test. From figure 3.23 it can be seen that the effect of the friction coefficient and the conicity on the error are negligible. In return, the differences are probably caused by the nonlinear nature of the bogie model. Since an analytical solution of the gradient calculation for the nonlinear model is not available the results can not be validated. None of them can be seen as the reference calculation.

The gradient calculated by the automatic differentiation approach gives the same result as the numeric gradient. This shows that the automatic differentiation is a suitable approach for the calculation of the gradient even for a complexe system solved by numerical integration methods.

The adjoint method has been implemented in the gradient based optimiza-

tion methods. If the numeric gradient calculation in the Newton and Trust region method is replaced by the gradient from the adjoint state approach the same optimization result is obtained.

From the sensitivity analysis in section 3.2 it is found that the misfit function relative to the stiffnesses c_x and c_y has several local minima. By regularizing the misfit function these local minima could be eliminated. However, in general the solution surface of the misfit function is not known a priori and local minima can occur. Therefore, the exclusive use of local methods is unsuitable since the convergence towards the global minimum is not guaranteed. The results of section 3.3.1.2 showed that the local optimization methods converge to the minimum closest to the initial parameter values.

3.3.3 Parameter identification with simulated annealing from Matlab reference simulation

In order to identify the global minimum of the misfit function the simulated annealing method is applied. As outlined in chapter 1 it is a global method able to leave the attractor region of a local minimum in order to converge to the global minimum of the solution space.

In a first step the simulated annealing method is applied to the bogie model for the identification of the stiffnesses c_x and c_y using a Matlab simulation as virtual experimental data. The choice of control parameters has an important effect on the results. From the considerations in chapter 1 it is known that if too fast the decrease of the temperature parameter can cause a convergence to a local minimum since the local search characteristics are emphasized.

The choice of the temperature algorithm and the number of function evaluations for every temperature is difficult since standard adjustments of the control parameters are not known yet. In this work several adjustments have been tested and compared. Another difficulty which all global methods have in common is the choice of a termination condition. Here, the temperature parameter and the number of iterations are used.

The nominal and the initial value as well as the constraints of the parameters are given in table 3.11.

The control parameters for which the simulated annealing is performed are

Stiffness parameters of bogie model				
Parameter	stiffness [N/m]			
	true	initial	min	max
cx	5.2e7	4.5e7	4e7	6.4e7
cy	3.5e6	3.2e6	3e6	4e6

Table 3.11: Parameters used for the simulated annealing method

listed in table 3.12:

Control parameter			
Parameter	**Configurations**		
number of consecutive rejections	10000	10000	10000
number of tries within one temperature	10000	10000	10000
number of successes within one temperature	20	20	20
reduction of temperature	10%	40%	60%

Table 3.12: Control parameters for the simulated annealing method

with:

- Number of consecutive rejections:
  Number of consecutive iterations for which the new misfit function value is not accepted. If this number is achieved the simulated annealing algorithm is terminated.

- Number of tries within one temperature:
  Number of misfit function evaluations in one temperature step. A large number leads to a accentuation of the global exploratory properties of the algorithm.

- Number of successes within one temperature:
  Number of evaluations for which the new misfit function value is accepted.

- Reduction of temperature:
  Percentage the temperature is reduced from one temperature level to the next. A slow reduction also accentuates the global exploratory properties of the algorithm.

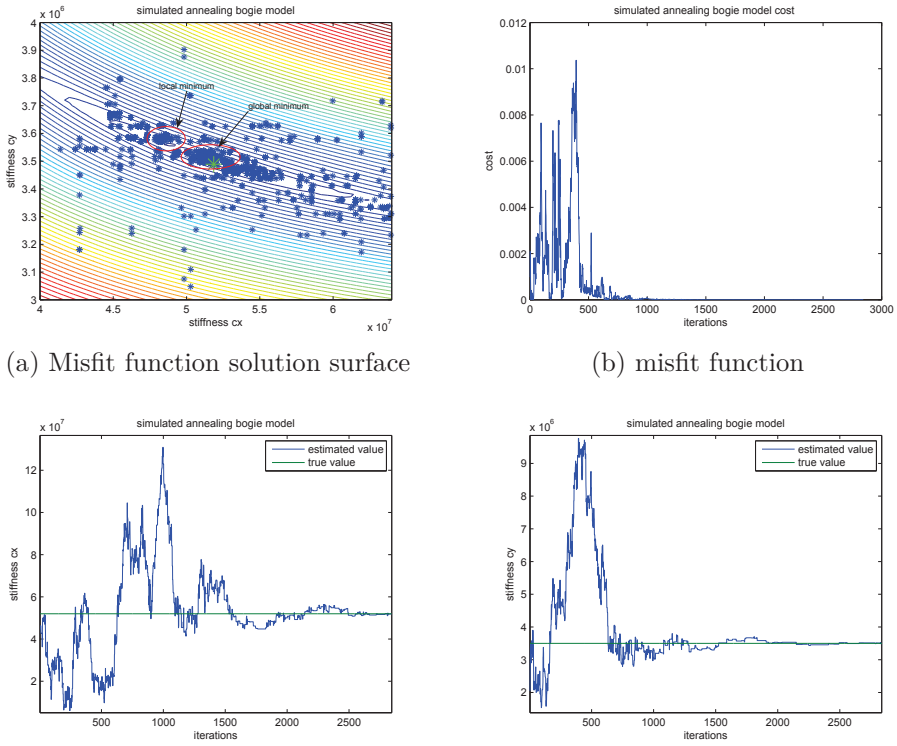

(a) Misfit function solution surface

(b) misfit function

(c) Stiffness cx

(d) Stiffness cy

Figure 3.25: Simulated annealing for the stiffnesses c_x and c_y with 10% temperature reduction

Optimization 1:

With a temperature reduction of 10% the algorithm converges to the global minimum of the misfit function.

In figure 3.25a an accumulation of parameter trials in three regions is recognisable. These regions represent the local and the global minimum of the misfit function surface. Due to the slow reduction of the temperature the exploratory properties of the algorithm are accentuated and the local minimum is left. In return, the number of iterations is high. The true parameter values are identified after about 2500 iterations.

Optimization 2:

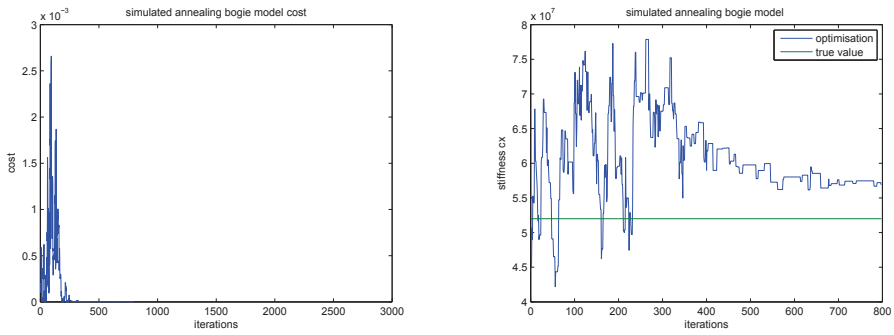

(a) misfit function

(b) Stiffness cx

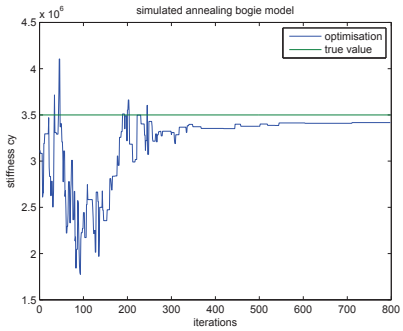

(c) Stiffness cy

Figure 3.26: Simulated annealing for the stiffnesses c_x and c_y with 60% temperature reduction

If the temperature is reduced with 60% the simulated annealing algorithm

becomes ineffective after a relatively short number of iterations. The algorithm then behaves like a local method and converges to a local minimum.

The results show that the global search characteristics of the simulated annealing algorithm should be emphasized at the beginning of the analysis. In order to reduce the number of iterations the change from global to local search characteristics can be accelerated if the convergence to the initially found global minimum remains guaranteed.

3.3.4 Parameter identification with simulated annealing from Vampire reference simulation

In the section 3.3.3 a simulation with the Matlab bogie model has been used as virtual measurement data for the parameter identification. The measurement and simulation data was therefore obtained from the same model. This explaines that the optimization algorithm converges to the exact parameter values used in the reference simulation. The misfit function becomes zero. Of course, in reality this is not possible. Since the model is a simplified representation of the real system it can not reproduce the measurement exactly. Therefore, in order to analyse the performance of the model and the parameter identification real measurement data should be used. If measurement data is not available, the simulation results of another model, preferably with a more complexe structure can be used. Therefore in this section the simulation result obtained from the Vampire bogie model will be used.

Several identifications are performed. First, the convergence of the simulated annealing algorithm has been tested for the case that the initial parameters of the Matlab model corresponds to the nominal parameters used in the Vampire model. Afterwards, the simulated annealing algorithm has been applied to the case of different initial parameter values. The parameter values and the degrees of freedom used for the definition of the misfit function are summarized in table 3.13.

Besides, different misfit functions are compared. For the Vampire model the response at all degrees of freedom is available, allowing to define the misfit function with all 10 degrees of freedom. However, when measurement data is used, the response is not available at all degrees of freedom. In order to analyse the effect of reduced misfit functions two different cases are studied. In one case only lateral displacements in the wheelsets are used while in the

other case six degrees of freedom are taken into account. The different cases studied are summarized in table 3.13.

Cal	Vampire Model			Bogie Model			Misfit function					
	suspension parameters			inital suspension parameters			degrees of freedom					
	c_x [N/m]	c_y [N/m]	c_z [N/m]	c_x [N/m]	c_y [N/m]	c_z [N/m]	$u_{y,ws1}$	$\delta_{z,ws1}$	$u_{y,ws2}$	$\delta_{z,ws1}$	$u_{y,b}$	$\delta_{z,b}$
1	5.2e7	3.5e6	1.0e6	5.2e7	3.5e6	1.0e6	+	-	+	-	-	-
2	5.2e7	3.5e6	1.0e6	5.2e7	3.5e6	1.0e6	+	+	+	+	+	+
3	5.2e7	3.5e6	1.0e6	2.0e7	1.0e6	0.5e6	+	-	+	-	-	-

Table 3.13: Parameters and degrees of freedom in misfit function

For the computations 1 and 2 the nominal values of the Vampire model are used as initial values for the bogie model. The simulated annealing algorithm converges to different values due to the differences in the structure of the two models. The degrees of freedom used in the misfit function play an important role. If only the lateral displacements are used (calculation 1) different parameter values are obtained for c_x and c_z.

For the calculations with the nominal values as initial values a reduction of the misfit function is obtained. In the figures 3.30a to 3.30f the response of the Vampire model is compared with the response of the Matlab model before and after the optimization. The distance between Matlab and Vampire model remains important according to the small reduction of the misfit function observed before. This schows that the distance between the response are due to structural differences in the model and not due to inaccurate parameter values.

3.3.5 Parameter optimization for the bogie model: conclusions

In this chapter the parameter identification has been applied to the Matlab bogie model. Both, local gradient optimization and the global simulated annealing method have been tested. Since no measurement data for a single bogie is available the result of a simulation with nominal parameters has been used as virtual measurement data. Both, the Matlab model and the Vampire bogie model have been used in order to obtain the virtual measurement data.

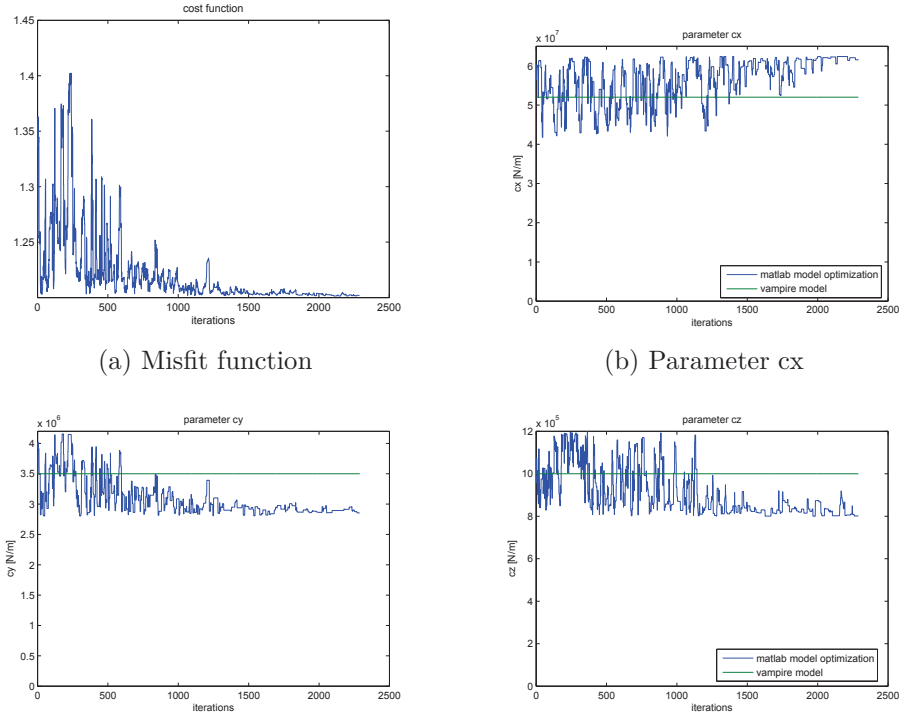

(a) Misfit function

(b) Parameter cx

(c) Parameter cy

(d) Parameter cz

Figure 3.27: Identification of Matlab model parameters from Vampire model result with: Initial values Matlab model = from Vampire, 2 dof measured

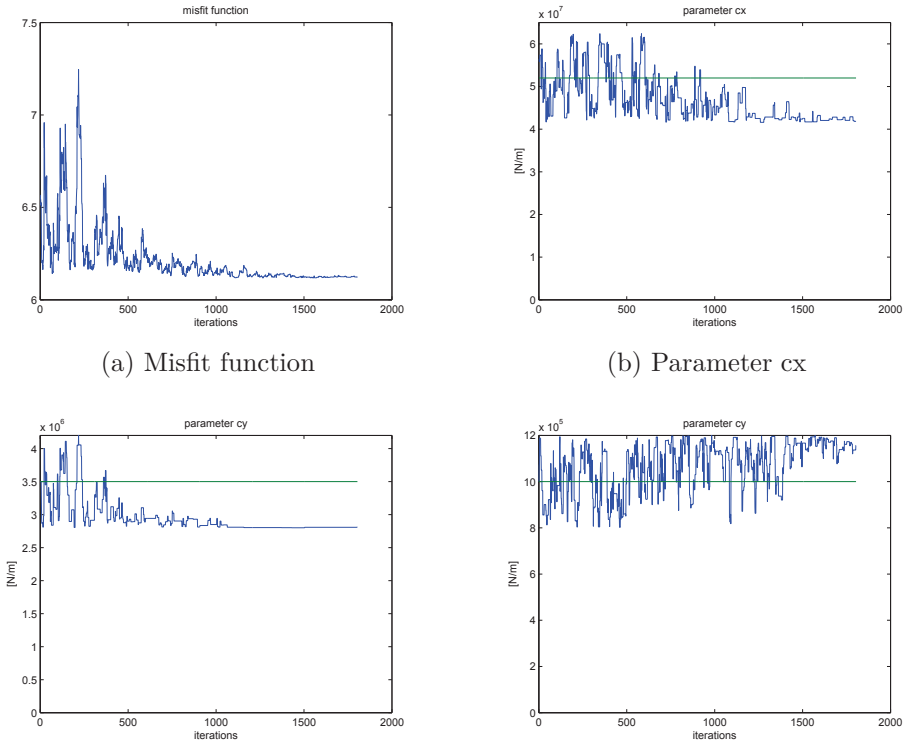

(a) Misfit function

(b) Parameter cx

(c) Parameter cy

(d) Parameter cz

Figure 3.28: Identification of Matlab model parameters from Vampire model result with: Initial values Matlab model = from Vampire, 6 dof measured

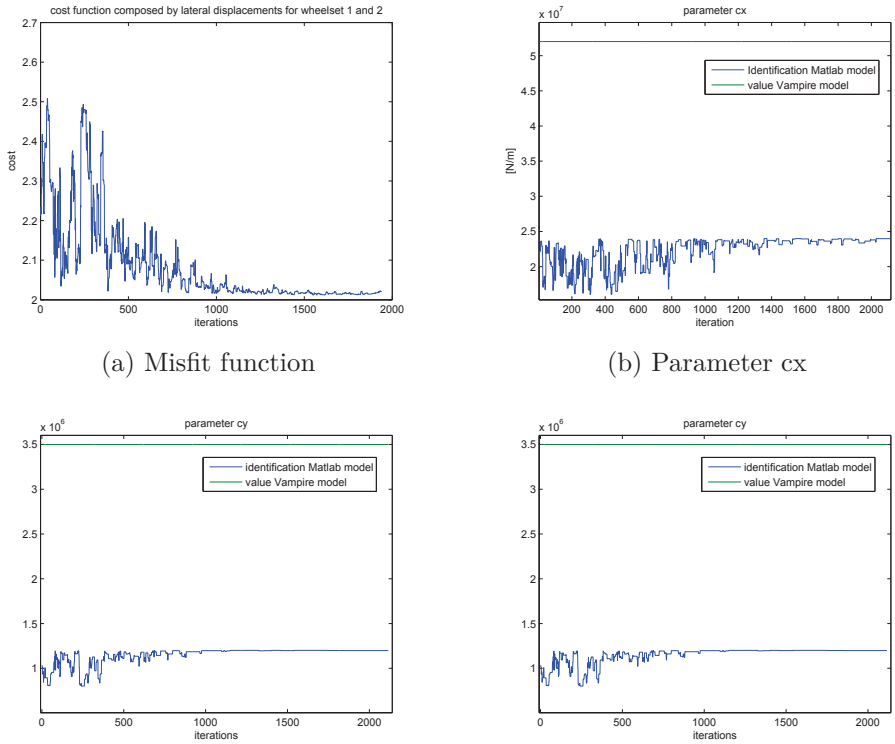

(a) Misfit function

(b) Parameter cx

(c) Parameter cy

(d) Parameter cz

Figure 3.29: Identification of Matlab model parameters from Vampire model result with: Initial values Matlab model $\neq$ from Vampire, 2 dof measured

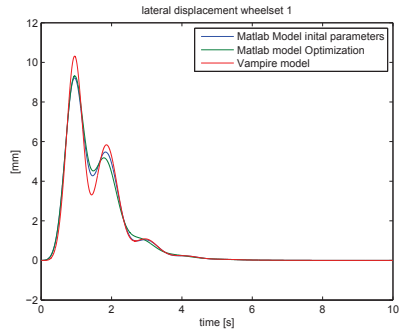

(a) Lateral displacement wheelset 1

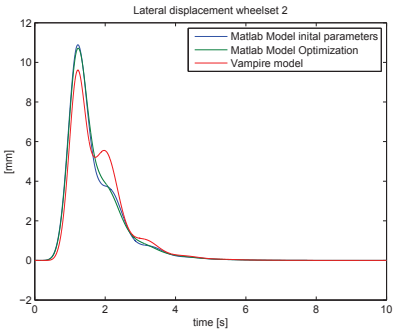

(b) Lateral displacement wheelset 2

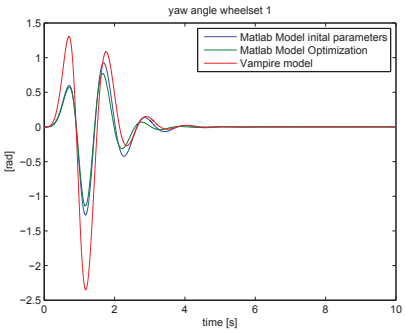

(c) Yaw angle wheelset 1

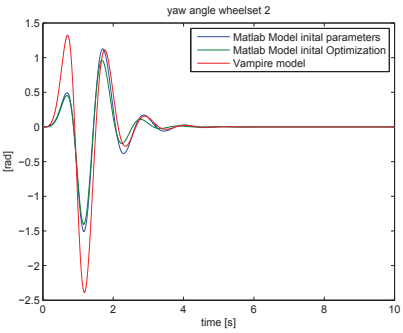

(d) Yaw angle wheelset 2

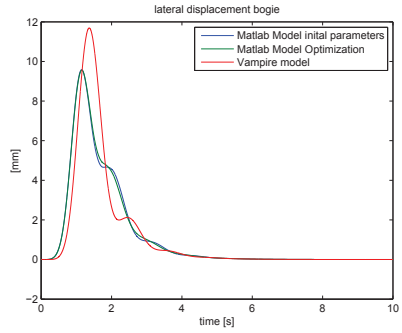

(e) Lateral displacement bogie

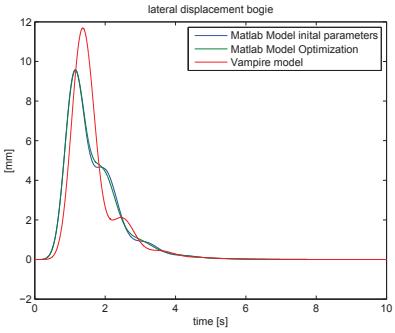

(f) Yaw angle bogie

Figure 3.30: Comparison of time data response for the Vampire model and the Matlab model with initial and optimized parameters

If the Matlab model is used the exact identification of the parameter values is possible. Then the global simulated annealing method converges to the global minimum given that the temperature reduction is sufficiently slow. The local gradient methods using the adjoint state approach are also able to converge to the global minimum if a regularization of the misfit function is used.

Chapter 4

Application of the parameter identification to the TGV model

4.1 Introduction

In the previous chapter the parameter identification problem was applied to the model of a single bogie. The identifiable parameters have been chosen using a sensitivity analysis. Then both local and global optimization methods have been applied in order to estimate the parameter values. However, for this simple model a parameter identification based on real measurement data was not possible. The simulation result obtained from the Vampire bogie model has been used as virtual measurement data. Measurement noise has not been considered but could be taken into account by adding a white noise to the Vampire simulation results.

In this chapter the approach outlined previously will be applied to the model of the TGV train. For the definition of the misfit function real measurement data will be used.

For the parameter identification many references to the steps outlined in the previous chapter will be found. This concerns mainly the choice of the parameters which have an influence on the vehicle response using a sensitivity analysis and the application of different optimization methods. However, the application to a far more complicated model and the use of real measurement data require additional steps on which this chapter will focus.

The parameter identification is not applied under well-defined laboratory conditions. Instead, the measurements used in the misfit function are obtained from operational measurements of a TGV train running on a real track with varying properties. It is therefore necessary to characterise the measurement conditions and analyse their influence on the parameter identification problem. The same concerns the vehicle. From chapter 2 it is known that the TGV train is a complex coupled system with a number of nonlinear effects. They are caused by the wheel-rail contact and several nonlinear suspension elements like the airspring and rubber springs. It is important to know the influence of these nonlinearities on the vehicle response in order to choose an adapted identification method. Finally, it is indispensable to validate the initial model with the measurement data. This allows to define the frequency range for which the model is valid, to know the performance of the model for different running conditions and to detect possible modelling errors.

These questions are discussed in the first section of this chapter. It analyses the influence of different running conditions on the vehicle dynamics and model performance using both the measurement data and simulation results. It aims at evaluating the influence of nonlinearities on the identification problem and it presents a validation of the model using the correlation and misfit function between simulation and measurement. Finally, it uses the sensitivity analysis developed in the previous chapter in order to analyse the coupling of the model and to detect the parameters which have an influence on the defined misfit functions.

The second section discusses the identification. Misfit functions defining the distance between simulation and measurement results are defined and minimized by the simulated annealing and genetic algorithm method. It will be shown that global optimization methods are required due to the presence of many local minima in the solution surface of the misfit functions and the under-determined problem.

In the third section the results are discussed and conclusions about the application of the parameter identification to the TGV model are presented.

4.2 System analysis and calibration of the initial model

4.2.1 Analysis of the vehicle-track system with regard to the parameter identification problem

The parameter identification is performed for operational measurements of a TGV Duplex train running on the east-European high-speed line. The main excitation of the train is the track characterised by a theoretical design and the track irregularities indicating the divergence of the real track from the theoretical design. Both properties have an important influence on the vehicle dynamics and have to be taken into account for the parameter identification.

An identification using all available measurement information for the whole line is practically impossible to perform due to the enormous amount of data. The identification has to be restricted to some sections which give representative results. These so-called learn sections should cover different running conditions for example straight and curved track as well as different line speed or track quality levels. For a reliable identification of the suspension parameters it has to be assured that the estimated values do not depend considerably on the running conditions used in the identification problem.

4.2.1.1 Analysis of the main excitation of the system : the track

The theoretical design describes the construction parameters of the railway line. It is given by the radii of the curves, the cant (or superelevation) of the curves, the construction speed and the cant insufficiency. The cant describes the difference in elevation between the outer and inner rail. It allows to reduce the component of the centrifugal force parallel to the track surface. For a given curve radius and speed the component of the centrifugal and gravitation force parallel to the track surface cancel out each other. Since the cant is limited with regard to vehicles at standstill and a high contruction speed is seeked the parallel component of the centrifucal force is not completely compensated. This deficieny of cant is called insufficieny. It corresponds to an uncompensated centrifugal force.

Figure 4.1 shows the track design for the east-European high-speed line used in this work. The main parameters whose influence on the vehicle response and parameter identification have been studied are the speed and the curve

radius.

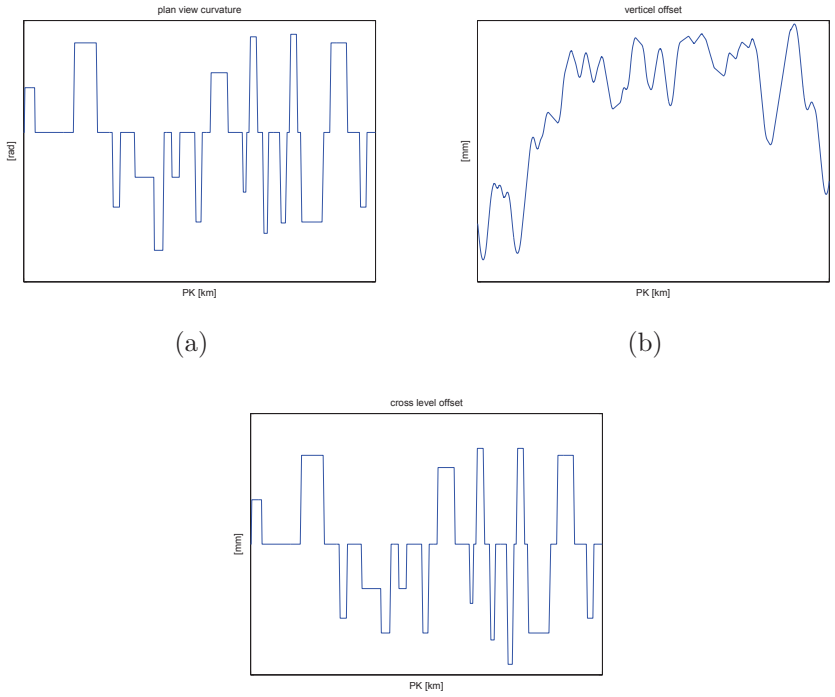

(a) (b)

(c)

Figure 4.1: Track design PK30 - PK100: Plan view curvature (a), vertical offset (b), superelevation (c)

The divergence of the real track position from the theoretical design is described by the track irregularities. They are expressed by four degrees of freedom either using the vertical and lateral displacement of the left and right rail or the parameterization shown in figure 4.2. The irregularities are described by the vertical and lateral displacement of the track centreline as well as the cross-level and gauge failure.

In order to identify possible correlations between the track irregularities and the performance of the simulation model the track irregularities have been characterized both in the spatial and frequency domain. At SNCF the track irregularities on high-speed lines are measured by the IRIS 320 test train, a TGV train equipped with an optical measurement system. It is an inertial measurement system which uses the laser cut method and the acceleration

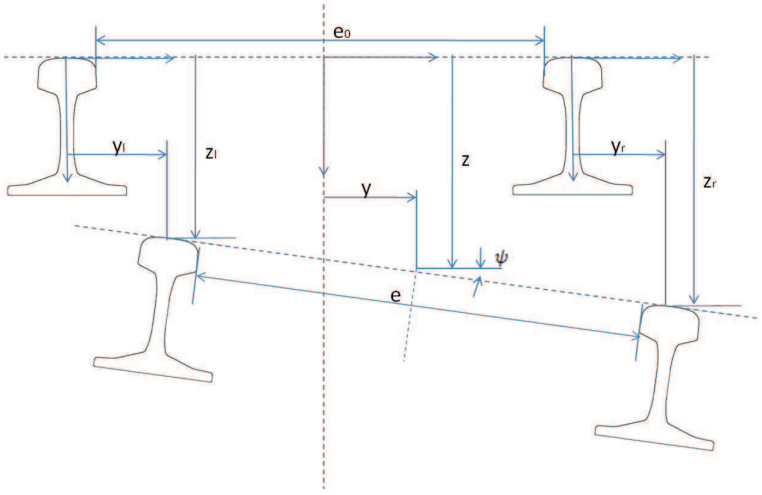

Figure 4.2: Track irregularities (vertical z, lateral y, cross level ψ, gauge e)

measured in the bogie in order to calculate the absolute track position. The laser cut method is based on the principle of triangulation. A line is projected on the rail by a laser. The picture of the line is registered by an electronical camera and transformed in 3D coordiantes of the rail position. Since the camera is installed on the bogie the position of the bogie has to be known in order to calculate the absolute rail position.

Spatial description of the track irregularities The spatial description of the track irregularities is obtained by parameterizing the track with the amplitude and wavelength of each defect as shown in figure 4.3. This is done by representing the measured track irregularities by simple geometric elements. Afterwards the maxima and standard deviations of the track defect parameters amplitude and amplitude over wavelength are calculated for sections of 250m length. As an example the result of this analysis is shown for the cross-level in figure 4.4. The segmentation for 250m will be used also for the misfit function thus allowing to study the influence of the track excitation on the model performance. The results for vertical, lateral and gauge irregularities can be found in annexe D.

Frequency description of the track irregularities The analysis has also been performed in the frequency domain. A computation of the power spectral density for the whole line using the Welch method gives an indica-

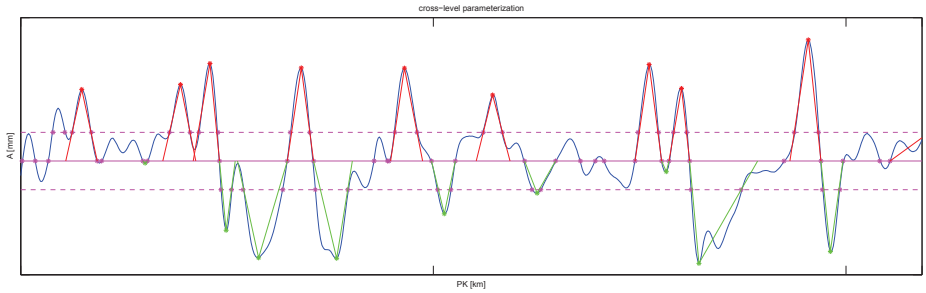

Figure 4.3: Parametrization of the track irregularities using the amplitude and the length of the track defects

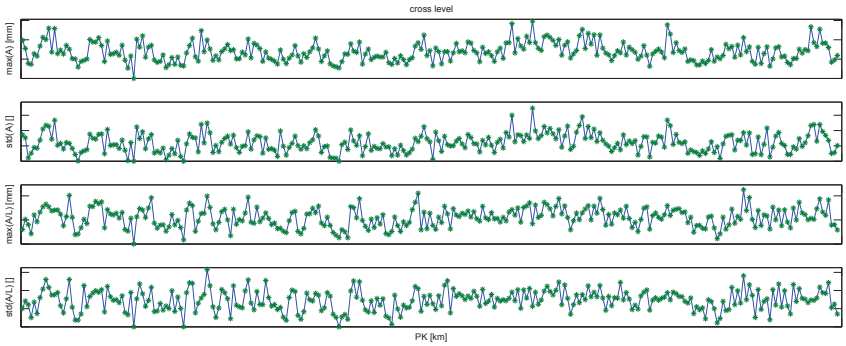

Figure 4.4: Maxima and standard deviation of amplitude and amplitude/wavelength for cross-level, section length=250m

tion on the frequency content but does not contain any spatial information. Due to the averaging the instationary characteristic of the track is not visible. Therefore the Short-time Fourier Transform (STFT) has been used. The spectra are computed for short sections of 50m thus allowing to have both frequency and spatial information on the track irregularities. An example is shown in figure 4.5 for the cross-level irregularity. Since the vehicle response spectra are expressed in [Hz] the spatial frequency [1/m] of the track irregularity is transformed in Hz using the mean vehicle speed per section.

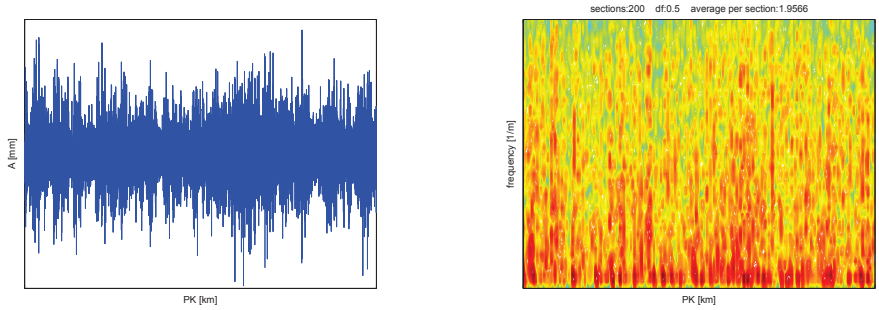

(a) Spatial signal (b) STFT

Figure 4.5: Spatial signal and Short Time Fourier transform for cross level irregularity

The complete results can be found in annexe D.

4.2.1.2 Analysis of the response of the system to track excitation using transfer functions

The description of the track design and irregularities beeing available the next step is to study the effect of the track excitation on the response of the real vehicle and of the model. This can be done both in the spatial and in the frequency domain. In this section the analysis is performed in the frequency domain using transfer functions.

The transfer functions are calculated for the primary and secondary suspension both in vertical and lateral direction in order to identify the suspension modes. Figure 4.6 illustrates the different approaches for the real system and the model.

In the case of the real system the excitation can not be chosen. It is given by the design and irregularities of the real track as well as the vehicle speed.

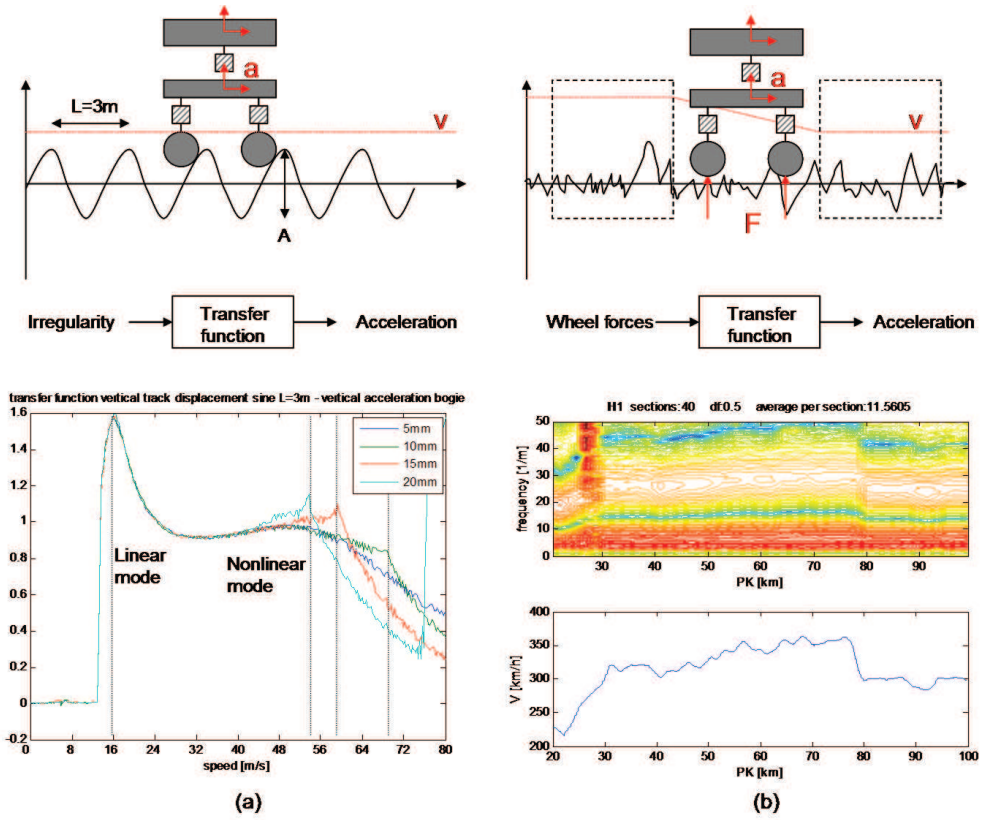

Figure 4.6: Calculation of the transfer function for the model with analytical track excitation (a) and for the TGV train under real track excitation (b)

Therefore the transfer functions are calculated between the measured wheel-forces and the accelerations in the bogie and the car body. For the calculation the auto- and cross spectra are used. This is possible since the track excitation has a broad band characteristic in the frequency range of interest. In order to take into account the unstationary process the transfer functions are calculated for short sections following the principle of the short time Fourier analysis.

For the model the transfer functions can be calculated for different clearly defined track design and irregularity conditions. This allows to study the influence of the curve radius, the wavelength and the amplitude of the track defects. The transfer function is calculated between the amplitude of the track defect and the response of the model.

Effect of the track design At first the influence of the track design on the transfer functions has been analysed. Figure 4.7 shows the transfer functions of the primary suspension in bogie A for a straight track and a curve with radius 4100m (smallest admissible radius at 320km/h). The track elevation is 180mm. For the track excitation a sine with an amplitude of 8mm and a wavelength of 3m is used in vertical and lateral directions. The wavelength of 3m corresponds to the axle distance of the bogie thus allowing the wheels of a bogie to move in phase. It is found that the curve changes considerably the modes of the primary suspension in lateral direction. This shows that some suspension elements are only sollicitated in curve or straight track. The influence of a suspension parameter will therefore change depending on if the vehicle is running in a curve or on a straight track.

Coupling of vertical and lateral modes In figure 4.8 another important effect is illustrated: the coupling between the vertical and lateral direction. For the example of bogie 3 it is found that the vertical response depends mostly on the vertical track excitation. Since the coupling between purely lateral excitation and vertical modes is very low the influence of lateral suspension parameters on the vertical vehicle response will also be low. This is not the case for the lateral response of the vehicle. Figure 4.8 shows that the vertical excitation has an important effect on the lateral mode. For frequencies above 23Hz it is more important than the lateral excitation. The comparison between the transfer function for a combined vertical and lateral track excitation with the sum of the transfer functions for separated vertical and lateral excitation shows important differences, indicating the coupling of

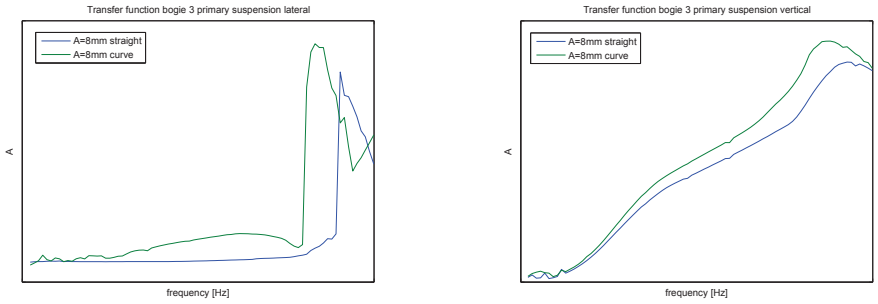

(a) Lateral (b) Vertical

Figure 4.7: Transfer function of primary suspension bogie A in lateral and vertical direction for a straight track and a curve

the system. The combined track excitation leads to a significant increase of the vehicle response.

The same behaviour can be observed for bogie 1 shown in figure 4.9 for the vertical and lateral response.

Effect of the wavelength With its two wheelsets positioned at a distance of 3m the bogie acts as a filter. Figure 4.10 shows the transfer fucntion between vertical track displacement and the displacement in the middle of the bogie as a function of the track wavelength. Depending on the wavelength contained in the track irregularity the transfer function amplitude will vary and modify the influence of modes and suspension parameters. If the track used in the simulation is filtered this might have an important effect on the parameter identification.

In figure 4.11 the transfer functions are compared for a sinusoidal track of 3 and 4 m wavelength. While for a wavelength of 3m corresponding to the axle distance of the bogie all wheels are moving in phase a wavelength of 4m leads to pitch and roll movements of the bogie frame. In particular on the lateral mode this movement has an important effect.

4.2.1.3 Detection of nonlinearities using transfer functions

The effect of nonlinearities on the dynamic behaviour of the system and their correct representation in the model is of high importance for the parameter identification problem. If a nonlinear behaviour of the real system is repre-

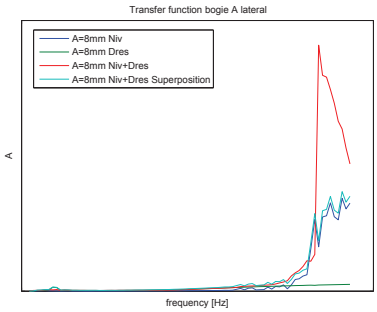

(a) Lateral

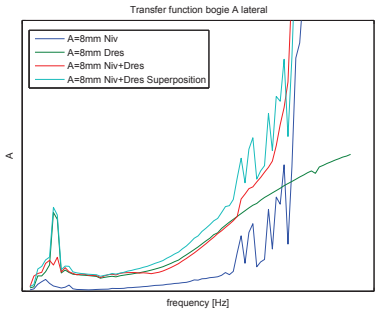

(b) Lateral zoom

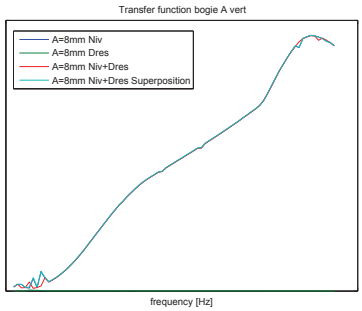

(c) Vertical

Figure 4.8: Transfer function of primary suspension for bogie 3 in lateral and vertical direction for vertical, lateral and combined sinusoidal track excitation (Niv: vertical track displacement, Dres: lateral track displacement, Niv+Dres: vertical and lateral track displacement, Niv+Dres superposition: sum of the vertical and lateral transfer function)

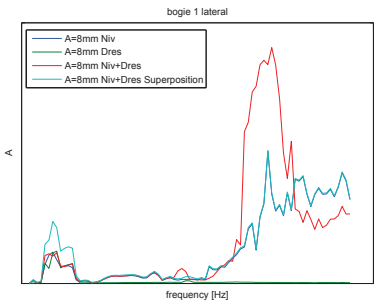

(a) Lateral

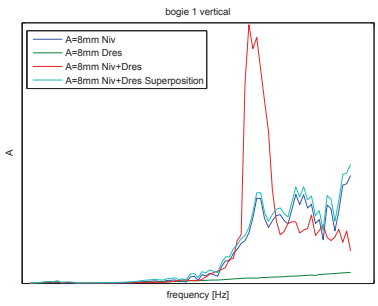

(b) Vertical

Figure 4.9: Transfer function of primary suspension for bogie 1 in lateral and vertical direction for vertical, lateral and combined sinusoidal track excitation

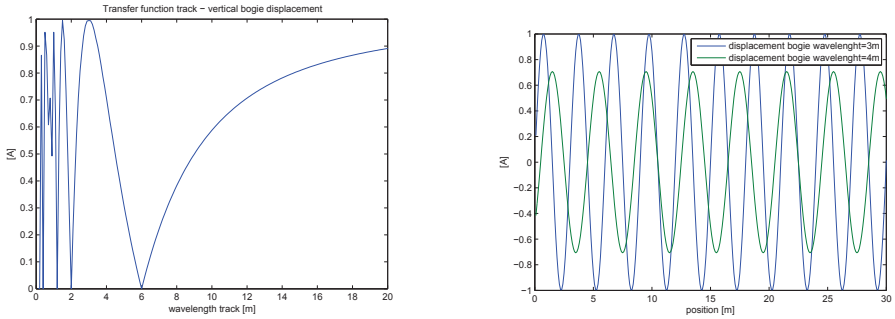

(a) (b)

Figure 4.10: Transfer function between track and bogie displacement as a function of the track wavelength (a) and bogie displacement for 3 and 4 m wavelength (b)

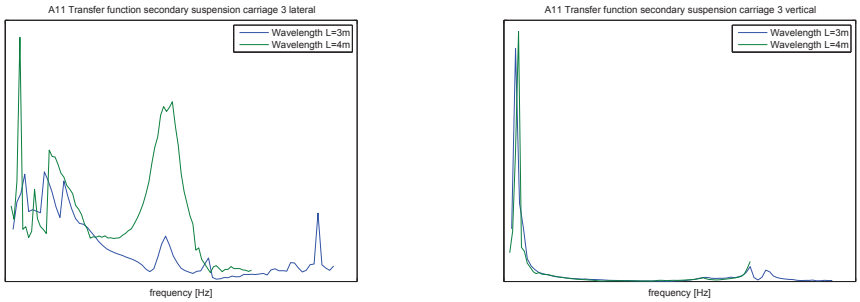

(a) Lateral (b) Vertical

Figure 4.11: Transfer function of secondary suspension in bogie 3 in lateral and vertical direction for track wavelengths 3m and 4m

sented by a linear or unsuitable nonlinear model the model will not be able to reproduce the real system behaviour at different excitation conditions. The application of the parameter identification at one defined running and excitation condition would lead to an adjustment of the model at this working point.

From the previous results it is known that the running conditions have an important influence on the dynamic behaviour of the vehicle. A model which is able to reproduce the real system behaviour at these different conditions requires thus a correct representation of the nonlinearities.

For the detection and characterisation of nonlinearities the transfer functions are a suitable tool. As outlined in figure 4.6 they are calculated both for the model and the real system. For the model the response is calculated for sinusoidal track excitation with different amplitudes. For the real system the transfer functions are calculated from the wheel-forces and the accelerations in the bogies and car bodies. Since the wavelengths and amplitudes of the track irregularities vary randomly along the track a comparison of the modes for different track defects is not possible. However, from a Short time Fourier Transform of the wheel forces a dependence on the vehicle speed is found. Figure 4.12 shows the vertical force in bogie A.

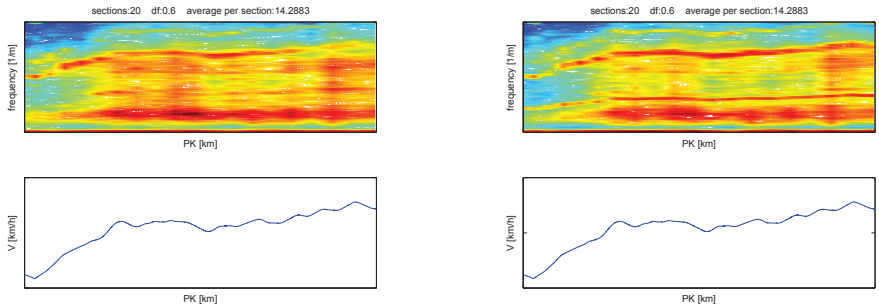

(a) STFT of the vertical wheelforce 11 in bogie A wheel

(b) STFT of the vertical wheelforce 21 in bogie A wheel

Figure 4.12: STFT of wheelset forces in bogie A in vertical direction

Since the transfer functions are calculated between the wheel-forces and the accelerations the comparison at different speeds is equivalent to different excitation levels allowing thus to study the effect of nonlinearities. In figure 4.13 the transfer functions for the model and the real system are compared

for the lateral direction of the primary suspension of bogie A. In both cases a nonlinear mode is found between 20 and 30 Hz representing the primary suspension.

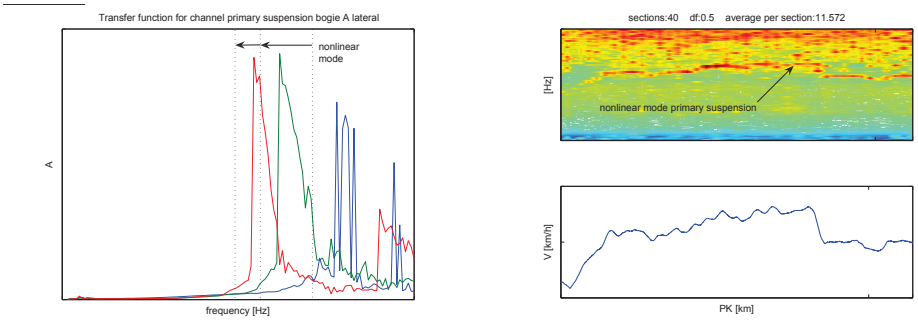

(a) Model (b) Measurement

Figure 4.13: Transfer function of primary suspension in bogie A in lateral direction: sine excitation at three different amplitudes A (a) and STFT of measurement (b)

As outlined before the transfer function is calculated from the auto- and crossspectra using a spatial sectioning. The choice of the section length and number of averages per section as illustrated in figure 4.14 is important for the detection of the nonlinear mode.

If the number of sections is chosen too large as in figure 4.15 (a) the nonlinear mode is rarely visible due to the unsteady excitation caused by the track irregularities. By reducing the number of sections to 80 and averaging over around 1km using the Welch method 4.15(b) the effect of the track irregularities is reduced and the nonlinear speed-dependent mode is better visible. If the section is much larger than the speed variation the speed dependence of the mode is not clearly visible either as it can bee seen in figure 4.15(c). The complete results of the transfer function analysis can be found in appendix D. They show the important effect of nonlinearities on many transfer functions. In general, the influence of nonlinearities on vertical modes is low while for the lateral modes nonlinearities can not be neglected.

4.2.1.4 Detection of nonlinearities from phase plots

The nonlinearities of the model have been represented using phase plots. For a linear system the response to a sinusoidal excitation is likewise a sine. A

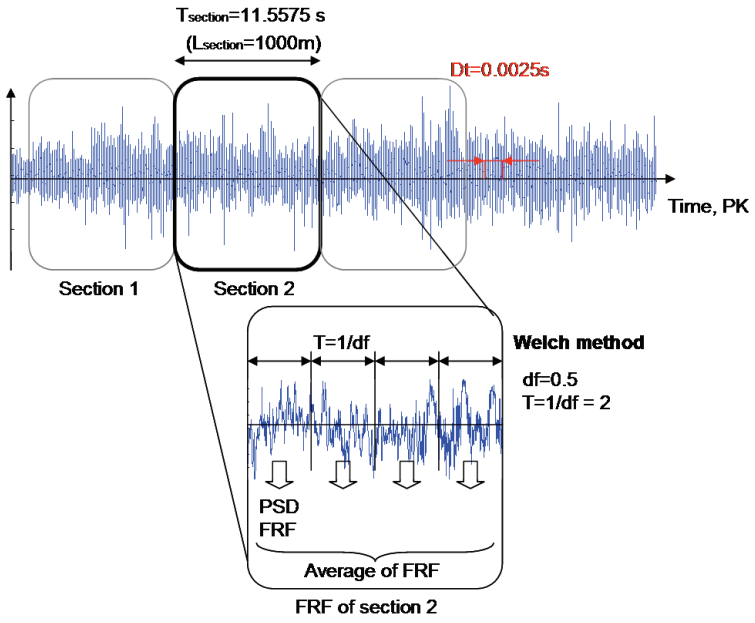

Figure 4.14: Computation of the power spectral density and transfer function for each section using the Welch method

deformation of the sinusoidal signal indicates nonlinearities. By plotting the displacement and the force together a phase plot is obtained. Since the effect of the nonlinearities depends on the excitation frequency the phase plots have been calculated at three different frequencies. Figure 4.16 shows the phase plot and the plots relating the displacements in bogie and carbody of carriage 3 for different frequencies. The deformation of the phase plot from the elliptical shape at 2Hz in lateral direction indicates a nonlinear behaviour.

4.2.2 First Calibration of the initial model estimated from the correlation and misfit function

Before applying the parameter identification the initial model is calibrated. The calibration requires a comparison of the model response with the measurement in order to quantify the performance of the model for the initial parameter values as a function of the different running conditions and in order to detect possible modelling errors.

Due to the important effect of nonlinearities and different running conditions the parameter identification will be performed in the time domain using ac-

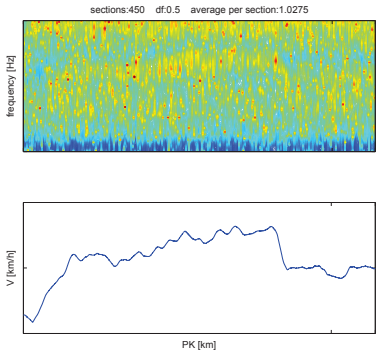

(a) 450 sections, no averaging

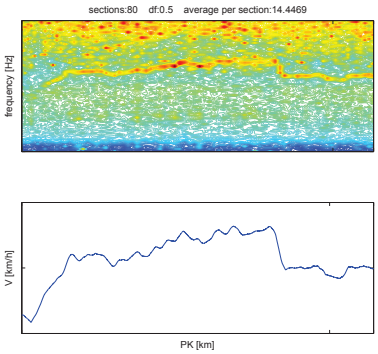

(b) 80 sections, average of 14 blocks

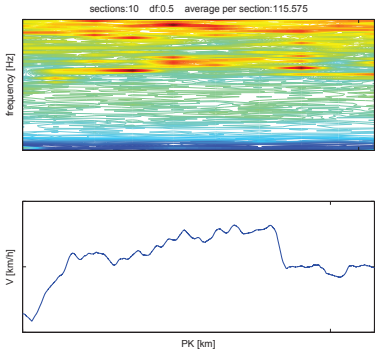

(c) 10 sections, average of 110 blocks

Figure 4.15: Transfer function for different numbers of sections: 450 (a), 80 (b), 10 (c)

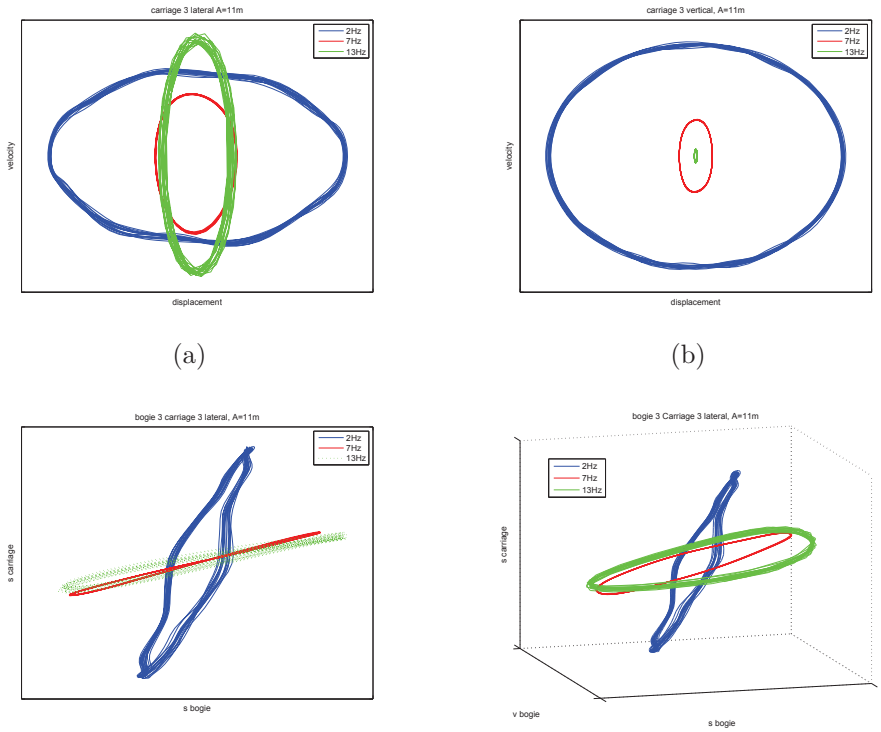

Figure 4.16: Phase plot for the carriage 3 in lateral (a) and vertical (b) direction at excitation frequency 2Hz, 7Hz, and 13Hz. In (c) the displacements of bogie and car-body are plotted. In (d) the speed in the bogie is added

celeration signals directly. It is therefore reasonable to proceed in the same way as for the validation of the bogie model. The time signals of the measured accelerations and forces are compared directly to the results of the simulation and a misfit function calculated from the least-square distance is defined.

A visual comparison of the time signals for the whole line is not possible and calculating only one misfit function value for the whole line leads to a complete loss of spatial information. Therefore a sectioning is used in the same way as for the track irregularities in section 4.2.1.1. As illustrated in figure 4.17 the response signals are divided in sections of 250m length and the correlation and misfit functions are calculated.

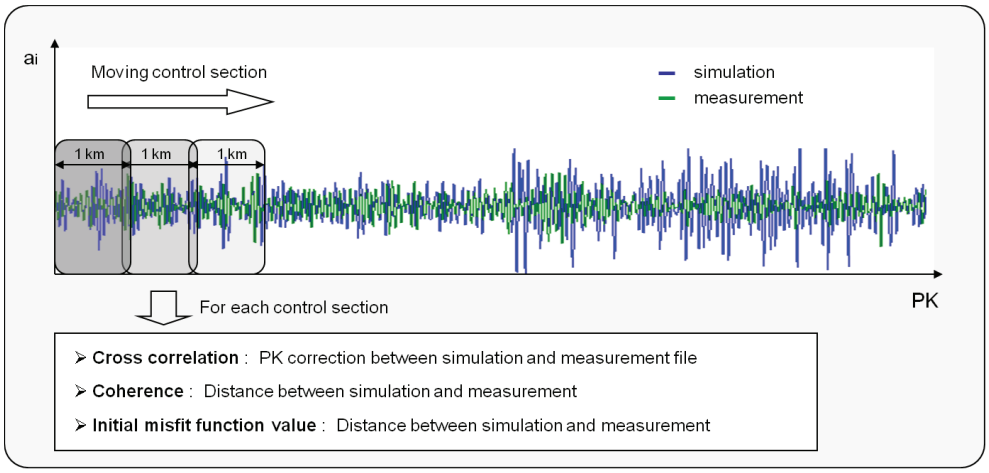

Figure 4.17: Comparison of measurement and simulation for every channel by calculating the correlation, coherence and misfit function or each section

A difficulty becomes obvious when the time signals are compared. Between the measurement and the simulation result a shift in the kilometre signal (PK) appears which depends on the position along the line and the considered acceleration signal.

4.2.2.1 Correction of the PK shift

A PK shift between the measurement and simulation signal leads to important misfit function values so that the misfit function does not represent the actual distance between measurement and simulation. A precise correction of the PK shift is therefore indispensable in order to obtain reliable misfit

function values.

The PK shift is caused by the fact that the track irregularities and the vehicle response are not measured in the same train. The track irregularities are measured in the IRIS 320 test train while for the vehicle response a TGV Duplex has been used. Inaccuracies in the PK measurement systems lead to errors in the PK position.

In order to adjust the PK position of the accelerations signals relatively to the track irregularities their cross correlation function is used. Since the signals are non-periodic stochastic signals a distinct peak is obtained indicating the shift. Although this correction can be applied to all acceleration signals the best coherence is obtained between the vertical irregularity and the vertical axle-box acceleration signals. The axle-box acceleration is measured below the primary suspension thus avoiding the effect of nonlinearities. It serves quasi as a sensor for the vertical track defect. The PK correction is illustrated in figure 4.18.

4.2.2.2 Computation of the correlation and misfit function per section

After dividing the measurement and simulation signals in sections of equal length (250m) the previously described PK correction is applied to each section. In the case that the coherence between the signals is too poor and no distinct shift is obtained, an interpolation from the neighbouring sections is used.

Having the PK shift corrected, the power spectral density, the coherence function and the misfit function are calculated. The power spectral density and the coherence function indicate the correlation between measurement and simulation as a function of frequency. They allow to choose the frequency range for which the parameter identification is performed. Additionally the transfer functions calculated in section 4.2.1.2 can be used. As an example figure 4.19 shows the PSD and the coherence function for the lateral acceleration in bogie A at PK51. A good correlation between model and simulation until 12Hz is found. The divergence at higher frequencies might be due to elastic modes in the real structure.

Finally for the chosen frequency range the initial misfit function is calculated. For the previous example a low misfit function value of 26.5% relative to the measurement is obtained (figure 4.20). Finally, the result for the misfit func-

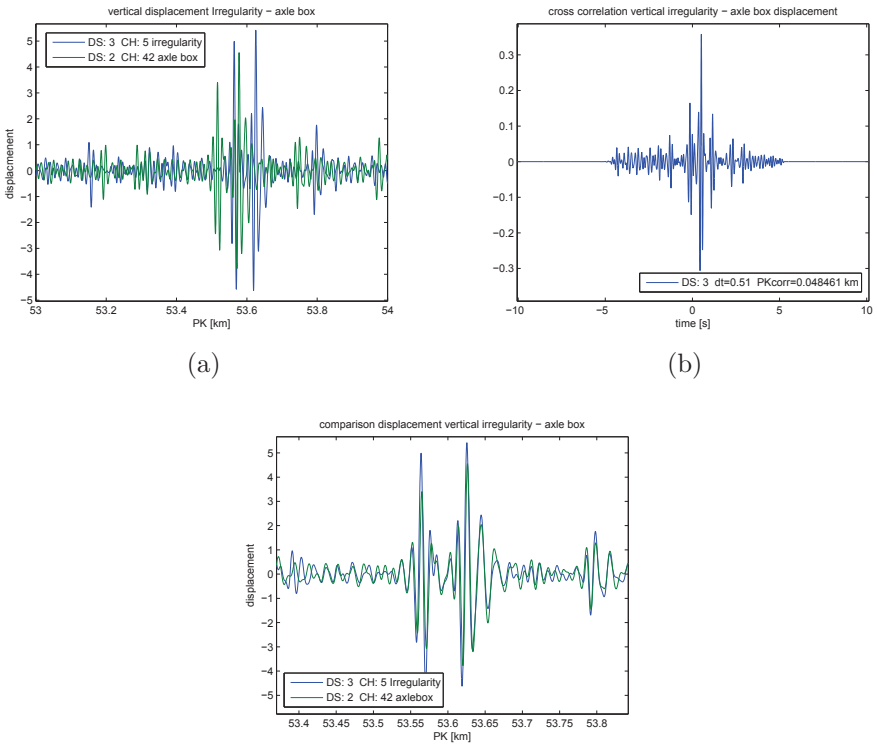

Figure 4.18: Correction of the kilometer position (PK): time signal of the track irregularity and axlebox acceleration signal before correction (a), cross correlation function between vertical track irregularity and vertical axlebox acceleration (b), corrected time signal (c)

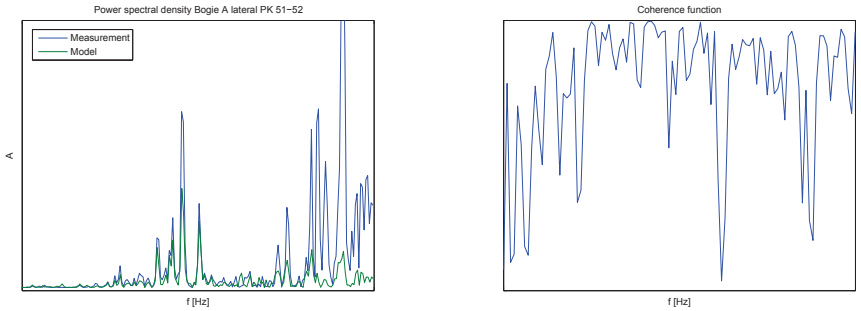

(a) Power spectral density (b) Coherence function

Figure 4.19: Power spectral density and coherence function for PK 51-52 for bogie A lateral

tion is plotted for all sections as a function of the PK position in figure 4.21.

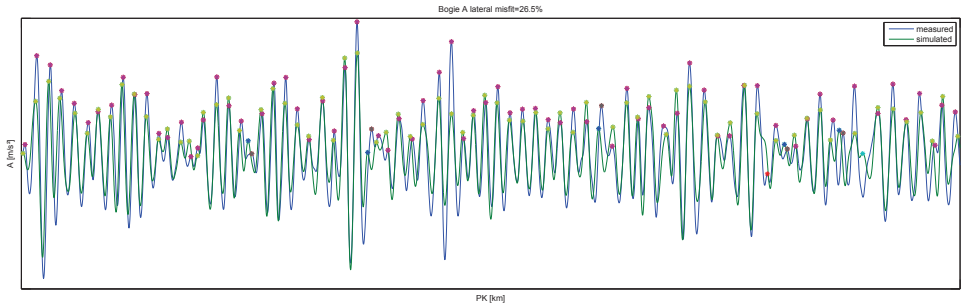

Figure 4.20: Comparison of measurement and simulation for the lateral acceleration in bogie A giving a misfit function value of 26.5%

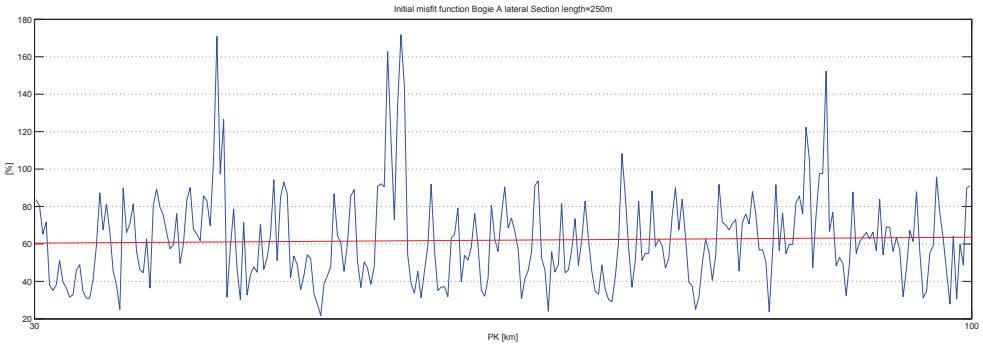

Figure 4.21: Misfit function describing the distance between measured and simulated acceleration in bogie A calculated for sections of 250m length

Figure 4.21 shows an important variation of the misfit function values between 20% indicating a very good conformity between model and measurement and 170% for the worst section. How can this variability of the misfit function be explained? One approach is to consider the correlation of the misfit function values with the previously defined track irregularities and design. Figure 4.22 shows the correlation between the maximum of the amplitude and of the amplitude/wavelength coefficient with the misfit function for bogie A lateral for 300 sections between PK 30 and PK 100. Even though no important correlation is observed it is found that the misfit function is

lower for higher amplitude and amplitude/wavelength values. One explanation is that for sections with very low irregularity levels the vehicle response is controlled by other excitations or the eigendynamics of the vehicle.

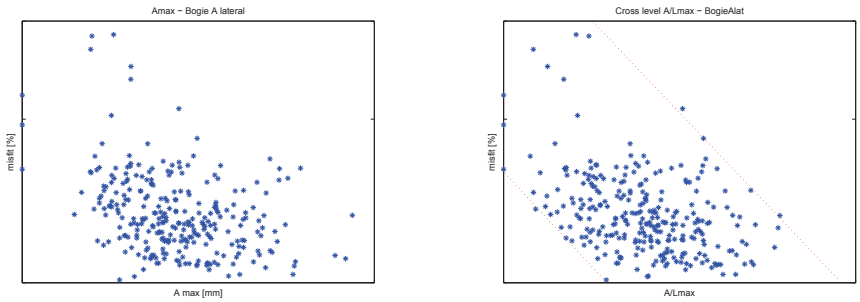

(a) Amplitude - misfit function

(b) Amplitude/wavelength - misfit function

Figure 4.22: Correlation between the cross-level defect amplitude and amplitude/wavelength with the misfit function in bogie A lateral

Figure 4.23 illustrates the correlation between the track curvature and cross-level offset. It can be seen that low misfit function values appear in straight track (curvature=0) while the highest values appear in curves. The model reproduces better the behaviour on a straight track.

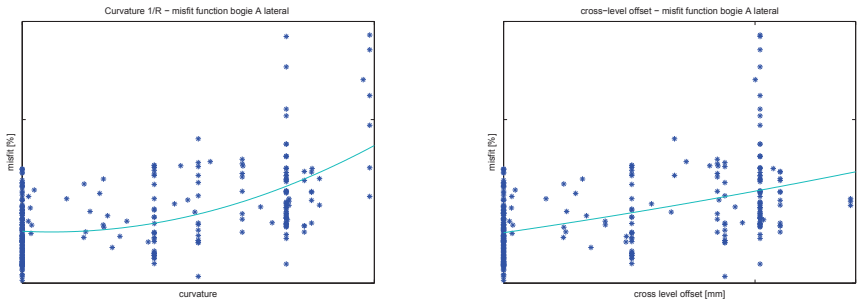

(a) Curvature - misfit function

(b) Cross-level offset - misfit function

Figure 4.23: Correlation between the curvature and the cross-level offset with the misfit function in bogie A lateral

The complete results of the model validation can be found in the appendix E. In general, the misfit function is worse for the lateral direction characterized

by important nonlinear effects. While the misfit function for the vertical wheel forces is mainly around 15% the lateral forces are worse reproduced by the model with misfit function values between 40% and 90%. Finally it is observed, that the misfit function deteriorates for accelerations measured above the secondary suspension.

4.2.3 Sensitivity analysis: coupling between substructures and choice of identifiable parameters

A requirement for the definition of the identification problem is a detailed knowledge about the coupling of the system and the identifiability of the model parameters.

Coupling describes the interaction between different degrees of freedom of the system. For the TGV model the coupling between the different substructures (bogie and car body for the traction units and the carriages) as well as the vertical and lateral direction is considered. It describes the influence of a suspension element acting in one defined direction on the vehicle response in other substructures and directions.

The identifiability of the model parameters is strongly related to their influence on the vehicle response. Only parameters having an influence on a model response for which measurement data is available can be estimated. Parameters which are not identifiable are excluded from the identification problem.

Both problems require to calculate the influence of all parameters of interest on the model response. This is done by applying the sensitivity analysis which has been used already for the bogie model in chapter 3. Both the local screening and the global Morris method are applied. As for the bogie model the least-square misfit function between the model response for nominal parameter values and the response for the modified parameter value is used as criterion.

Correlation between parameter values When applying the sensitivity analysis to the TGV model it is necessary to determine wether or not the model parameters are correlated. In order to correctly answer this question a statistical analysis of a sufficiently large number of parameter measurements or a very precise physical model would be required. Both are not available.

The measurement of the parameter values would require to measure the suspension elements separately on a test rig.

In the absence of this correlation information two estimations are compared:

- One assumes that all parameters values of the same element type are completely correlated corresponding to a correlation factor of 1. This means that all elements of the same type are described by the same value. Values of different element types are not correlated. This approach has been used for the definition of the identification problem in the next section.
- The other estimation assumes that no correlation exists even between the parameter values of the same element type. In practice the second approach is difficult to implement since the number of parameter increases drastically.

4.2.3.1 Calculation of the solution surface by varying one parameter

The screening method is applied to 117 model parameters using a tolerance of 50%. A list of the analysed parameters can be found in appendix B. The misfit functions are calculated for each bogie and car body in vertical and lateral direction giving in total 36 misfit functions (figure 4.24).

For each couple parameter-misfit function the result is obtained in form of a graph describing the misfit function value as a function of the parameter value. Figure 4.25 shows as an example the influence of the coil spring stiffnesses cy and cz of the primary suspension in the traction unit on the vertical bogie accelerations. It can be seen that the vertical stiffness has an important influence on the vertical acceleration in the bogies of the traction unit described by a convex misfit function (b). The influence on the vertical acceleration on the carriage bogies is negligible. In vertical direction the coupling between traction unit and carriages is very low. The lateral stiffness has a negligible influence on the vertical acceleration of all bogies (a).

As a second example the nonlinear yaw damper is regarded in figure 4.26. It has a strong influence at low values. The solution surface of the misfit function shows many local minima.

For the representation of the coupling of all parameters with the vehicle response in total 4212 misfit function have to be taken into account. In order

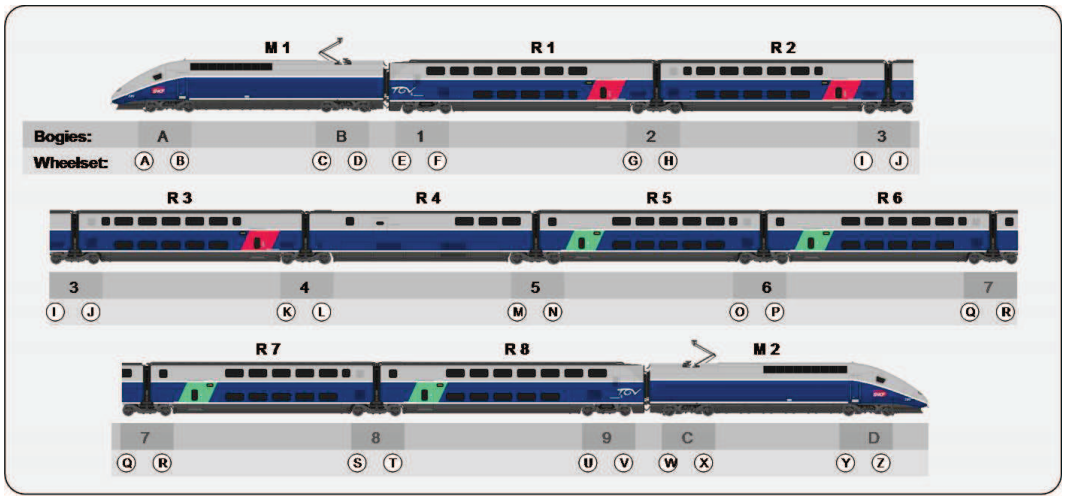

Figure 4.24: Numeration of car bodies, bogies and wheelsets for the TGV Duplex train

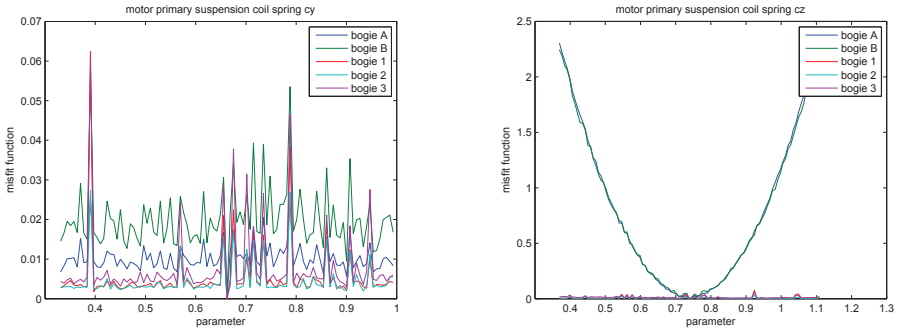

(a) Coil spring cy (b) Coil spring cz

Figure 4.25: Sensitivity of the vertical bogie accelerations with respect to the lateral (a) and vertical stiffnesses (b) of the coil spring in the primary suspension of the traction unit

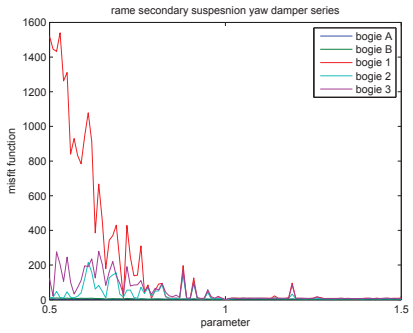

Figure 4.26: Sensitivity of the lateral accelerations in bogies A,B,1,2 and 3 with respect to the series stiffness of the yaw damper

to simplify the analysis of the result a more compact representation of the results is used in the following which describes each misfit function by only one value. As shown in figure 4.27 this value can be either the maximum, the mean or the standard deviation value of the misfit function over the defined parameter tolerance. A comparison of the values gives qualitatively the same results. Then these values are arranged in a table with the model parameters on the x- and the misfit function values on the y-axis. Their amplitude is expressed by a color bar as shown in figure 4.28.

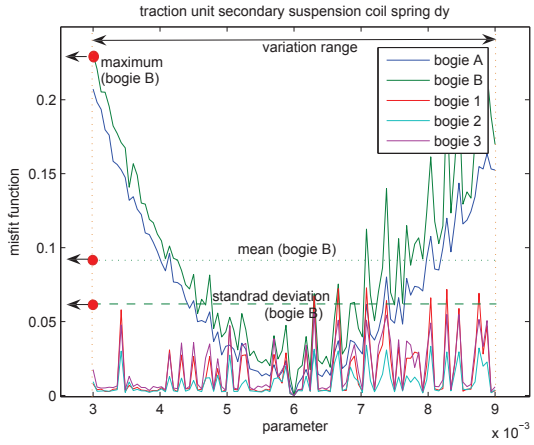

Figure 4.27: Representation of the sensitivity by one value: maximum, standard deviation or mean value

Figure 4.29 shows the result of the screening analysis for the bogies using

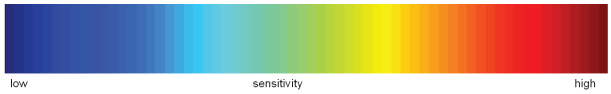

Figure 4.28: Intensity of parameter sensitivity used in table representation

the standard deviation. Several important results appear. The coupling of the system differs completely between the vertical and lateral direction. In vertical direction the coupling is low. The vertical response of the traction unit bogies is controlled by vertical suspension parameters of the traction unit. The same is valid for the bogies of the carriages. In lateral direction in contrary all parameters have an important influence on the model response. Some parameters like the airspring and the yaw damper stick out. The system is strongly coupled and the minimization of a misfit function requires to take into account a large number of parameters. In general the same result is obtained for the car bodies as shown in figure 4.30. The influence of the parameters in lateral directions differs more than for the bogie response.

4.2.3.2 Sensitivity taking into account the parameter interaction

The sensitivity of a parameter on the vehicle response obtained from the screening analysis does not take into account the interaction of the parameters. It can cause changes of the sensitivity of one parameter due to changes of the other parameter values. In order to take into account this interaction, important in particular for nonlinear systems, the Morris method is applied to the TGV model.

For each misfit function the result is obtained in form of a point distribution with the overall effect indicated on the x- and the coupling on the y-axis. As an example figure 4.31 shows the result for the bogie A in lateral and vertical directions. The result is conform with the result obtained from the screening analysis. In vertical direction only some vertical suspension parameters of the traction unit have an influence (vertical damper, coil spring, etc.) The interaction between them is important. All other parameters have a negligible influence. In lateral direction on the contrary an important interaction between a large number of parameters is found with the anti-yaw damper as an element which is particularly important. In both cases the bogie mass has an outstanding influence.

As a second example the car body acceleration of carriage 2 is regarded in figure 4.32. In general, the influence of the parameters on the lateral response

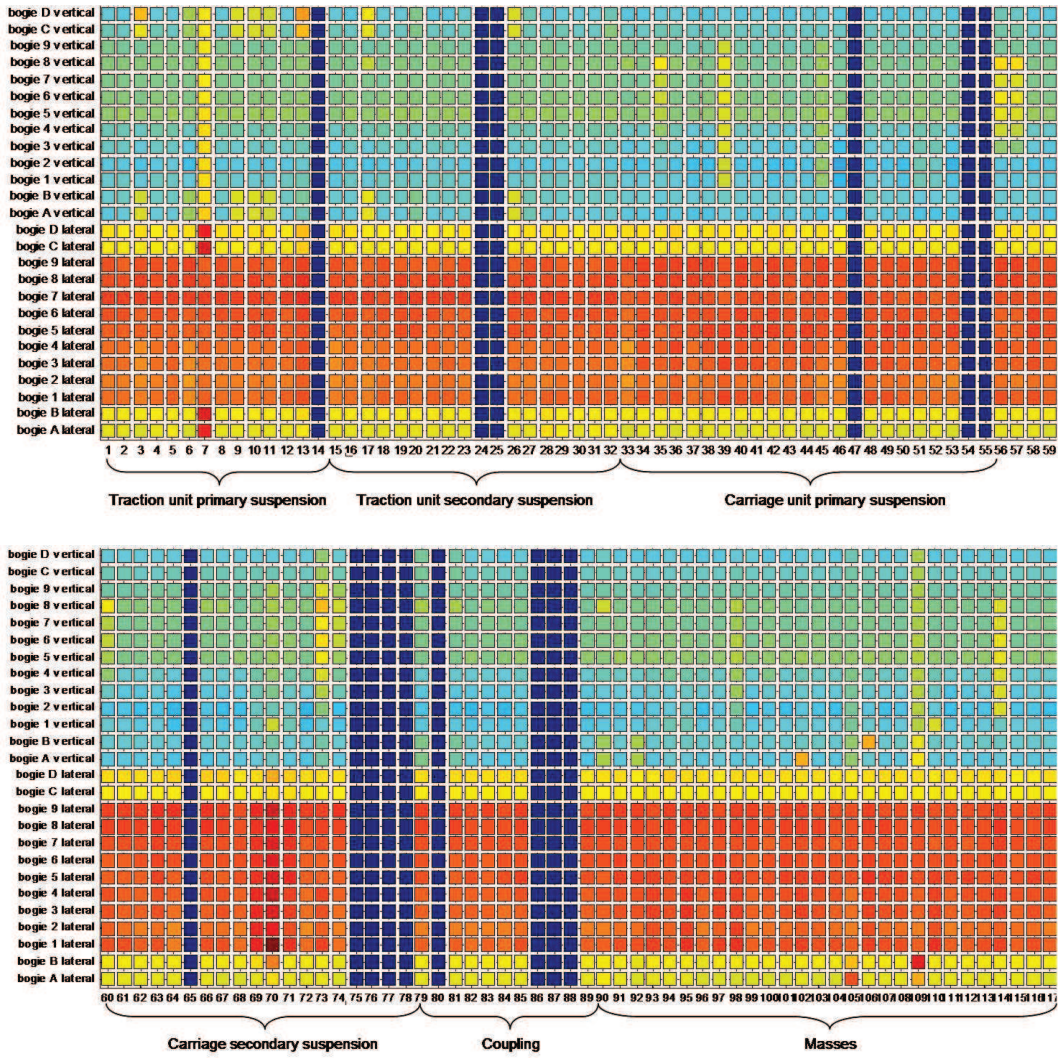

Figure 4.29: Screening for the accelerations in the bogies in vertical and lateral direction with 50 % variance using the standard deviation

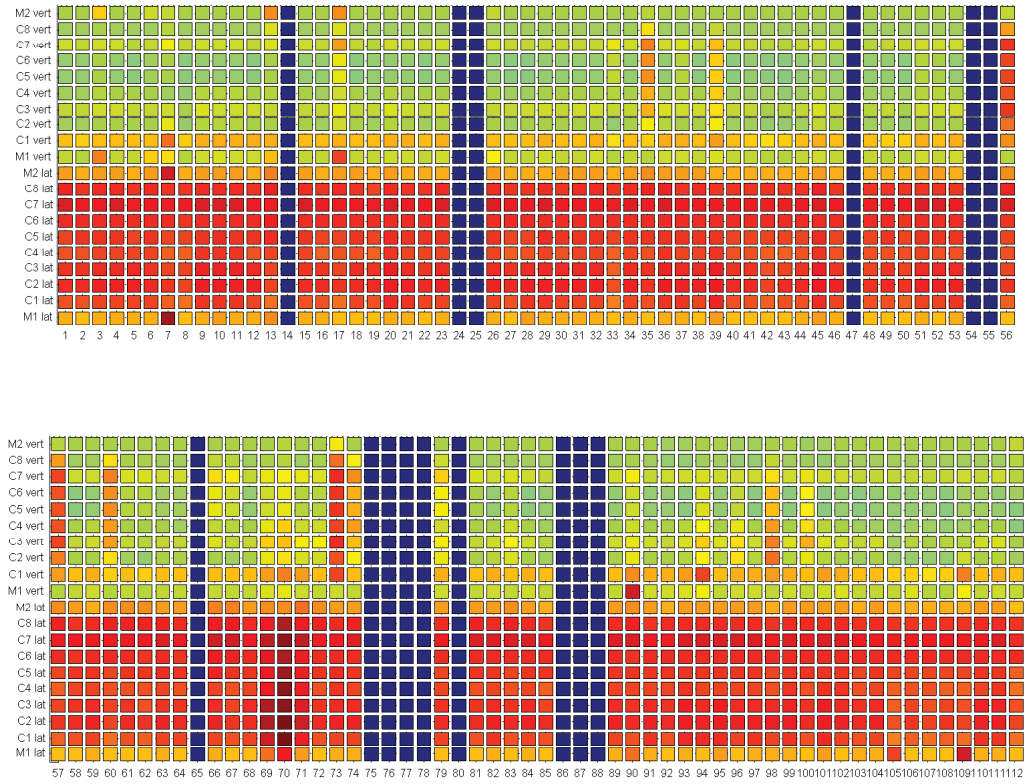

Figure 4.30: Screening for the accelerations in car bodies in vertical and lateral direction with 50 % variance using the standard deviation

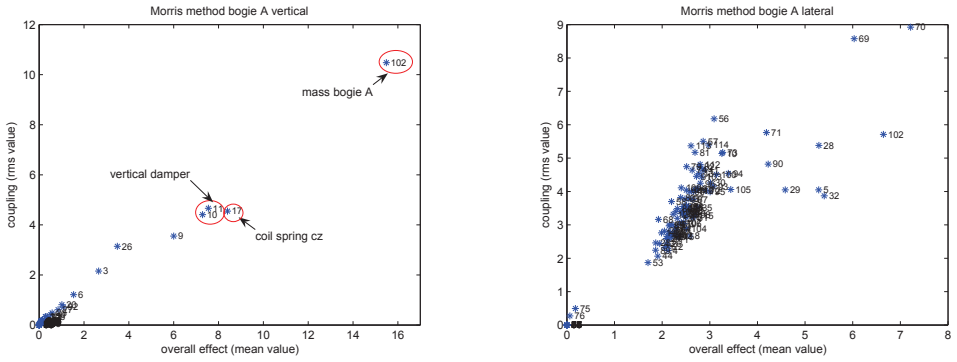

(a) Vertical (b) Lateral

Figure 4.31: Morris method for bogie A vertical (a) and lateral(b)

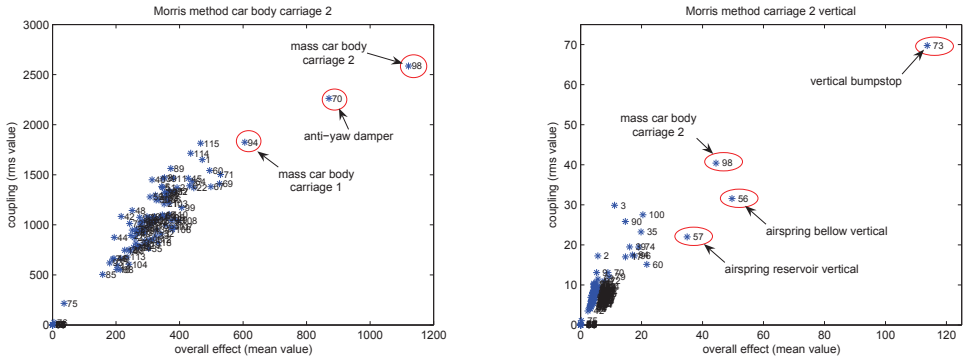

(a) Lateral (b) Vertical

Figure 4.32: Morris method for carriage 2 in lateral (a) and vertical direction (b)

is much higher. The interaction between a large number of parameters is important. The vertical response is less sensitive to parameter changes and controlled by few parameters notably the airspring.

In the same way as for the screening analysis the results are visualised in table format. Figure 4.33 shows the overall effect of 117 parameters on the bogie misfit functions. In figure 4.34 the coupling is represented in the same form. If the results are compared to the screening analysis in figure 4.29 the same parameters as for the screening analysis are pointed out. However, especially in vertical direction the Morris method shows that more paramters have an important effect of the vehicle response. Examples are the coil spring damping of the secondary suspension in the traction unit (20) or the nonlinear vertical damper of the primary suspension of the carriages (51, 52). Figure 4.35 shows the overall effects of the parameters on the carriage misfit functions.

4.2.3.3 Sensitivity for independent suspension parameters

For the sensitivity analysis and the identification of the parameters it is supposed that all parameters of the same element type are completely correlated corresponding to a correlation factor of one. For an adjustment of the model to the measurements this appraoch is considered as sufficient. It has the advantage that the number of parameters taken into account stays manageable. Besides, information about the real correlation between the parameter values is not available. The other estimation which can be applied assumes

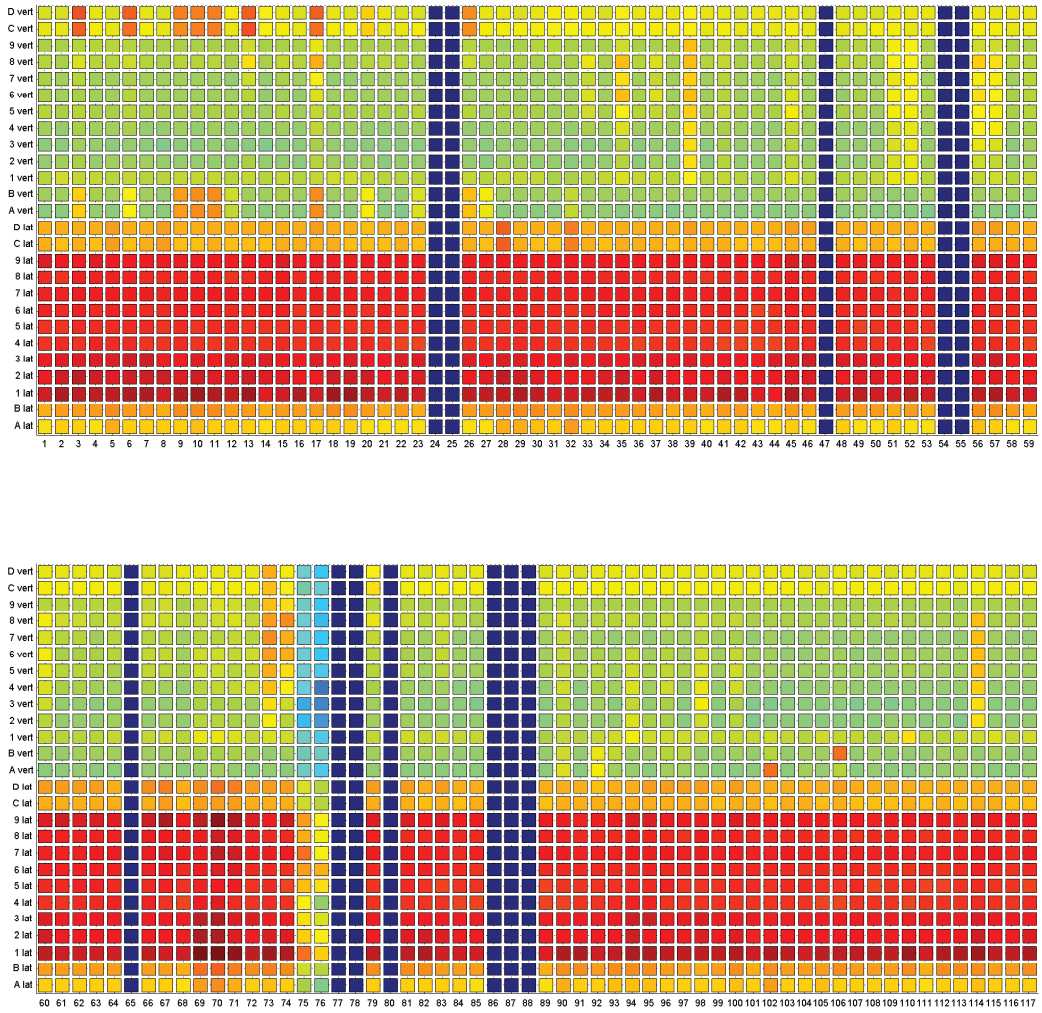

Figure 4.33: Morris method for the bogies in vertical and lateral direction for the overall effect using real track excitation

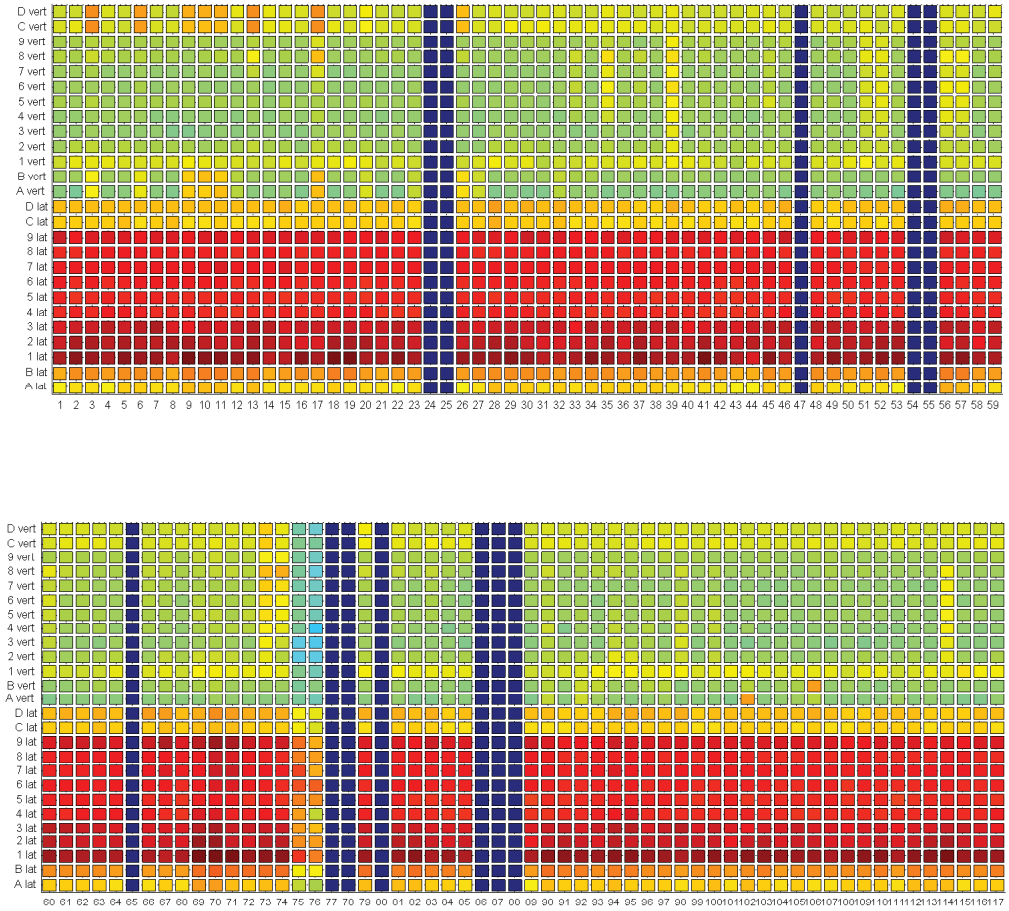

Figure 4.34: Morris method for the bogies in vertical and lateral direction for the coupling effect using real track excitation

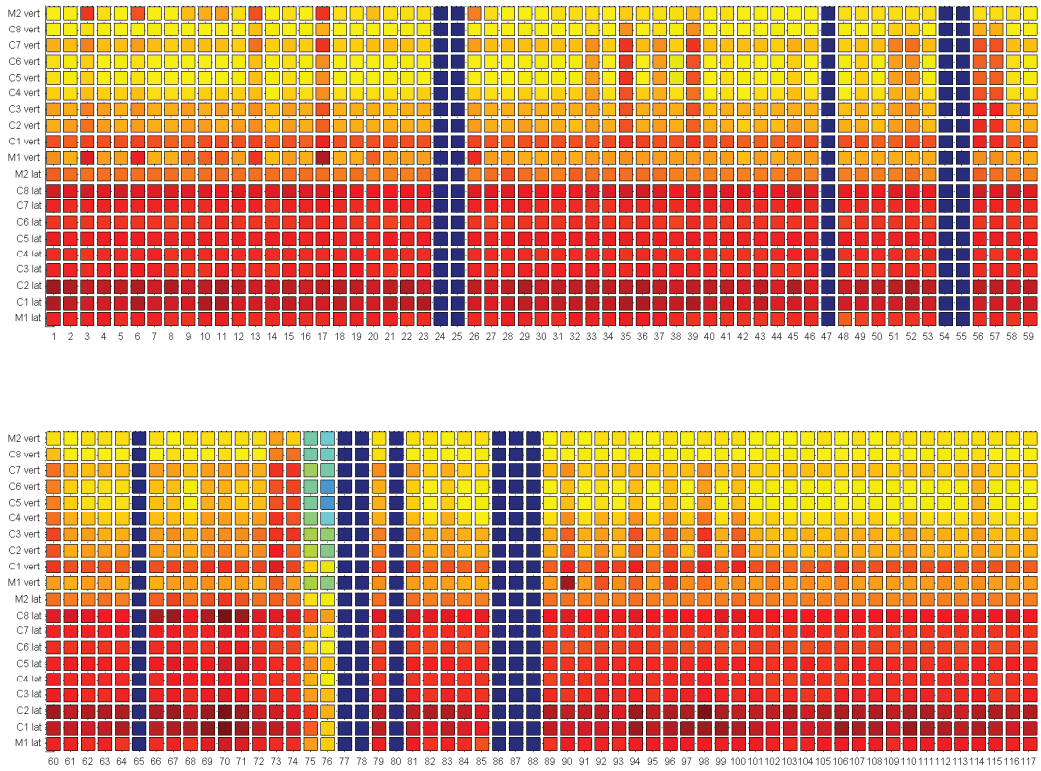

Figure 4.35: Morris method for the carriages in vertical and lateral direction for the overall effect using real track excitation

in contrary that no correlation exists between the parameter values of the same element type. This approach leads to a drastic increase of the number of parameters and has not been completly implemented. Therefore only an example is shown here. It presents the results for the parameters of the primary suspension in the carriages. For every wheelset 24 parameters are needed: 6 stiffnesses for all degrees of freedom and 6 damping values both for the left and right side. Calculated for the bogies 1 to 7 336 parameters are considered in total. Figure 4.36 shows the result for the parameters 1 to 200. It reveals an important coupling between the carriages of the train. Only the vertical stiffness and damping parameters have a distinctive local effect on the vertical response. In lateral direction no local effects are visible due to the high coupling. Both for the vertical and lateral direction the effect of parameters changes is more distinct in the middle of the train.

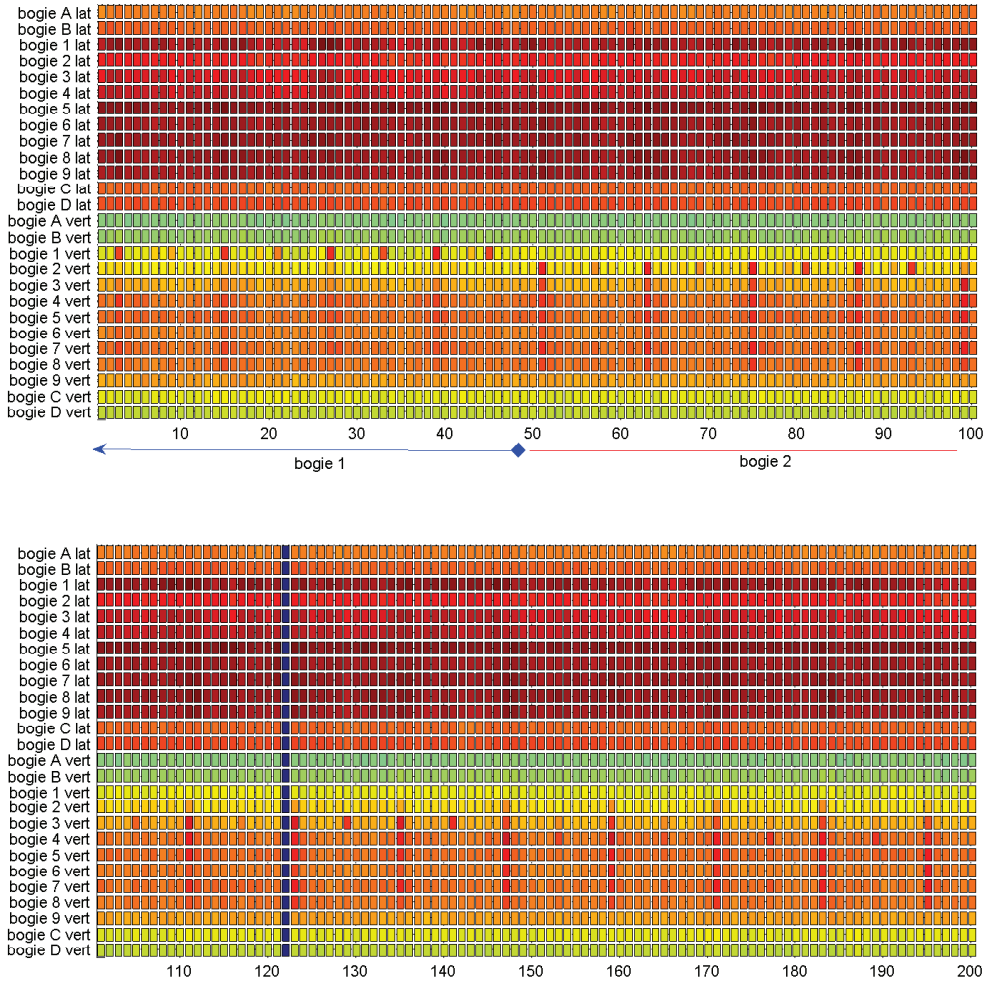

Figure 4.36: Morris method for the bogies in vertical and lateral direction for the overall effect using real track excitation and independent parameters of the primary suspension

4.3 Parameter identification

From the first section of this chapter all the information is available which allows the definition of the parameter identification problem.

From the coupling analysis it is known that for a minimisation of the vertical vehicle response the substructures traction unit and carriages can be considered independently. For the vertical response of bogie A only 8 parameters have been identified as important: coil spring stiffness cz of the primary suspension, the guidance spring damping dx and dz, the vertical damper characteristic, the vertical bumpstop, the coil spring stiffness cz and the vertical damper of the secondary suspension. A minimisation of the misfit functions for the lateral vehicle response requires to take into account most of the parameters.

The nonlinearities detected from the transfer function analysis are taken into account for the choice of the identification method. Taking the previous example the vertical response of bogie A is not influenced by nonlinearities. The misfit function found for the coil spring has a convex form allowing the use of local methods. The lateral vehicle dynamics are characterised by important nonlinearities leading to complex solution surfaces with local minima. A minimization of these misfit functions can only be obtained when global algorithms are used.

4.3.1 Misfit function

For the identification problem the misfit functions are defined between the measured and simulated vehicle response. Since the accelerations are not measured in the centre of gravity the result obtained from the simulation have to be recalculated for the exact measurement position taking into account the rotation of the body. This is done using the rotational matrix R. In order to identify the exact accelerometer position which is not always known a priori the misfit function has been calculated as a function of the accelerometer position. The acceleromter position is varied in the range of geometrically possible values and the misfit function is calculated.

Figure 4.37 shows the misfit function for the vertical acceleration in bogie A as a function of the longitudinal and lateral accelerometer position. A distinct minimum is found at x=0.84m and y=-1m relative to the centre of gravity of the bogie. This corresponds approximately to the theoretical position defined at the primary suspension. Using this accelerometer position

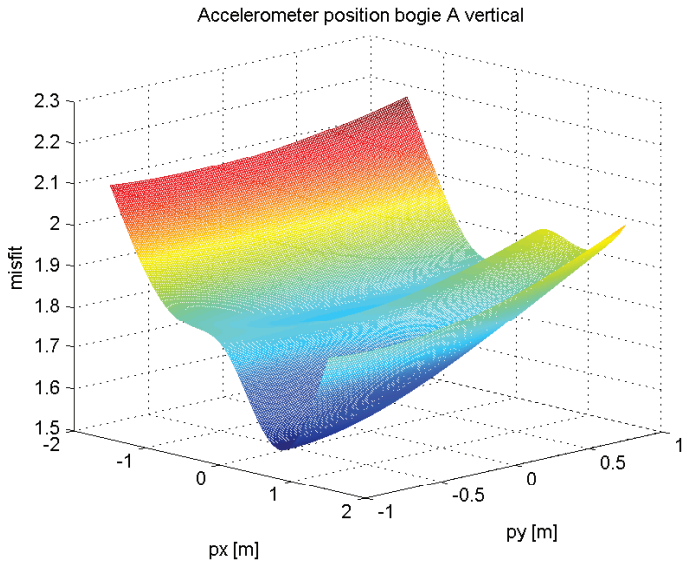

Figure 4.37: Misfit function for the vertical acceleration in bogie A as a function of the accelerometer position

the measured signals are much better described by the simulation as shown in figure 4.43 for the previous example.

Misfit function criteria For the misfit function two different criteria have been used: the least-square criterion already used for the bogie model and a criterion taking into account only the maxima of the response. This is reasonable since for the analysis of the comfort and security only the peaks of the vehicle response are of interest. The maxima criterion is illustrated in figure 4.39. It is based on the detection of the maxima of the measured and simulated response. For each measured maximum the existence of a corresponding simulation maximum is checked. In a first step simulation maxima in a certain control region around the measured maxima are identified giving well defined couples. If the number of simulated and measured maxima between two of these couples is the same further couples are taken into account. The misfit function is then defined using the amplitude and position distance of each couple as well as the difference in the number of maxima per section.

Frequency range The frequency range for which is misfit fucntion is calculated depends on the model description and the frequency content of the excitation signal. As outlined before the validity of the model is limited

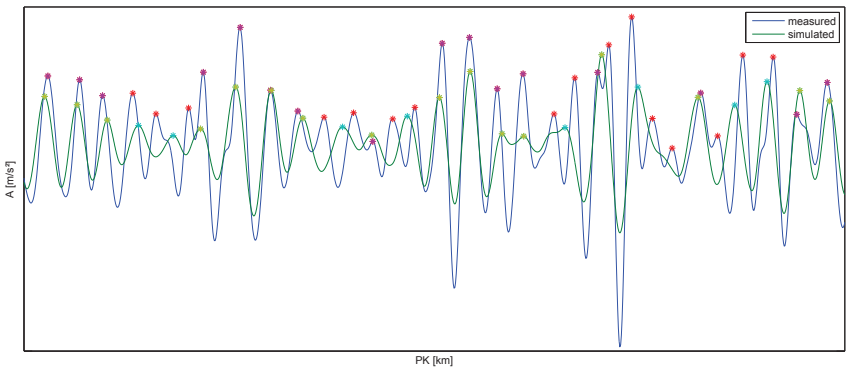

(a)

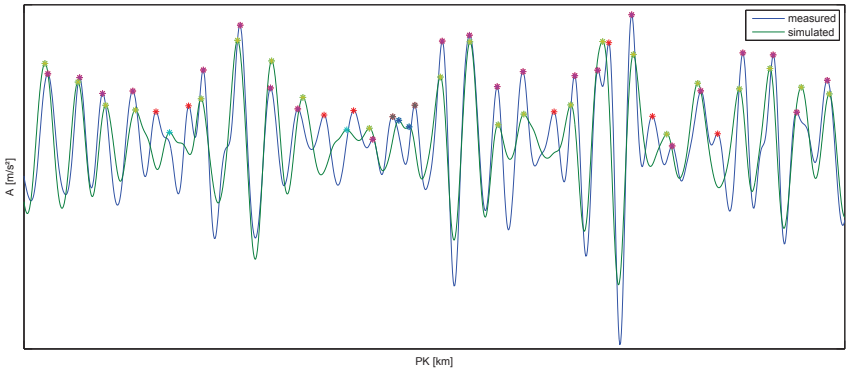

(b)

Figure 4.38: Accelerations signals for bogie A vertical without (a) and with (b) correction of accelerometer position

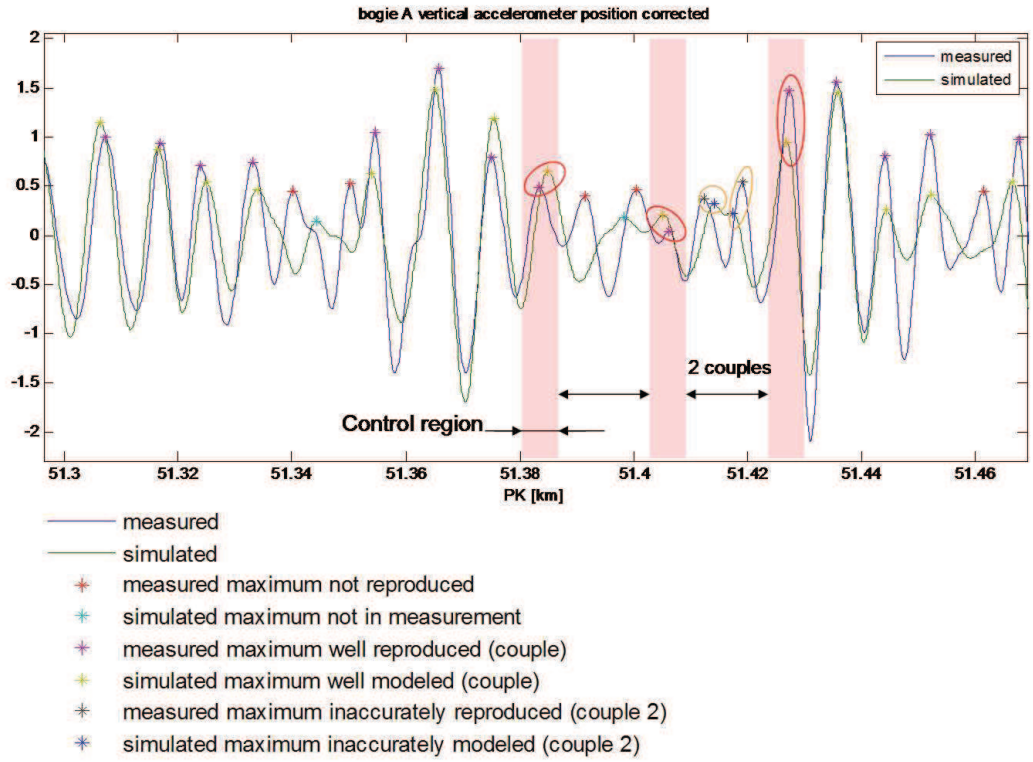

Figure 4.39: Misfit function criterion based on the maxima values of the time signal

by the fact that elastic modes are not taken into account. The maximal frequency considered in the misfit function is given by the lowest eigenfrequencies of the elastic modes which have an influence on the vehicle response. The second limitation is given by the frequency range of the excitation signal. For the IRIS320 measurement train which measures the track irregularities between 3m and 200m the excitation signal contains frequencies between 0,4 and 28Hz at a speed of 300km/h.

4.3.2 Identification problems

Taking into account the coupling and influence of nonlinearities different identification problems have been defined. They are summarized in table 4.1 and their results discussed in the following sections.

The notation used in the tables:

- Optimization methods (Opt): SA: Simulated annealing, GA: Genetic algorithm, PS: Pattern Search
- Misfit function criterion (C): LS: Least aquares, Max: maximal values
- Channel type: TU: Traction unit, C: Carriage, PS: Primary suspension, SS: secondary suspension
- Track type (T): s: straight track, c: curved track
- Masses (M): cb: car body

4.3.2.1 Bogie A vertical

At first only the vertical acceleration of bogie A is used for the misfit function. The optimization is performed for the global simulated annealing and genetic algorithm method as well as for the local pattern search method. For the misfit function the least-square and the maxima criteria are used.

The identification is performed for several different configurations. An important distinction is the number of model parameters taken into account. In the simplest case the parameter vector is formed by eight parameters of the suspension of traction unit 1 which have been identified from the sensitivity analysis. By introducing the PK correction between measurement and simulation signal as additional parameter possible shifts due to changes in the eigenfrequencies can be corrected during the optimization process. In another configuration all suspension parameters are taken into account. The

	Misfit function						Parameters								
Opt	C	Bogie		Car body		dof	Suspension				PK	M	T	Tol	Num
		lat	vert	lat	vert		TU PS	TU SS	C PS	C SS					
SA	LS Max	-	A	-	-	3	3 6 9 10 11	17 20 26	-	-	yes no	-	s,c	50, 10	8
SA	LS Max	-	A	-	-	3	3 6 9 10 11	17 20 26	-	-	yes no	cb	s,c	50, 10	8
SA	LS Max	-	A	-	-	3	all	all	all	all	yes no	-	s,c	50, 10	76
SA	LS Max	-	A	-	-	3	all	all	all	all	yes no	cb	s,c	50, 10	76
GA	LS	-	A	-	-	3	3 6 9 10 11	17 20 26	-	-	yes no	-	s	50, 10	8
GA	LS	-	A	-	-	3	all	all	all	all	yes no	-	s	50, 10	76
GA	LS	-	A	-	-	3	all	all	all	all	yes no	cb	s	50, 10	88
PS	LS	-	A	-	-	3	3 6 9 10 11	17 20 26	-	-	yes no	-	s	50, 10	8
PS	LS	-	A	-	-	3	all	all	all	all	yes no	-	s	50, 10	76
SA	LS Max	-	-	R2	-	3	all	all	all	all	yes no	-	s	50, 10	76
SA	LS	-	-	R2	-	3	all	all	all	all	yes no	cb	s	50, 10	76
GA	LS	-	-	R2	-	3	all	all	all	all	yes no	-	s	50, 10	76
SA	LS	A B	A B	M1	M1	11	all	all	all	all	yes no	-	s	50, 10	76
GA	LS	A B	A B	M1	M1	11	all	all	all	all	yes no	-	s	50, 10	76
SA	LS	A B 1 2 3	A B 1 2 3	M1 R1 R2 R3	M1 R1 R2 R3	22	all	all	all	all	yes no	-	s	50, 10	76
SA	LS	A B 1 2 3	A B 1 2 3	M1 R1 R2 R3	M1 R1 R2 R3	22	all	all	all	all	yes no	cb	s	50, 10	76
GA	LS	A B 1 2 3	A B 1 2 3	M1 R1 R2 R3	M1 R1 R2 R3	22	all	all	all	all	yes no	-	s	50, 10	76
PS	LS	A B 1 2 3	A B 1 2 3	M1 R1 R2 R3	M1 R1 R2 R3	22	all	all	all	all	yes no	-	s	50, 10	76

Table 4.1: Parameter identification methods and test configurations

configuration with the highest number of parameters includes also masses and inertia.

In order to study the effect of the running conditions the identification is applied both to a section of straight track (PK 51-52) and to a section of curved track (PK 41-42).

Finally the optimization is performed for three different parameter tolerances: unconstrained, 50% and 10%. In the first case the parameter values are not restricted to a certain range. A convergence to values outside the physically possible range can indicate modelling errors. In the second and third case the range of admissible parameter values is limited to 50% and 10% of the nominal value respectively.

The results for this first identification problem are summarized in table 4.2. The most important reduction of the misfit function of 62% is obtained for the highest number of parameters on straight track for the unconstrained optimization (case 15). The obtained parameter values are nevertheless outside the range of realistic values indicating that the algorithm has not converged to the sought minimum. By restricting the variation range to 50% around the nominal value 50% reduction are obtained (case 5). A further reduction of the variation range to 10% reduces the gain considerably (case 17).

If only 8 parameters are considered the gain is slightly reduced to 42% (case 2) for 50% variation. This indicates the importance of these parameters for the model response. The inclusion of the PK correction as an optimization parameter has a small positive effect comparing cases 1 to 2 and 4 to 5.

As an example figure 4.40 shows the optimization result for case 1. The misfit function is reduced by 41.5%. As a convergence criterion the stabilization of the misfit function is used. If its value has not varied more than 1% over the last 1000 iterations the optimization is finished. Eventually a local search has been performed afterwards. Figure 4.41 shows the vehicle response for the estimated parameter values. The simulation reproduces well the measurement.

If the three different optimization methods are compared for the same configuration approximately the same misfit function gain is observed. For the pattern search method (case 20) this is interesting since it indicates the convex form of the solution surface which has been found already from the screening analysis in figure 4.25.

Bogie A vertical (frequency range 1-10Hz, 3 dof)											
Configuration								Misfit gain			
	Meth	Crit	PK	Num	Tol [%]	T	L [km]	init [%]	end [%]	red [%]	Iter
1	SA	LS	no	8	50	s	1	37.2	21.8	41.5	15000
2	SA	LS	yes	8	50	s	1	37.2	21.4	42.4	15800
3	SA	Max	yes	8	50	s	1	38.8	28.4	26.8 (42.6)	13000
4	SA	LS	no	76	50	s	1	37.2	19.3	48.3	12000
5	SA	LS	yes	76	50	s	1	37.2	18.9	49.5	11000
6	SA	LS	yes	76	50	s	2	130	18.9	20	-
7	SA	Max	yes	76	50	s	1	37.7	30.5	21.2 (35)	-
8	SA	LS	no	8	50	c	1	37.7	28.9	23.6	-
9	SA	LS	yes	8	50	c	1	37.5	28.9	22.8	-
10	SA	Max	yes	8	50	c	1	146.3	110	24.8 (-7)	-
12	SA	LS	no	76	50	c	1	37.6	27.3	27.4	-
12	SA	LS	yes	76	50	c	1	37.8	26.7	29	-
13	SA	Max	yes	76	50	c	1	146.3	12.63	14 (2)	-
14	SA	LS	no	76	-	s	1	37.4	14	63.3	11000
15	SA	LS	yes	76	-	s	1	37.4	16.2	57	11000
16	SA	LS	yes	88	-	s	1	37.3	14.4	61.5	11000
17	SA	LS	no	8	10	s	1	36.14	35.2	2.5	-
18	SA	LS	yes	76	10	s	1	37.26	34.87	6.7	-
19	SA	LS	yes	88	10	s	1	37.3	34.5	7.5	-
20	PS	LS	no	76	-	s	1	37.3	20.78	44.16	-
21	GA	LS	no	8	50(g)	s	1	37.5	20.6	45.1	-0
22	GA	Max	no	8	50(g)	s	1	39	19	51.26	-
23	GA	LS	no	76	50(g)	s	1	37.5	21.54	42.56	-
24	GA	LS	no	76	-	s	1	37.4	19	49.2	-
25	GA	LS	no	88	-	s	1	37.3	17.7	52.6	-

Table 4.2: Comparison of different configurations for the identification using the vertical accelerations in bogie A

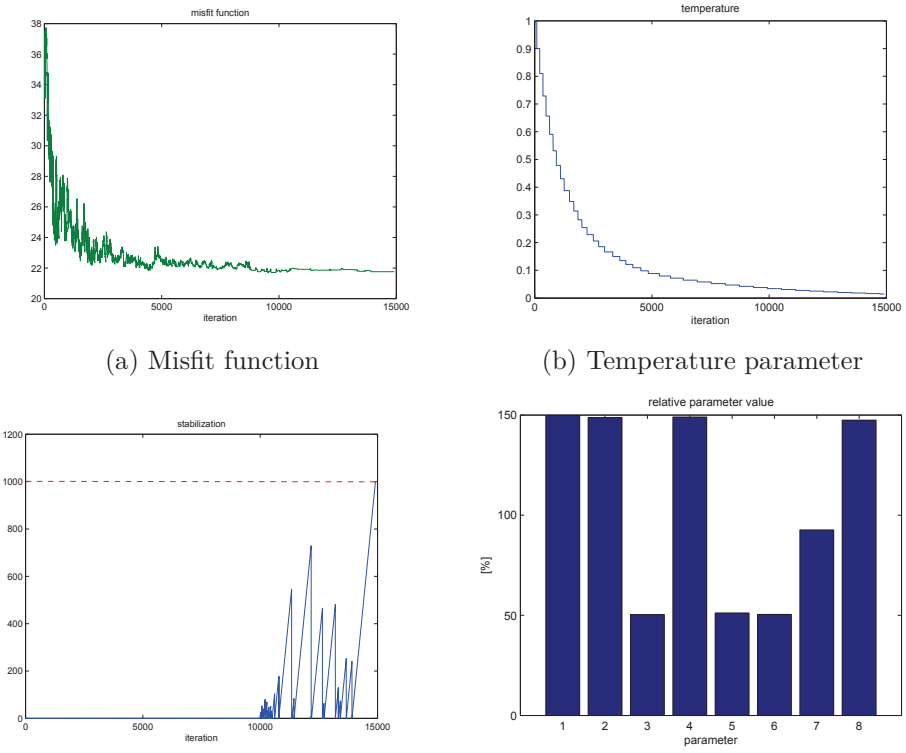

(a) Misfit function

(b) Temperature parameter

(c) Stabilization

(d) Relative parameter

Figure 4.40: Misfit function (a), temperature (b), stabilization (c) and parameters (d) for case 1

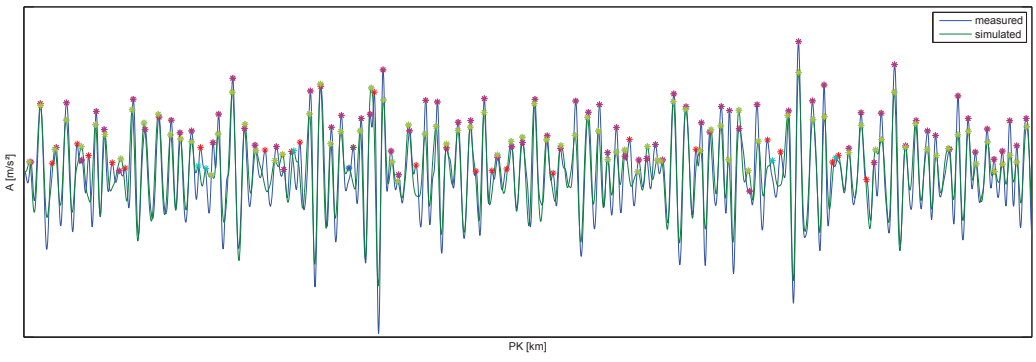

Figure 4.41: Measured and simulated acceleration signals for bogie A vertical after optimization for case 1

From the sensitivity analysis an influence of the track design on the model performance was found. Therefore the optimization has been performed both for straight and curved track. The misfit function gain is lower for curved track (PK 41-42) and the estimated parameter values differ from the straight track case (figure 4.42 and 4.43).

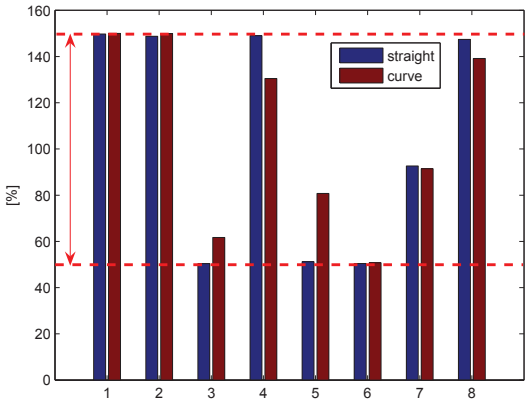

Figure 4.42: Estimated parameter values for straight and curved track with least square criterion (cases 1 and 8)

In figure 4.44 the relative parameter values are compared for the case that 76 parameters are considered. It is found that some parameter values differ considerably between straight track and curve. In particular lateral and longitudinal parameters which have an import influence on the dynamic behaviour in the curve are concerned. The guidance spring stiffness cx (4) is increased 50% for the straight track but reduced 50% for the curve. This might indicate that the nonlinear behaviour of the guidance spring is not well represented by the model. But if the sensitivity analysis is considered (figure 4.45) it is found, that the longitudinal stiffnesses of the coil and the guidance spring have a small influence on the considered vehicle response in straight track. The identification of these parameters from the straight track section is therefore not reliable. Instead, for the vertical stiffnesses (3) and (6) of these elements which have a strong effect on the vehicle response the same values are found for straight and curved track.

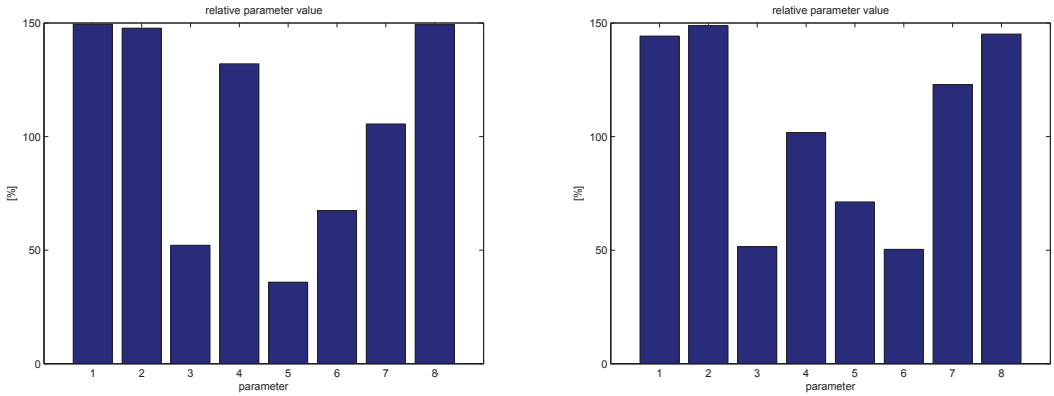

(a) straight line (b) curve

Figure 4.43: Estimated parameter values for straight and curved track with maxima criterion (cases 3 and 10)

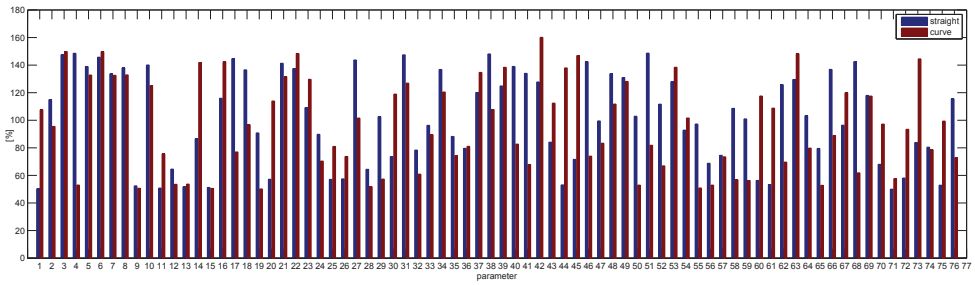

Figure 4.44: Estimated parameter values for straight and curved track with least square criterion (cases 5 and 9)

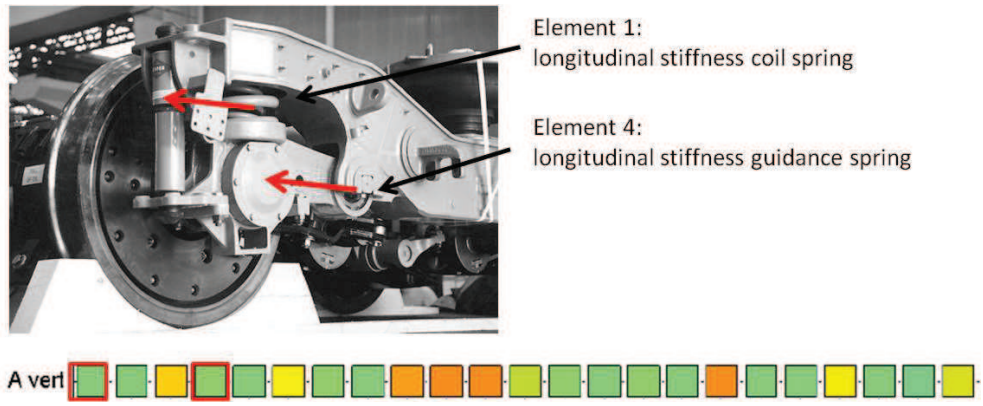

Figure 4.45: Sensitivity analysis for elements 1 and 4

4.3.2.2 Carriage 2 lateral

The second parameter identification problem studied in this work uses the lateral acceleration of carriage 2 in the misfit function. Its properties differ considerably from the first one. Due to the secondary suspension and nonlinear effect the initial misfit function value is worse. The least square criterion gives a value of 88%. The strong coupling in lateral direction found from the sensitivity analysis necessitates to take into account 76 suspension parameters. The problem is therefore highly under-determined. Besides, from the solution surface of the misfit functions the existence of many local minima was observed. The use of local optimization methods is therefore not possible.

The studied configurations and corresponding results are summarized in table 4.3.

Carriage 2 lateral (frequency range 1-10Hz, 3 dof)											
Configuration								Misfit gain			
	Meth	Crit	PK	Num	Tol [%]	T	L [km]	init [%]	end [%]	red [%]	Iter
1	SA	LS	no	76	50	s	1	92	56	39	6500
2	SA	Max	no	76	50	s	1	7	3	44.3	6000
3	SA	LS	yes	88	10	s	1	88	58	34	9100
4	GA	LS	no	76	1	s	1	88	51	42	177

Table 4.3: Comparison of different configurations for the identification using the lateral accelerations in carriage 2

The reduction of the misfit function obtained for 50% parameter tolerance is, with a value of 39%, lower than for the first optimization case. In comparison to the first identifcation problem an interesting result is obtained when the parameter tolerance is reduced to 10%. In contrast to the case of the vertical bogie acceleration the misfit function gain does not drop significantly when the tolerance is reduced to 10%. While it was reduced from 42.4% (2) to 6.7% (18) for the first optimization case the gain decreases only slightly to 34% for the lateral acceleration in the carriage. This indicates the important influence of the parameters on the lateral vehicle dynamics. Even small errors in the parameter values have an important effect on the model performance. In lateral direction the model is less robust. Figure 4.46 shows the relative change of the parameter values for a tolerance of 10%. It can be seen that some parameters - 4 of 8 airspring parameters - reach the defined boundaries. It illustrates the difficulty when a simple suspension element model is replaced by a more complicated one. The nominal parameters of the thermodynamic airspring model which replaced the simple equivalent stiffnesses are not well known and increase the complexity of the identification problem.

Using the Genetic algorithm with 1% admissible variation per generation a slightly higher misfit function gain of 42% is obtained. The figures 4.47 and 4.48 show the lateral acceleration signal in carriage 2 before and after the optimization for case 1.

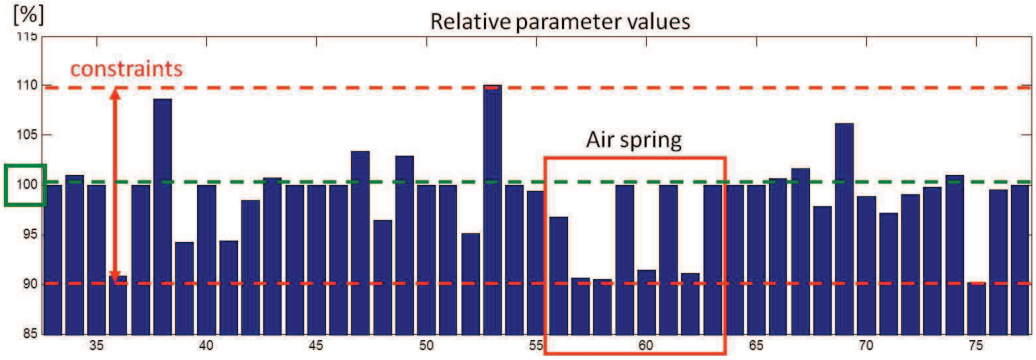

Figure 4.46: Relative changes of parameter values for a misfit function using the lateral acceleration in carriage 2

Figure 4.49 shows the misfit function calculated for sections of 250m length before and after the parameter identification. The misfit function is reduced for most of sections.

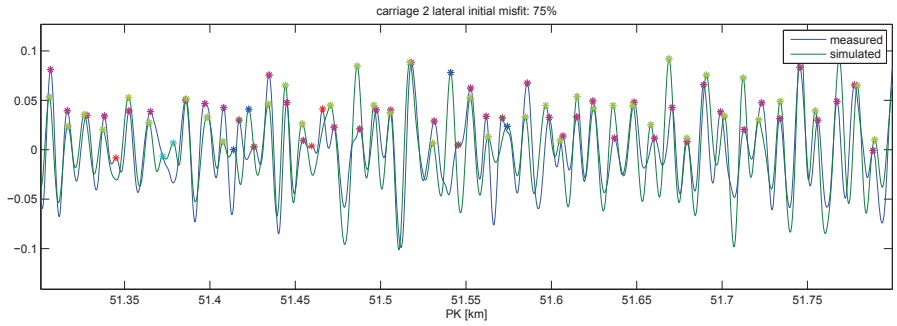

Figure 4.47: Measured and simulated acceleration signals for carriage 2 lateral before optimization for case 1

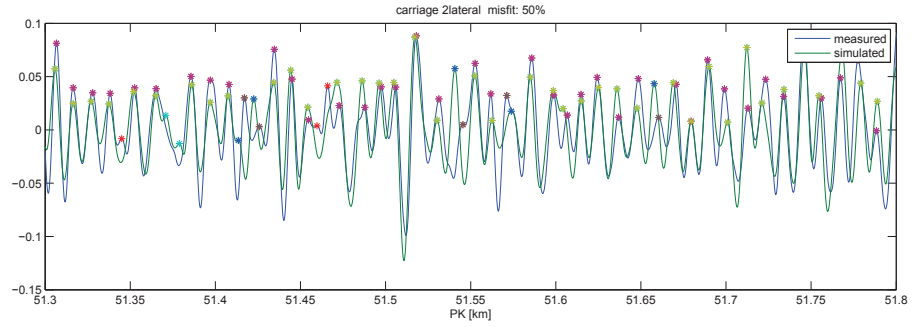

Figure 4.48: Measured and simulated acceleration signals for carriage 2 lateral after optimization for case 1

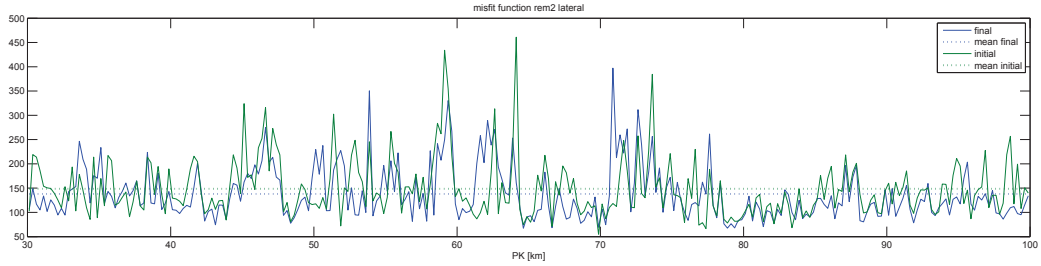

Figure 4.49: Misfit function before and after the parameter identification for section of 250m length for the lateral acceleration in carriage 2

4.3.2.3 Traction unit 1: bogies, car bodies, vertical, lateral

In the third identification problem the number of degrees of freedom considered in the misfit function is increased by including all available accelerations measured in traction unit 1. The misfit function therefore includes both vertical and lateral accelerations in the bogie and car body. Taking into account the rotations in total 11 degrees of freedom are considered. The number of parameters is 76 without and 88 with mass parameters. The coupling of the system in lateral direction requires to take into account also suspension parameters of the carriages.

The studied configurations and corresponding results are summarized in table 4.4.

Traction unit 1 (frequency range 1-10Hz, 11 dof)											
Configuration								Misfit gain			
	Meth	Crit	PK	Num	Tol [%]	T	L [km]	init [%]	end [%]	red [%]	Iter
1	SA	LS	no	76	50	s	1	42.2	40.5	4	4500
2	SA	LS	yes	76	50	s	1	44.2	39.3	11.2	9700
3	SA	Max	no	76	50	s	1	45.2	36.2	19.8	4500
4	SA	LS	yes	76	10	s	1	42.2	41.1	2.6	6500
5	SA	LS	yes	88	10	s	1	42.2	40.7	3.6	-
6	GA	LS	no	76	1	s	1	42.2	39.3	6.8	170
7	PS	LS	no	76	1	s	1	42.2	41.5	1.6	34

Table 4.4: Comparison of different configurations for the identification using vertical and lateral accelerations in traction unit 1

The combination of vertical and lateral responses in the misfit function leads to an important degradation of the misfit function gain. For a parameter tolerance of 50% only 11% reduction are obtained. This might indicate a conflict in the choice of the parameter values for vertical and lateral direction.

Due to the presence of local minima the pattern search method is not suitable for this identification problem.

4.3.2.4 Traction unit, carriages

The last identification problem studied in this work uses accelerations both from the traction unit and the carriages 1 and 2. In total 23 degrees of

freedom are considered. All model parameters are included in the parameter vector.

The studied configurations and corresponding results are summarized in table 4.5.

Traction unit 1 + Carriages 1, 2 (frequency range 1-10Hz, 23 dof)											
Configuration								Misfit gain			
	Meth	Crit	PK	Num	Tol [%]	T	L [km]	init [%]	end [%]	red [%]	Iter
1	SA	LS	no	76	50	s	1	47	40.6	13.6	9500
2	SA	LS	yes	76	50	s	1	47	40.3	14.3	7000
3	SA	LS	yes	88	50	s	1	47	39	17	5600
4	SA	LS	yes	76	-	s	1	47	38.3	18.6	5600
5	SA	LS	yes	76	10	s	1	47	43.3	7.9	11000
6	SA	LS	yes	76	10	s	1	47	43.3	7.9	11000
7	SA	LS	yes	88	10	s	1	47	42.5	9.6	8500
8	SA	LS	yes	32	10	s	1	47	44.3	5.8	11000
9	PS	LS	no	76	-	s	1	47	43.4	7.7	33
10	GA	LS	no	76	1	s	1	47	40.5	13.9	170
10	GA	LS	no	76	10	s	1	47	38.3	18.5	80
11	GA	LS	no	88	10	s	1	47	38	19.2	80

Table 4.5: Comparison of different configurations for the identification using vertical and lateral accelerations in traction unit 1

The highest reduction of the misfit function, obtained both for the simulated annealing (case 4) and the genetic algorithm method (case 11), is around 19% when the parameter values are not constrained. By constraining the parameter values to a range of 50% the reduction is reduced to 14% in case 2.

4.4 Conclusions

4.4.1 Discussion of errors in the parameter identification problem

The application of optimization methods on the parameter identification problems defined in the previous section allowed to adjust the model to the measurement. Reductions of the misfit function up to 60% could be obained. But even though the performance of the model could be improved important differences between the responses of the model and the measurement persist. For the response with the best conformance, the vertical acceleration in bogie A, the misfit function could not be reduced under 14%. For the other cases much higher differences persist.

The reasons for these errors are both modelling errors and measurement uncertainties. Modelling errors are due to the fact the the model is not an exact representation of the real system. In order to obtain a model with reasonable complexity and computation times not all physical effects of the real system can be taken into account. The second source of errors is measurement uncertainties. The excitations and the response of the real system can not be measured exactly.

4.4.1.1 Modelling errors

For the TGV model the restriction to rigid bodies is the most important limitation. The multi-body model is not able to reproduce the dynamic behaviour due to elastic modes. The modal analysis of the car body of a TGV train in [93] shows that the first eigenmodes lie at frequencies under 20Hz. The first vertical bending mode of the car body is found at 14.6Hz. It falls into the considered frequency range and can explain the divergence between model and measurement for frequencies above 15Hz. Other modes which might influence the result are the first torsional mode at 19.7Hz, the first lateral bending mode at 17,8Hz as well as a torional mode opposite to the axcitation at 14Hz. The modal shapes show that the primary suspension is not close to the nodal points. The identified modes can therefore be excited under operation.

The other important source of modelling errors is the suspension elements. The degradation of the misfit function observed for accelerations above the secondary suspension relative to the accelerations in the bogie illustrates this. For suspension elements with a complex physical behaviour in particular the

airspring and rubber spring elements simplified models are used. Moreover, a correct choice of the suspension parameters is made difficult by the lack of measured information on the real system behaviour. Only for some acceleration elements the measured nonlinear characteristics are available.

Varying conicity and friction conditions are not taken into account by the model either. Since no measurement information about these parameters is availbale constant values are used in the model.

Some physical effects are not considered by the model. For the TGV model excitations due to aerodynamic effects are not taken into account. Aerodynamic forces act on the car body and can explain the lower conformity between model and measurement above the secondary suspension. As shown in [6] they have a significant influence on the dynamic behaviour.

Unsteady aerodynamic forces on the train can be caused by side winds and turbulences due to bodies along the line (bridges) or trains passing on the opposite track. The last point is of importance since the measurement where performed during daytime and normal operation on the line.

Modelling erros can explain the convergence of parameter values to the boundary of the defined tolerances and different identification results on straight and curved track. As an example, the guidance spring stiffness cx value obtained by the identification increases 50% for straight track while a reduction of 50% was obtained for curved track. The differences in the mistfit function are likewise important with 19% for the straight and 27% for the curved track. In the curve many suspension elements are exposed to higher forces and modelling errors become apparent. Then the optimization for one running conditions leads to an adjustment at a certain working point but not for the whole operation range. Besides, the sensitivity analysis of the guidance spring stiffness cx showed that its influence is low on straight track. The identifiaction is therefore not possible.

4.4.1.2 Measurement uncertainties

Although modelling errors represent the main source of errors in the identification problem the influence of measurement uncertainties has to be considered also. The measurement of the track excitation and accelerations is corrupted by measurement noise and unknown systematic errors. Important to mention are the not exactly known accelerometer positions and the shift in the kilometer position (PK). The influence of these errors on the parameter

identification has been analyzed by repeating the identification for varying errors. As reference for the identification a simulation with the known parameter values is used. The effect of the PK and accelerometer position error on the parameter estimation is illustrated in figure 4.50 for the example of the coil spring stiffness in bogie A. It is found that already small uncertainties in the position of the accelerometer and a kilometer shift lead to an important difference between estimated and real parameter value.

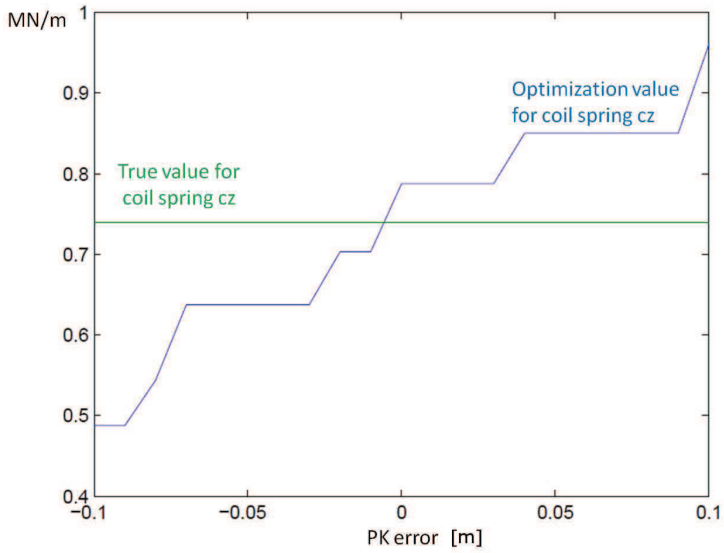

Figure 4.50: Influence of the PK error on the identification result for coil spring stiffness cz

Therefore the correction of the PK shift is essential for a reliable parameter identification. It is performed using the cross-correlation function between measurement and simulation result calculated per section. The shift is obtained in the time domain and translated to a spatial shift using the mean velocity of the section. The correction is therefore a mean value per section and different section length might lead to different results. The section in figure 4.51 has been devided in several numbers of subsections and the PK correction values are calculated. Figure 4.52 shows the obtained PK corrections for each subsection together with the mean value of all subsections. It is found that uncertainties in the PK position up to 50cm have to be considered. According to the result in figure 4.50 this leads to an important increase of the misfit function and errors in the identified parameters.

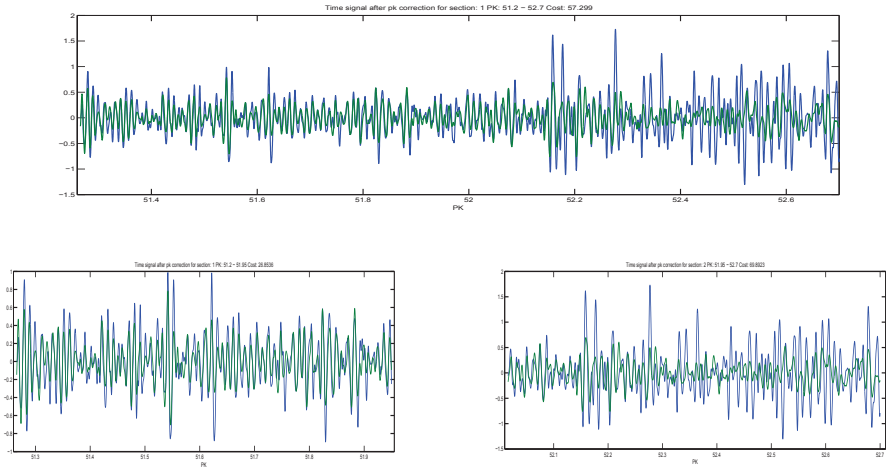

Figure 4.51: Section of 1.5km length is devided in subsections

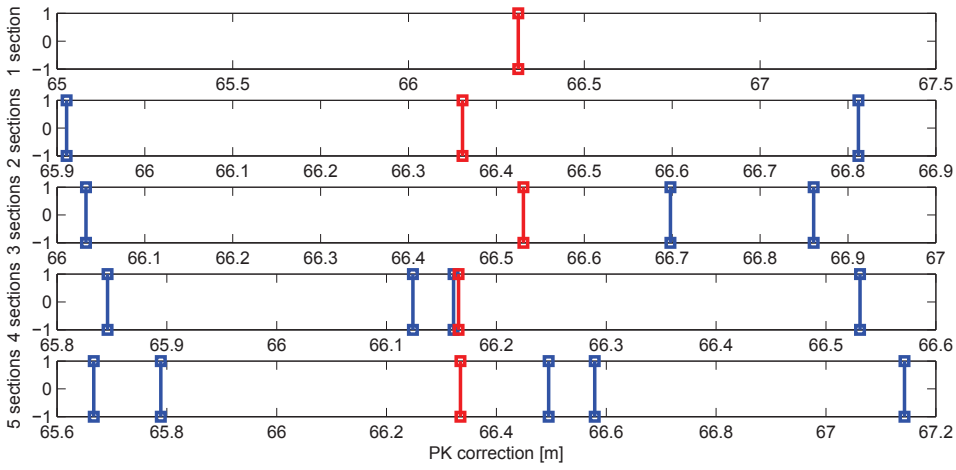

Figure 4.52: PK correction for complete section and subsections (blue) given with their mean values (red)

4.4.2 Discussion and Perspectives

The application of the parameter identification problem to the TGV train revealed the important potential for improved vehicle dynamics simulations but also the limitations due to the model. For the first identification problem using the vertical response of bogie A the least square misfit function could be reduced, depending on the defined parameter tolerance, up to 60%. However, in order to avoid that the estimated parameter values lie outside the range of realistic values the parameter tolerances have to be chosen carefully. Otherwise the global optimization algorithm might converge to a minimum which gives unrealistic estimates. For 10% tolerance a reduction of only 10% was obtained indicating well estimated initial parameter values and robustness of the traction unit model in vertical direction.

For the second identification problem using the lateral acceleration in carriage 2 an important reduction of the misfit function of 35% could be obtained for 10% parameter tolerance. Due to the strong sensitivity in lateral direction the model is less robust and small changes in parameter values have an important effect on the misfit function.

For the more complicated identification problems 3 and 4 taking into account several acceleration in traction unit and carriages the misfit function gain is smaller.

In general, the misfit function gains obtained from the genetic algorithm method and the simulated annealing method are of the same order. Differences in the obtained parameter values are due to complex solution surface with many local minima. By introducing a regularization function the number of local minima might be reduced and the optimization improved in the same way as for the bogie model. The choice of a suitable regularization function therefore should be part of the further work.

Differences in the parameter values were likewise obtained for straight and curved track. This indicates an inadequate model structure. Possible improvement of the model concern a more detailed description of the suspension elements, the consideration of variable friction conditions and elastic modes.

These limitations of the actual model complicate the appication of the parameter identification to a model-based condition monitoring which could allow to detect the degradation of the suspension elements. The monitoring application would also require reduced computation times. For the model

used in this work the dynamic equations are not available. Therefore for the computation of the gradients only the numeric finite differences method could be applied. For the large number of parameters considered, especially if suspension parameters of the same element type are assumed to be independent, improved gradient computation methods are needed. The adjoint method is an interesting approach due to the lower computational cost.

Conclusions and perspectives

This work showed the applicability and the potential of parameter identification methods for the complex nonlinear system of a railway vehicle. Measured forces and accelerations of the vehicle can be used in order to adjust the simulation model to the real system. This is necessary since many vehicle parameters are not exactly known: stiffness and damping coefficients of the suspension are subject to important variations.

The identification problem has been applied to two different models: the model of a single bogie developed in Matlab and the model of a complete TGV train implemented in the multibody simulation code Vampire.

The model of the bogie is composed of the bogie frame and two wheelsets connected by the primary suspension. Thanks to the known mathematical description the adjoint state method can be applied to the model. Even though with 10 degrees of freedom the model is relatively simple it includes a full description of the nonlinear wheel-rail contact using the theory of Kalker. The wheel is represented by a cone and the rail by a circular profile. The conicity and the friction coefficients are important parameters which control the dynamic behaviour of the model together with the suspension parameters. The suspension is described by the stiffness and damping coefficients in vertical, lateral and longitudinal directions. The model is excited by the track irregularities described by a vertical and lateral displacement of the left and the right rails.

The dynamic behaviour of the bogie model for different parameter values and velocities has been analyzed and compared to a bogie model implemented in Vampire. It is found that the model reproduces correctly the dynamics of bogie and wheelsets. The wheelsets perform the typical hunting movement, a combination of lateral displacement and yaw-rotation. Above a critical speed which depends on the suspension parameters this movement becomes instable and a limit-cycle is obtained. The bogie model implemented in Vampire

gives generally the same results. Smaller differences in the vehicle response may be caused by differences in the model structure which is not completely known for the Vampire model.

The aim of the identification is to find the correct parameter values of the model from measurement data. For the bogie model only the suspension parameters stiffness and damping coefficients are taken into account. The parameters of the wheel-rail contact - the profil shape, the conicity and the friction coefficients - are important also but more difficult to identify due to their non-steady characteristics. They have not been considered in this work but should be taken into account in future work.

Due to the nonlinear behaviour of the system the time-domain based model updating has been identified as the most suitable method. It requires the definition of a misfit function in the time domain and the minimization of this function. The fastest convergence is in general obtained by the use of local gradient methods. These methods require the calculation of the first and second order derivatives of the misfit function relatively to every parameter. A calculation of the gradients from finite differences is time consuming and less accurate. Therefore the application of the adjoint state method to the bogie model has been developed. The gradients can be calculated from a misfit function defined with the displacements, the velocities or the accelerations of the vehicle response. Which of these approaches provides the best result depends on the available data and the error introduced by integrating or differentiating the time signals. It was found that the differentiation leads to numeric errors and should be avoided. Therefore the displacements and velocities have been used for the bogie model. Since no measurement data is available for the bogie model, virtual measurement data obtained from a reference simulation of the Matlab model has been used for the application of the gradient method. Using the gradient method with the adjoint state approach the stiffness parameters of the suspension could be identified. Due to their negligible influence on the misfit function the identification of the damping coefficients is not possible. The gradient calculation using the adjoint method is a promising approach which will show its adavantage of reduced calculation costs when applied to vehicle models with more parameters in future work.

A difficulty for the use of local gradient methods is the presence of several local minima in the misfit function. Depending on the initial parameter values the optimization converges to the closest local minimum and the parameter values are not correctly identified. In order to avoid this, the Tikhonov

regularization has been used. By adding a polynomial function to the misfit function a solution surface with one minimum is obtained. The regularization parameter has been chosen according to the discrepancy principle such that the error introduced by the regularization is not larger than the measurement noise. Since no information about the measurement noise was available a regularization factor has been assumed. For future work an estimation of the noise level from statistical analysis of measurement data or from technical knowledge about the measurement chaine should be used in order to define the regularization parameter.

The model of the TGV train is more complicated. It includes two traction units and 9 carriages with over 300 degrees of freedom. The model is implemented in the multi-body tool Vampire. Therefore the mathematical description of the model is not completely known and the application of the adjoint state method has not been possible. As for the bogie model the time-domain based model updating has been used due to the nonlinear characteristics of the system. The analysis of the transfer functions of the primary and secondary suspension at different velocities and running conditions showed the important influence of nonlinearities on the vehicle behaviour. A second important aspect is that the identification is performed using operational measurements. The real track irregularities are measured by the track inspection train and used as excitation signal in the multi-body simulation. The track irregularities represent a transient signal with varying frequency content. Therefore the linearization for a defined operating point is not possible. A comparison of the transfer functions and the transient response obtained from the measurement and simulation showed that the nonlinear behaviour is in general reproduced by the model. Going more in detail, the misfit function indicates larger differences for the car body accelerations than for the bogie. This is due to the complex nonlinear behaviour of the secondary suspension with the air spring element.

The identification problem is applied to more than 100 parameters including both suspension and inertia parameters. For the same reasons named above the parameters of the wheel-rail contact are not considered. The solution surface of the misfit functions reveals local minima distributed over the whole parameter range. This impedes to obtain a minimization problem with a unique solution. In this work the non-regularized optimization problem has been used for the TGV model. The definition of a suitable regularization function taking into account the characteristic of the solution surface and the range of the parameter values is proposed for future work.

Consequently, the use of global optimization methods is a suitable approach. The simulated annealing and genetic algorithm methods have been applied. Misfit functions with and without the kilometric correction taken into account as an optimization parameter have been compared. Generally, important reductions of the misfit function up to 60% have been obtained. The parameter values obtained from the different optimization methods and running conditions have been compared. For the first case using the vertical acceleration in bogie A qualitatively the same modifications of the parameter values are obtained. The misfit function reaches values lower than 20% indicating a very good correlation between model and measurement. However, differences between the identification for straight and curved track are observed. Besides, some parameter values reach the boundaries of the defined tolerances indicating the need of modifications of the model structure. If the response in the carriage is used the differences between model and measurement remain larger. For the second case using the lateral acceleration in carriage 2 misfit function values of 50% are obtained. In opposite to the first case, an important reduction of 34% even for 10% parameter tolerance showed that the initial parameters were not correctly choosen.

The variability of the misfit function along the TGV east line stays large even after the identification. In order to explain this strong variability of the model performance the correlation with the track design and the track irregularities has been analyzed. It explains only partly the results of the misfit function. It is supposed that the dynamic behaviour of the TGV train is controlled by other excitations and dynamic properties which are not taken into account by the model. The importance of elastic modes and aerodynamic forces should be mentioned. The first elastic modes of the carriages lie at 15Hz thus in the frequency range considered in this work.

The result of this work opens the perspective to further applications. Up to now only suspension parameters have been identified for the bogie model. As mentioned before the parameters of the wheel-rail contact have an important influence on the vehicle dynamics. Since exact information about the conicity and friction coefficients is often not available they add uncertainty to the simulation results. An identification of these parameters from measurement data could help to better understand the vehicle behaviour under different running conditions and improve the simulation results.

An interesting application of the parameter identification is the condition monitoring. A continuous or repeated identification of parameters values during operation would allow the detection of changes in suspension elements.

This information could be used for the identification of damage models of the suspension elements leading to improved maintenance procedures.

The condition monitoring would require to apply the parameter identification to many runs on the same line. Already the computation of the forward model would be very time consuming. The two-timescale homogenization presented in [3],[4] and [10] could be used to reduce the computational time. It is based on the idea to describe the dynamic behaviour of the system by two different time-scales. One describing the short-time dynamics and another describing slower effects. In this case the transient response due to the track irregularities represents the vehicle dynamics at a fast time scale while the evolution of the vehicle behaviour due to element damages takes place at a slow time scale. The homogenization method would allow to calculate the evolution due to several runs on a certain line by taking into account the averaged effect of the transient dynamics at each run. Since the track irregularities do not represent a periodic excitation the principles of non-periodic homogenization from [10] would have to be applied.

In this work the model parameters are considered as deterministic. For the identifiable suspension parameters deterministic values were obtained and for other model parameters constant parameters taken. In reality some of these parameters are not exactly known and may vary during a measurement. In particular for the wheel-rail contact parameters friction coefficient and conicity this is the case. Besides, the measured accelerations are always corrupted by noise introducing uncertainty to the identification results.

It is therefore reasonable to consider these parameters as stochastic parameters with a certain probability distribution. A probabilistic model is obtained and the identified suspension parameters will be stochastic values also. The variability of the input parameters propagates to the output. Different methods as the Monte Carlo or the Bayesian network could be used to perform the parameter identification in a probabilistic way. While the vehicle parameters have been considered as completely dependent or independent in this work, probabilistic approach could account for the conditional dependencies between parameter values.

Appendix A

Multi-body model of bogie

Kinematic equations

The solution for the nonlinear kinematic equations of the wheelset with circular wheel and rail profiles is:

$$\Delta r \cong \lambda u_y \tag{A.1}$$

$$\tan \delta_{l(r)} \cong \tan \delta_0 \pm \epsilon \frac{2}{e_0} u_y \tag{A.2}$$

$$\delta_x \cong \sigma \frac{2}{e_0} u_y \tag{A.3}$$

$$u_z = \frac{1}{2}\zeta u_y^2 - \frac{1}{2}\xi \delta_z^2 \tag{A.4}$$

It describes the relation between the dependent parameters vertical displacement u_z, rotation around x-axis δ_x and difference between right and left contact radii Δr relative to the degrees of freedom of the wheelset. In [52] the geometric parameters λ, ϵ, σ, ζ and ξ are defined as:

$$\lambda = \lim_{R_R \to \infty} \left(\frac{R_R \sin \delta_0}{(R_R - R_S)} \frac{(\frac{1}{2}e_0 + R_S \sin \delta_0)}{(\frac{1}{2}e_0 \cos \delta_0 - r_0 \sin \delta_0)}\right) = \sin \delta_0 \frac{\frac{1}{2}e_0 + R_S \sin \delta_0}{\frac{1}{2}e_0 \cos \delta_0 - r_0 \sin \delta_0} \tag{A.5}$$

$$\epsilon = \lim_{R_R \to \infty} \left(\frac{\frac{1}{2}e_0}{R_R - R_S} \frac{\frac{1}{2}e_0 + R_R \sin \delta_0}{\frac{1}{2}e_0 \cos \delta_0 - r_0 \sin \delta_0}\right) = \frac{\frac{1}{2}e_0 * sin(\delta_0)}{\frac{1}{2}e_0 cos(\delta_0) - r_0 sin(\delta_0)} \tag{A.6}$$

$$\sigma = \frac{\frac{1}{2}e_0 \sin\delta_0}{\frac{1}{2}e_0 \cos\delta_0 - r_0 \sin\delta_0} \tag{A.7}$$

$$\begin{aligned}\zeta = \lim_{R_R \to \infty} (&\frac{\sin\delta_0}{\frac{1}{2}e_0 \cos\delta_0 - r_0 \sin\delta_0} + \frac{(\frac{1}{2}e_0 + R_R \sin\delta_0)(\frac{1}{2}e_0 + R_S \sin\delta_0)}{(R_R - R_S)\cos\delta_0(\frac{1}{2}e_0 \cos\delta_0 - r_0 \sin\delta_0)^2}) \\ &= \frac{\sin\delta_0}{\frac{1}{2}e_0 \cos\delta_0 - r_0 \sin\delta_0} + \frac{\sin\delta_0(\frac{1}{2}e_0 + R_S \sin\delta_0)}{\cos\delta_0(\frac{1}{2}e_0 \cos\delta_0 - r_0 \sin\delta_0)^2}\end{aligned} \tag{A.8}$$

$$\xi = \tan\delta_0(\frac{1}{2}e_0 - r_0 \tan\delta_0) + \frac{(\frac{1}{2}e_0 - r_0 \tan\delta_0)^2}{(R_R - R_S)} = tan\delta_0(\frac{1}{2}e_0 - r_0 \tan\delta_0) \cong \frac{1}{2}\delta_0 e_0 \tag{A.9}$$

Lagrange equations

For the setup of the equations of motion the Lagrange approach based on the kinetic energy is used. For each degree of freedom x_i of the vector of generalized coordinates the Lagrangian equations have the form:

$$\frac{d}{dt}(\frac{\partial E_c}{\partial \dot{x}_j}) - \frac{\partial E_c}{\partial x_j} = d_j, \qquad j = 1, ..., 10 \tag{A.10}$$

E_c is the kinetic energy of the system calculated with the translational velocity v_i and rotation velocity ω_i at the centre of gravity for every body i described by its mass m_i and inertia J_i:

$$E_c = \frac{1}{2}\sum_{i=1}^{3}(v_i^T m_i v_i + \omega_i^T J_i \omega_i) \tag{A.11}$$

Calculation of velocities

The Lagrange equations require the translational and rotational velocities for every body. They are calculated from the vector $\underline{q}$ of generalized coordinates.

$$\underline{q} = \begin{pmatrix} r_{bxI} \\ r_{byI} \\ r_{bzI} \\ \delta_{bxI} \\ \delta_{byI} \\ \delta_{bzI} \\ u_{e1y} \\ u_{e2y} \\ \delta_{e1z} \\ \delta_{e2z} \end{pmatrix} \tag{A.12}$$

The position vectors of the three bodies are expressed with these generalized coordinates. For the bogieframe this is obvious since all three coordinates are independent:

$$\underline{r}_{bI}(\underline{q}, t) = \begin{pmatrix} r_{bxI} \\ r_{byI} \\ r_{bzI} \end{pmatrix} \tag{A.13}$$

For the wheelset the position vector is given by the kinematic relations derived in chapter 2.

$$\underline{r}_{e1I}(\underline{q}, t) = \begin{pmatrix} r_{e1xI} \\ r_{e1yI} \\ r_{e1zI} \end{pmatrix} = \begin{pmatrix} \frac{1}{2}s \\ u_y \\ r_0 + d_z - \frac{1}{2}r_0(\gamma_d)^2 + \frac{1}{2}\zeta(u_y - d_y + r_0\gamma_d)^2 - \frac{1}{2}\xi\delta_z^2 \end{pmatrix} \tag{A.14}$$

The translational speed of each body is received from a total derivation of the position vector:

$$\underline{v}_i = \frac{d\underline{r}_i}{dt} = \frac{\partial \underline{r}_i}{\partial q_1}\frac{dq_1}{dt} + \frac{\partial \underline{r}_i}{\partial q_2}\frac{dq_2}{dt} + ... + \frac{\partial \underline{r}_i}{\partial q_f}\frac{dq_f}{dt} + \frac{\partial r_i}{\partial t} \tag{A.15}$$

Using the Jacobian matrix of translation $\underline{\underline{J}}_{Ti}$ the translational speed can be written as:

$$\underline{v}_i = \underline{\underline{J}}_{Ti}(\underline{q}, t)\dot{\underline{q}} + \hat{\underline{v}}_i(\underline{q}, t) \tag{A.16}$$

with the Jacobian matrix of translation given by:

$$\underline{\underline{J}}_{Ti} = \begin{pmatrix} \frac{\partial r_{xi}}{\partial q_1} & \frac{\partial r_{xi}}{\partial q_2} & ... & \frac{\partial r_{xi}}{\partial q_f} \\ \frac{\partial r_{yi}}{\partial q_1} & \frac{\partial r_{yi}}{\partial q_2} & ... & \frac{\partial r_{yi}}{\partial q_f} \\ \frac{\partial r_{zi}}{\partial q_1} & \frac{\partial r_{zi}}{\partial q_2} & ... & \frac{\partial r_{zi}}{\partial q_f} \end{pmatrix} \tag{A.17}$$

$\underline{\hat{v}}_i(\underline{q},t)$ is the so-called local velocity describing the direct derivation relative to time:

$$\underline{\hat{v}}_i(\underline{q},t) = \begin{pmatrix} \frac{\partial r_{xi}}{\partial t} \\ \frac{\partial r_{yi}}{\partial t} \\ \frac{\partial r_{zi}}{\partial t} \end{pmatrix} \tag{A.18}$$

Again for the bogie frame the description is simple. Since all coordinates are independent the Jacobian matrix becomes:

$$\underline{\underline{J}}_{Tb} = \begin{pmatrix} 1 & 0 & 0 & 0 & ... & 0 \\ 0 & 1 & 0 & 0 & ... & 0 \\ 0 & 0 & 1 & 0 & ... & 0 \end{pmatrix} \tag{A.19}$$

The translative speed is then calculated as:

$$\underline{v}_{bI}(\underline{q},t) = \begin{pmatrix} \dot{r}_{bxI} \\ \dot{r}_{byI} \\ \dot{r}_{bzI} \end{pmatrix} \tag{A.20}$$

For the wheelset the following Jacobian matrix is obtained:

$$\underline{\underline{J}}_{Te1} = \begin{pmatrix} 0 & 0 & 0 & 0 & 0 & 0 & 0 & 0 & 0 & 0 \\ 0 & 0 & 0 & 0 & 0 & 0 & 1 & 0 & 0 & 0 \\ 0 & 0 & 0 & 0 & 0 & 0 & \zeta(u_{e1y} - d_y + r_0\gamma_d) & 0 & -\xi\delta_{e1z} & 0 \end{pmatrix} \tag{A.21}$$

This gives for the translational velocity:

$$\begin{aligned} \underline{v}_{e1I}(\underline{q},t) = & \begin{pmatrix} 0 \\ \dot{u}_{e1y} \\ \dot{u}_{e1y}\zeta(u_{e1y} - d_y + r_0\gamma_d) - \dot{\delta}_{e1z}\xi\delta_{e1z} \end{pmatrix} + \\ & \begin{pmatrix} 0 \\ 0 \\ \dot{d}_z - r_0\gamma_d\dot{\gamma}_d + \zeta(u_{e1y} - d_y + r_0\gamma_d)(-\dot{d}_y + r_0\dot{\gamma}_d) \end{pmatrix} \end{aligned} \tag{A.22}$$

The rotational velocity is derived from the rotational matrix $\underline{\underline{R}}$. In the following description it has to be distinguished between the coordinate system $\hat{K}$ attached to the body in the centreof gravity and the system K which is also attached at the centre of gravity but remains always parallel to the

inertial system. The two coordinate systems are related by the rotational matrix $\underline{\underline{R}}$ so that a position vector $\underline{r}_{iK}$ is given by:

$$\underline{r}_{iK} = \underline{\underline{R}}_i \underline{r}_{i\hat{K}} \tag{A.23}$$

Since $\underline{r}_{i\hat{K}}$ is a constant vector describing the position on the body the velocity expressed in system K is:

$$\Rightarrow \dot{\underline{r}}_{iK} = \dot{\underline{\underline{R}}}_i \underline{r}_{i\hat{K}} \tag{A.24}$$

replacing $\underline{r}_{i\hat{K}}$ by:

$$\underline{r}_{i\hat{K}} = \underline{\underline{R}}_i^{-1} \underline{r}_{iK} = \underline{\underline{R}}_i^T \underline{r}_{iK} \tag{A.25}$$

the derivative of $\underline{r}_{iK}$ is given by:

$$\Rightarrow \dot{\underline{r}}_{iK} = \dot{\underline{\underline{R}}}_i \underline{\underline{R}}_i^T \underline{r}_{iK} = \underline{\omega}_i \times \underline{r}_{iK} = \tilde{\underline{\omega}}_i \underline{r}_{iK} \tag{A.26}$$

with:

$$\tilde{\underline{\omega}}_i = \dot{\underline{\underline{R}}}_i \underline{\underline{R}}_i^T = [\frac{\partial \underline{\underline{R}}_i}{\partial q_1}\frac{dq_1}{dt} + \frac{\partial \underline{\underline{R}}_i}{\partial q_2}\frac{dq_2}{dt} + ... + \frac{\partial \underline{\underline{R}}_i}{\partial q_f}\frac{dq_f}{dt} + \frac{\partial R_i}{\partial t}]\underline{\underline{R}}_i^T \tag{A.27}$$

In the same way as for the translational velocity the rotational velocity $\underline{\omega}_i$ can be written as the time derivative of the generalized coordinates and the rotational Jacobian matrix $\underline{\underline{J}}_{Ri}(\underline{q}, t)$:

$$\Rightarrow \underline{\omega}_i = \underline{\underline{J}}_{Ri}(\underline{q}, t)\dot{\underline{q}} + \hat{\underline{\omega}}_i(\underline{q}, t) \tag{A.28}$$

The rotational Jacobian matrix is defined by:

$$J_{Ri} = \frac{\partial \underline{r}_i}{\partial \underline{q}^T} = \begin{pmatrix} \frac{\partial r_{xi}}{\partial q_1} & \frac{\partial r_{xi}}{\partial q_2} & \cdots & \frac{\partial r_{xi}}{\partial q_f} \\ \frac{\partial r_{yi}}{\partial q_1} & \frac{\partial r_{yi}}{\partial q_2} & \cdots & \frac{\partial r_{yi}}{\partial q_f} \\ \frac{\partial r_{zi}}{\partial q_1} & \frac{\partial r_{zi}}{\partial q_2} & \cdots & \frac{\partial r_{zi}}{\partial q_f} \end{pmatrix} \tag{A.29}$$

its elements are calculated according to the definition of the rotational velocity as:

$$\frac{\partial \underline{\underline{R}}_i}{\partial q_j} \underline{\underline{R}}_i{}^T = \begin{pmatrix} 0 & -\frac{\partial r_{iz}}{\partial q_j} & \frac{\partial r_{iy}}{\partial q_j} \\ \frac{\partial r_{iz}}{\partial q_j} & 0 & -\frac{\partial r_{ix}}{\partial q_j} \\ -\frac{\partial r_{iy}}{\partial q_j} & \frac{\partial r_{ix}}{\partial q_j} & 0 \end{pmatrix} \tag{A.30}$$

Starting the bogie the rotational matrix is:

$$\underline{\underline{R}}_b = \begin{pmatrix} 1 & 0 & 0 \\ 0 & \cos\delta_{bx} & -\sin\delta_{bx} \\ 0 & \sin\delta_{bx} & \cos\delta_{bx} \end{pmatrix} \begin{pmatrix} \cos\delta_{by} & 0 & -\sin\delta_{by} \\ 0 & 1 & 0 \\ \sin\delta_{by} & 0 & \cos\delta_{by} \end{pmatrix} \begin{pmatrix} \cos\delta_{bz} & -\sin\delta_{bz} & 0 \\ \sin\delta_{bz} & \cos\delta_{bz} & 0 \\ 0 & 0 & 1 \end{pmatrix} \tag{A.31}$$

The elements of the first row of the Jacobian matrix corresponding to the first degree of freedom are calculated as:

$$\begin{aligned} \frac{\partial \underline{\underline{R}}_{Tb}}{\partial \delta_{bx}} \underline{\underline{R}}_{Tb}^T &= \begin{pmatrix} 0 & 0 & 0 \\ 0 & -\sin\delta_{bx} & -\cos\delta_{bx} \\ 0 & \cos\delta_{bx} & -\sin\delta_{bx} \end{pmatrix} \underline{\underline{R}}_{by} \underline{\underline{R}}_{bz} \underline{\underline{R}}_b^T = \\ &\begin{pmatrix} 0 & 0 & 0 \\ 0 & -\sin\delta_{bx} & -\cos\delta_{bx} \\ 0 & \cos\delta_{bx} & -\sin\delta_{bx} \end{pmatrix} \underline{\underline{R}}_{by} \underline{\underline{R}}_{bz} \underline{\underline{R}}_{bx}^T \underline{\underline{R}}_{by}^T \underline{\underline{R}}_{bz}^T = \\ &\begin{pmatrix} 0 & 0 & 0 \\ 0 & 0 & -1 \\ 0 & 1 & 0 \end{pmatrix} \end{aligned} \tag{A.32}$$

In the same way the components of the Jacobian matrix are calculated for the other degrees of freedom. The complete Jacobian matrix then becomes:

$$\underline{\underline{J}}_{br} = \begin{pmatrix} 1 & 0 & \sin\delta_{by} & 0 & \dots & 0 \\ 0 & \cos\delta_{bx} & -\sin\delta_{bx}\cos\delta_{by} & 0 & \dots & 0 \\ 0 & \sin\delta_{bx} & \cos\delta_{bx}\cos\delta_{by} & 0 & \dots & 0 \end{pmatrix} \tag{A.33}$$

Since the local rotational velocity for the bogie is zero the rotational velocity is diretly obtained as:

$$\underline{\omega}_b = \begin{pmatrix} \dot{\delta}_{bx} + \sin(\delta_{by})\dot{\delta}_{bz} \\ \cos(\delta_{bx})\dot{\delta}_{by} - \sin(\delta_{bx})\cos(\delta_{by})\dot{\delta}_{bz} \\ \sin(\delta_{bx})\dot{\delta}_{by} + \cos(\delta_{bx})\cos(\delta_{by})\dot{\delta}_{bz} \end{pmatrix} \tag{A.34}$$

Due to the kinematic relations the calculation of the rotational velocity of the wheelsets is more complicated. The rotational matrix is given by:

$$\underline{\underline{R}}_e = \begin{pmatrix} 1 & 0 & 0 \\ 0 & \cos\delta_{ex} & -\sin\delta_{ex} \\ 0 & \sin\delta_{ex} & \cos\delta_{ex} \end{pmatrix} \begin{pmatrix} \cos\omega t & 0 & -\sin\omega t \\ 0 & 1 & 0 \\ \sin\omega t & 0 & \cos\omega t \end{pmatrix} \begin{pmatrix} \cos\delta_{ez} & -\sin\delta_{ez} & 0 \\ \sin\delta_{ez} & \cos\delta_{ez} & 0 \\ 0 & 0 & 1 \end{pmatrix} \tag{A.35}$$

By inserting the term for the rotation angle δ_{e1x} the rotational matrix becomes:

$$\underline{\underline{R}}_e = \begin{pmatrix} 1 & 0 & 0 \\ 0 & \cos\left(\gamma_d + \sigma\frac{1}{e_0}(u_y - d_y + r_0\gamma_d)\right) & -\sin\left(\gamma_d + \sigma\frac{1}{e_0}(u_y - d_y + r_0\gamma_d)\right) \\ 0 & \sin\left(\gamma_d + \sigma\frac{1}{e_0}(u_y - d_y + r_0\gamma_d)\right) & \cos\left(\gamma_d + \sigma\frac{1}{e_0}(u_y - d_y + r_0\gamma_d)\right) \end{pmatrix} \begin{pmatrix} \cos\omega t & 0 & -\sin\omega t \\ 0 & 1 & 0 \\ \sin\omega t & 0 & \cos\omega t \end{pmatrix} \begin{pmatrix} \cos\delta_{e1z} & -\sin\delta_{e1z} & 0 \\ \sin\delta_{e1z} & \cos\delta_{e1z} & 0 \\ 0 & 0 & 1 \end{pmatrix} \tag{A.36}$$

The rotational Jacobian matrix is calculated for the two degrees of freedom for the wheelset:

$$\underline{\underline{J}}_{eR} = \begin{pmatrix} 0 & \ldots & 0 & 2\frac{\sigma}{e_0} & 0 & \sin(\omega t) & 0 \\ 0 & \ldots & 0 & 0 & 0 & -\cos(\omega t)\sin\left(\frac{\gamma_d e_0 + 2\sigma u_y - 2\sigma d_y + 2\sigma r_0\gamma_d}{e_0}\right) & 0 \\ 0 & \ldots & 0 & 0 & 0 & \cos(\omega t)\cos\left(\frac{\gamma_d e_0 + 2\sigma u_y - 2\sigma d_y + 2\sigma r_0\gamma_d}{e_0}\right) & 0 \end{pmatrix} \tag{A.37}$$

The rotational speed depends also on the track irregularities which are a function of displacement and for the constant vehicle speed of time:

$$\underline{\omega}_e = \begin{pmatrix} \frac{-2\sigma\dot{d}_y + e_0\dot{\gamma}_d + 2\sigma r_0\dot{\gamma}_d}{e_0} \\ \omega\cos\left(\frac{\gamma_d e_0 + 2\sigma u_y - 2\sigma d_y + 2\sigma r_0\gamma_d}{e_0}\right) \\ \omega\sin\left(\frac{\gamma_d e_0 + 2\sigma u_y - 2\sigma d_y + 2\sigma r_0\gamma_d}{e_0}\right) \end{pmatrix} \tag{A.38}$$

The rotational speed for the wheelset is therefore:

$$\underline{\omega}_e = \begin{pmatrix} 2\dot{u}_e\frac{\sigma}{e_0} + \dot{\delta}_{ez}\sin(\omega t) + \frac{-2\sigma\dot{d}_y + e_0\dot{\gamma}_d + 2\sigma r_0\dot{\gamma}_d}{e_0} \\ -\dot{\delta}_{ez}\cos(\omega t)\sin\left(\frac{\gamma_d e_0 + 2\sigma u_y - 2\sigma d_y + 2\sigma r_0\gamma_d}{e_0}\right) + \omega\cos\left(\frac{\gamma_d e_0 + 2\sigma u_y - 2\sigma d_y + 2\sigma r_0\gamma_d}{e_0}\right) \\ \dot{\delta}_{ez}\cos(\omega t)\cos\left(\frac{\gamma_d e_0 + 2\sigma u_y - 2\sigma d_y + 2\sigma r_0\gamma_d}{e_0}\right) + \omega\sin\left(\frac{\gamma_d e_0 + 2\sigma u_y - 2\sigma d_y + 2\sigma r_0\gamma_d}{e_0}\right) \end{pmatrix} \tag{A.39}$$

With the translational and rotational velocity of the bodies known the kinetic energy can be calculated:

$$E_c = \frac{1}{2}\sum_{i=1}^{3}(v_i^T m_i v_i + \omega_i^T J_i \omega_i) \tag{A.40}$$

Calculation of suspension forces

Beside the kinetic energy the generalized forces are required in the Lagrange equations. They are calculated with the forces and moments acting on every body.

In order to calculated the suspension forces the position vector of the coupling points have to be expressed in the inertial system. For the bogie frame this relation is for a coupling point i:

$$\underline{r}_i = \underline{r}_b + \underline{\underline{R}}_b \underline{r}_{i\hat{K}} \tag{A.41}$$

With relative displacement between two coupling points and the stiffness of the suspension element the force is obtained.

For the calculation of the damping forces the local speed at the coupling points is required. It is obtained from the translational and rotational speed of the body as well as the rotational matrix as:

$$\underline{v}_i = \underline{v}_b + \underline{\omega}_b \times \underline{\underline{R}}_b \underline{r}_{i\hat{K}} \tag{A.42}$$

Calculation of contact forces

The contact forces are distinguished in the normal and tangential forces. The normal forces are composed by a static part due to the weight of the vehicle and a dynamic part. In order to calculate the dynamic part $F_{dyn} = ma$ the acceleration of the bodies have to be known. Since the actual acceleration at the time step i is not known without the forces the acceleration calculated at the previous time step i-1 has to be used.

For the calculation of the adjoint state the derivatives of the dynamic equations have to be calculated symbolically. Therefore the dynamic part of the normal force has been neglected.

Hertz Theorie

With the normal forces known the contact surface can be computed using the Hertz theory. It allows to calculate the contact radii of the contact ellipse as well as the static deflection and the stress. The input parameters are the normal force and the radii of curvature for the rail and wheel profile. The

following illustration is based on the book on railway vehicle dynamics [52].

The normal force is computed from the equilibrium of forces and moments for the wheelset. The forces which have to be considered are the normal forces for the left N_l and right wheel N_r, the gravitational force $m_w g$ as well as the spring F_c and damper forces F_d of the primary suspension:

$$m_w a_{wz} = N_l + N_r - m_w g - F_{cl} - F_{cr} - F_{dl} - F_{dr} \tag{A.43}$$

$$J_{exx}\dot{\delta}_{ex} = -(F_{cl} + F_{dl})l_{sp} + (F_{cr} + F_{dr})l_{sp} + N_l e_0 - N_r e_0 \tag{A.44}$$

The normal forces are computed as:

$$N_R = \frac{(-(F_{cl} + F_{dl}) + (F_{cr} + F_{dr}))l_{sp}}{2e_0} \tag{A.45}$$

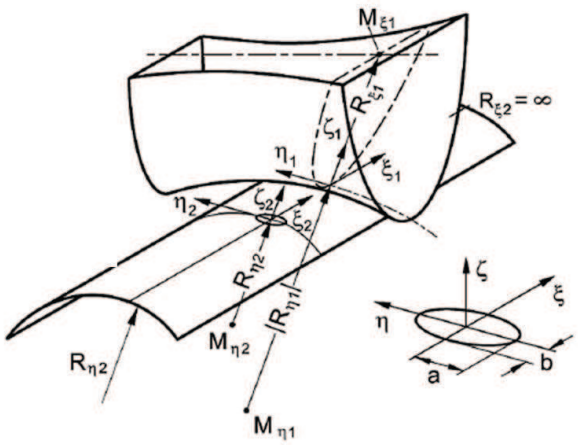

Figure A.1: Calculation of the contact ellipse according to Hertz

The next step is to combine the surfaces of the wheel and the rail described by the radii of curvature $R_{1\epsilon}$, $R_{2\epsilon}$, $R_{1\eta}$ and $R_{2\eta}$ to a equivalent surface. The radii of curvature are shown in figure A.1.

$$\frac{1}{R_\epsilon} = \frac{1}{R_{1\epsilon}} + \frac{1}{R_{2\epsilon}} \tag{A.46}$$

$$\frac{1}{R_\eta} = \frac{1}{R_{1\eta}} + \frac{1}{R_{2\eta}} \tag{A.47}$$

From the equivalent radii of curvature an averaged radius R_m is calculated:

$$R_m = \sqrt{R_\epsilon R_\eta} \tag{A.48}$$

Under the assumption that the wheel and the rail are from the same material the module of elasticity is:

$$E^* = \frac{E}{2(1-\nu^2)} \tag{A.49}$$

Then the contact radii a and b of the ellipse can be calculated based on the approach proposed by Johnson. This is done by determining the averaged radius of curvature $c = \sqrt{ab}$ from the R_m:

$$c = \sqrt[3]{\frac{3}{4}\frac{1}{E^*}NR_m}F_1(e) \tag{A.50}$$

The factor F_1 is received from a graphical representation as a function of the relation between the relative radii of curvature. Besides, the relation between a and b is given graphically so that a and b can be calculted.

$$a = c\sqrt{\frac{a}{b}} \tag{A.51}$$

$$b = c\sqrt{\frac{b}{a}} \tag{A.52}$$

Appendix B

Vampire model of the TGV train

Suspension elements

The suspension elements of the TGV Duplex train are represented by physical models. The parameter of the suspension elements are summarized in table B.1. They are organised with respect to their position in the primary or secondary suspension of the traction unit or car bodies. The keyword motor describes elements in the traction unit and rame elements in the carriages.

Parameters		
num	suspension type	element
1	motor primary suspension	coil spring cx
2	motor primary suspension	coil spring cy
3	motor primary suspension	coil spring cz
4	motor primary suspension	guidance spring cx
5	motor primary suspension	guidance spring cy
6	motor primary suspension	guidance spring cy
7	motor primary suspension	guidance spring dx
8	motor primary suspension	guidance spring dy
9	motor primary suspension	guidance spring dz
10	motor primary suspension	vertical damper velocity
11	motor primary suspension	vertical damper force
12	motor primary suspension	vertical damper series
13	motor primary suspension	vertical bumpstop displacement
14	motor primary suspension	vertical bumpstop displacement
15	motor secondary suspension	coil spring cx
16	motor secondary suspension	coil spring cy
17	motor secondary suspension	coil spring cz
18	motor secondary suspension	coil spring dx
19	motor secondary suspension	coil spring dy
20	motor secondary suspension	coil spring dz
21	motor secondary suspension	coil spring sx
22	motor secondary suspension	coil spring sy
23	motor secondary suspension	coil spring sz
24	motor secondary suspension	transversal bumpstop displacement
25	motor secondary suspension	transversal bumpstop force
26	motor secondary suspension	vertical damper linear d
27	motor secondary suspension	vertical damper linear c serial
28	motor secondary suspension	transversal damper linear d
29	motor secondary suspension	transversal damper linear c serial
30	motor secondary suspension	antiyaw damper velocity
31	motor secondary suspension	antiyaw damper force
32	motor secondary suspension	antiyaw damper series
33	rame primary suspension	coil spring cx
34	rame primary suspension	coil spring cy
35	rame primary suspension	coil spring cz
36	rame primary suspension	coil spring ca
37	rame primary suspension	coil spring cb
38	rame primary suspension	coil spring cg
39	rame primary suspension	coil spring dx
40	rame primary suspension	coil spring dy

Table B.1: Suspension parameters considered in sensitivity analysis

Parameters		
num	suspension type	element
41	rame primary suspension	coil spring dz
42	rame primary suspension	coil spring da
43	rame primary suspension	coil spring db
44	rame primary suspension	coil spring dg
45	rame primary suspension	guide arm cx
46	rame primary suspension	guide arm cy
47	rame primary suspension	guide arm cz
48	rame primary suspension	guide arm ca
49	rame primary suspension	guide arm cy
50	rame primary suspension	guide arm cg
51	rame primary suspension	vertical damper velocity
52	rame primary suspension	vertical damper force
53	rame primary suspension	vertical damper series
54	rame primary suspension	vertical bumpstop displacement
55	rame primary suspension	vertical bumpstop force
56	rame secondary suspension	airspring vertical bellow
57	rame secondary suspension	airspring vertical reservoir
58	rame secondary suspension	airspring vertical damping
59	rame secondary suspension	airspring vertical area
60	rame secondary suspension	airspring lateral displacement
61	rame secondary suspension	airspring lateral force
62	rame secondary suspension	airspring lateral damping
63	rame secondary suspension	airspring lateral force
64	rame secondary suspension	vertical damper linear d
65	rame secondary suspension	transversal damper displacement
66	rame secondary suspension	transversal damper force
67	rame secondary suspension	transversal damper series
68	rame secondary suspension	antiyaw damper displacement
69	rame secondary suspension	antiyaw damper force
70	rame secondary suspension	antiyaw damper series
71	rame secondary suspension	traction bogie-carbody0
72	rame secondary suspension	vertical bumpstop displacement
73	rame secondary suspension	vertical bumpstop force
74	rame secondary suspension	transversal bumpstop displacement
75	rame secondary suspension	transversal bumpstop force
76	rame secondary suspension	transversal bumpstop 2 displacement
77	rame secondary suspension	transversal bumpstop 2 force
78	rame secondary suspension	anti-roll bar
79	traktion unit-coach	coupler stiffness
80	traktion unit-coach	buffer damping

Table B.2: Suspension parameters considered in sensitivity analysis

Parameters		
num	suspension type	element
81	coach-coach	pivot joint cx
82	coach-coach	pivot joint cy
83	coach-coach	pivot joint cz
84	coach-coach	pivot joint cg
85	coach-coach	pivot joint dz
86	coach-coach	longitudinal damper velocity
87	coach-coach	longitudinal damper force
88	coach-coach	longitudinal damper series
89	coach-coach	transersal damper linear d
90	masse car body	Traction unit 1 masse
91	masse car body	Traction unit 1 Jx
92	masse car body	Traction unit 1 Jy
93	masse car body	Traction unit 1 Jz
94	masse car body	carriage 1 masse
95	masse car body	carriage 1 Jx
96	masse car body	carriage 1 Jy
97	masse car body	carriage 1 Jz
98	masse car body	carriage 2 masse
99	masse car body	carriage 2 Jx
100	masse car body	carriage 2 Jy
101	masse car body	carriage 2 Jz
102	masse bogie	bogie A masse
103	masse bogie	bogie A Jx
104	masse bogie	bogie A Jy
105	masse bogie	bogie A Jz
106	masse bogie	bogie B masse
107	masse bogie	bogie B Jx
108	masse bogie	bogie B Jy
109	masse bogie	bogie B Jz
110	masse car body	bogie 1 masse
111	masse bogie	bogie 1 Jx
112	masse bogie	bogie 1 Jy
113	masse bogie	bogie 1 Jz
114	masse bogie	bogie 2 masse
115	masse bogie	bogie 2 Jx
116	masse bogie	bogie 2 Jy
117	masse bogie	bogie 2 Jz

Table B.3: Suspension parameters considered in sensitivity analysis

Thermodynamic airspring model

The thermodynamic airspring model developed by Krettek gives the most accurate results and forms the basis to the air spring models in ADMAS rail and Simpack. The equations are developed for the simple physical air spring model shown in figure B.1.

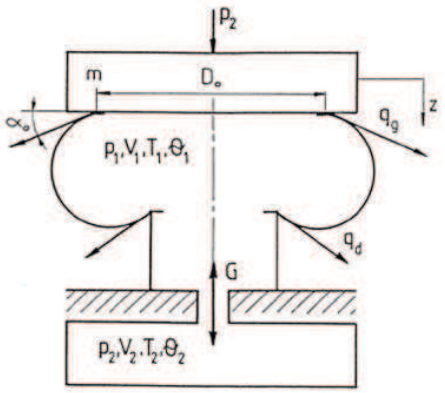

Figure B.1: Physical air spring model

It is composed of the air spring bellow, a surge pipe with an orifice and the reservoir. The relative displacements between the car body and the bogie lead to pressure differences between the bellow and the reservoir which are compensated by an air exchange between the two volumes. The spring characteristic depends on the air spring surface A_e, the volumes of bellow V_1 and reservoir V_2, the air pressure in the system but also on the form and material of the air spring bellow. Krettek [54] determined the spring characteristic for an air spring with no reservoir experimentally. An almost linear relation was found between the force and the spring compression. This does not hold any longer if an airspring with a reservoir and a surge pipe is analysed. The spring characteristics then becomes strongly nonlinear.

The thermodynamic model developed by Krettek is based on the energy balance, the mass balance and the ideal gas law. With respect to the air mass, the bellow, surge pipe and reservoir form a closed system. The total air mass remains constant. For the energy balance this is not the case. Energy is exchanged with the environment in form of work (spring compression and depression) and heat. The change of the inner energy U is therefore determined by the heat transfer Q_{12}, the volume work $\int_1^2 dW = \int_1^2 pdV$ and the

dissipation $(W_{diss})_{12}$.

$$U_2 - U_1 = Q_{12} - \int_1^2 pdV + (W_{diss})_{12} \tag{B.1}$$

The air is considered as an ideal gas described by the ideal gas law:

$$pV = nRT \tag{B.2}$$

with: p: pressure, V: volume, n: amount of substance, R: ideal gas constant, T: temperature.

Then the energy balance, mass balance and ideal gas law for the bellow and the reservoir are set up. For the air bellow they are:

$$-Q_1 + dQ_D = dU_1 + dW \tag{B.3a}$$
$$dM_1 = -Gdt \tag{B.3b}$$
$$p_1 dV_1 + V_1 dp_1 = R(M_1 dT_1 + T_1 dM_1) \tag{B.3c}$$

and for the reservoir :

$$-Q_2 - dQ_D = dU_2 \tag{B.4a}$$
$$dM_2 = Gdt \tag{B.4b}$$
$$V_2 dp_2 = R(M_2 dT_2 + T_2 dM_2) \tag{B.4c}$$

with: $Q_{1(2)}$: heat transfer with environment, Q_D: heat transfer between air bellow and reservoir, $dU_{1(2)}$: change in inner energy, $Q_{1(2)}$: air mass in air bellow and reservoir, G: mass stream between air bellow and reservoir.

In order to derive the thermodynamic equations for the air spring the different termes in the equations have to be specified. The volume work due to a compression or expansion of the air bellow is given

$$dW = -p_1 dV_1 = -p_1 A dz \tag{B.5}$$

From the specific heat capacity for a constant volume c_v the inner energy of the air bellow and reservoir is calculated:

$$U_1 = c_v T_1 \tag{B.6}$$

$$U_2 = c_v T_2 \tag{B.7}$$

The heat flow between the air bellow T_1 and the environment T_0 and between the reservoir T_2 and the environment is calculated from the temperature differences and the heat transfer coefficients β :

$$\frac{dQ_1}{dt} = \beta_1(T_1 - T_0) \tag{B.8}$$

$$\frac{dQ_2}{dt} = \beta_2(T_2 - T_0) \tag{B.9}$$

Between the air bellow and the reservoir heat is transported with the air mass stream. The heat flow is therefore depending on the direction of the mass flow. For $p_1 > p_2$ the heat stream is:

$$dQ_d = c_p T_1 dM_1 \tag{B.10}$$

and for $p_2 > p_1$:

$$dQ_d = c_p T_2 dM_2 \tag{B.11}$$

Now all termes of the mass and energy balance equation are specified for the air spring system. If they are introduced in the equations B.3 and B.4 the relations for the pressure and temperature changes of the air bellow and the reservoir are obtained. The equations can be found in [29].

The only term which has not been specified yet is the mass stream G between the air bellow and the reservoir. For the pipe flow other assumptions have to be made. In order to consider the friction the air can not be treated as an ideal gas any longer. Due to the vehicle vibrations and the large exchanged air masses the flow in the pipe is turbulent. The air exchange is therefore described by the Saint Venant equations. For pressure relations between bellow and reservoir larger than 0.5282 they are given by:

$$G = \mu \frac{\pi d_0^2}{4} \sqrt{\frac{2\kappa}{\kappa - 1} \frac{p_1^2}{RT_1} [\frac{p_1}{p_2}^{\frac{2}{\kappa}} - \frac{p_2}{p_1}^{\frac{\kappa+1}{\kappa}}]} \tag{B.12}$$

for $p_2 > p_1$ and

$$G = -\kappa\mu \frac{\pi d_0^2}{4} \sqrt{\frac{2\kappa}{\kappa - 1} \frac{p_2^2}{RT_2} [\frac{p_1}{p_2}^{\frac{2}{\kappa}} - \frac{p_2}{p_1}^{\frac{\kappa+1}{\kappa}}]} \tag{B.13}$$

for $p_1 > p_2$.

The air spring model based on the thermodynamic equations presented above has been implemented in Vampire and ADAM rails. It is supposed to give the most accurate results for the modelling of the air spring.

Appendix C

Optimization methods

Newton method

The Newton method seeks to minimize the quadratic approximation $m(p)$ of the misfit function:

$$m(d_k) = J(p_k) + d_k^T \nabla J(p_k) + \frac{1}{2} d_k^T \nabla^2 J(p_k) d_k \tag{C.1}$$

p_k is the parameter vector at iteration step k and d_k the search direction. If the Hessian matrix $\nabla^2 J(p_k)$ is positive definite, $p_k + d_k$ is the solution of $min\ m(d_k)$.

$$\nabla m(d_k) = \nabla J(p_k) + \nabla^2 J(p_k) d_k = 0 \tag{C.2}$$

$$\nabla^2 J(p_k) d_k = -\nabla J(p_k) \tag{C.3}$$

$$d_k = -(\nabla^2 J(p_k))^{-1} \nabla J(p_k) \tag{C.4}$$

Instead, if the Hessian matrix $\nabla^2 J(p_k)$ is not positive definite it is possible that the Newton search direction does not satisfy the condition $\nabla J(p_k)^T d_k < 0$ or is not defined. In this case the steepest descent direction is used.

A drawback of the Newton method is the use of the Hessian matrix whose calculation can become very costly. By replacing the Hessian matrix by an approximation the calculation time can be reduced. This is done in the Quasi-Newton method.

Quasi-Newton method

Instead of the Hessian Matrix an approximation B_k is used which is updated at every iteration:

$$d_k = -B_k^{-1} \nabla J(p_k) \tag{C.5}$$

Among the approximation of the Hessian matrix the BFGS method is well known. Outgoing from an initial estimation which can be the identity matrix the approximation is calculated from the gradients as:

$$B_{k+1} = B_k + \frac{q_k q_k^T}{q_k^T s_k} - \frac{B_k^T s_k^T s_k B_k}{s_k^T B_k s_k} \tag{C.6}$$

with:

$$s_k = x_{k+1} - x_k \tag{C.7}$$

$$q_k = \nabla J(x_{k+1}) - \nabla J(x_k) \tag{C.8}$$

Levenberg-Marquardt method

The Levenberg-Marquardt method completes the Newton method with a regularization. The Tikhonov regularization is applied to the inverse matrix for the calculation of the search direction d_k:

$$d_k = -[\nabla^2 J(p_0)^T \nabla^2 J(p_0) + \nu I]^{-1} \nabla^2 J(p_0)^T \nabla J(p_0) \tag{C.9}$$

The search direction is controlled by the parameter ν. For $\nu = 0$ the method corresponds to the Newton method and for $\nu = \inf$ to the steepest descent method

Conjugated gradient method

The conjugate gradient method initially developed for the solution of large linear problems has been adapted to non-linear problems. Its advantage is a fast convergence and low memory needs.

In the case of a non-linear system the methods allows to solve iteratively the system:

$$Ax = b \tag{C.10}$$

The solution of the linear system corresponds to the minimisation problem:

$$min\ \phi(x) = \frac{1}{2}x^T Ax - x^T b \tag{C.11}$$

The gradient of ϕ is equal to the residuum of the linear system.

$$\nabla\phi(x) = Ax - b = r(x) \tag{C.12}$$

The method is based on the creation of conjugated vectors defined by:

$$p_i^T Ap_j = 0 \quad for\ all\ i \neq j \tag{C.13}$$

The introduction of conjugated vectors allows to minimize ϕ successively by a minimisation in every direction.

$$x_{k+1} = x_k + \alpha_k p_k \tag{C.14}$$

α_k is the iteration step of the function ϕ. If x is replaced in the function ϕ by $x_k + \alpha_k p_k$ the iteration step α_k is calculated by:

$$\alpha_k = -\frac{r_k^T p_k}{p_k^T Ap_k} \tag{C.15}$$

It is possible to show that the sequence x_k converges to the solution of the linear system. For the conjugate directions the eigenvalues of the matrice A or a Gram-Schmidt orthogonalization can be used. However, both approaches are relatively costly. By using the conjugated gradient method for the calculation of the conjugated vectors the complexity can be reduced. For the calculation of the preceding search direction only the previous direction is used:

$$p_k = -r_k + \beta p_{k-1} \tag{C.16}$$

β is determined from the condition that p_{k-1} and p_k are conjugated relative to A. The method is therefore composed by two steps: with the actual search direction p_k and the residuum r_k the step length and the new parameter values x_{k+1} and residues r_{k+1} are calculated. Then the new search direction is calculated.

The Fletcher Reeves method is the extension to non-linear functions. The residue is the gradient of the non-linear misfit function. Then a unidimensional search is performed i the direction p_k in order to identify the minimum.

$$x_{k+1} = x_k + \alpha_k p_k \tag{C.17}$$

Trust region methods

Trust region methods are composed by two steps: the identification of a suitable trust region and the solution of the subproblem in this region given by a quadratic constrained optimization problem. The radius of the trust region has an important effect on the performance of the method. A radius which is chosen too small leads to a large number of iterations and a slow convergence. In return, if it is chosen too large the quadratic approximation is not valid any longer. The radius is chosen by comparing two iterations of the misfit function $J(p)$ and the quadratic approximation $m(p)$:

$$\rho_k = \frac{J(p_k) - J(p_k + d_k)}{m(0) - m(d_k)} \tag{C.18}$$

If the value of ρ_k is close to one the approximation describes well the misfit function and the next point is accepted. If, instead, ρ_k is close to zero or even negative the radius is reduced.

The next step is the minimisation of the quadratic approximation considering the constraint given by the trust region radius. The quadratic approximation is obtained by a Taylor development:

$$J(p_k + d_k) = J(p_k) + \nabla J(p_k) d_k + \frac{1}{2} d_k^T \nabla^2 J(p_k) d_k \tag{C.19}$$

The minimisation is therefore given by:

$$min\ m_k(d_k) = J(p_k) + \nabla J(p_k) d_k + \frac{1}{2} d_k^T B_k d_k \quad \|d_k\| \leq \triangle_k \tag{C.20}$$

with: d_k: search direction

In the same way as for the line search methods the subproblem is solved in the steepest descent direction. If only the first derivative is used a linear problem is solved:

$$d_k = \ min\ J(p_k) + \nabla J(p_k) d \tag{C.21}$$

by minimizing:

$$\tau_k = \ min\ m_k(\tau d_k) \quad \|\tau d_k\| \leq \triangle_k \tag{C.22}$$

The solution of d_k is the gradient normalized by the radius of the trust region:

$$d_k = -\frac{\triangle_k}{\|\nabla J(p_k)\|}\nabla J(p_k) \tag{C.23}$$

If the function m_k is monotone in the trust region the solution corresponds to the point on the radius of the trust region $\tau_k = 1$. For a convex misfit function m_k τ_k is either the local minima of m_k or the radius.

Tensor algebra for solution of the adjoint Method

The adjoint equation using the displacements in the misfit function is given by:

$$\int_0^T \mathbf{z}^T(D_x\mathbf{M}\ddot{\mathbf{x}}\delta\mathbf{x})dt + \int_0^T \mathbf{z}^T(\mathbf{M}\delta\ddot{\mathbf{x}})dt + \int_0^T \mathbf{z}^T(D_x\mathbf{F}\delta\mathbf{x})dt + \int_0^T \mathbf{z}^T(D_{\dot{\mathbf{x}}}\mathbf{F}\delta\dot{\mathbf{x}}) = \int_0^T (\mathbf{x}-\mathbf{x}_{exp})^T\delta\mathbf{x}dt \tag{C.24}$$

The term D_xM describes the derivative of the matrix M with respect to a vector x giving a tensor of order 3. The calculation of the gradient is based on the following gradient definition for a scalar $\delta = \delta(p_1, p_2, ..., p_n)$ a vector $x = x(p_1, p_2, ..., p_n)$ and a matrix $A = A(p_1, p_2, ..., p_n)$. Here the orthonormal basis in the euclidean space is used for which the covariant derivative and the contravariant derivatives are equal $e_i = e^i$. The basis vectors are self-dual.

$$grad\delta = \delta|_i e_i \tag{C.25}$$

$$gradx = x_j|_i e_j \otimes e_i \tag{C.26}$$

$$gradA = A_{kl}|_i e_k \otimes e_l \otimes e_i \tag{C.27}$$

with: $|_i$ differential operator

$\mathcal{E} = (e_1, e_2, ..., e_n)$ is the basis of the n-dimensional Euclidean space with orthonormal vector e_i:

$$e_i.e_j = \delta_{ij} \tag{C.28}$$

Tensors of second and third order are expressed by their coefficents a_{ij} and a_{ijk} respectively and the tensor product of the basis vectors e:

$$a_{i,j}e_j \otimes e_i \tag{C.29}$$

This gives a tensor of order 3 expressed as:

$$\frac{\partial M}{\partial x} = \frac{\partial m_{i,j}}{\partial x_s} e_i \otimes e_j \otimes e_s \tag{C.30}$$

The contraction of a third order tensor with a vector is defined as:

$$(u \otimes v \otimes w)x = (w.x)(u \otimes v) \tag{C.31}$$

If the derivative of M is contracted with the vector $\ddot{x}$ a second order tensor is obtained:

$$(\frac{\partial m_{i,j}}{\partial x_s} e_i \otimes e_j \otimes e_s)\ddot{x} = \frac{\partial m_{i,j}}{\partial x_s}(e_s, \ddot{x})e_i \otimes e_j = \frac{\partial m_{i,j}}{\partial x_s}(\ddot{x}_s)e_i \otimes e_j \tag{C.32}$$

Accordingly, an index appearing twice in a multiplicative term represents a summation. The equation above can therefore be written as:

$$\sum_s \ddot{x}_s \frac{\partial m_{i,j}}{\partial x_s} e_i \otimes e_j \tag{C.33}$$

For the calculation of the adjoint equation from the derivative of the Lagrange equation the gradient of the matrix M is contracted two times with a vector. Then a scalar product of this vector is calculated. For the transform described in equation C.32 the order of these operations has to be altered. The scalar product is associativ so that:

$$\underline{a}.\underline{b} = a_i b_i (e_i.e_i) \tag{C.34}$$

The contraction of a matrix A with a vector x is given by:

$$A_{ij}(e_i \otimes e_j)x = A_{ij}e_i(e_j.x) = A_{ij}e_i(x_j) \tag{C.35}$$

The scalar product of this vector with another vector y gives:

$$A_{ij}e_i(x_j).(e_i y_i) = A_{ij}x_j y_i.(e_i.e_i) \tag{C.36}$$

If now the vector x and y are permuted the following result is received:

$$A_{ij}e_i(y_j).(e_i x_i) = A_{ij}y_j x_i.(e_i.e_i) \tag{C.37}$$

The two results are equal if the indices of matrix A a permuted. This corresponds to the calculation of the transposition of the matrix A:

$$(A^T)_{ij} = A_{ji} \tag{C.38}$$

By neglecting small movements the matrix M becomes independent of x. The derivative of M leading to tensors of order 3 is avoided and the adjoint state equation simplifies to:

$$M\ddot{x} + D_x F^T z - (D_{\dot{x}} F^T z)' = \ddot{x} - \ddot{x}_{exp} \tag{C.39}$$

Appendix D

Analysis of measurement data and calibration of model

In order to analyse the measurement and calibrate the model three types of signals are available: the simulated response of the model, the measured response of the TGV train and the measured track irregularities. The properties of the signals are summarized in table D.1. Both, the simulation and the measurement are time-based giving discretization with constant time-steps. The PK signal is thus calculated using the vehicle speed. The time step of the simulation has been chosen 2.5 times smaller than for the measurement in order to allow a correct resampling.

Data analysis			
Signal	**Model**	**System**	**Track**
Type	Accelerations Forces	Accelerations Forces	Displacement
Time	$\Delta t = 0.001$	$\Delta t = 0.0025$	-
PK	$\Delta PK = variable$, recalculation using speed: $\Delta PK_i = v_i \Delta t$	$\Delta PK = variable$, recalculation using speed: $\Delta PK_i = v_i \Delta t$	$\Delta PK = 0.25m$
Speed	$v = measured$	$v = measured$	-
Sampling frequency	$f_s = 1/\Delta t = 1000Hz$	$f_s = 1/\Delta t = 400Hz$	$f_s = 1/\Delta PK = 4[1/m]$ or calculation for a defined vehicle speed: $f_s = 1/\Delta t$ with $dt_i = \Delta PK/v_i f_s$ variable

Table D.1: Parameters of signal analysis

Transfer functions

In order to detect nonlinearities the transfer function of the model and the measured system are analysed. The transfer functions are compared for the primary and secondary suspension in the traction unit and the carriage. For the measurement the transfer functions are computed in the frequency domain betwene the vertical and lateral forces on the wheel and the accelerations in bogie and car body. Since the measured wheel forces are only available for the bogies A and 3 they have been used for this analysis. Their position in the train can be found in figure D.1.

Transfer function for model

For the model a modal analysis with a sine excitation at different frequencies is reproduced. For every simulation the train is running with a slightly increased speed over a track with sinusoidal irregularities of 3m wavelength. In order to detect nonlinearities this analysis has been repeated for different amplitudes of the track irregularities.

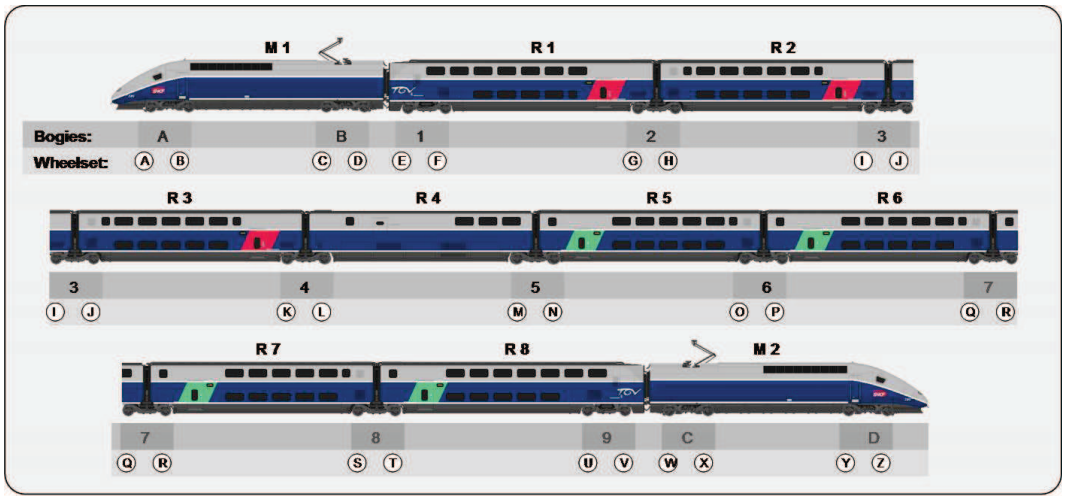

Figure D.1: Numeration of the wheelsets, bogies and car bodies of the TGV Duplex train

Transfer function for measurement

The transfer functions are calculated in the frequency domain separately for short sections allowing to detect changes in the eigenfrequencies due to non-linearities. As illustrated in figure D.2 the signal is separated in a certain number of sections. Then for each section the power spectral densities and transfer functions are calculated using the Welch method. Depending on the required frequency resolution the section is divided in several blocks which might overlap. The PSD and transfer function is calculated for each block and averaged over all blocks in one section.

The choice of the section length has been made from experience with the aim to identify linear and nonlinear modes from the transfer function. If the number of sections is chosen too large the nonlinear mode is rarely visible due to the instationarities caused by the track irregularities. By reducing the number of sections to 80 and averaging over around 1km using the Welch method the effect of the track irregularities is reduced and the nonlinear speed depended mode is better visible.

Traction unit vertical direction

The transfer function of the primary suspension in vertical direction for the model (figure D.3 a) shows a nonlinear mode with an eigenfrequency between

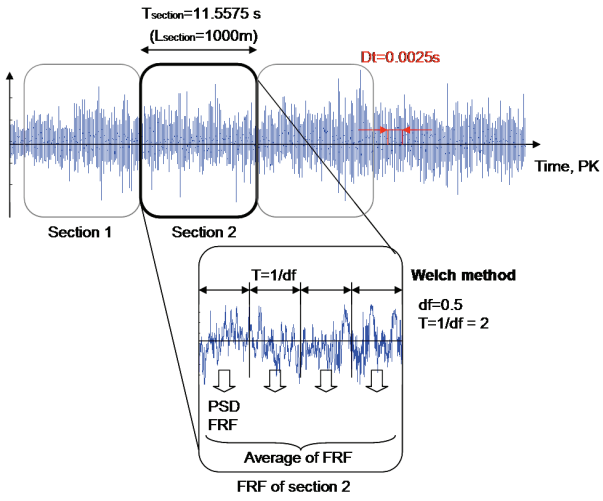

Figure D.2: Computation of the power spectral density and transfer function for each section using the Welch method

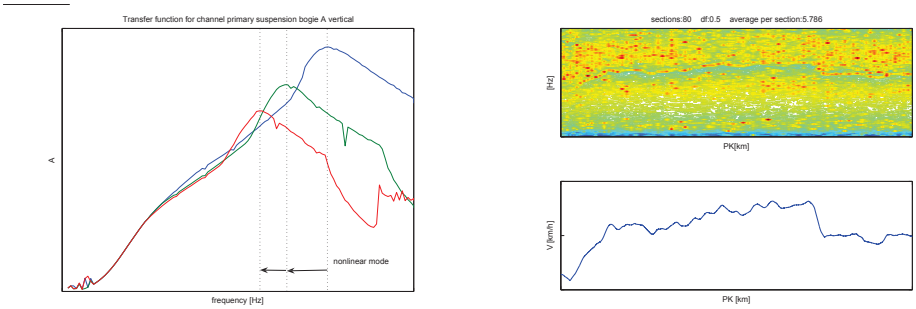

(a) Model (b) Measurement

Figure D.3: Transfer function of primary suspension bogie A in vertical direction

Short time Fourier analysis			
Parameter	**Formule**	**Value**	**Explication**
PK Start-End [km]	-	20-100	section with important speed variations
Number sections N	-	80	resolution adapted to speed changes
Length section L[m]	-	approximately 1000	variable, depending on speed
Time step $\Delta t[Hz]$	-	0.0025	defined by measurement system
Datapoints total N_{tot}	-	369841	all sections
Datapoints section $N_{section}$	N_{tot}/N	4623	one sections
Length section $T_{section}$ [t]	$N_{section}\Delta t$	11.5575	time length of one sections
Required frequency resolution $\Delta f[Hz]$	-	0.5	detection of modes possible
Welch method: blocklength $T_{block}[s]$	$1/\Delta$ f	$1/0.5 = 2$	averaging over section length
Welch method: nfft	$T_{block}/\Delta t$	$2/0.0025 = 800$	
Welch method: overlap [%]	-	60	
Welch method: averages per section	$N_{section}/(nfft0.4)$	14	

Table D.2: Parameters of the test section for computing the transfer functions

20 and 30Hz. It is probably due to the rubber spring in the primary suspension. The mode is not clearly visible in the measurements but a nonlinear mode can be found between 20 and 30Hz.

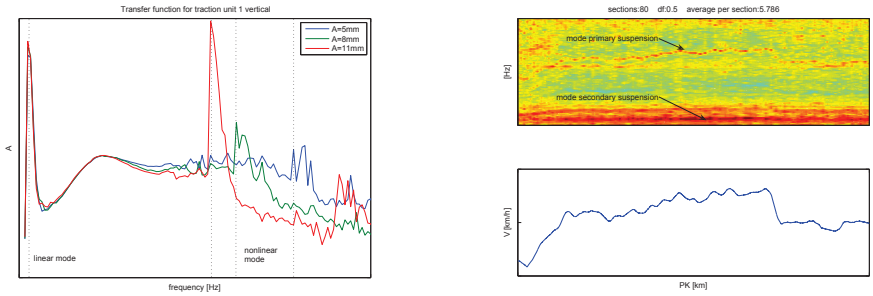

(a) Model (b) Measurement

Figure D.4: Transfer function of primary + secondary suspension bogie A in vertical direction

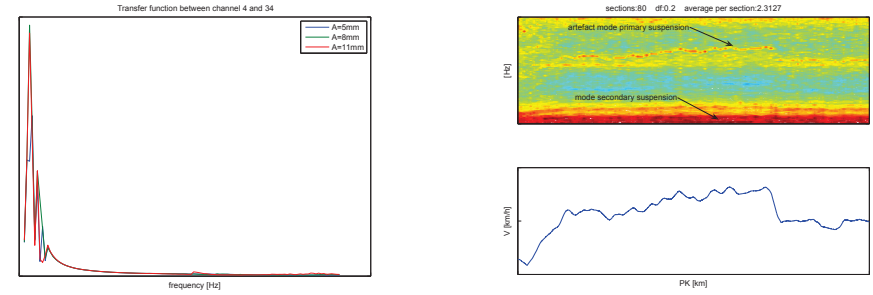

(a) Model (b) Measurement

Figure D.5: Transfer function of secondary suspension bogie A in vertical direction

From figure D.5 linear modes are found at 2 and 4Hz for the secondary suspension of the model. These modes are also present in the measurement. Besides, a nonlinear mode is visible between 20 and 30Hz which is probably an effect due to the primary suspension.

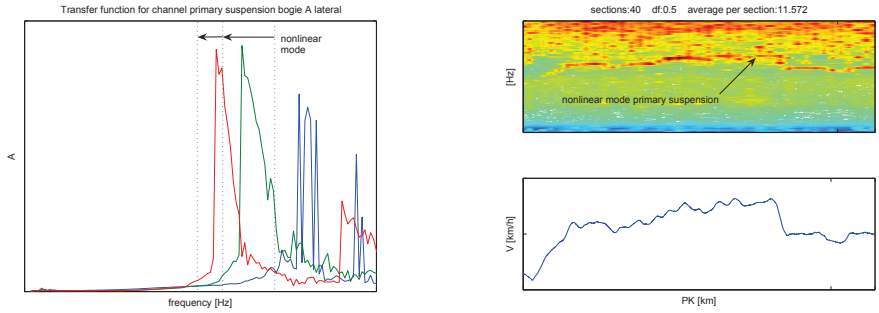

(a) Model (b) Measurement

Figure D.6: Transfer function of primary suspension bogie A in lateral direction

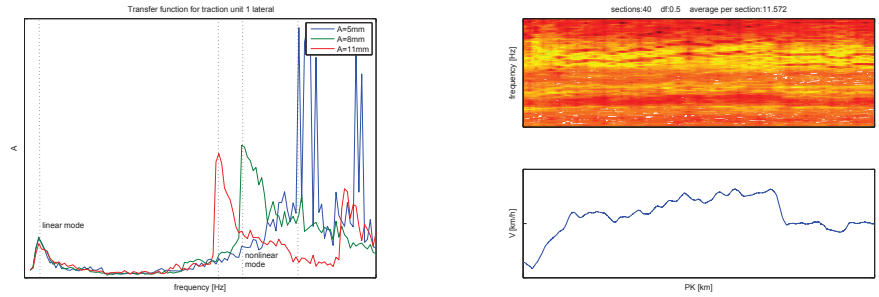

(a) Model (b) Measurement

Figure D.7: Transfer function of primary + secondary suspension bogie A in lateral direction

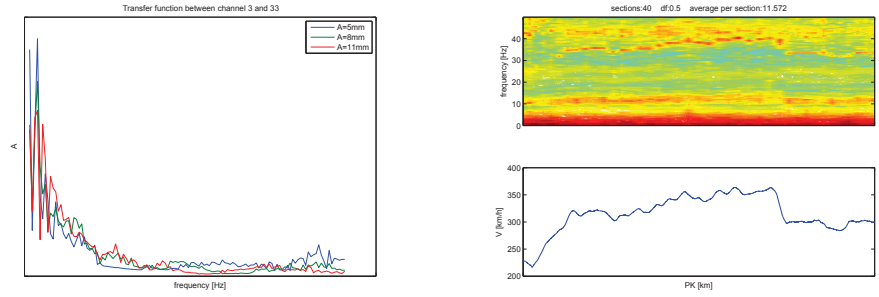

(a) Model (b) Measurement

Figure D.8: Transfer function of secondary suspension bogie A in lateral direction

Traction unit transversal direction

In lateral direction a highly nonlinear mode is found in the primary suspension between 25 and 35Hz both for the simulation and the measurement. The confirms the importance of nonlinearities in the lateral vehicle dynamics. The secondary suspension is characterized by a quite linear mode at around 2 to 3Hz. At higher frequencies nonlinear effects are visible which might be caused by the primary suspension.

Carriage vertical direction

Force measurements have been performed also for bogie 3. In order to take into account the different suspension elements in the carriages and the effect of the Jacobs bogies the transfer functions are computed for bogie 3 and carriage 2.

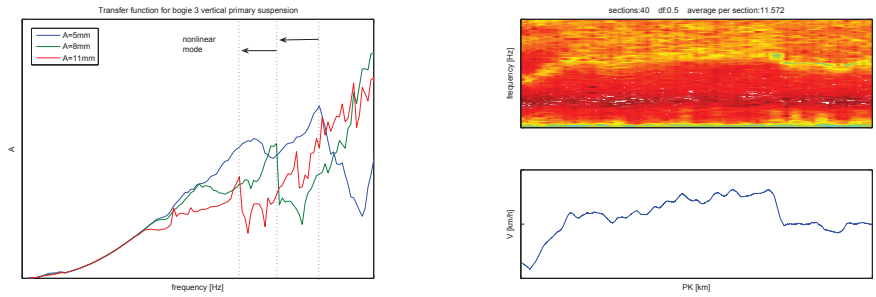

(a) Model (b) Measurement

Figure D.9: Transfer function of primary suspension bogie 3 in vertical direction

For the primary suspension in vertical direction (figure D.9) a nonlinear mode is found between 25 and 35Hz. It is supposed that this nonlinear mode is caused by the rubber spring elements in the primary suspension acting both in vertical and lateral direction. While the nonlinear mode is isolated in lateral direction the vertical direction shows a linear component due to the coil spring.

In the transfer function of the secondary suspension (figure D.10) a linear mode is found at 2Hz both in the measurement and the model. It corresponds to the vertical airspring. Besides, a nonlinear mode is visible in the measurements. It is not correctly reproduced by the model where a second linear mode can be seen.

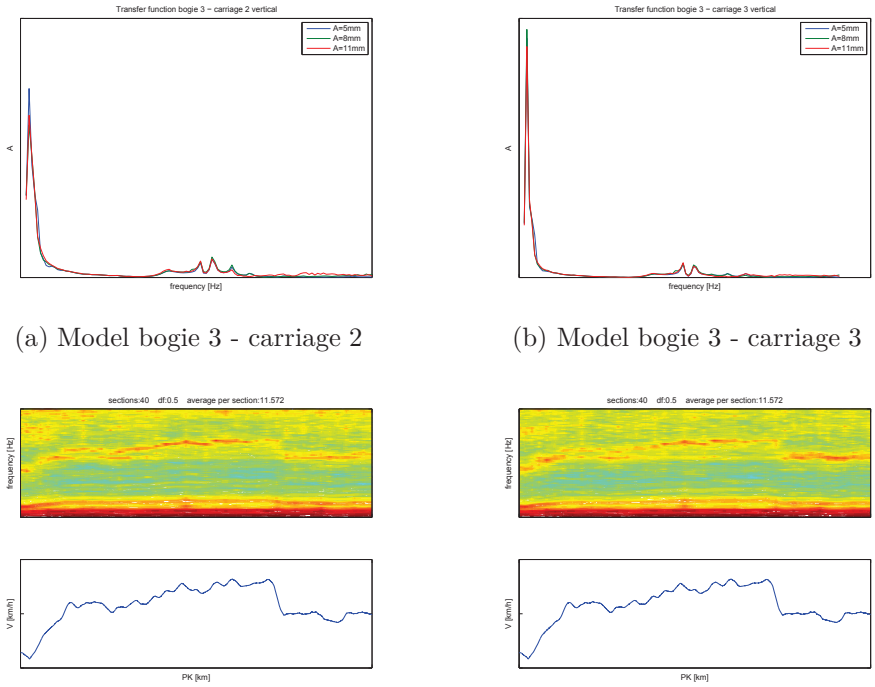

(a) Model bogie 3 - carriage 2

(b) Model bogie 3 - carriage 3

(c) Measurement bogie 3 - carriage 2

(d) Measurement bogie 3 - carriage 3

Figure D.10: Transfer function of secondary suspension bogie 3 in vertical direction

Carriage transversal direction

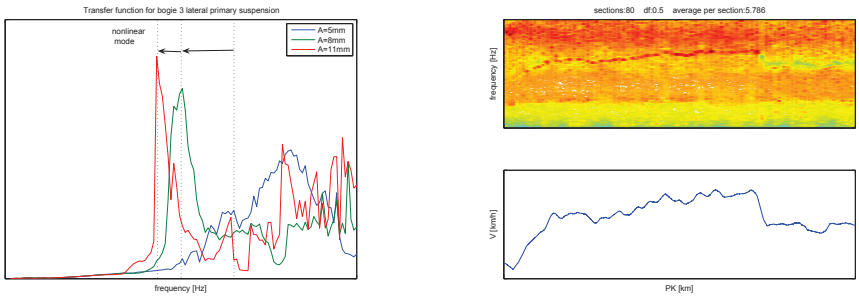

(a) Model (b) Measurement

Figure D.11: Transfer function of primary suspension bogie 3 in lateral direction

In lateral direction (figure D.12) a distinct nonlinear mode is found in the primary suspension both in the model and in the measurement between 18 and 30Hz. Again, the influence of nonlienarities on the lateral vehicle behavior is important. The nonlinearity of the wheel-rail contact and rubber spring elements can explain this behavior. In the secondary suspension (figure D.13) nonlinear effects appear for the mode of the airspring between 2 and 5Hz but also at higher frequencies.

Wheel rail contact

In order to characterize the effect of the wheel-rail contact the transfer functions have been calculated between the measured wheel forces and axle-box accelerations in vertical and lateral direction. Figure D.14 shows the spectra of the vertical wheel-forces on the left and right wheel of wheelset A. They show clear peaks at several frequencies.
The results for the transfer functions are shown in figure D.15. In vertical direction the transfer function does not shown important modes. Vertical forces and the axle-box acceleration are directly coupled in the low frequency range. This is due to the geometric constraint in vertical direction and the fact that at low frequencies track and wheel can be considered as rigid. In lateral direction this direct coupling is not valid. The possible relative movement between track and wheel as a function of the slip and friction forces leads to a more complicated behavior and a transfer function with several modes. Finally, it has to be considered that wheelsets and bogie are excited

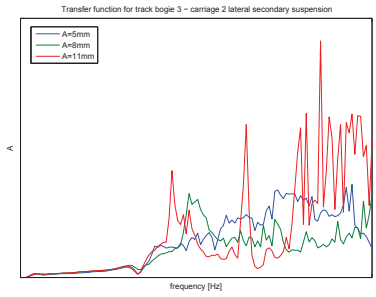

(a) Model bogie 3 - carriage 2

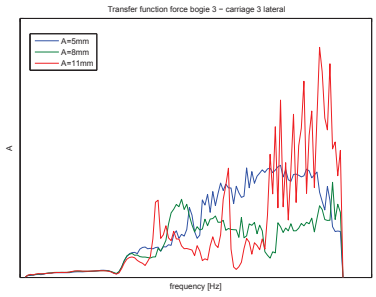

(b) Model bogie 3 - carriage 3

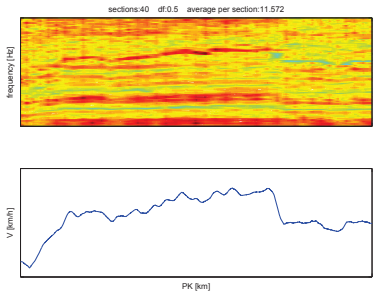

(c) Measurement forceQ11 bogie 3 - Carriage 2

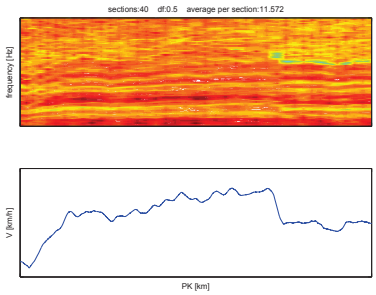

(d) Measurement forceQ11 bogie 3- Carriage 3

Figure D.12: Transfer function of primary + secondary suspension bogie 3 in lateral direction

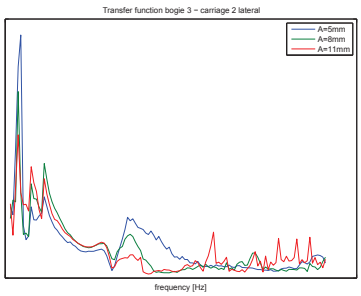

(a) Model bogie 3 - carriage 2

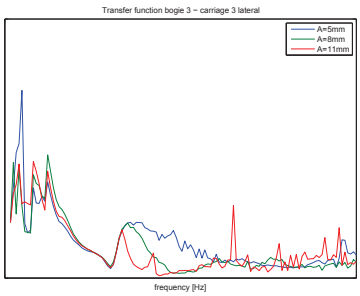

(b) Model bogie 3 - carriage 3

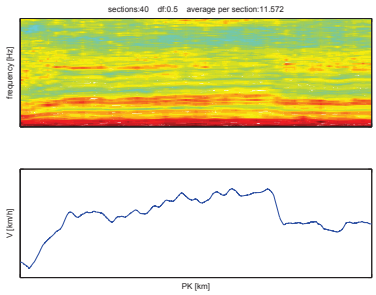

(c) Measurement bogie 3 - carriage 2

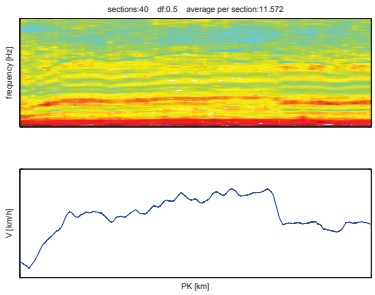

(d) Measurement bogie 3 - carriage 3

Figure D.13: Transfer function of secondary suspension bogie 3 in lateral direction

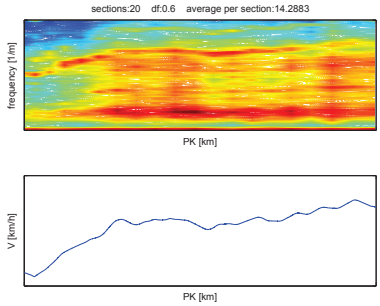

(a) STFT of the vertical wheelforce 11 in bogie A wheel

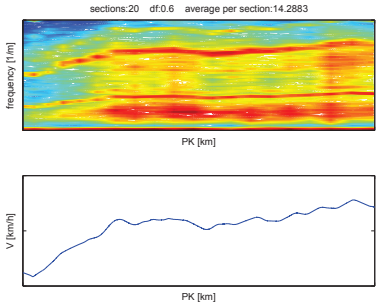

(b) STFT of the vertical wheelforce 21 in bogie A wheel

Figure D.14: STFT of wheelset forces in bogie A in vertical direction

simultaneously by several correlated forces. This can introduce errors when calcualting the transfer function between one force and the vehicle response.

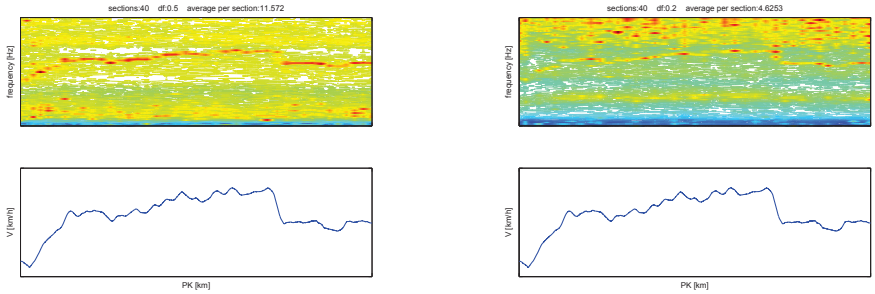

(a) Vertical (b) Lateral

Figure D.15: Transfer function H2 of wheel rail contact (force - acceleration axle box) : vertical (a) lateral (b) of measurement

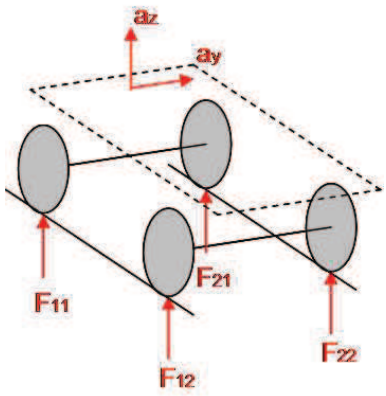

Figure D.16: Measured wheel forces and accelerations in the bogie

Appendix E

Calibration of the initial model using coherence and misfit functions

The quality of the initial model is evaluated by analysing the differences between the measured and simulated vehicle response. Therefore the vehicle response is devided in sections of 250m length. After an automatic correction of the kilometric shift using the cross-correlation function the coherence function and the misfit function are calculated. This analysis is applied to the wheel forces, the axle-box accelerations, the bogie accelerations and the car-body accelerations.

Wheel forces

Bogie A and 3 are equiped with measurement wheelsets allowing to measure vertical and lateral wheel forces. The frequency range for which the model response is valid can be obtained from the power spectral density. For the vertical wheel forces a very good correlation is found between 5 and 15 HZ while most of the signal energy is contained between 5 and 25Hz. The coherence calculated for each section shows an important variability with most of the values between 0.8 and 1. However, some sections for example between PK55 and 60 shows significantly lower coherence values. The results for the coherence function correlates with the misfit fucntion. Most of the values lie between 15 and 50% error with a mean of 30%. The good reproducibility of the vertical wheel force by the model can be explained by the direct mechanical coupling between rail and wheel in vertical direction and the mainly linear characteristics of the vertical suspension generating the dynmic part

of the vertical wheel force.

For the lateral wheel forces the distance between model and measurement is higher. Misfit function values between 40 and 1000% are obtained. The reason is the complicated kinematics and the nonlinear behavior of lateral suspension elements.

Model calibration	
Signal type	Wheel force
Frequency range	5 to15/25Hz
Section length	250m
Overlap	50%
Position	Bogie A, vertical, lateral wheel 11

Table E.1: Control parameters

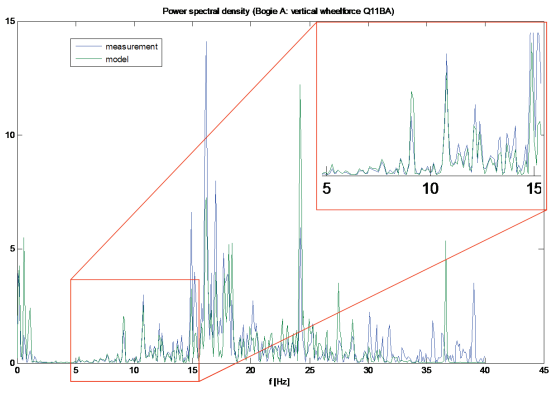

Figure E.1: Measured and simulated power spectral density for choice of frequency range

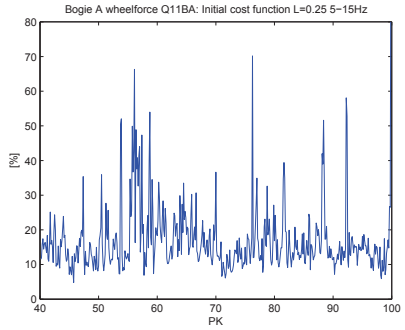

(a) Initial misfit function

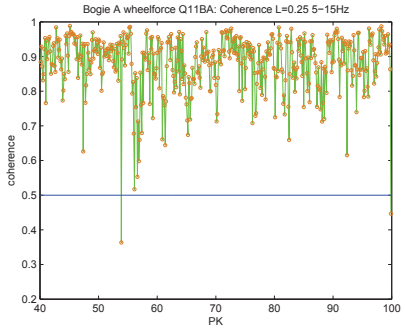

(b) Coherences

Figure E.2: Initial misfit function and coherence function for vertical wheelforce Q11 bogie A for frequency range 5 to 15Hz

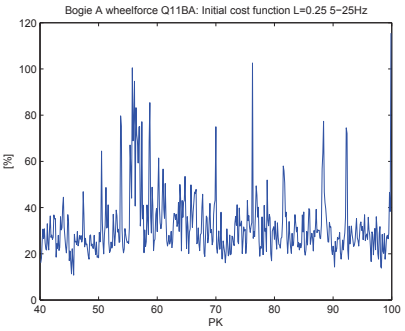

(a) Initial misfit function

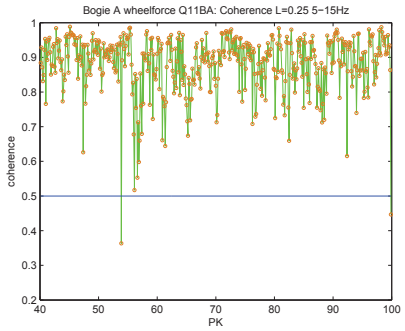

(b) Coherences

Figure E.3: Initial misfit function and coherence function for vertical wheelforce Q11 bogie A for frequency range 5 to 25Hz

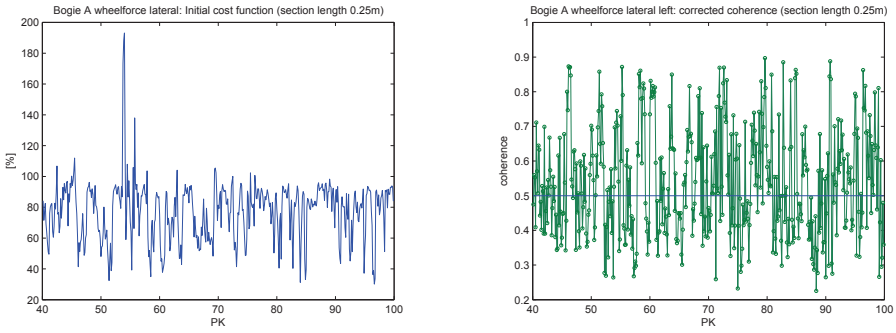

(a) Initial misfit function (b) Coherences

Figure E.4: Initial misfit function and coherence function for lateral wheelforce Y11 bogie A for frequency range 5 to 25Hz

Axle box acceleration

Axle box accelerations are measured on the wheelsets A and I in transversal and vertical direction. Measured on the wheelset running on the track without any suspension they show the same characteristics as the wheelset forces. In vertical direction direction a good correlation between measurement and simulation is obtained. Due to the geometric constraint in vertical direction the acceleration depends directly on the vertical track irregularity. In lateral direction the misfit function shows higher values. The axle box acceleration depends on the nonlinear contact geometry and the friction forces in the wheel rail contact.

Model calibration	
Signal type	Axle-box acceleration
Frequency range	5 to 25Hz
Section length	250m
Overlap	50%
Position	Wheelset A lateral/vertical

Table E.2: Control parameters

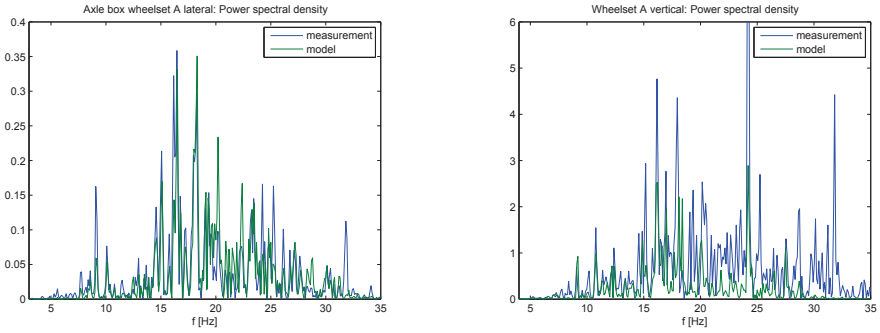

(a) PSD lateral (b) PSD vertical

Figure E.5: Measured and simulated power spectral densities of axle-box acceleration in vertical and lateral direction

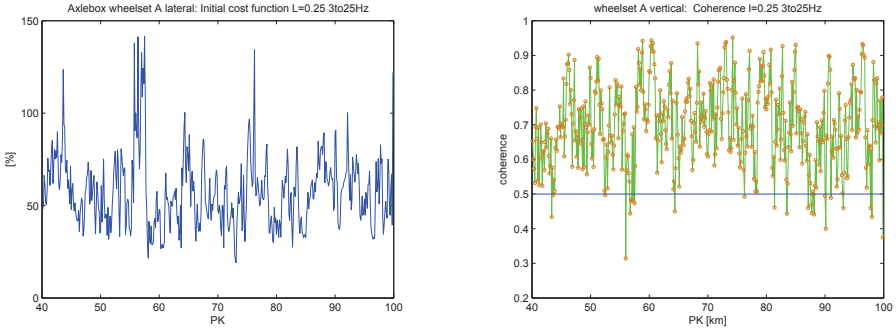

(a) Initial misfit function (b) Coherences

Figure E.6: Initial misfit function and coherence function for lateral axle-box acceleration in wheelset A for frequency range 5 to 25Hz

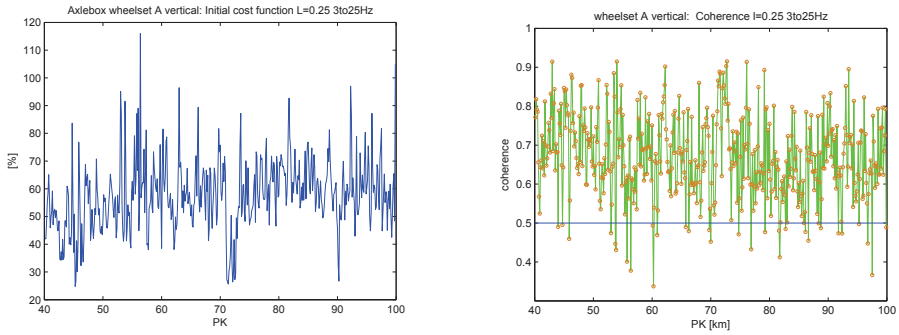

(a) Initial misfit function

(b) Coherences

Figure E.7: Initial misfit function and coherence function for vertical axlebox acceleration in wheelset A for frequency range 5 to 25Hz

Traction unit bogie acceleration

Model calibration	
Signal type	Traction unit bogie acceleration
Frequency range	1 to 11Hz
Section length	250m
Overlap	50%
Position	bogie A lateral/vertical

Table E.3: Control parameters

The distance between measured and simulated accelerations in the traction unit bogie are analysed. From the power spectral density it can be seen that the model is only valid up to frequencies of 14Hz in lateral and 10Hz in vertical direction. This is probably due to the effect of elastic modes or suspension modes not represented in the model. The misfit function and coherence function values are good both for the vertical and lateral direction with values between 40 and 80%. However, again important variations for the sections can be observed.

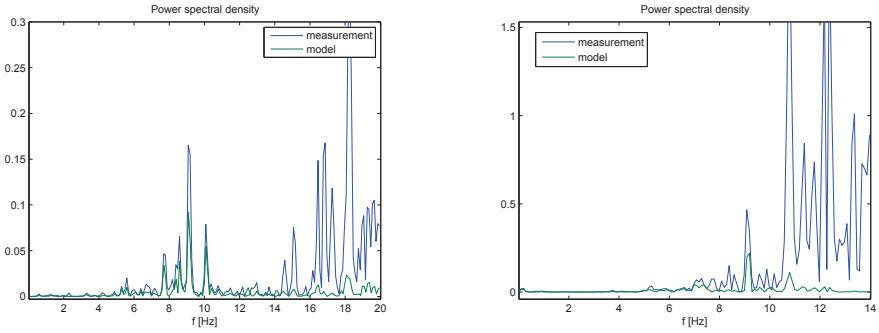

(a) PSD lateral (b) PSD vertical

Figure E.8: Measured and simulated power spectral densities of bogie A acceleration in vertical and lateral direction

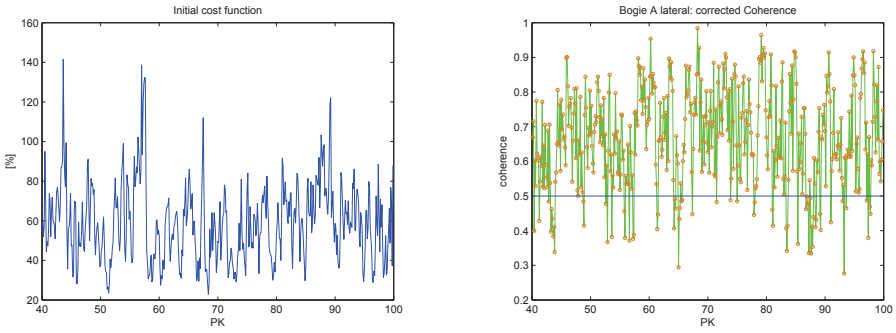

(a) Initial misfit function (b) Coherences

Figure E.9: Initial misfit function and coherence function for lateral acceleration in bogie A

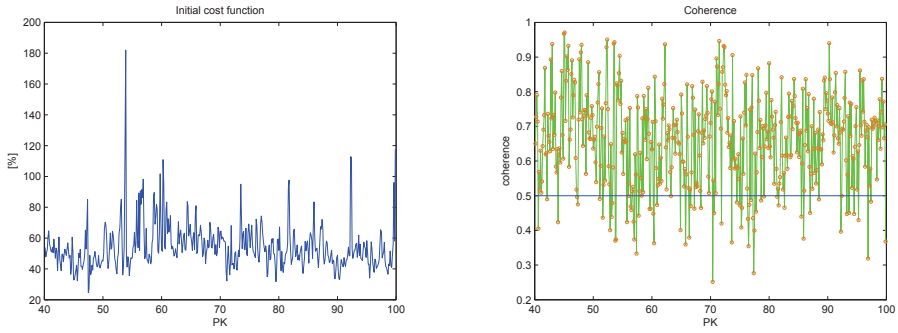

(a) Initial misfit function (b) Coherences

Figure E.10: Initial misfit function and coherence function for vertical acceleration in bogie A

Traction unit car body acceleration

Model calibration	
Signal type	Traction unit car body acceleration
Frequency range	1 to 11Hz
Section length	250m
Overlap	50%
Position	Traction unit 1 lateral/vertical

Table E.4: Control parameters

The analysis of the power spectral density of the car body accelerations shows important differences. This can be due to the complex behavior of the secondary suspension which is not correctly represented in the model.

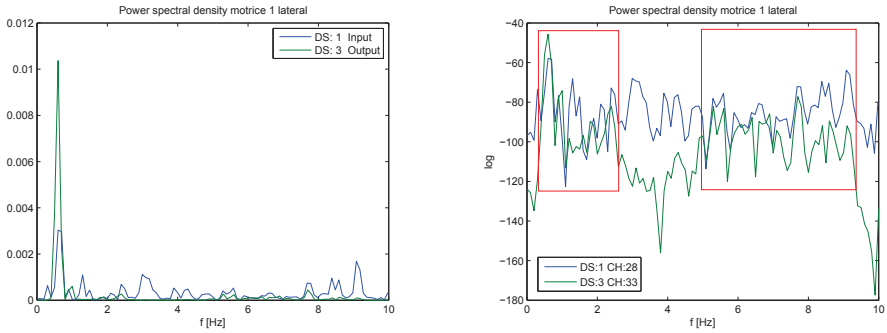

(a) PSD lateral (b) PSD vertical

Figure E.11: Measured and simulated power spectral densities of traction unit 1 acceleration in vertical and lateral direction

Bibliography

[1] M. Alexe, A. Sandu *Forward and adjoint sensitivity analysis with continuous explicit Runge-Kutta schemes*, Applied Mathematics and Computation 208, p.328-346, 2009.

[2] S. W. Anzengruber, R. Ramau *Morozov's Discrepancy Principle for Tikhonov-type functionals with non-linear operators*, Radon Institute for Computational and Applied Mathematics, Linz, 2009.

[3] D. Aubry, G. Puel *CCF modelling with use of a two-timescale homogenization model*, Procedia Engineering 2, p.787-796, 2010.

[4] D. Aubry, G. Puel *Two-timescale homogenization method for the modeling of material fatigue*, IOP Conf. Series: Materials Science and Engineering 10, 2010.

[5] N. Azizi, S. Zolfaghari *Adaptive temperature control for simulated annealing: a comparative study*, Computers and Operational Research, Vol. 31, 14, p.2439-2451, 2004.

[6] C.J. Baker, A. Bouferrouk, J. Perez, S.D. Iwnicki *The integration of cross wind forces into train dynamic calculations*, School of Engineering, University of Birmingham, 2008.

[7] M. Berg *A non linear rubber spring model for rail vehicle dynamic analysis*, Vehicle System Dynamics 30, p.197-212, 1998.

[8] B. Bergander, G. Dendl, A. Nefzger, D. Nicklisch *Die Entwicklung von Rad- und Schieneprofilen*, Glasers Annalen 127, 2003.

[9] J.-U. Bruns *Detektion und Identifikation von Nichtlinearitäten in mechanischen Schwingungssystemen*, Dissertation, Universität Hannover, 2004.

[10] Y. Capdeville, L. Guillot, J.-J. Marigo *1-D non-periodic homogenization for the seismic wave equation*, Geophysical Journal International 181, p.897-910, 2010.

[11] M. Cardiff, P. K. Kitanidis *Efficient solution of nonlinear, underdetermined inverse problems with a generalized PDE model*, Computer and Geoscience, 2008.

[12] H.C. Chan, C.W. Cai, Y.K. Cheung *Exact analysis of structures with periodicity using the U-Transformation*, World scientific, 1999.

[13] G. Charles, R. Dixon, R. Goodall *Condition monitoring approaches to estimating wheel-rail profile*, Loughborough university, 2008.

[14] F. Clément, N. Khvoenkova, A. Cartalade, P. Montarnal *Analyse de sensibilité et estimation de paramètres de transport pour une équation de diffusion, approche par état adjoint*, Institut de la recherche en informatique et en automatique, 2004.

[15] L.P.M. Dias *Sensitivity analysis of rigid-flexible multibody systems*, Multibody System Dynamics, p.303-322, 1997.

[16] J.Y Ding, Z.K. Pan, L.Q. Chen *Second order adjoint sensitivity analysis of multibody systems described by differential-algebraic equations*, Multibody System Dynamics 18(4), p.599-617, 2007.

[17] H. W. Engl, K. Kunisch, A. Neubauer *Convergence rates for Tikhonov regularization of non-linear ill-posed problems*, Kluver Academic Publishers, 1999.

[18] U. Feldmann, E. Kreuzer, F. Pinto *Dynamic diagnosis of railway tracks by means of the Karhunen-Loeve transformation*, Kluver Academic Publishers, 1999.

[19] S. A. Forth, M. M Edvall *User guide for Mad - a Matlab Automatic Differentiation Toolbox TOMLAB/MAD Version 1.4*, Tomlab Optimization, 2007.

[20] Y. Gao, M.J. Brennan, P.F. Joseph *A comparison of time delay estimators for the detection of leak noise signals in plastic water distribution pipes*, Journal of sound and vibration, 292, 2006.

[21] C. Geiger, C. Kanzow *Numerische Verfahren zur Lösung unrestringierter Optimierungsaufgaben*, Springer, 2002.

[22] R. Giering *Recipes for Adjoint Code Construction*, Max-Planck-Institut für Meteorologie, 1998.

[23] M. B. Giles *An introduction to the adjoint approach to design*, Flow, Turbulence and Combustion, 56, 2000.

[24] P. Glösmann, E. Kreuzer *Nonlinear system analysis with Karhunen-Loève Transform*, Nonlinear Dynamics, 41, 2005

[25] G. Gloth, D. Göge *Detektierung und Charakterisierung von Nichtlinearitäten im Rahmen von Standschwingversuchen*, VDI-Berichte, 1825, 2004.

[26] G. Gloth, M. Sinapius *Analysis of swept-sine runs during modal identification*, Mechanical systems and signal processing 18, 2004.

[27] D. Göge, U. Füllekrug *Analyse von nichtlinearen Schwingungsverhalten bei grossen Luft-und Raumfahrtstrukturen*, VDI-Berichte, 1825, 2004.

[28] C. Gontier, D. George, M. Raffy *Energetic mode contributions in stochastic modal analysis: An application to mode classification*, Journal of sound and vibration 294, p.944-965, 2006.

[29] J. Grajnert, O. Krettek *Zur Phänomenologie und Ersatzmodelbildung von Luftfedern*, Glasers Annalen 115, Nr. 7/8, 1991.

[30] J. Grajnert, Z. Chabras, P. Wolko *Airspring modeled in MATLAB/Simulink as a force element in ADAMS*, MDI conference, 2001.

[31] A. Griewank *Evaluating Derivatives*, Society for Industrial and Applied Mathematics, Philadelphia, 2000.

[32] W. Hanneforth, W. Fischer *Laufwerke*, Transpress, VEB Verlag für Verkehrswesen, Berlin, 1986.

[33] E. J. Haug, K. K. Choi, V. Komkov *A time and frequency domain approach for identifiying nonlinear mechanical system models in the absence of an input measurement*, Journal of Sound and Vibration 283, 2005.

[34] E. J. Haug, K. K. Choi, V. Komkov *Design Sensitivity Analysis of Structural Systems*, Mathematics in science and engineering, Vomlume 177, Academic Press, 1986.

[35] W. Heylen, S. Lammens, P. Sas *Modal analysis theory and testing*, Katholieke Universiteit Leuven, B-3001 Leuven, Belgium, 1997.

[36] L. Hermans, H. Van der Auweraer *Modal testing and analysis of structures under operational conditions: industrial applications*, Mechanical Systems and Signal processing, 13(2), p.193-216, 1999.

[37] D. Hickey, K. Worden, M. Platten, J. Wright *Higher-order spectra for identification of nonlinear modal coupling*, Mechanical Systems and Signal Processing, 23, 2009.

[38] K.J. Hollenbeck, K.H. Jensen *Maximum-likelihood estimation of unsaturated hydraulic parameters*, Journal of Hydrology 210, p.192-205, 1998.

[39] B. Hu *Korrelationsbasierte Methode zur Parameteridentifikation nichtlinearer mechanischer Systeme*, Fortschrittsberichte VDI, 257.

[40] A. Ismael, L.N. Vicente *A particle swarm pattern search method for bound constrained nonlinear optimization*, 2006.

[41] S. Iwnicki *Handbook of railway vehicle dynamics*, Taylor and Francis, 2000.

[42] T. A. Johansen *On Tikhonov Regularization, Bias and variance in nonlinear system identification*, Automatica, Vol.33, No.3, p.441-446, 1997.

[43] K.L. Johnson *Contact mechanics*, Cambridge University Press, 1985.

[44] J.J. Kalker *Three-Dimensional Elastic Bodies in Rolling Contact*, Kluwer Academic Publishers, 33 AA Dordrecht, Netherlands, 1990.

[45] J.J. Kalker *A fast algorithm for the simplified theory of rolling contact*, Vehicle System Dynamics 11, 1982.

[46] J.J. Kalker *Wheel-rail rolling contact theory*, Wear, 144, 243-261, 1991.

[47] J. S. Kang *Structural system identification in time domain using measured acceleration*, Kluwer Academic Publishers,33 AA Dordrecht, Netherlands, 2005.

[48] M. Kern *Problèmes inverses aspects numériques*, École Superieure d 'Ingénieurs Léonard de Vinci, 2003.

[49] M. Kern *Problèmes inverses*, École Superieure d 'Ingénieurs Léonard da Vinci, 2003.

[50] G. Kerschen, K. Worden, A. F. Vakakis, J.-C. Golinval *Past, present and future of nonlinear system identification in structural dynamics*, Mechanical Systems and Signal Processing 20, p.505-592, 2006.

[51] G. Kerschen, M. Peeters, J.C. Golinval, A.F. Vakakis *Nonlinear normal modes, Part I: A useful framework for the structural dynamicist*, Mechanical Systems and Signal Processing 23 , p.170-194, 2009.

[52] K. Knothe, S. Stichel *Schienenfahrzeugdynamik*, Springer-Verlag Berlin Heidelberg, 2003.

[53] K. Knothe, J. Piotrowski *Heinrich Hertz und Ferdinand Redtenbacher*, Glasers Annalen 129, 2005.

[54] O. Krettek, J. Grajnert *Zur luftfeder- und schwingungstechnischen Auslagung des TGV Atlantique*, Springer-Verlag Berlin Heidelberg, 2003.

[55] O. Krettek, J. Grajnert *Die Modeldarstellung pneumatischer Fahrzeugfederungen und die Vorauswahl der Modellparameter*, Glasers Annalen 115, Nr. 5, 1991.

[56] J. Lardies, N. Larbi *A new method for model order selection and modal parameter estimation in time domain*, Journal of Sound and Vibration, 245, 2001.

[57] M. Laroussi *Analyse de sensibilité 3D par la méthode de l'état adjoint - application au forgeage*, Thèse de doctorat, Ecole Nationale Supérieure des Mines de Paris, 2003.

[58] R. M. Lewis, V. Torczon, M. W. Trosset *Why pattern search works*, NASA/CR-1998-208966, 1998.

[59] P. Li, Roger Goodall *Estimation of railway vehicle suspension parameters for condition monitoring*, Control Engineering Practice 15, 2007.

[60] J. Martins, J. Alonso, J. Reuther *A coupled-adjoint sensitivity analysis method for high fidelity aero-structural design*, Springer, 2005.

[61] R. van Marrewijk, E. de Jong, R. Ahrens *Implementation of multiple thermodynamic airspring systems in ADAMS*, NedTrain Consulting, Alstom LHB.

[62] L. Mauer *Die modulare Beschreibung des Rad/Schiebe-Kontaktes im linearen Mehrkörperformalismus*, Technische Universität Berlin, 1988.

[63] Z. Michalewicz *Genetic Algorithms + Data Structures = Evolution Programs*, Springer-Verlag Berlin Heidelberg, 1996.

[64] K. Miettinen, M.M. Mäkelä, H. Maaranen *Efficient hybride methods for global continuous optimization based on simulated annealing*, Computers and Operational Research, Volume 33, Issue, 4, p.1102-1116, 2006.

[65] M. Molodova, Z. Li, R. Dollevoet *Simulation of dynamic responses of vehicle-track system for detection of track short wave defects*, Conference paper CM2009, 2009.

[66] S.M. Moore, J.C.S. Lai, K. Shankar *ARMAX modal parameter identification in the presence of unmeasured excitation-I: Theoretical background*, Conference paper CM2009, 2009.

[67] S.M. Moore, J.C.S. Lai, K. Shankar *ARMAX modal parameter identification in the presence of unmeasured excitation-II: Numerical and experimental verification*, Conference paper CM2009, 2009.

[68] Klaus Mosegaard, Albert Tarantola *Monte Carlo sampling of solutions to inverse problems*, Journal of Geophysical research, Vol. 100, 1995.

[69] J. Nocedal, S. J. Wright *Numerical Optimization*, Optimization and Engineering, 6, p.33-62, 2005.

[70] N. Oda, S. Nishimura *Vibration of air suspension bogies and their design*, Bulletin of the JSME, Vol. 13, No. 55, 1970.

[71] D.I. Padadimitriou; K.C. Giannakoglou *The continuous direct-adjoint approach for second order sensitivities in viscous aerodynamic inverse design problems*, Computer ad Fluids 38, 1839-1548, 2009.

[72] M. Peeters, G. Kerschen, J.C. Golinval *Dynamic testing of nonlinear vibrating structures using nonlinear normal modes*, Journal of Sound and Vibration, Volume 330, Issue 3, p.486-509, 2011.

[73] M. Peeters, R. Viguié, G. Sérandour, G. Kerschen, J.-C. Golinval *Nonlinear normal modes, Part II: Toward a practical computation using numerical continuation techniques* Mechanical Systems and Signal Processing, Volume 23, Issue 1, p.195-216, 2009.

[74] K. A. Petsounis, S. D. Fassois *Parametric time domain methods for the identification of vibrating structures - a critical comparison and assessment*, Mechanical systems and signal processing 15, 2001.

[75] M. Presthus *Derivation of air spring model parameters for train simulation*, Lulea university of technology, master thesis, 2002.

[76] B. Protas *A computational framework for the regularisation of adjoint analysis in multiscale PDE systems*, Journal of computational physics 195, 2004.

[77] R. Pytlak *Conjugate Gradient Algorithms in Nonconvex Optimization*, Springer, 2009.

[78] A. Rahrooh, S. Shepard *Identification of nonlinear systems using NARMAX model*, Nonlinear Analysis 71, 2009.

[79] C. Rathod, A. Shabana *Geometry and differentiability requirements in multibody railroad vehicle dynamic formulations*, Nonlinear Dynamics 47, p.249-261, 2007.

[80] C.M. Richards, R. Singh *identification of multi-degree-of-freedom nonlinear system under random excitations by the reverse path spectral method*, Journal of Sound and Vibration, 213, 1998.

[81] E. de Rocquigny *La maîtrise des incertitudes dans un contexte industriel*, Nonlinear Dynamics 47, p.249-261, 2007.

[82] A. Saltelli, Stefano Tarantola, Francesca Campolongno, Marco Ratto *Sensitivity analysis in practice*, Wiley, 2004.

[83] A. Saltelli *Variance based sensitivity analysis of model output. Design and estimator for the total sensitivity index*, Computer Physics Communication 181, p.259-270, 2010.

[84] A. Sandel *Outils symboliques pour l'écriture de modèles et l'étude de sensibilité des systèmes multicorps*, Thèse INSA Lyon, 2007.

[85] A.Schmidt-Fellner, J.-U. Bruns, K. Popp *Identifikation nichtlinearer Koppelelemente*, Forschung im Ingenieurwesen 69, p.82-89, Springer-Verlag, 2005.

[86] A. A. Shabana, M. Tobaa, H. Sugiyama, K. E. Zaazaa *On the computer formulations of the wheel/rail contact problem*, Nonlinear dynamics, 40, 2005.

[87] J. J. Schneider *Stochastic optimisation*, Springer, 2007.

[88] R. Serban, J.S. Freeman *Identification and Identifiability of unknown parameters in multibody dynamic systems*, Springer, 2002.

[89] R. Serban, E.J. Haug *Analytical derivatives for multibody system analysis*, University of Pennsylvania, 2007.

[90] W. Sextro *Dynamical contact problems with friction*, Springer, 2002.

[91] K. Shimozawa, T. Tohtake *An air spring model with nonlinear damping for vertical motion*, Quarterly report of RTRI, Vol. 49, No. 4, Nov. 2008.

[92] M. Sjöberg *On dynamic properties of rubber isolators*, Doctoral thesis, KTH Stockholm, 2002.

[93] SNCF *Analyse modal TGV*, Document technique SNCF, 1983.

[94] M. Syrjakow *Verfahren zur effizienten Parameteroptimierung von Simulationsmodellen*, Dissertation, Universität Karlsruhe, 1997.

[95] M.J.G. Tarrago, J. Vinolas, L. Kari *Axial stiffness of carbon black filled rubber bushings*, Rohstoffe und Anwendungen, 2007.

[96] H.A.L. Thi, D.T. Pham *Combination between gobal and local methods for solving an optimization problem over the efficient set*, European journal of operational research, Volume 142, Issue 2, pp. 258-270, 2002.

[97] H. True *Nichtlineare Schienenfahrzeugdynamik, neue Grundlagen, Methoden und Ergebnisse*, Glasers Annalen 128, 2004.

[98] G. Vohla *Werkzeuge zur realitätsnahen Simulation der Laufdynamik von Schienenfahrzeugen*, Fortschritt-Berichte VDI: Reihe 12, Verkehrstechnik, Fahrzeugtechnik, Nr. 270, VDI-Verlag, Düsseldorf, 1996.

[99] E. Walter, L. Pronzato *Identification of Parametric Models from Experimental Data*, Springer, 1997.

[100] E. Walter, L. Pronzato *On the identifiability and distinguishability of nonlinear parametric models*, Mathematics and computes in simulation 42, p.125-134, 1996.

[101] J. Wingren *Track to Carbody vibration transfer for a bogie rail vehicle*, TRITA-FKT 1997:07, KTH Stockholm, 1997.

[102] K.A. Woodbury *Inverse Engineering Handbook*, CRC Press, 2003.

[103] Vampire *Vampire Manual*,Version 4.31.

[104] P. Verboven, P. Guillaume, S. Vanlanduit, B. Cauberghe *Assessment of nonlinear distorsions in modal testing and analysis of vibration automotive structures*, Journal of sound and vibration 293, 299-319, 2006.

[105] C. Xu, G. Gertner *Extending a global sensitivity analysis technique to models with correlated parameters*, Computational Statistics and Data Analysis, Vol. 51, Issue 12, 2007.

[106] W. Yu, T.J. Harris *Parameter uncertainty effects on variance-based sensitivity analysis*, Reliability Engineering and system safety 94, p.596-603, 2009.

[107] K. E. Zaazaa, A. L. Schwab *Review of Joost Kalkers wheel-rail contact theories and their implementation in multibody codes*, proceedings of the ASME 2009 International Design Engineering Technical Conference, 2009.